~~CONFIDENTIAL~~

NATIONAL AERONAUTICS AND SPACE ADMINISTRATION
CONTRACT NO. NASW-6

Report No. 20-123

Juno IV Rocket Vehicle System

J. D. Burke
D. R. Bartz
A. Briglio
C. R. Gates

JET PROPULSION LABORATORY
CALIFORNIA INSTITUTE OF TECHNOLOGY
PASADENA, CALIFORNIA

December 27, 1960

~~CONFIDENTIAL~~

CONTENTS

CONTENTS (Cont'd)

APPENDIXES:

TABLES

FIGURES

FIGURES (Cont'd)

FIGURES (Cont'd)

FIGURES (Cont'd)

ABSTRACT

This Report has been prepared as a record of the engineering investigations made at JPL during 1958, when one of the several space-vehicle projects that were being proposed at that time was given a go-ahead and later cancelled. Some of the results of the ARPA-sponsored *Juno IV* studies reported here were carried over into the NASA-sponsored *Vega* project, which was authorized and subsequently cancelled during 1959.

The *Juno IV* vehicle was to consist of a Jupiter IRBM booster plus guided liquid-propelled upper stages including a second stage of 45,000-lb thrust and a third stage of 6,000-lb thrust. The program was authorized and preliminary funds released in August 1958; the program was cancelled in October 1958.

The Report is divided into three main parts. The first part describes the 45,000-lb-thrust propulsion system, the second part summarizes work done on the 6,000-lb-thrust powerplant, and the third part describes the guidance, control, and telemetry systems that were proposed for the *Juno IV* vehicle.

I. INTRODUCTION

Late in 1957, shortly after the beginning of the *Explorer* project, the Jet Propulsion Laboratory and the Army Ballistic Missile Agency began studies aimed at defining a satellite and space-vehicle program to extend beyond the end of the International Geophysical Year. These studies resulted in the recommendation of a so-called *Juno* program, the object of which was to exploit the existing capability of the Army's large rockets, while at the same time expanding this capability by means of new developments in propulsion, guidance, and long-range communications. The rocket configurations studied were as follows:

1. *Juno I* (previously called *Redstone RTV* or *Jupiter C*): the *Explorer* launching vehicle.
2. *Juno II*: a lunar probe or earth-satellite vehicle consisting of a *Jupiter* IRBM booster plus *Explorer*-type upper stages.
3. *Juno III*: *Jupiter* plus enlarged upper stages similar to those of *Juno I* and *II*, i.e., an unguided, spinning cluster of solid-propellant rockets.
4. *Juno IV*: *Jupiter* plus guided, liquid-propelled upper stages.

The *Juno I* and *Juno II* programs were accepted for use during and after the IGY; the *Juno III* vehicle was studied briefly and then abandoned in favor of *Juno IV*. During the summer of 1958, *Juno IV* went through several proposal stages, and in August a program was authorized, preliminary funds being released by the Advanced Research Projects Agency. In October the project was canceled.

The first joint JPL-ABMA proposal for an improved space vehicle based on the *Jupiter* booster was presented in November, 1957. This was the *Juno III* proposal, in which the upper stages were to consist of rotating clusters

of solid-propellant rockets similar to but larger than clusters used in *Juno I* and *II*. It was soon decided that this vehicle, while having the advantages of quick, cheap development and reasonable certainty of success, was not really compatible with the expected course of developments in the field of guidance and payload experiments. Therefore, in May, 1958, another proposal was submitted to ARPA. This, the first of the *Juno IV* proposals, envisioned a vehicle with guided, liquid-propelled upper stages which could be developed on a schedule calling for a first flight in March, 1959. During the next few months the design studies were continued, with JPL concentrating on lunar and space missions and ABMA concentrating on earth-satellite missions. It was found that near-optimum vehicles for all missions could be obtained merely by altering the tank sizes in the various stages. Thrust levels for the upper-stage powerplants were selected on the basis of a compromise between performance and convenience of development; the design vacuum thrust levels of the second and third stages were to be 45,000 and 6,000 lb, respectively. It was proposed that two parallel second-stage engine developments be carried on: one by ABMA based on existing hardware (the GE 405H engine, with about 33,000 lb of thrust), the other by JPL based on a new design for the 45,000-lb-thrust engine. When it became apparent that funds would not be sufficient to carry both programs, the GE engine was dropped. It was clear, however, that the original flight schedule could not be maintained, especially in view of the expected time required for the 45,000-lb-thrust engine development. Therefore, it was proposed that the early flights be made with a vehicle having only two stages, the *Jupiter* plus an enlarged 6,000-lb-thrust stage. Such a vehicle would have a respectable earth-satellite performance but would have no lunar or space-probe capability.

In August, 1958, ARPA Orders 15-59 and 16-59 were issued, authorizing the *Juno IV* project and releasing preliminary funds. These orders called for earth-satellite missions only. The emphasis on lunar and space missions being reduced, JPL and ABMA began at once on the design and construction of the earth-satellite vehicles. A program consisting of three two-stage and three three-stage firings was proposed, the first firing being scheduled for June, 1959. Because of the limited payload capacity of the two-stage vehicles, it was decided to use a lightweight guidance system, to be supplied by JPL, in the first three firings. An alternate program was offered, contingent upon additional funds, incorporating the GE engine for the first three firings, so that all vehicles would have three stages.

In September, 1958, the earth-satellite missions were reviewed and it was found that the proposed vehicles could meet all of the payload and altitude requirements, provided that a transfer-orbit or "kick" technique was used for the higher-altitude missions. In order to improve the prospects of meeting all the scheduled flight dates, it was decided to defer the introduction of the JPL 45,000-lb-thrust engine and to make the six requested flights with three two-stage vehicles and three three-stage vehicles incorporating the GE second-stage powerplant. On October 16, 1958, the project was canceled by ARPA. This report summarizes the work done up to the time of cancellation.

II. PRELIMINARY DESIGN

The primary design criteria were that the *Juno IV* vehicle have the accuracy, versatility, and performance required for all space missions contemplated and that, at the same time, its development make progress toward the ideal of reliability and simplicity in liquid-rocket powerplants. It was intended that during the program it would be possible at any time to exploit the maximum performance capability of the existing *Jupiter* version by having available upper stages of near-optimum size.

A. Selection of Propellants and Pumping Scheme for the Upper Stages

Over a period of years, propulsion research personnel at JPL and elsewhere have become convinced that the next major advance in the liquid-rocket field will result from the use of noncryogenic, pressure-fed systems (which are inherently more simple and reliable than the large rocket powerplants now in use) with high-performance propellants such as N_2O_4 and N_2H_4. Such systems are particularly suitable for use in the upper stages of space vehicles because (1) ability to operate at low chamber pressure makes a pressurized system competitive in weight with a pumped system and (2) in some missions long coasting periods occur before firing, so that the cryogenic liquefied-gas propellants may not be used.

When the *Juno IV* program was proposed, experimental work on injectors, cooling, gas-generation pumping, and other aspects of powerplant design was sufficiently advanced at JPL to justify a proposal for the immediate development of engines based on the principles just described. Among the several propellant combinations that could be considered, N_2O_4 and N_2H_4 were selected as best on the basis of performance and development experience. In the tests that have been made since the project was approved, these propellants have demonstrated excellent performance at the flight-design thrust levels.

B. General Configuration Studies

The rocket design studies were all based on the known present characteristics of the *Jupiter* booster plus reasonable assumptions as to the performance of future improved versions. Given a certain maximum weight allowable at takeoff, the first task in such studies is to determine the weight distribution among stages that maximizes the payload. The results of these studies are summarized in Table 1. Concurrently with the weight-distribution study, it was necessary to select thrust levels for the upper stages. Some early calculations for the three-stage version showed that (1) earth-satellite payload increased significantly as second-stage thrust was raised from 25,000 to 50,000 lb, (2) lunar payload decreased slightly over the same interval, and (3) the payload for both missions was insensitive to the value of third-stage thrust. On the basis of these results a compromise value of 45,000 lb was selected for the JPL second-

Table 1. Weight Distribution

Mission and Date	Gross Weight Allowable, lb	Propellant Weight lb				Gross* Payload Weight, lb	Remarks**
		Stage 1	Stage 2	Stage 3	Stage 4		
Earth Satellite, *Juno IVA*, 1959	136,000	113,500	9,000	—	—	1,090	at 260-mile altitude
Earth Satellite, *Juno IVB*, 1960	137,500	90,000	24,550	7,480	—	2,200	at 260-mile altitude
24-hr Satellite, *Juno IVB*, 1960	137,850	98,100	22,400	3,950	270	290	at 22,300-mile altitude
Lunar Vehicle, *Juno IVB*, 1960	137,600	98,100	22,360	4,000	—	360	82-hr flight time
Mars, *Juno IVB*, 1960	136,000	94,000	20,900	6,300	930	370	180-day flight time

*Gross payload weight includes all weight ahead of the empty power plant at injection into orbit; i.e., it includes, in addition to the "net" experimental payload, the guidance, communication, and power equipment, plus all associated structure. When terminal maneuvers are used, the (loaded) weight of the necessary rockets is also included.
**All east from AMR.

stage engine development. A value of 6,000 lb was chosen for the third stage largely because of compatibility with existing test facilities.

Further calculations showed that a vehicle consisting only of the *Jupiter* and a 6,000-lb-thrust stage could perform usefully as an earth-satellite launcher. (see Fig. 1), provided that the tanks in both stages were enlarged. In order to achieve early flights, such a vehicle, designated *Juno IVA*, was to have been built.

C. Structural Arrangement

Because the JPL upper-stage power plants were pressure fed, structural efficiency of the propellant tanks and other pressure vessels was essential to the success of the design. After studies of various tank arrangements for the 6,000-lb-thrust stage had been made, it was decided to make a tank of nearly spherical shape, with an internal bulkhead dividing the two propellants as the design goal. For interim use on the early vehicles, however, separate spherical tanks were selected on grounds of simpler and more reliable development. A weight penalty of the order of 50 lb was associated with the use of the separate tanks. A maximum diameter of 70 in. for both upper stages was chosen for compatibility with ABMA airframe tooling. The first earth-satellite version of *Juno IVA* is shown in Fig. 2. The guidance compartment and interstage structures were to be of conventional light-alloy, semimonocoque construction similar to that used in the *Redstone* and *Jupiter*. The propellant tanks for the 6,000-lb-thrust

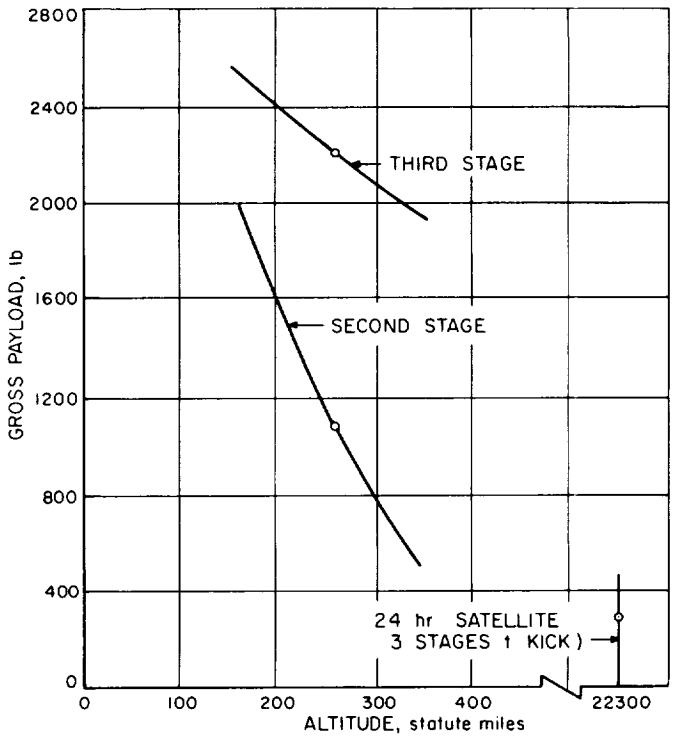

Fig. 1. Gross Payload vs Altitude for Atlantic Missile Range Launching Eastward

stage were to be made from 2014-T6 aluminum alloy, formed, chem-milled, and welded by techniques similar to those used in the *Thor* and WS117L. The payload structure was unspecified.

Appendices A through F present material pertaining to the separation mechanics and tank fabrications.

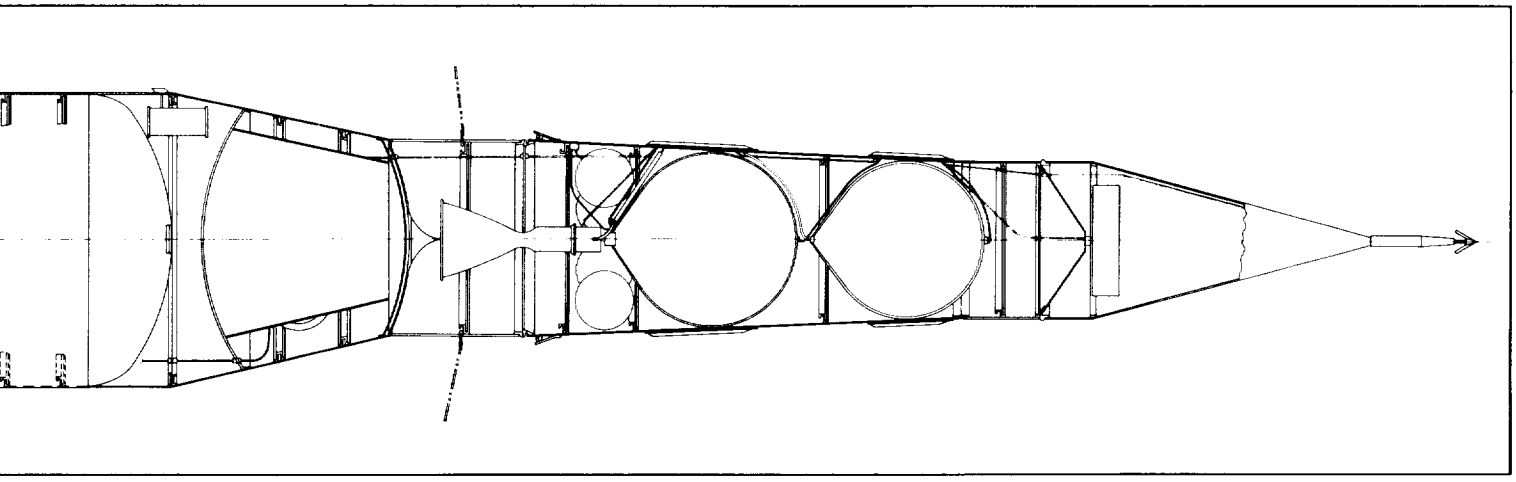

Fig. 2. First Earth-Satellite Version of *Juno IVA*

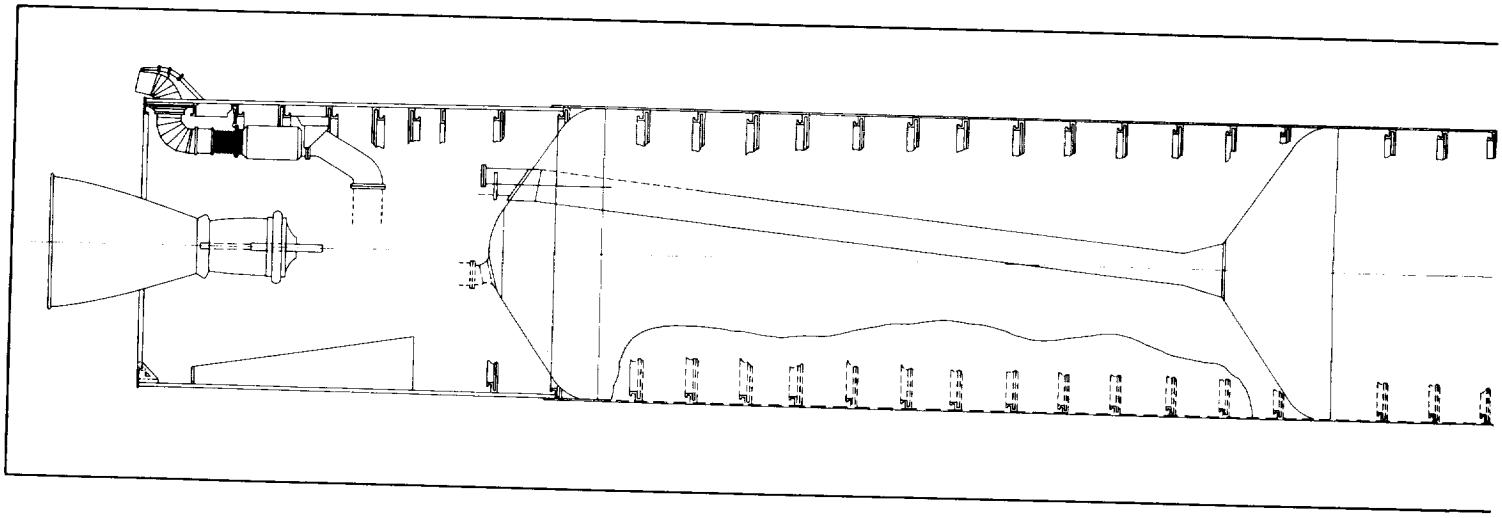

III. PROPULSION SYSTEM, 45,000-LB-THRUST STAGE

The following summary represents the work done on the 45,000-lb-thrust (45K) powerplant at the termination of the *Juno IV* Program:

1. A schematic diagram of the "heated hybrid" system was completed. A preflight and in-flight operational analysis of the system was also completed.

2. Preliminary layouts of the 45K propulsion system in the 70-in.-diameter second-stage missile configuration were made which demonstrated the method of system packaging.

3. Heat-transfer studies were completed on the 45K thrust chamber and actual tube wall chamber drawings were commenced. The individual tube configuration was completed; assembly drawings were not finished.

4. Drawings of the flight-weight injector and preliminary drawings of the chamber injector assembly were laid out; various preliminary layouts of the dual-ball-valve-injector assembly were drawn.

5. Various methods of chamber construction and fabrication were considered; small-scale test samples were made up and evaluated.

6. The selection of the vendors to supply the necessary components for the 45K system was nearly completed; various vendors were being considered for thrust-chamber fabrication.

7. Uncooled short-duration 45K firings were made; the injector optimization and design c* goal was reasonably in sight.

A. System Design

The proposed JPL 45K second-stage propulsion system for *Juno IV* had the following gross characteristics:

Propellant combination: nitrogen tetroxide (N_2O_4) and hydrazine (N_2H_4)
Vacuum thrust: 45,000 lb
Approximate burning time: 135 sec
Pumping system: "heated hybrid" gas pressurization (Fig. 3)

It was believed that the development of a 45K N_2O_4 – N_2H_4 second-stage propulsion system would greatly increase the reliability and growth potential of the *Juno IV* vehicle. The four factors that would have contributed most directly to increased reliability were propellant storability, propellant hypergolicity, monopropellant fuel, and a simplified pumping system.

The following facts are of interest as related to growth potential: (1) the similarity of the 45K second stage to the JPL third-stage propulsion system made it a logical choice as the top stage of future high-payload orbital and space vehicles; (2) the characteristics of the proposed system would have greatly simplified the problem of its eventual adaptation to repeated on-off operation; (3) development of the monopropellant runout technique would have afforded a direct approach to the problem of maximum propellant utilization; and (4) the experience gained in the development of this system would have provided valuable background information in the development of high-thrust-level, storable-propellant engines.

The selection of a vacuum-thrust level of 45,000 lb was based on gravity-turn-trajectory studies wherein *Jupiter*-based three-stage vehicles with various second-stage thrust levels (first-stage and third-stage thrust levels held constant) were run on the computer for both the satellite and lunar missions. The over-all effect of burning time and second-stage propulsion system weight on payload could then be discerned and the thrust for maximum payload realized. The following general conclusions were drawn from this study:

1. For a three-stage *Jupiter*-based (liquid oxygen – N_2H_4 satellite vehicle, a second-stage vacuum thrust of 50,000 to 65,000 lb permits the largest payload capability. The third-stage burning time has relatively no effect on payload capability, and other considerations such as allowable downrange burnout dictate the selection of third-stage thrust.

2. Because of the flatness of the lunar trajectory, a low-thrust, second-stage engine (a lighter propulsion system than the high-flow-rate, high-thrust systems) gives maximum payload for a three-stage vehicle. A vacuum thrust of the order

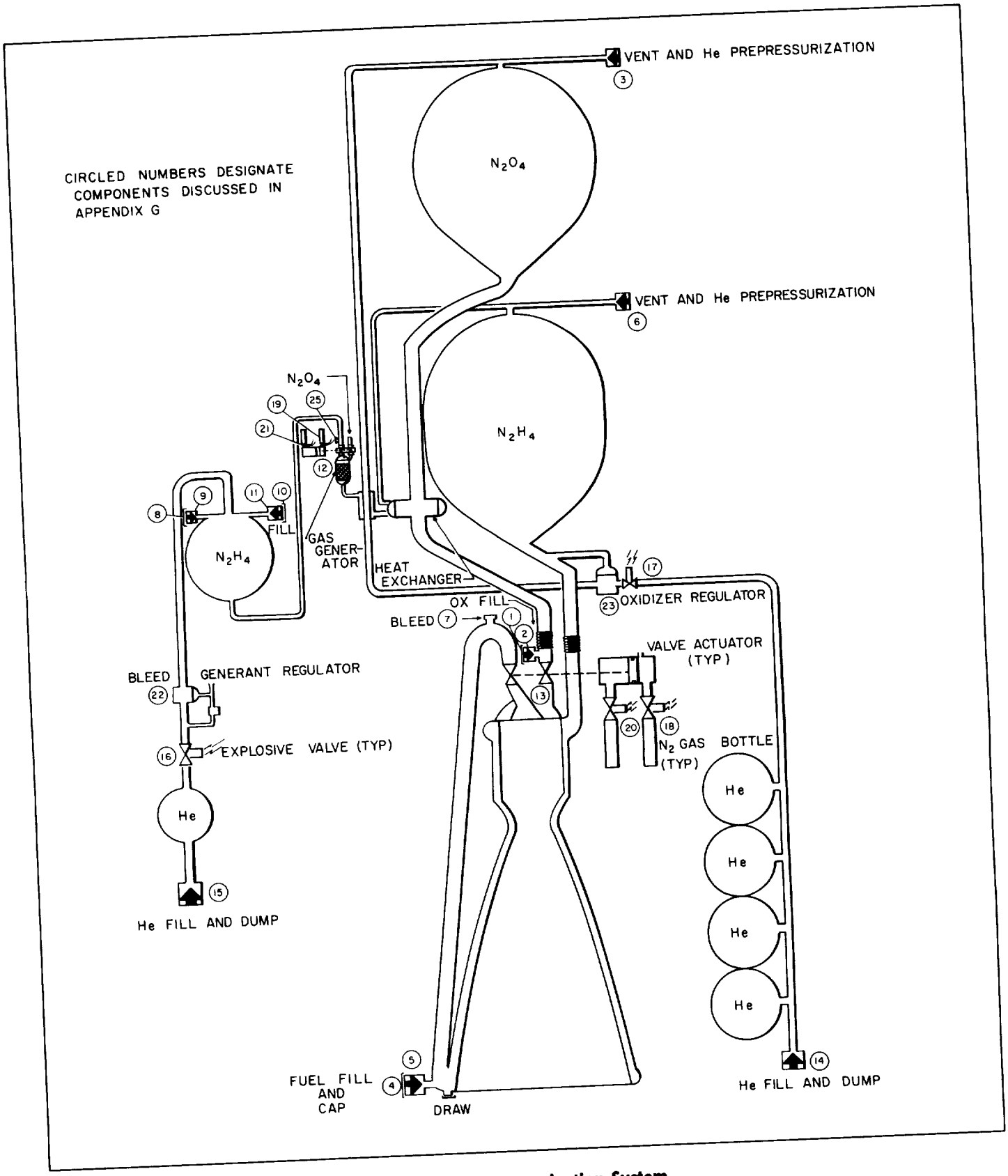

Fig. 3. Gas Pressurization System

of 20,000 to 25,000 lb appeared best for this mission. It should be noted, however, that for certain launch sites a higher second-stage thrust might be required for the lunar mission. More nearly vertical trajectories would be required during certain periods of the year at such locations.

The 45K engine represented a compromise between the optimum thrust level for the satellite mission and the optimum thrust level for the lunar mission. The 45K thrust level also suggested a reasonable "scale-up" from a 20K sea-level-thrust $N_2O_4 - N_2H_4$ engine successfully run at the Edwards Test Station.

Since a gas-pressurization system was selected as the propellant transfer method, it was apparent that a low-chamber-pressure engine (i.e., low tank pressures) was desirable. If experimental performance is invariant with chamber pressure, the optimum chamber pressure occurs below 150 psia; however, a chamber-pressure survey on the 20K $N_2O_4 - N_2H_4$ engine indicated a substantial loss in performance below chamber pressures of 200 psia. A chamber pressure of 200 psia was therefore selected on the basis of expected performance characteristics.

It was believed that pressurized-gas propellant-transfer systems offered the best combination of weight, reliability, and simplicity. A fairly comprehensive study of gas-pressurization systems was conducted in order to select a feasible high-performance propellant-transfer system for the second stage. The following eight systems were evaluated:

Dual-gas generation

1. Monopropellant gas generator pressurizes fuel tank; oxidizer-rich bipropellant gas generator pressurizes oxidizer tank.

Single-gas generation

2. Heat-exchanger-cooled hydrazine gas-generant products pressurize both tanks. (Expulsion bladder located in oxidizer tank.)

3. Ammonia-quenched hydrazine gas-generant products pressurize both tanks. (Expulsion bladders located in both tanks.)

4. Helium-quenched hydrazine gas-generant products pressurize both tanks. (Expulsion bladder located in oxidizer tank.)

5. Helium heated by gas-generator products pressurizes oxidizer tank; gas-generator products pressurize hydrazine tank.

6. Helium heated by decomposition products pressurizes both propellant tanks; generant products dumped overboard.

7. Cold helium pressurizes oxidizer tank; hydrazine products pressurize fuel tank.

Compressed gas

8. Oxidizer and fuel tanks pressurized by common reservoir of compressed helium.

A complete weight breakdown of the eight systems was made on the basis of 21,600 lb of propellant being pumped at a flow rate of 151 lb/sec. A propellant mixture ratio of 1.10 and a tank pressure of 335 psia were assumed. The results showed that systems (2) and (3) were the lightest of the systems evaluated; system (8) was the heaviest and represented approximately a 50-lb loss in lunar payload capability when compared with systems (2) and (3). The system selected for further detailed study as the second-stage pumping system was the "heated hybrid" system (5). This system offered the most satisfactory combination of weight efficiency and developmental simplicity.

Figure 3 represents the propulsion system as it was envisioned. This "hybrid" system utilized an N_2H_4 monopropellant gas generator to pressurize the fuel-tank (N_2H_4) and helium heated by exchange with the gas-generator products to pressurize the oxidizer (N_2O_4) side. Although cooled somewhat by the helium, the generator products were brought to acceptable tank temperatures by the N_2O_4 heat exchanger located in the oxidizer line. The system as depicted by the schematic diagram utilized a gimbaled thrust chamber for yaw and pitch control. No means of roll control is depicted. However, a hot-gas bypass from the gas generator would have been used for roll control contingent upon the development of a hot-gas swivel nozzle.

An in-flight and preflight operational analysis of the 45K propulsion system described in Fig. 3 is given in Appendix G.

B. Components of the 45,000-Lb-Thrust Stage

1. GAS GENERATOR-DECOMPOSITION CHAMBER

The gas-generator decomposition chamber was designed for an ammonia dissociation value of 75% in order to obtain an outlet temperature of 1460°F. This particular dissociation value was selected in order to obtain the lowest practical decomposition gas average molecular weight without a severe component weight penalty due to decomposition chamber size.

The flow rate necessary for main system fuel expulsion, based upon a tank pressure of 335 psia and a mean tank gas temperature of 100°F, was calculated to be 0.861 lb/sec. The additional flow required for roll control was 0.162 lb/sec. A decomposition chamber pressure of 485 psia was selected after completion of a study of system weight vs gas-generator chamber pressure and also in order to allow for a high gas pressure drop through the oxidizer heat exchanger. The gas generator design, based on the parameters stated above, consisted of a decomposition chamber of 6.25 in. in diameter and 6.50 in. long utilizing type H-A-3 catalyst. The weight of the decomposition chamber assembly was calculated to be 17.5 lb. A prototype gas generator was constructed by modification of an existing similar unit. This modified chamber was used for the development of an efficient bipropellant ignition technique and was scheduled for tests with the gas analyzer system prior to final design and construction of the flight-weight unit.

2. GAS GENERATOR-IGNITION SYSTEM

In order to provide an efficient method for initiating monopropellant operation of the gas generator, a simple bipropellant ignition system was designed and tested. This system consisted of a small cartridge which was preloaded with nitrogen tetroxide, pressurized with nitrogen, and then sealed. Energizing the fire valves opens both circuits allowing the fuel to enter from its regulated source and the oxidizer cartridge to "blow down," injecting the slug of nitrogen tetroxide into the chamber in the process.

A total of 36 tests was conducted with varying amounts of oxidizer. Reliable ignition was obtained without adverse effect on the catalyst bed when a 150-cc cartridge was preloaded with 15 to 50 cc of oxidizer and prepressurized to 600 psig. Essentially full chamber pressure was developed within 200 millisec of valve actuation. The optimum cartridge for the 45,000-lb-thrust gas-generation system appears to be one of 50-cc capacity preloaded with 15-cc of oxidizer.

3. ROLL-CONTROL SYSTEM

In order to fully exploit the advantages of the gas-generation system it is desirable to utilize generated gases for the vehicle roll-control system. Based upon the specified required moment of 105-ft-lb, a single roll-control nozzle of 35-lb thrust was determined to be sufficient. The following design parameters were utilized: $T_{gas} = 1360°F$, $\overline{M} = 12.0$, $P_c = 485$ psia, expansion ratio = 35:1. A weight flow of 0.162 lb/sec conservatively satisfies the stated requirements.

In order to utilize the 35-lb thrust level it is necessary that the nozzle rotate plus or minus 90 deg from the aft, or normal, position. Representatives of commercial organizations were contacted to determine the availability of a hot gas swivel nozzle with such a capability. The best available unit had a gimbal capability of only plus or minus 8 deg.

A brief development program was undertaken to determine the feasibility of a unit utilizing a carbon face seal, which had shown promise during a previous program. Results of preliminary tests indicated that the carbon face seal design possessed enough merit to warrant further investigation. In lieu of development of a reliable seal utilizing the 1350°F gases, it would be possible through a heat exchanger to cool the gases to almost any arbitrary temperature prior to routing these gases to the roll-control nozzle. Although this system would be less efficient, and hence require more propellant, more conventional seal materials could be used.

4. HEAT EXCHANGER (HYDRAZINE DECOMPOSITION PRODUCTS TO HELIUM)

In order to optimize the helium system used for oxidizer pumping it is desirable to add heat to the helium in order

to obtain the lowest possible $\overline{M}/T$. The helium temperature is the limiting factor inasmuch as its maximum value is determined by propellant tank temperature-strength characteristics. A temperature of 200°F was determined to be the maximum feasible helium temperature for the system.

A simple concentric tube arrangement was designed to furnish the necessary heat transfer surface to meet the design objective. This preliminary study indicated that a stainless steel tube of 0.75-in. diameter inside a similar tube of 1.125-in. diameter would be satisfactory. The length of the unit was determined to be 18 in. A heat exchanger of these dimensions would assure that the initial helium temperature did not exceed 200°F and would provide sufficient surface area to furnish helium gas at 70°F at the end of main engine operation. This design was not finalized at the time of program termination.

5. HEAT EXCHANGER (HYDRAZINE DECOMPOSITION PRODUCTS TO NITROGEN TETROXIDE)

To avoid the possibility of a reaction occurring between the gaseous hydrazine decomposition products and the liquid hydrazine, it was decided that 150°F would be the maximum allowable gas temperature. Several commercial organizations were contacted in reference to designing and constructing an optimum heat exchanger to accomplish this cooling by using the main system oxidizer as a cooling medium. In addition, a design study was undertaken to provide a backup unit for this purpose. The design requirements for such a unit are as follows:

Hot Gas		Liquid	
In temperature	1460°F	In temperature	75°
Out temperature	150°F	Flow	80 lb/sec
Flow	0.861 lb/sec	Pressure drop	25 psi max
Pressure drop	100-125 psi		

The most promising design was that submitted by United Aircraft Products, Inc., Dayton, Ohio. Their design consists of a compact tube bundle with dimensions of 5.5 in. in diameter and 13.0 in. in length. The dry weight of this unit is given as 14.0 lb. No unit cost quotation nor final negotiations had been undertaken with United Air Products, Inc. at the termination of the *Juno IV* program.

6. GAS-GENERANT TANK

The total weight of hydrazine required for the decomposition chamber in order to pump the main fuel tank dry and to furnish roll control throughout the stage burning period was calculated to be 153.1 lb. This weight included a 5% reserve for the roll-control system in order to allow for variations in duration.

The tank volume required to hold this amount of generant fuel, with a 3% ullage allowance, was calculated to be 2.5 cubic ft. A spherical tank of this capacity of aluminum would be 20.2-in. in diameter, with a calculated weight of 18.45 lb.

7. GAS-GENERANT HELIUM RESERVOIR

A generant helium tank was designed upon the following parameters: initial pressure, 3000 psia, regulated pressure, 600 psia, final pressure, 650 psia, mean specific heat ratio, 1.45, volume to be pressurized, 2.5 ft^3. Application of these parameters resulted in a tank volume of 0.925 ft^3. A standard 1 ft^3 tank could undoubtedly be used with only a small weight penalty. A spherical tank of such volume would be 14.9 in. in diameter and would weigh 17.0 lb.

8. CONTROL SYSTEM

A study was conducted of various control systems whose function would be to maintain the fuel and oxidizer tank pressures at the design point. Control systems studied include the following:

1. A two-stage gas generator injection system. The gas generator would have a high flow and a low flow injection system. The generator would normally operate on the low flow system until a signal was received from a differential pressure switch connected to each of the main system tanks. It would then operate on the high flow function until the tank pressures equalized.

2. A fuel dome loaded helium regulator which would maintain the oxidizer helium system at the same pressure as the gas generator fed fuel system.

3. A so-called "flow divider" which would sense gas generator output just prior to the fuel tank entrance and would adjust the helium pressure accordingly.

4. A system much like (1) except on the oxidizer which would control high and low flow of helium to the oxidizer tank by sensing the oxidizer or fuel-tank pressure through an accurate pressure switch.

It was expected that the control system to be employed would depend greatly upon the system that proved best in the earlier developed 6,000-lb-thrust propulsion system.

C. Test Program

Injector development tests on the 45,000-lb-thrust scale with $N_2O_4 - N_2H_4$ began in June, 1958, using heavy-walled uncooled engines. The design point was taken to be:

$$p_c = 200 \text{ psia}$$
$$r = 0.9$$
$$c^* = 5550 \text{ ft/sec}$$

This performance corresponds to a vacuum I_{sp} of about 304 lb-sec/lb for the shockless nozzle of 25:1 expansion ratio which was being considered for the flight engine.

Thirty-nine firing tests were made with the uncooled engines, using chambers of two chamber-to-throat contraction ratios, 1.6 and 2, with the same injector and the same nozzle. The injector was a splash-plate type and had 80 pairs of orifices, each oxidizer stream impinging on one fuel stream. The surface of this splash plate was located at the impingement points. The injector design was based on that of a 20,000-lb-thrust (sea-level) engine which gave a peak c^* of about 5500 ft/sec at its design point of $p_c = 300$ psia and $r = 1.0$. The 45K uncooled engine had a throat area of 128 sq in. and a nozzle expansion ratio of 2.95, which gave optimum expansion of the combustion gases when operated at its design chamber pressure of 200 psia at the Edwards Test Station (atmospheric pressure of 13.5 psia). Under such conditions, the thrust was about 33,500 lb. The throat area was selected on the basis of giving a vacuum thrust of 45,000 lb for a p_c of 200 psia and using a nozzle with an expansion ratio of 15. The expansion ratio was subsequently changed to 25 to obtain higher specific impulse.

The purpose of varying the contraction ratio was to determine the effect of this variable on performance, holding L^* constant at 40 in. Twenty-five tests were made at a contraction ratio of 1.6, and 14 tests at a contraction ratio of 2. For each contraction ratio, tests were first made using short orifices (having length-to-diameter ratios of about 2.5) in the injector (see Fig. 4). Additional tests were then made wherein the short orifices were replaced by longer orifices (having length-to-diameter ratios of about 10) in the injector (Fig. 5). The greater length gave better liquid impingement by producing streams with less breakup and better direction. The engine in its static test installation is shown in Fig 6.

In these tests, the orifices had the following inside diameters: oxidizer, 0.1565 in., fuel, 0.1862 in. These diameters were selected on the basis of giving pressure drops of 70 psi on the oxidizer side and 50 psi on the fuel side, for nominal flow rates of 75 lb/sec for both oxidizer and fuel. The pressure drop of 50 psi for the fuel side of the injector was determined by selecting the ratio of the injector-pressure drop to the chamber pres-

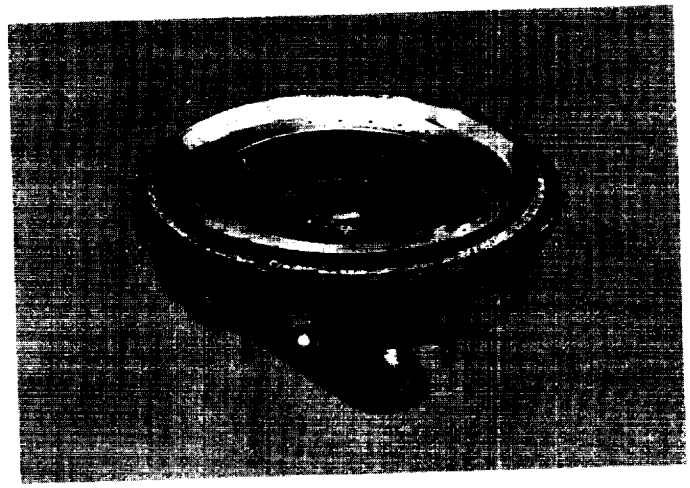

Fig. 4. Splash Plate Injector With Short Orifices for Development of 45,000-lb Vacuum-Thrust Engine

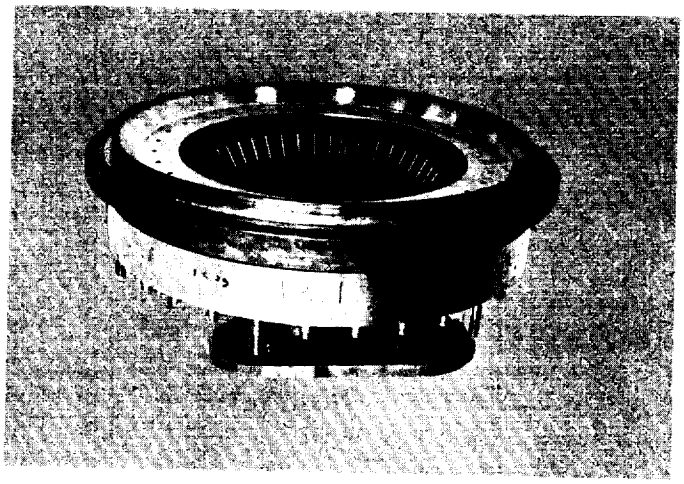

Fig. 5. Splash Plate Injector With Long Orifices for Development of 45,000-lb Vacuum-Thrust Engine

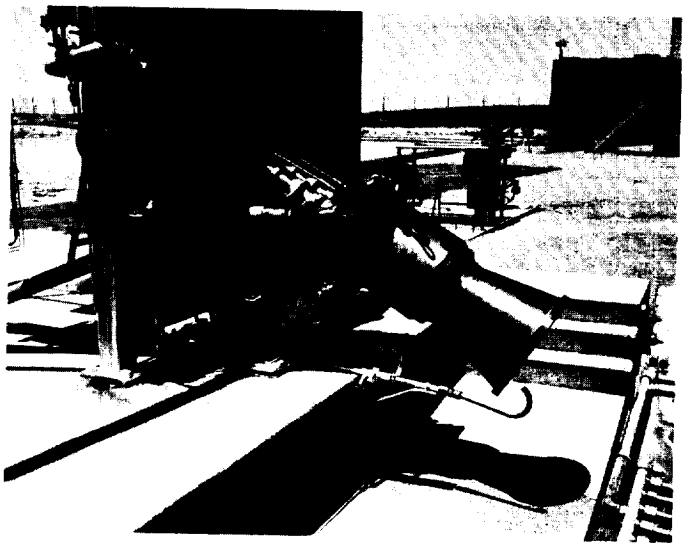

Fig. 6. Static Test Installation of Uncooled Engine for Development of 45,000-lb Vacuum-Thrust Engine

sure to be 0.25. It was considered desirable to have the propellant-tank pressures equal to each other. The fuel-pressure drop in the engine cooling jacket was estimated to be about 30 psi. The oxidizer-pressure drop in the heat exchanger (which, in the case of the heated-hybrid pressurizing system being considered, was to cool the gas generation products to about 150°F) was estimated to be 10 psi. Therefore, the injector-pressure drop on the oxidizer side was taken to be 70 psi, 20 psi higher than that on the fuel side.

The ratio of orifice diameters determined on the preceding basis was 0.840. Hydraulic studies (Ref. 1) conducted at this Laboratory with nonreacting fluids have shown that for a pair of impinging streams (in the absence of any splash plate) having suitable hydraulic characteristics, including similar and symmetrical velocity profiles, uniform-mixture-ratio distribution of the two fluids in the resulting spray is obtained, provided the following equation is satisfied:

$$\frac{\delta_1 V^2{}_1 D_1}{\delta_2 V^2{}_2 D_2} = 1$$

where δ, V, and D are the fluid density, stream velocity, and orifice diameter, respectively. This equation reduces to the form

$$r_u = \sqrt{\frac{\delta_O \ D_O{}^3}{\delta_F \ D_F}}$$

where r_u is the mixture ratio (oxidizer-weight flow rate to fuel-weight flow rate) at which uniform mixture ratio of fluids would be obtained in the resulting spray, and the subscripts refer to oxidizer and fuel.

For the case of $D_O/D_F = 0.840$, and taking the densities of the propellants at 60°F ($\delta_{N_2O_4} = 1.46$, $\delta_{N_2H_4} = 1.01$), a value of 0.925 for r_u is calculated. The performance data for the injector having orifice diameter ratios of 0.840 are presented in Fig. 7 (for tests at a chamber contraction ratio of 1.6) and Fig. 8 (for tests at a chamber contraction ratio of 2).

For both contraction ratios, the performances for short orifices were similar over the range of mixture ratio covered, peaking at fuel-rich mixture ratios ($r = 0.7$). The data obtained at a contraction ratio of 1.6 are about 1% higher than those for $f_c/f_t = 2$, the peak values being as follows: $c^* = 5430$ ft/sec, $I_{sp} = 220$ lb-sec/lb.

In the tests with long orifices, the performances peaked at mixture ratios ($r = 1$ to 1.3) in the vicinity of the peak theoretical performance point. The data obtained at a contraction ratio of 1.6 are about 3% higher than those for $f_c/f_t = 2$, the peak values being as follows: $c^* = 5440$ ft/sec, $I_{sp} = 215$ lb-sec/lb.

The peak experimental value of c^*, 5440 ft/sec, corresponds to 93.5% of the peak theoretical c^* (5820 ft/sec) calculated for equilibrium flow at a p_c of 200 psia for $N_2O_4 - N_2H_4$, or to 95% of the peak theoretical c^* (5730 ft/sec) calculated for frozen flow. The experimental value, which is only 2% lower than the design goal, was not corrected for the heat loss to the engine walls, this loss corresponding to about 1% in performance. In a previous program wherein small-scale engines (about 20-lb

UNCOOLED ENGINE EMPLOYING SPLASH-PLATE INJECTOR:
ϵ = 2.95 AND L^* = 40 in.
ORIFICE DIAMETER: OXIDIZER = 0.1565 in. AND
FUEL = 0.1862 in.
F = 33,600 lb AT p_c = 200 psia AND p_o = 13.5 psia
p_c = 200 psia NOMINAL, EXCEPT AS NOTED
$r = w_o / w_f$

EACH SET OF POINTS AT A GIVEN MIXTURE RATIO
REPRESENTS DATA FROM A SINGLE TEST
DATA UNCORRECTED FOR HEAT LOSS TO ENGINE WALLS
● SHORT INJECTOR ORIFICE
\+ LONG INJECTOR ORIFICE
--- THEORETICAL PERFORMANCE AT p_c = 200 psia,
p_o = 13.5 psia, ϵ = 2.95

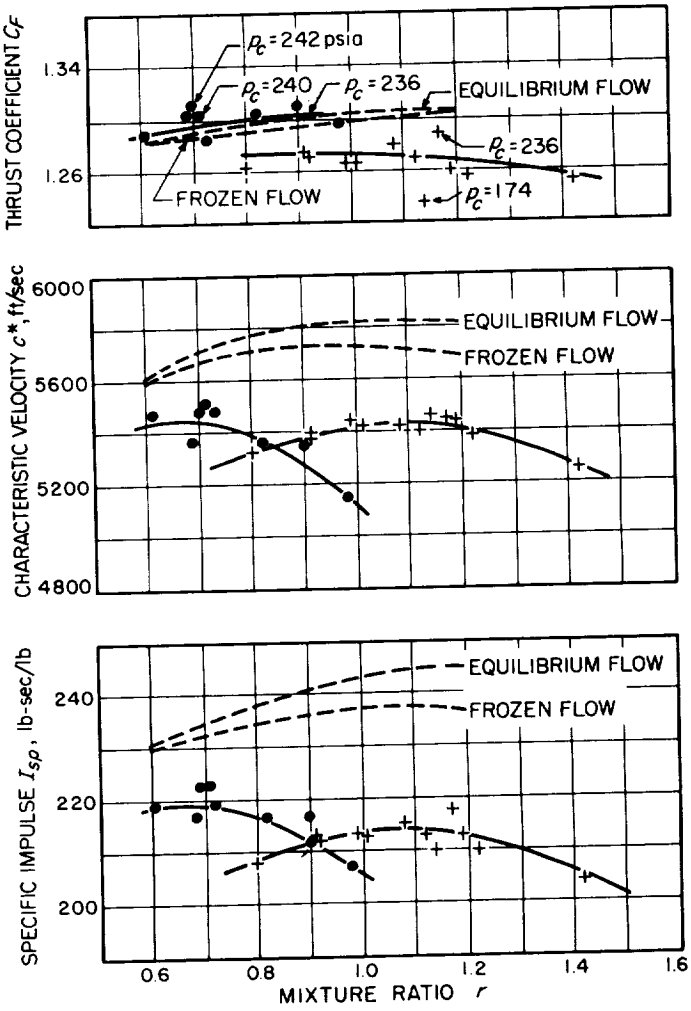

Fig. 7. Performance Data (Short Orifices in Injector)

UNCOOLED ENGINE EMPLOYING SPLASH-PLATE INJECTOR:
ϵ = 2.95 AND L^* = 40 in.
ORIFICE DIAMETER: OXIDIZER = 0.1565 in. AND
FUEL = 0.1862 in.
F = 33,600 lb AT p_c = 200 psia AND p_o = 13.5 psia
p_c = 200 psia NOMINAL, EXCEPT AS NOTED
$r = w_o / w_f$

EACH SET OF POINTS AT A GIVEN MIXTURE RATIO
REPRESENTS DATA FROM A SINGLE TEST
DATA UNCORRECTED FOR HEAT LOSS TO ENGINE WALLS
● SHORT INJECTOR ORIFICE
\+ LONG INJECTOR ORIFICE
--- THEORETICAL PERFORMANCE AT p_c = 200 psia,
p_o = 13.5 psia, ϵ = 2.95

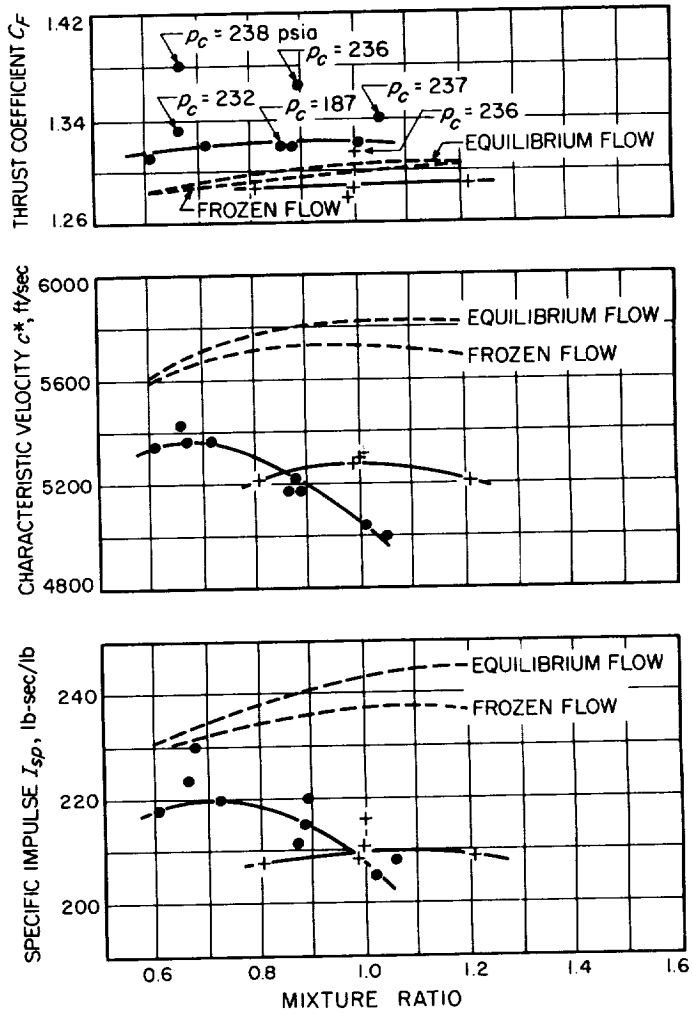

Fig. 8. Performance Data (Long Orifices in Injector)

thrust) using the system FNA-N_2H_4 were operated water-cooled and fuel-cooled, gains in performance of as high as 300 ft/sec in c^* were obtained when engines were operated fuel-cooled compared with the performance of water-cooled engines. The improvement is believed to have resulted from improved combustion resulting from heating the fuel. For these reasons, it is believed that the 45K injector might give close to the desired performance when operated in a fuel-cooled engine.

The reason for the difference in the mixture ratios corresponding to the peak-performance points for short and long orifices is not definitely known. Such a difference might possibly result from changed mass distribution of propellant caused by the difference in control of the impingement process due to variations in stability of streams produced by short and long orifices.

There are three reasons why the mixture ratio uniformity criterion would not be expected to apply to the 45K tests. The first is that the conditions under which the criterion was established were not fully satisfied. For example, the streams produced by the injector orifices did not have the necessary hydraulic properties as far as stability and stream profile were concerned. Secondly, tests with $N_2O_4 - N_2H_4$ using transparent-walled engines have shown that impinging streams react so rapidly that the streams tend to become blown apart. In such a case, the uniformity criterion would not be expected to apply. Thirdly, the criterion was established for streams which impinged in the absence of a splash plate, and the effect of a splash plate on propellant distribution is not known.

For purposes of determining the effect of varying the ratio of orifice diameters, five tests were made at a contraction ratio of 1.6 in which the long 0.1565-in. diameter oxidizer orifices were replaced by long orifices of 0.1862-in. diameter. For this case of $D_O = D_F = 0.1862$ in., r_u has a value of 1.20, and a shift in the peak mixture ratio to a higher value would be expected if uniformity of mixture ratio contributes to increased performance. Such a shift was actually obtained, the performance peaking at $r = 1.35$. However, the peak performance was decreased about 3% by enlarging the oxidizer orifice diameter, the peak c^* being about 5300 ft/sec. It is possible that this decrease was associated with the decrease in the energy of mixing of the streams due to the lower injection velocity of the oxidizer, resulting in an increased tendency of the propellant streams to blow apart.

A few tests (Figs. 7 and 8) were made to determine dependence of performance on p_c for fairly small changes in p_c, for both short and long orifices (oxidizer orifice diameter 0.1565 in., fuel orifice diameter 0.1862 in.). Little or no improvement in c^* was generally obtained by raising p_c, except possibly for the tests at a contraction ratio of 1.6 with short orifices in the injector (Fig. 7). For this case, three tests at p_c values ranging from 236 to 242 psia gave c^* values averaging 80 ft/sec above those for $p_c = 200$ psia. However, scatter of ± 60 ft/sec is present in the data at $p_c = 200$ psia.

Measurements of chamber heat flux were made in all tests except that for the engine having a chamber contraction ratio of 2 and employing short orifices. For a chamber-to-throat contraction ratio of 2, a chamber heat flux of 2.7 Btu/in.^{2}-sec was predicted. Experimentally, for the injector with long orifices, the chamber heat flux at the peak performance point was 3.8 Btu/in.^{2}-sec, or 40% higher than predicted. For a chamber-to-throat contraction ratio of 1.6, chamber heat flux of 3.1 Btu/in.^{2}-sec was predicted, whereas measured values were higher by 29% for short orifices and 45% for long orifices. In case the heat flux throughout the engine was higher than predicted by the same percentages, the desired margin on cooling would not exist. For purposes of determining whether the heat flux in the nozzle exceeded the predicted values, some tests were made in which nozzle heat fluxes were measured. Predicted and measured values agreed closely, indicating that adequate cooling could be easily achieved.

All measurements of heat flux were made by the use of a plug of metal fabricated from the same material as the wall of the engine and pressed into the wall. A thermocouple was located in the plug close to the end surface exposed to the combustion gases. Another thermocouple was attached to the outside surface of the engine close to the plug. The voltages of the thermocouples were recorded by means of an oscillograph, and inside wall temperature, heat transfer, and heat-transfer coefficients were computed as functions of time and wall temperature. The values of heat flux at an inside wall temperature of 800°F are presented herein, since the hot wall temperature of the fuel-cooled engine would be in the neighborhood of 800°F.

IV. PROPULSION SYSTEM OF THE 6000-LB-THRUST STAGE

A. Introduction

The Jet Propulsion Laboratory 6000-lb-thrust high-altitude propulsion system is comprised of a liquid bipropellant rocket motor, suitable propellant tanks, and a gas-supply system for propellant transfer. The propellants are nitrogen tetroxide and anhydrous hydrazine. The rocket motor employs a splash-plate type of injector, a lightweight, high-expansion-area-ratio thrust chamber of advanced design, and valves so designed that the total impulse delivered can be closely controlled by means of fast, reproducible cutoff. The design of the propulsion system provides for simplified ground handling owing to the use of storable liquid propellants, for the easy starting attendant on the use of hypergols, and for the growth potential of tank pressurization by means of controlled decomposition of the monopropellant fuel, hydrazine.

In the development of this propulsion system, three different combinations of stage control and tank pressurization were given consideration. Preliminary consideration was given to a system using three small monopropellant hydrazine motors for control of the stage in pitch, yaw, and roll. This type of system was considered to be desirable for those applications in which attitude control of the stage was required after the main propulsion motor was shut off. The thrust chamber in this case was fixed; the propellant tanks were pressurized by helium gas. This system is identified in the following discussion as system A, vernier motor control and helium pressurization.

Most of the development effort was concentrated on the second system, in which stage control was exercised by gimbaling the thrust chamber. This system was considered to be simpler than the vernier motor system and thus more apt to meet the required time schedule. In this system, roll control was to be maintained by a separate gas roll-control nozzle. Pressurization of the propellant tanks was by helium gas, which was to be warmed by heat exchange with the liquid oxidizer. Thus it is referred to as the "heated helium" system and is identified in the following discussion as system B, gimbal motor control and heated helium pressurization.

A considerable improvement in payload is possible by the use of a gas-generation system (in place of the helium gas system) to pressurize the propellant tanks. In the third system considered, it was proposed to incorporate part of this improvement by pressurizing the fuel tank by means of a monopropellant hydrazine gas-generation system and to pressurize the oxidizer tank with helium gas which had been warmed by heat exchange with the gas generator. Thus it is referred to as the "heated hybrid" system and is identified in the following discussion as system C, gimbal motor control and gas-generation pressurization of fuel tank.

B. System Concept

1. PROPELLANTS

In choosing the propellant combinations for the stages of the *Juno IV* vehicle, three items in particular were considered: (1) reliability, (2) high performance, and (3) a reasonable time schedule. It was proposed that the *Jupiter* vehicle should be used as the first stage, and that, in order to maintain a reasonable time schedule, the standard propellant combination LOX-RP should be retained for the first vehicle.

One important facet of reliability for satellite and space vehicles is the ability to launch "on time." Thus, elimination of last-minute loading of propellants would be an important consideration from this standpoint of reliability; therefore, storable propellants are desirable for the high-speed stages of the vehicle, provided the requirements of high performance and a reasonable time schedule could be met by the storable propellants chosen.

The two storable propellant combinations having the highest performance are nitrogen tetroxide – hydrazine and chlorine trifluoride – hydrazine. The Laboratory has done a considerable amount of research with both these propellant combinations. It was believed that a reasonable time schedule could be maintained if the N_2O_4-N_2H_4 propellant combination was used for the high-speed stages of the *Juno IV* vehicles. Although the performance of the ClF_3-N_2H_4 propellant combination is higher than that of N_2O_4-N_2H_4 (due to the higher density of ClF_3; the specific impulses are equal), it was believed that the handling of ClF_3 was not well enough known for use in the first vehicles on a reasonable time schedule.

Thus, it was concluded that the first series of *Juno IV* vehicles should consist of a *Jupiter* first stage using LOX-RP, and high-speed stages using the storable, high-performance propellant combination nitrogen tetroxide-hydrazine. Considerable growth potential exists by substituting other propellant combinations in the stages as these propellants are brought to operational status.

2. SYSTEM A, VERNIER-MOTOR AND HELIUM PRESSURIZATION.

The first model of the 6000-lb-thrust stage propulsion system considered for *Juno IV* was a gas-pressurized (helium) unit using a nitrogen tetroxide-hydrazine (N_2O_4-N_2H_4) main propulsion motor and three monopropellant hydrazine vernier-control motors. Control of the stage was to be accomplished (and final terminal velocity reached) by means of the three vernier-control motors, each rotating in a single plane. In operation, the three vernier-control motors are started before the main motor in order to separate this stage from the previous stage. The vernier motors are started before the motor of the previous stage is shut off in order to have positive acceleration on the stage at all times.

Since the vernier-control motors are started first and the main motor later, the main motor cannot be started by means of a simple burst diaphragm; the usual dual propellant valve is required. The vernier-control motors can be started by simple pressure-operated burst diaphragms.

Final terminal velocity is obtained by continued operation of the vernier-control motors after the main motor is shut off. The main motor is shut off when either (1) a predetermined velocity has been reached or (2) the oxidizer (N_2O_4) is depleted (except for that remaining in the propellant line). In either case, the vernier-control motors continue to operate on the remaining monopropellant (N_2H_4) until terminal velocity is reached.

The schematic diagram of propulsion system A is shown in Fig. 9. The helium gas tanks are pressurized through a quick-disconnect fitting (1)[1] when the vehicle is on the launcher. Helium is admitted to the system through an explosively operated valve (2). The propellant tanks are pressurized by means of a regulator (3); the dome of the regulator is pressurized through a pilot regulator (4). Helium is admitted to the propellant tanks through pressure-operated burst diaphragms and check valves (5).

The propellant tanks are filled while the vehicle is on the launcher. The oxidizer fills the tank and lines down to the pressure-operated burst diaphragm (6) just upstream from the propellant valve. A drain connection is provided just upstream from this burst diaphragm in case it is necessary to unload oxidizer from the vehicle. A relief valve is provided at the top of the tank to vent any excess pressure.

The fuel fills the tank, the thrust-chamber regenerative cooling passages, and the propellant lines down to the pressure-operated burst diaphragm (7). A bleed port is provided just upstream from the burst diaphragm in order to fill the circuit completely with liquid. A drain connection is provided at the nozzle end of the thrust-chamber cooling passage in case it is necessary to unload fuel from the vehicle. A relief valve is provided at the top of the tank to vent any excess pressure.

Just downstream from the burst diaphragm in the fuel line, a propellant line leads to the three vernier-control chambers which operate on monopropellant hydrazine and contain a catalyst which causes decomposition of the hydrazine. The vernier-control motors start operating when the burst diaphragm in the fuel line ruptures and are stopped by the explosively operated cutoff valve (8).

The main thrust motor is started and stopped by opening and closing the dual propellant valve (9). This propellant valve is opened and closed by a pneumatic cylinder (10). Pressure for opening the cylinder is obtained through an explosively opened valve (11) from a gas bottle (12) and is closed through a similar valve (13) and gas bottle (14).

The operation of the system during flight is as follows: When chamber pressure in the previous-stage motor drops during the cutoff period, a signal transmitted to the 6000-lb-thrust stage operates the explosively opened valve (2) in the high-pressure helium line. In turn, (a) the burst diaphragms in the propellant tank heads are ruptured, (b) the tanks pressurize, (c) burst diaphragms in the oxidizer and fuel propellant lines rupture, and (d) the vernier-control motors start operating. The vernier-control motors operate by themselves for a few seconds during which time the stage separates from the previous stage (actual separation from the launcher requires ap-

[1] Numbers in parentheses refer to component numbers on Fig. 9.

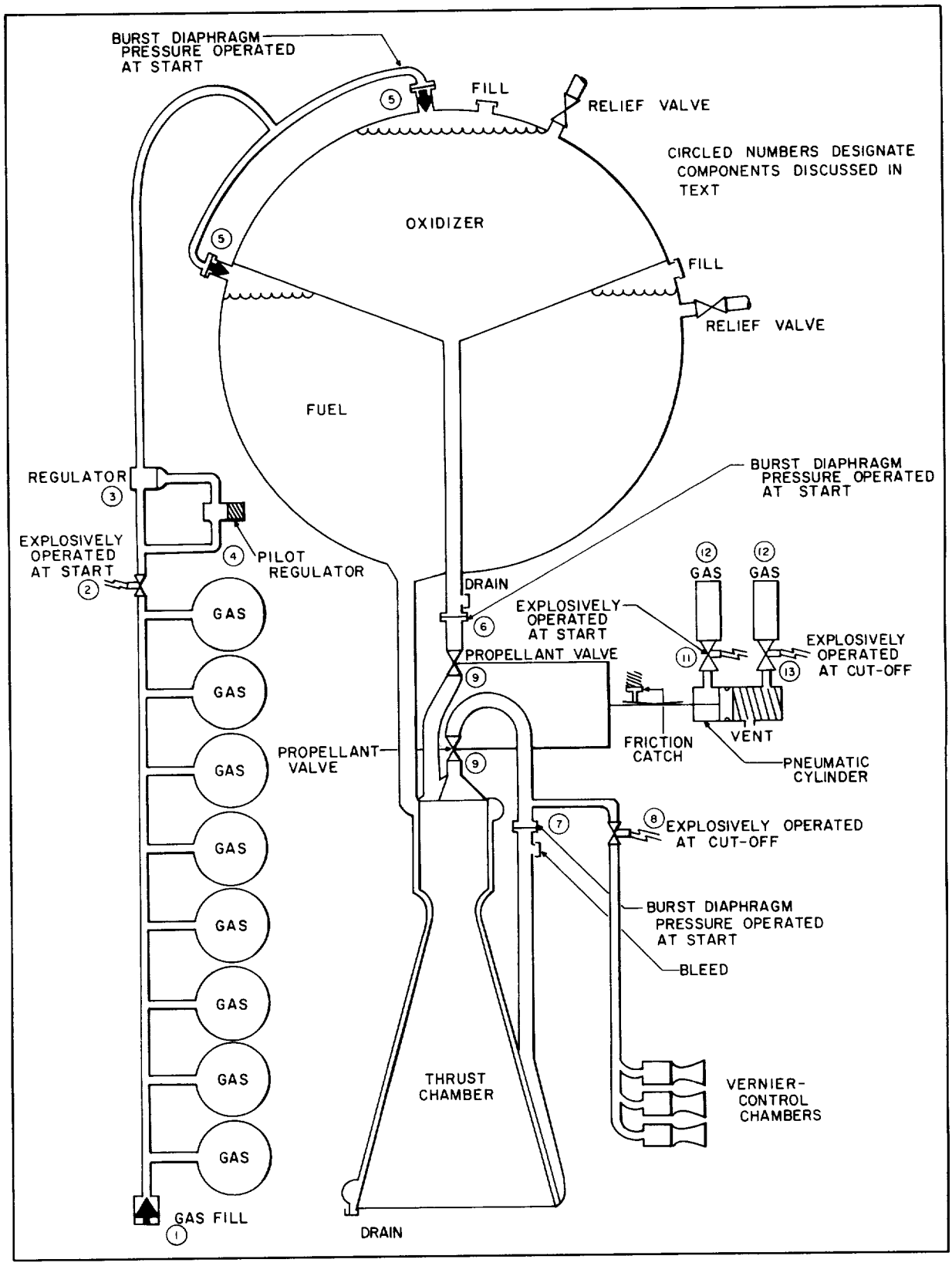

Fig. 9. Schematic Diagram of System A, Vernier Motor Control and Helium Pressurization

proximately 2 sec). The vernier-control motors should be locked in the direction of the vehicle axis during this period.

To start the main motor, a signal is transmitted to the explosively operated valve (11) which admits gas to the pneumatic cylinder and opens the main propellant valve. As the propellants (N_2O_4 and N_2N_4) are spontaneous, no ignition system is required.

The main propulsion motor continues to operate until one of two conditions is reached:

1. A predetermined velocity is reached; a signal then operates the explosively operated valve (13) which admits gas to the pneumatic cylinder and closes the main propellant valve, or
2. The oxidizer is depleted except for that remaining in the propellant line; a liquid-level detector then transmits a signal to the explosively operated valve (13) which admits gas to the pneumatic cylinder and closes the main propellant valve.

After the main propulsion motor stops operating from either of the above signals, the vernier-control motors continue to operate until the desired terminal velocity is reached; they provide both velocity increment and missile control during this period. When the desired terminal velocity is reached, a signal closes the explosively operated valve (8) in the vernier-control motor propellant line and shuts off the vernier-control motors.

The numerical values pertinent to this discussion are shown in Table 2.

Table 2. Numerical Values of System A, Control Motor Type

A. General

Gross weight, lb	4739
Velocity increment required, ft/sec	16,464
Oxidizer, nitrogen tetroxide (N_2O_4) specific gravity at 72°F	1.44
Fuel, hydrazine (N_2H_4) specific gravity at 72°F	1.005
Specific impulse, main motor, sec	300 (at altitude)
Specific impulse, control motors, sec	231 (at altitude)
Mixture ratio, over-all, W_{ox}/W_{fuel}	0.87

B. Pressurizing gas (Helium)

Initial pressure, psia	3000
Final pressure, psia	300
Regulated pressure, psia	250
Volume, ft³	8.0

C. Propellant weight, lb

	W_f	W_{ox}
Control motor start 2 sec before separation	3	—
Main stage and control operation for 99% of ΔV	2112	1798
Velocity vernier correction	18	—
Propellant reserve for 1% additional ΔV	8	7
Propellant reserve for 1% variation in I_{sp}	8	7
Unavailable propellant	4	10
Total	2153	1822
Total propellant weight, lb	3975	

D. Propellant tanks

Tank pressure, psia	250
Oxidizer tank volume (including 4% ullage), ft³	21.1
Fuel tank volume (including 4% ullage), ft³	35.4

It should be noted here that 30 lb of the fuel is carried in the main engine cooling passages. The use of control motors permits the drainage of the main motor. The actual propellant weights in the tank are, therefore,

Fuel, lb	2123
Oxidizer, lb	1822
Total, lb	3945

E. Main thrust chamber

Thrust (at altitude), lb	6000
Duration (nominal), sec	197
Nozzle throat area, in.²	23.08
Nozzle throat diameter, in.	5.42
Cylindrical chamber length, in.	14
Cylindrical chamber ID, in.	8.60
Contraction area ratio	2.5
Expansion area ratio	20.8
Oxidizer flow rate, lb/sec	10.0
Fuel flow rate, lb/sec	10.0
Mixture ratio, main engine W_o/W_p	1.0
Fuel flow rate through regenerative cooling circuit (includes flow to vernier-control motors), lb/sec	11.56
Chamber pressure, psia	150

Pressure drops (design or estimated), psia	Oxidizer	Fuel
a. Injector	55	50
b. Main propellant valve	3	3
c. Lines	8	14
d. Cooling jacket	—	15±6

F. Control motors (3 required)

Thrust, each, at altitude, lb	120
Nozzle throat area, in.²	0.453
Nozzle throat diameter, in.	0.758
Chamber ID, in.	3.5
Expansion area ratio	50
Cylindrical chamber length	3.5
Fuel flow rate (monopropellant), lb/sec	0.52
Chamber pressure, nozzle end, psia	150
Pressure drops (design or estimated), psia	
Injector	50
Valve	2
Lines	16
Estimated weight, per motor, lb	3.5

3. SYSTEM B, GIMBAL MOTOR CONTROL AND HELIUM PRESSURIZATION

For satellite missions, two configurations were considered. In the first of these, the *Jupiter* vehicle was used as a first stage, the 45,000-lb-thrust system was used as the second stage, and the 6,000-lb-thrust system was used as the third stage. The second configuration used the *Jupiter* as the first stage and the 6,000-lb-thrust system with greatly increased propellant quantity (9,000 lb) as the second stage. Although the first configuration was near optimum as far as payload capability was concerned, it was believed that the second configuration should be used for the first *Juno IV* vehicles in order to have an early launching capability.

a. Schematic diagram. The schematic diagram of the 6,000-lb-thrust propulsion system, system B, is shown in Fig. 10; it differs from the schematic diagram of system A (Fig. 9) primarily in the following respects:

1. Separate spherical tanks are used for each propellant instead of the integral tank with a separating diaphragm. Although this change adds some weight to the system (estimated as 40 lb), it simplifies the fabrication of the tanks and in addition simplifies operation of the system since there is no longer need for the close control of the differential pressure between the two tank compartments that was required with the integral tank construction.

2. Pitch and yaw are controlled by gimbaling the main motor rather than having the three separate vernier-control motors. This change was made primarily because attitude control was not required for the satellite mission after the main motor was shut off. Also, it was believed that a gimbaled main motor with separate roll control was simpler than the three separate vernier-control motors for pitch, yaw, and roll control and would thus more likely be able to meet the time schedule. Subsequent experimental results with the vernier-control motors indicated that there would probably have been no particular problems with the vernier-control motors.

3. Keeping in mind that the ability to restart the main motor would probably be required for some vehicle early in the launching schedule, some of the minor components in the schematic layout were changed so that this capability could be incorporated easily; for example, a solenoid valve was used in the helium pressurizing line in place of the explosive-type valve shown for system A.

b. System operation. A summary of the components pertinent to both the system B and system C is given in Table 3. The numbers correspond to those shown on the schematic diagrams, Figs. 10 and 11.

Table 3. Component Summary for System B and System C

Number*	Component	Normal Position
1	oxidizer fill and drain disconnect	closed, opened during fill
2	oxidizer fill and drain disc. cap	seals with a crush gasket
3	oxidizer vent disconnect — remote	closed, opened during fill
4	fuel vent disconnect — remote	closed, opened during fill
5	fuel fill and drain disconnect	closed, opened during fill
6	fuel fill disconnect cap	seals with a crush gasket
7	engine fuel bleed valve and cap	closed, opened for bleed
8	pressure equalizer	seals with a crush gasket
9	oxidizer pressurization valve	closed
10	fuel pressurization valve	closed
11	actuators for (9) and (10)	in closed position
12	regulator dome restrictor	
13	helium regulator	closed zero leak
14	dome loader bleed restrictor	
15	helium fill disconnect — remote	closed, open during fill
16	relief valve	closed, built-in restrictor
17	dome loader control valve	closed solenoid valve
18	dome loader regulator	
19	nitrogen fill valve and cap	closed
20	actuator opening valve	closed
21	actuator opening shutoff valve	open
22	actuator for propellant valves	closed, lock pin in place
23	oxidizer valve	closed
24	fuel valve	closed
25	actuator closing valve	
26	oxidizer trim orifice	mixture ratio calibration
27	main valve lock pin	
28	cap, gas generator	
29	gas flow divider	
30	oxidizer tank burst diaphragm	
31	fuel tank burst diaphragm	
32	gas-generator start valve	
33	gas-generator shutoff valve	
34	gas-generator helium regulator	
35	gas-generator pressurization valve	
36	gas-generator tank fill valve and cap	
37	gas-generator tank vent valve and cap	
38	gas-generator helium fill and vent disconnect	
39	pressurized gas-generator ignition cartridge, valve assembly	

*Numbers correspond to component numbers on schematic diagrams, Figs. 10 and 11.

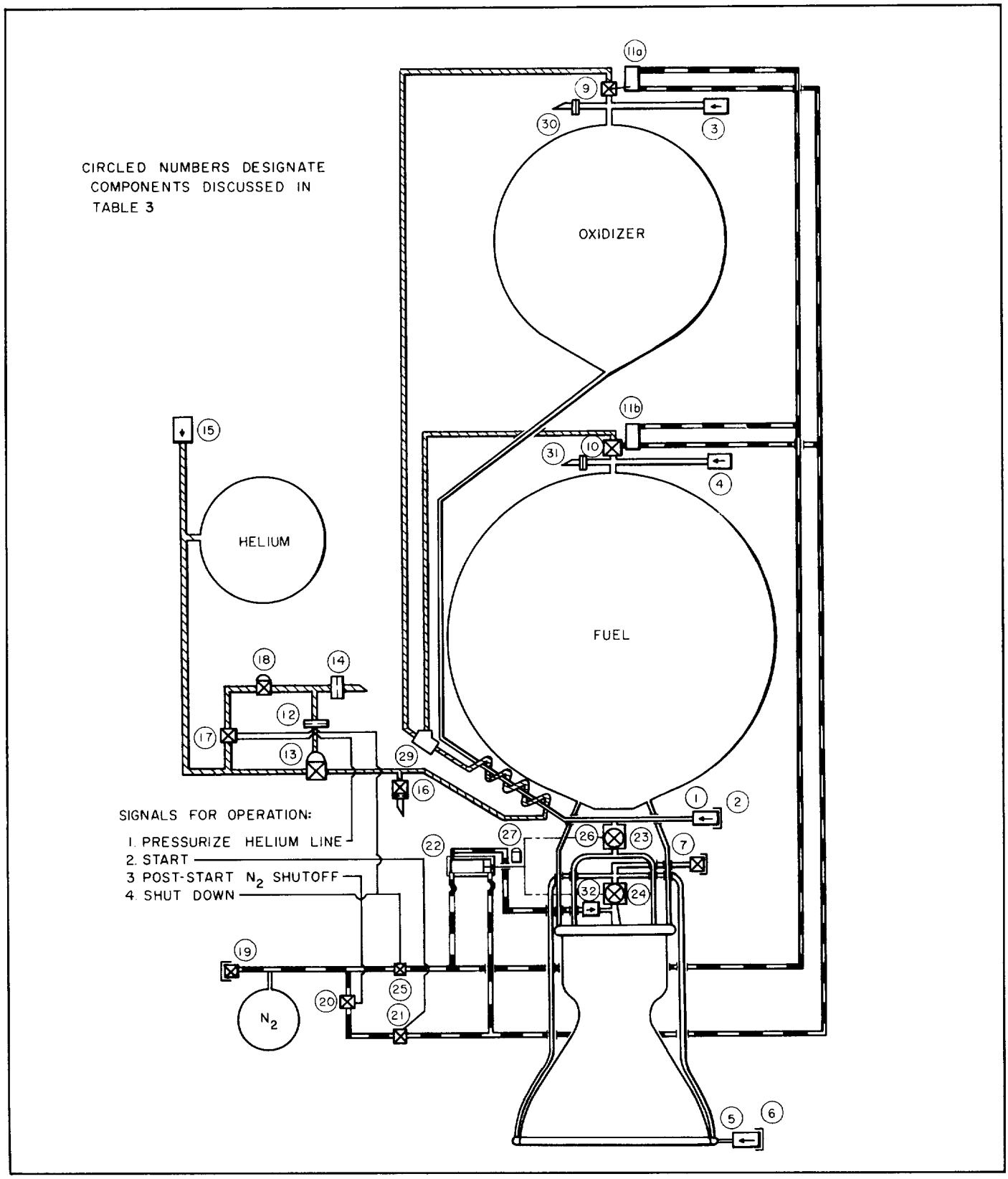

Fig. 10. Schematic Flow Diagram of Gimbal Motor Control and Heated Helium Pressurization

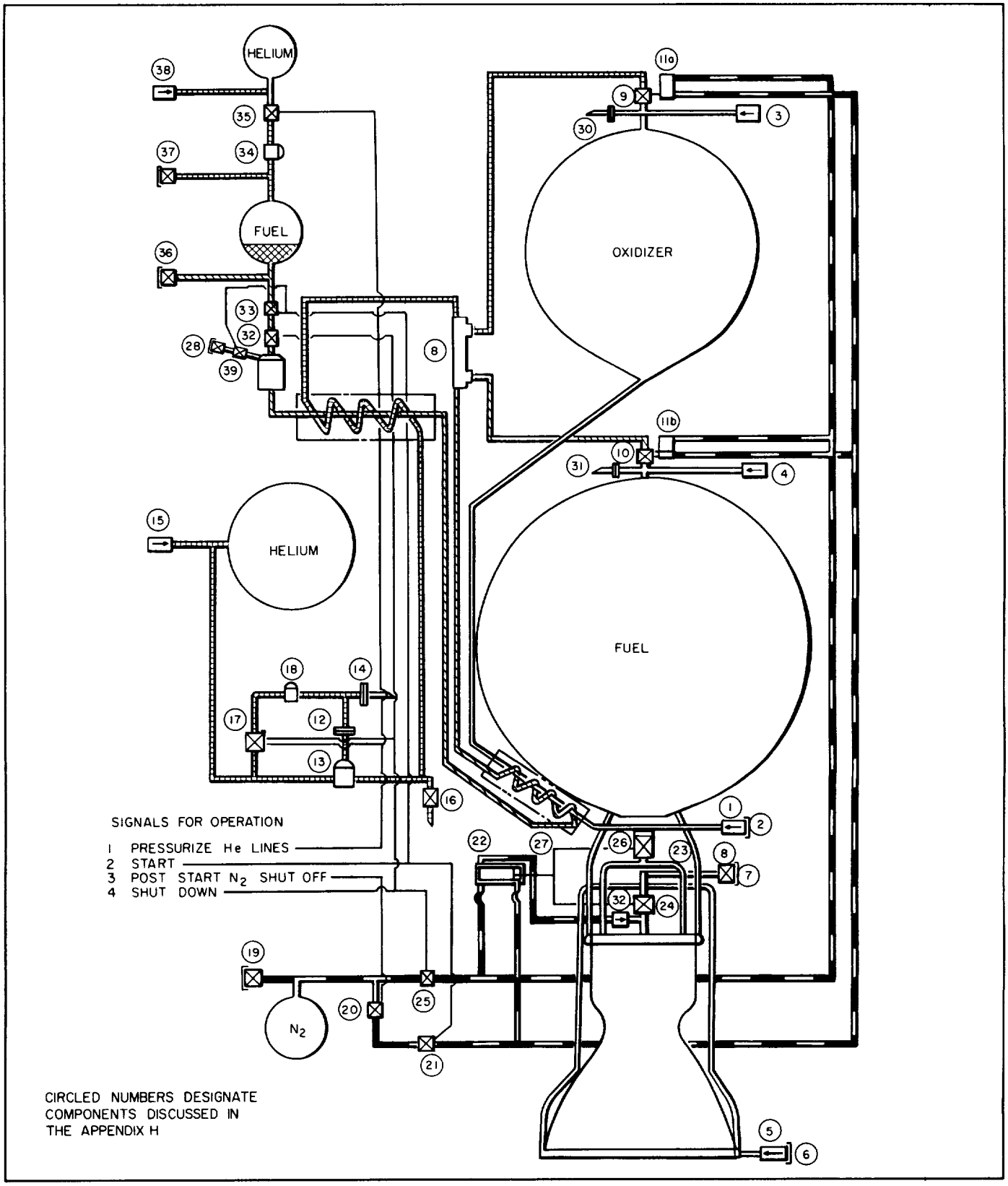

Fig. 11. Schematic Flow Diagram of Gimbaled Motor Control and Gas-Generation Pressurization of Fuel Tank

4. SYSTEM C, GIMBAL MOTOR CONTROL AND GAS-GENERATION PRESSURIZATION OF FUEL TANK

An appreciable increase in vehicle payload can be obtained by using a gas-generation system (in place of the helium pressurizing system) to pressurize the fuel tank. The increase in payload is estimated to be 174 lb as compared to a cold helium pressurizing system and 140 lb as compared to a heated helium pressurizing system.

The system is based on the use of monopropellant hydrazine decomposition gases to pressurize the fuel tank; the decomposition gases would be cooled from the reaction temperature (1460°F) to 150°F by heat exchange with the oxidizer flow to the main engine. Helium would be used to pressurize the oxidizer tank, and this helium would be warmed to 150°F by heat exchange with the N_2H_4 decomposition gases.

It was planned to incorporate this gas generation system into the propulsion systems of later *Juno IV* vehicles after the reliability of the system had been fully demonstrated by water and propellant pumping tests.

a. Schematic diagram and system operation. The schematic diagram of the 6,000-lb-thrust propulsion system using gas-generation fuel pressurization (system C) is shown in Fig. 11.

An operational analysis for both normal operation and malfunctions is given in Appendix H.

5. SYSTEM PERFORMANCE

a. Propellant reserve. An analysis was made of the propellant reserve required in the 6,000-lb-thrust stage of the *Juno IV* vehicle. The results of that analysis showed that propellant reserve is required to provide for the following items:

1. Variation in combustion efficiency which results in a variation in I_{sp}.

   For a missile with given velocity increment and gross weight, the variation in the required propellant weight due to a variation in I_{sp} is given by:

$$\Delta W_P = W_P \left(\frac{W_g}{W_P} - 1\right) \ln\left(1 - \frac{W_P}{W_g}\right) \frac{\Delta I_{sp}}{I_{sp}} \quad (1)$$

   where W_P is the burned propellant weight and W_g is the gross weight. The value of $\Delta W_P/W_P$ per percentage change in I_{sp} is plotted in Fig. 12 as a function of W_P/W_g. It is expected that for the present splash plate injector, the maximum variation in I_{sp} will be approximately 1%.

2. Correction of velocity increment of previous stages.

   For a missile with given I_{sp} and gross weight, the variation in the required propellant weight owing to a variation in ΔV, the velocity increment, is given by:

$$\Delta W_P = - W_P \left(\frac{W_g}{W_P} - 1\right) \ln\left(1 - \frac{W_P}{W_g}\right) \frac{\Delta(\Delta V)}{(\Delta V)} \quad (2)$$

   The value of $\Delta W_P/W_P$ per percentage change in ΔV is therefore given by Fig. 12. The velocity at ignition of the 6,000-lb-thrust stage was expected to be within 1% of the velocity increment of this stage.

3. Variation in mixture ratio.

   For a missile with given gross weight, velocity increment, and I_{sp}, the propellant reserve required by small variations in the flow rates of the propellants is given by:

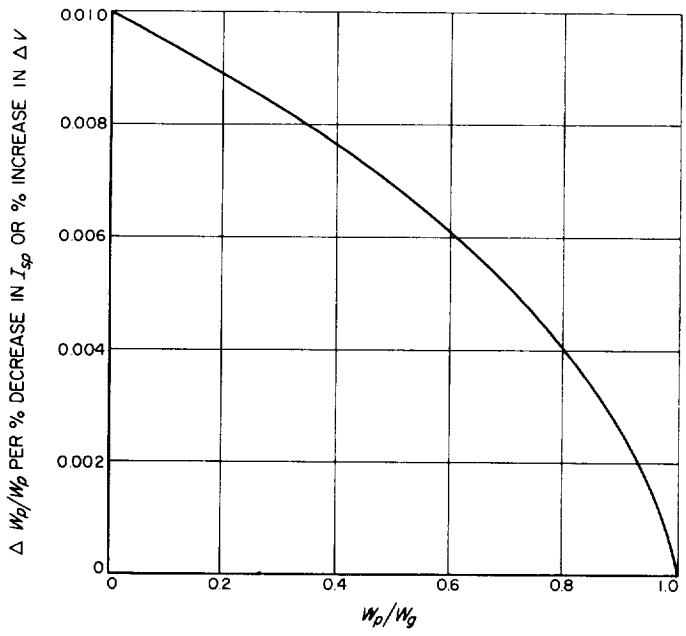

Fig. 12. Ratio of $\Delta W_p/W_p$ per Percentage Change in I_{sp} and Δ_V

$$\Delta W_P = \frac{2\left(\frac{\Delta \dot{W}_f}{\dot{W}_f} + \frac{\Delta \dot{W}_{ox}}{\dot{W}_{ox}}\right)}{r + 2 + \frac{1}{r}} W_P \qquad (3)$$

$\dot{W}_f$ is the fuel flow rate, $\dot{W}_{ox}$ is the oxidizer flow rate, where $\Delta \dot{W}_F$ is the variation in fuel flow rate, $\Delta \dot{W}_{ox}$ is the variation in oxidizer flow rate, and r is the mixture ratio (near unity).

The above propellant reserve is equally divided between fuel and oxidizer at all mixture ratios.

Since both tanks are pressurized from the same source, it is expected that the variations in the flow rates will not exceed 1% on the oxidizer side, and, due to the uncertain density of N_2H_4 in the cooling passages, 1.5% on the fuel side. In a very similar system, the *Corporal*, the flow uncertainties were kept to less than 1% each.

4. Holdup in tanks.

The holdup in the tanks is due to two causes, saturation of the pressurizing gas and propellant adhering to tank walls and lines. If it is assumed that the inert pressurizing gas is saturated with propellant vapors, then, at an ambient temperature of 80°F the weight of oxidizer in the vapor phase is given by:

$$\Delta \dot{W}_{ox} = 0.0030 \frac{r}{r+1} W_P \qquad (4)$$

Up to an ambient temperature of 150°F the weight of fuel in the vapor phase is less than 1 lb for a 5000-lb-capacity hydrazine tank; therefore, no allowance needs to be made.

Propellant held on tank walls and in lines is not quite proportional to propellant weight; however, for the simplicity of this analysis it will be considered as such. Under the assumption that a 1/16-inch-thick film of propellant is left on the tank walls and that the propellant lines are not drained, the total holdup is 12 lb for $W_P = 10{,}000$ lb. As a function of W_P the holdup is:

$$\Delta W_P = 0.0012 \; W_P \qquad (5)$$

The total propellant reserve at any mixture ratio, burned propellant weight, and gross weight can be computed by summing Eqs. (1) through (5).

Thus, the reserve on the oxidizer side is:

$$\Delta W_{ox} = \left[f\left(\frac{W_P}{W_g}\right)\left(\frac{\Delta I_{sp}}{I_{sp}} + \frac{\Delta(\Delta V)}{(\Delta V)}\right) + 0.0042 \right]\frac{r}{r+1} W_P + \frac{\frac{\Delta \dot{W}_f}{\dot{W}_f} + \frac{\Delta \dot{W}_{ox}}{\dot{W}_{ox}}}{r + 2 + \frac{1}{r}} W_P$$

where

$$f\left(\frac{W_P}{W_g}\right) = -\left(\frac{W_g}{W_P} - 1\right)\ln\left(1 - \frac{W_P}{W_g}\right)$$

and is plotted in Fig. 12.

The reserve on the fuel side is:

$$\Delta W_f = \left[f\left(\frac{W_P}{W_g}\right)\left(\frac{\Delta I_{sp}}{I_{sp}} + \frac{\Delta(\Delta V)}{(\Delta V)}\right) + 0.0012 \right]\frac{1}{r+1} W_P + \frac{\frac{\Delta \dot{W}_f}{\dot{W}_f} + \frac{\Delta \dot{W}_{ox}}{\dot{W}_{ox}}}{r + 2 + \frac{1}{r}} W_P$$

The total propellant reserve is:

$$\Delta W_P = \left[f\left(\frac{W_P}{W_g}\right)\left(\frac{\Delta I_{sp}}{I_{sp}} + \frac{\Delta(\Delta V)}{(\Delta V)}\right) + 0.0012 + \frac{2\left(\frac{\Delta \dot{W}_f}{\dot{W}_f} + \frac{\Delta \dot{W}_{ox}}{\dot{W}_{ox}}\right)}{r + 2 + \frac{1}{r}} + 0.0030 \frac{r}{r+1} \right] W_P$$

It should be pointed out that the reserve thus computed does not include the hydrazine in the motor cooling passages. For the tube-wall motor this amounts to approximately 30 lb and is included as part of the motor weight.

For the *Juno IVA* having $W_g = 11{,}475$ lb, $W_P = 9{,}000$ lb, and operating at unit mixture ratio, the propellant reserves shown in Table 4 are needed:

b. Weight breakdown. An analysis of the weight breakdown of the 6,000-lb-thrust propulsion system using three different pressurizing systems has been made and is

Table 4. Propellant Reserves

Item	ΔW_{ox}	ΔW_f	ΔW_P
Variation in I_{sp}, 1%	19	19	38
Additional ΔV, 1%	19	19	38
Mixture-ratio variation	56	56	112
Holdup in tanks	21	7	28
Total reserve	115	101	216

shown in Table 5. The three systems are cold helium, heated helium, and gas generation hybrid system.

c. Scaling formulae. During the course of the preliminary design of the 6,000-lb-thrust propulsion system, it was necessary to develop scaling formulae for the system and its major components. The final scaling formulae are given in terms of the nondimensional thrust F, the nondimensional chamber pressure P_c, and the nondimensional propellant weight W_P. The normalization is based on the present design, that is, all quantities are expressed as fractions of the parameters of the present design. Those parameters are: thrust, 6,000 lb; chamber pressure, 150 psia; and propellant weight, 9,000 lb.

The formulae are believed to be applicable in the range of about 2,000-to-8,000-lb thrust and for chamber pressures above 100 psia. Minimum material thicknesses are taken into account wherever applicable.

Owing to the limitations of cooling by the maximum allowable bulk temperature rise of the fuel, the mixture ratio has to be varied with chamber pressure and thrust. Since the performance of the N_2O_4-N_2H_4 system maximizes at a mixture ratio of about 1.1, the maximum operating mixture ratio commensurate with cooling requirements must be selected. The variation of the maximum permissible mixture ratio, r, with thrust and chamber pressure is given by:

$$r = 2\ P_c^{0.1}\ F^{0.1} - 1$$

This variation in mixture ratio is included in all scaling formulae.

Weight of gimbaled assembly, tube wall motor (W_{ga}):

$$W_{ga} = F^{1/2}\ (9\ P_c^{-1/2} + 4.5 + P_c^{1/2} + 7.2\ P_c) + F\ (34.8\ P_c^{-1} + 9.4\ P_c^{-1/2} + 9.4\ P_c^{1/2} + 5\ P_c) + F^{3/2}\ (1.7\ P_c^{-1} + 43.7\ P_c^{-1/2} + 1.9\ P_c^{1/2})$$

Weight of propulsion system components (W_{psc}). (These components refer to helium pressurization system and are not included when the hybrid system is used):

$$W_{psc} = 6.75 + 28.5F$$

Weight of cold helium supply, W_{Hc}:

$$W_{Hc} = W_p\,[30 + 183.6\ (P_c + 2/3)] + 3F\ (P_c + 2/3)$$

Weight of heated helium supply, W_{Hh}:

$$W_{Hh} = W_p\,[30 + 163\ (P_c + 2/3)] + 5.4F\ (P_c + 2/3)$$

Weight of gas-generation system:
Fuel side (W_{ggfs})

$$W_{ggfs} = 6.9\ F\ (P_c + 2/3) + 28.1\ W_p(P_c + 2/3)\ P_c^{-0.1}\ F^{-0.1}$$

Oxidizer side (W_{ggos})

$$W_{ggos} = 25.25\ F + 1.5\ F\ (P_c + 2/3) + 121.8\ W_p(P_c + 2/3)\ [1 - 0.5\ P_c^{-0.1}\ F^{-0.1}] + 15.0\ W_p$$

The propulsion system components for this system are included in the first term in the oxidizer-side weight equation, i.e., 25.25F.

Weight of electrical system (W_e):

$$W_e = 15.0$$

Weight of gimbal actuation system (W_{gas}):

$$W_{gas} = 80\ P_c^{-3/2}\ F^2$$

Weight of roll control (W_{RC}):

$$W_{RC} = 35\ FW_p$$

Weight of integral tanks (W_T):

$$W_T = 5 + 10F + 71.3FW_p^{2/3}\,(0.15F^{-0.1}\,P_c^{-0.1} + 0.7)^{2/3} + 3.17F\ W_p^{1/3}\,(0.15F^{-0.1}\,P_c^{-0.1} + 0.7)^{1/3}\,(P_c + 2/3) + 38.8W_p\,(0.15F^{-0.1}\,P_c^{-0.1} + 0.7) + 40.2W_p^{2/3}\,(0.15F^{-0.1}\,P_c^{-0.1} + 0.7)^{2/3} + 26.4W_p^{1/3}\,(0.15F^{-0.1}\,P_c^{-0.1} + 0.7)^{1/3} + 179W_p\,(P_c + 2/3)\ (0.15F^{-0.1}\,P_c^{-0.1} + 0.7) + 56.7W_p^{1/3}\,(P_c + 2/3)\,(0.15F^{-0.1}\,P_c^{-0.1} + 0.7)^{1/3}$$

Table 5. 6,000-lb-Thrust Engine Weight Breakdown for *Juno IVA*, W_P = 9,000 lb Consumed

Component			Cold Helium Supply	Heated Helium Supply	GG Hybrid System
A. Gimbaled Assembly					
1. Thrust Chamber					
Tubes (111 required, 0.702 OD to 0.156 OD, 0.016 wall)		32.5	123.2	123.2	123.2
Braze (nickel base, 25% filling between tubes)		8.0			
Wire wrapping (combustion chamber out to A/A* = 3.5, 0.022 diameter, coated with epoxy resin)		4.4			
Stiffening rings		5.0			
Inlet manifold		3.0			
Exit manifold		5.4			
Coolant return tubes (4, ⅜ × 0.020 tubes)		3.0			
Uncooled exit skirt		6.8			
Dry weight	68.1				
Propellant holdup in tube wall		19.7			
Propellant holdup in manifolds		4.9			
Propellant holdup in coolant return tubes		2.1			
Thrust chamber propellant holdup	26.7				
Thrust chamber wet weight	94.8				
2. Valves, Lines, and Injector					
Injector		8.0			
Oxidizer valve		2.0			
Oxidizer distribution manifold		0.5			
Fuel valve		3.0			
Ball		0.5			
Injector support bracket		1.0			
Valve actuation system		4.0			
Fuel inlet tubes to injector		1.0			
Fuel inlet tubes to thrust chamber manifold (¾ in. flex.)		2.2			
Oxidizer inlet tubes to injector (½ in. flex.)		2.0			
Pressure relief tubes, (¾ in. flex.)		2.5			
Propellant holdup in injector and associated lines		1.7			
Dry weight	28.4				
Total Wet weight	123.2				
B. Component Summary			35.25	35.25	25.25
1. Oxidizer fill and drain disconnect	0.5	0.5			
2. Oxidizer fill and drain disconnect cap					
3. Oxidizer vent disconnect, remote	0.5	0.5			
4. Fuel vent disconnect, remote	0.5	0.5			
5. Fuel fill and drain disconnect	0.5	0.5			
6. Fuel fill disconnect cap					
7. Engine fuel bleed disconnect	0.5	0.5			
8. Engine fuel disconnect cap					
9. Oxidizer pressurization valve	—	2.5			
10. Fuel pressurization valve					
11. Actuator for (9) and (10)					
12. Regulator dome restrictor	—	—			
13. Helium regulator	2.0	2.0			
14. Dome loader bleed restrictor	—	—			
15. Helium fill disconnect, remote	0.5	0.5			
16. Relief valve	0.5	0.5			
17. Dome loader control valve	1.0	1.0			

Table 5 (Cont'd)

Component			Cold Helium Supply	Heated Helium Supply	GG Hybrid System
18. Dome loader regulator	1.0	1.0			
19. Nitrogen fill disconnect	0.5	0.5			
20. Actuator opening valves	0.5	0.5			
21. Actuator opening shutoff valve	0.5	0.5			
22. Actuator for propellant valves	Eng	Eng			
23. Oxidizer valve }	Eng	Eng			
24. Fuel valve }					
25. Actuator closing valve	0.5	0.5			
26. Oxidizer trim orifice	Eng	Eng			
27. Main valve lock pin	Eng	Eng			
28. Nitrogen fill disconnect cap	—	—			
29. Gas flow divider	0.25	0.25			
30. Diffuser oxidizer	0.5	0.5			
31. Diffuser fuel	0.5	0.5			
32. Nitrogen bottle	3.0	3.0			
33. Nitrogen and exp. valve, 2 act. brackets	2.0	2.0			
34. Miscellaneous brackets	2.0	2.0			
35. 50 ft ¼-in. lines and fittings	2.5	5.0			
36. 20 ft ¾-in. lines and fittings	5.0	10.0			
	25.25	35.25			
C. Flight Instrumentation			3.0	3.0	3.0
Temperature		.25			
T_1 helium supply					
T_2 fuel in tank					
T_3 fuel downstream of coolant passage					
T_4 oxidizer in tank					
Pressure		2.0			
P_1 helium supply					
P_2 regulated helium					
P_3 oxidizer manifold					
P_4 fuel manifold					
P_5 injection end of chamber					
P_6 N_2 tank					
P_7 oxidizer tank					
P_8 fuel tank					
Position indicators		0.75			
Main valve actuator, start and full open					
Pressurization valve actuators, full open	3.0				
D. Helium Supply, Cold			341.0		
1. Tanks and bosses and fittings		270.0			
2. Manifold and T's and tubing		5.0			
3. Supports		30.0			
4. Helium		36.0			
E. Helium Supply, Heated	341.0			310.5	
1. Tanks and bosses and fittings		240.0			
2. Manifold		5.0			
3. Supports		30.0			
4. Helium		31.5			
5. Heat exchanger	310.5	4.0			
F. GG-Hybrid System					177.3
Fuel side					
Gas generator		1.5			
GG tank		3.10			
Propellant		38.30			

Table 5 (Cont'd)

Component			Cold Helium Supply	Heated Helium Supply	GG Hybrid System
Helium		0.70			
Heat exch. valves, lines, etc.		10.00			
Helium tank	58.3	4.7			
Oxidizer side					
Helium tanks		90.0			
Manifold		2.5			
Mounting		15.0			
Helium		11.5			
	119.0				
	177.3				
Totals for engine			502.4	472.0	328.7

Propellant holdup (W_{ph}):

$$W_{ph} = \left[-0.015 \left(\frac{W_G}{W_p} - 1 \right) \ln \left(1 - \frac{W_p}{W_G} \right) + 0.0012 + 0.02 \ (P_c^{-0.1} \ F^{-0.1} - 0.5 P_c^{-0.2} \ F^{-0.2}) + 0.003 \ (1 - 0.5 \ P_c^{-0.1} \ F^{-0.1}) \right] W_p$$

Miscellaneous components (W_m):

$$W_m = 22 \ W_p$$

The total system weight is, of course, the summation of the appropriate components.

d. Flow-system analysis. The variation in many of the in-flight parameters (such as the chamber pressure, thrust, and burning time) and the propellant reserve are strongly affected by the accuracy of the flow-system calibrations. Since it is desirable to hold these variations and the propellant reserve to a minimum, an accurate calibration of the flow system must be made. In order to facilitate the calibration, a static analysis of the flow system is required.

The equations describing each component of the system can be written without difficulty and then may be solved for the two propellant flow rates. If such an analysis is made, the resultant equations are exceedingly complicated, and the effect of changes in system parameters on the flow rates is not apparent. The analysis presented here avoids algebraic complexity by differentiation of all system equations and clearly points out the effect of changes in system parameters on the propellant flow rates.

Let the fuel flow rate be denoted by $\dot{w}_f$ and the oxidizer flow rate by $\dot{w}_{ox}$. Further, let all line resistances and pressures be identified by the schematic diagram of the flow system in Fig. 18. The propulsion system is considered as consisting of three main parts, the motor, the feed system, and the pressurization system, as this treatment allows calibration of the flow system by parts. All system constants are assumed to be independent of flow, pressure, and density for small changes in these quantities.

The flow of propellants into the motor is described by the following set of equations:

$$P_{mox} - P_{cox} = K_{mox} \ \rho_{ox}^{-1} \ \dot{w}_{ox}^2 \tag{6}$$

$$P_{mf} - P_{cf} = K_{mf} \ \rho_f^{-1} \ \dot{w}_f^2 \tag{7}$$

where ρ denotes the density.

In the above equations, P_{cox} and P_{cf} are the chamber pressures as seen by the oxidizer and the fuel, respectively. They are to be distinguished from the true chamber pressure, P_c, because of a pressure drop across and behind the splash plate. These apparent chamber pressures may be expressed to a very good approximation by:

$$P_{cox} = \alpha_{ox} \ (\dot{w}_{ox} + \dot{w}_f) \tag{8}$$

$$P_{cf} = \alpha_f \ (\dot{w}_{ox} + \dot{w}_f) \tag{9}$$

where

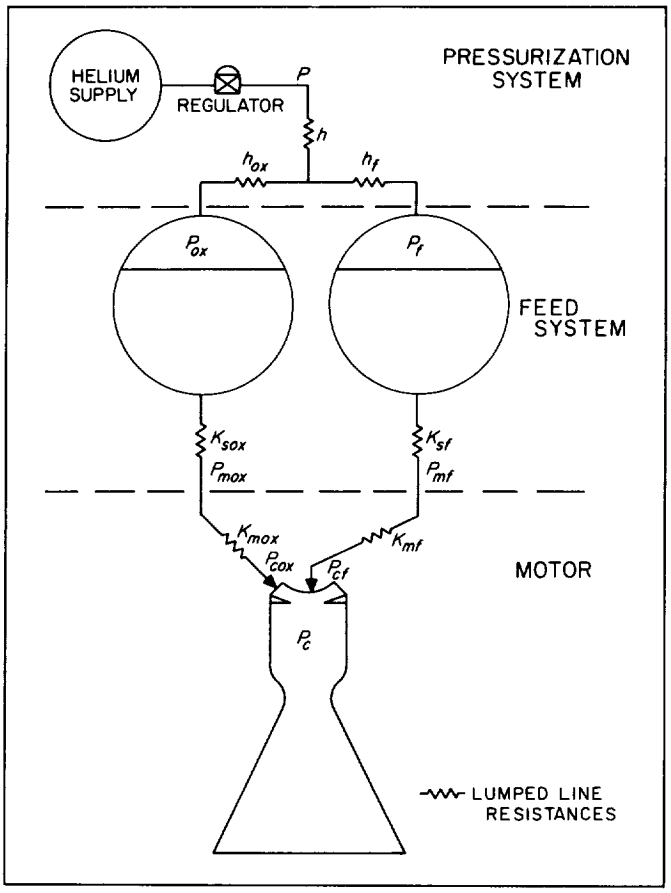

Fig. 13. Schematic Diagram of Flow System

$$\alpha_{ox} = (1 + \beta_{ox}) \frac{c^*}{A_{tg}} \tag{10}$$

$$\alpha_f = (1 + \beta_f) \frac{c^*}{A_{tg}} \tag{11}$$

and c^* is the characteristic exhaust velocity, A_t the throat area, g the gravitational constant (32.2 ft/sec), and β_{ox} and β_f are constants determined by the mixing and combustion characteristics of the injector and splash plate.

Equations (6) through (9) can be combined to give:

$$P_{mox} - \alpha_{ox} (\dot{w}_f + \dot{w}_{ox}) = K_{mox} \rho_{ox}^{-1} \dot{w}_{ox}^2 \tag{12}$$

$$P_{mf} - \alpha_f (\dot{w}_f + \dot{w}_{ox}) = K_{mf} \rho_f^{-1} \dot{w}_f^2 \tag{13}$$

The notation with α_{ox} and α_f rather than with β_{ox}, β_f, and c^* is used because of simplicity.

The feed system is described by the following two equations:

$$P_{ox} - P_{mox} = K_{sox} \rho_{ox}^{-1} \dot{w}_{ox}^2 \tag{14}$$

$$P_f - P_{mf} = K_{sf} \rho_f^{-1} \dot{w}_f^2 \tag{15}$$

The pressurization system is described by:

$$P - P_{ox} = h_{ox} \dot{w}_{ox}^2 - h (\dot{w}_f + \dot{w}_{ox})^2 \tag{16}$$

$$P - P_f = h_f \dot{w}_f^2 - h (\dot{w}_f + \dot{w}_{ox})^2 \tag{17}$$

No densities are included, since they are grossly variable for a blowdown system. Their effect is therefore absorbed in the constants. As mentioned above, if the equations describing the separate parts are combined, the resultant expressions for the flows become too complex to be useful. The complexity is avoided by first differentiating all pertinent equations and then solving the resultant linear equations for $d\dot{w}_{ox}$ and $d\dot{w}_f$. In the process the pressures at intermediate points are eliminated. Substitution of differences for differentials then results in a set of $\Delta\dot{w}_{ox}$ linear equations expressing the changes in flow rates due to changes in system parameters.

Application of this method to Eqs. (6), (7), (8), (9), (12), and (13) yields the following equations describing the interaction of chamber and feed system:

$$\frac{\Delta\dot{w}_f}{\dot{w}_f} = \frac{1}{c}\left[A_1 \frac{\Delta P_f}{P_f} + A_2 \frac{\Delta P_{ox}}{P_{ox}} + A_3 \frac{\Delta K_f}{K_f} + A_4 \frac{\Delta K_{ox}}{K_{ox}} + A_5 \frac{\Delta\alpha_f}{\alpha_f} + A_6 \frac{\Delta\alpha_{ox}}{\alpha_{ox}}\right] \tag{18}$$

$$\frac{\Delta\dot{w}_{ox}}{\dot{w}_{ox}} = \frac{1}{c}\left[B_1 \frac{\Delta P_f}{P_f} + B_2 \frac{\Delta P_{ox}}{P_{ox}} + B_3 \frac{\Delta K_f}{K_f} + B_4 \frac{\Delta K_{ox}}{K_{ox}} + B_5 \frac{\Delta\alpha_f}{\alpha_f} + B_6 \frac{\Delta\alpha_{ox}}{\alpha_{ox}}\right] \tag{19}$$

where

$$A_1 = \left[\alpha_{ox} + 2 \dot{w}_{ox} K_{ox}\right] \frac{P_f}{\dot{w}_f} \tag{20}$$

$$A_2 = -\alpha_f \frac{P_{ox}}{\dot{w}_f} \tag{21}$$

$$A_3 = -\left[\alpha_{ox} \dot{w}_f^2 + 2 \dot{w}_f^2 \dot{w}_{ox} K_{ox}\right] \frac{K_f}{\dot{w}_f} \tag{22}$$

$$A_4 = \alpha_f \dot{w}_{ox}^2 \frac{K_{ox}}{\dot{w}_f} \tag{23}$$

$$A_5 = -\left[\alpha_{ox} (\dot{w}_{ox} + \dot{w}_f) + 2 \dot{w}_{ox}^2 K_{ox} + 2 \dot{w}_{ox} \dot{w}_f K_{ox}\right] \frac{d\alpha_f}{\alpha_f} \tag{24}$$

$$A_6 = \alpha_f (\dot{w}_{ox} + \dot{w}_f) \frac{\alpha_{ox}}{\dot{w}_f} \quad (25)$$

$$B_1 = -\alpha_{ox} \frac{P_f}{\dot{w}_{ox}} \quad (26)$$

$$B_2 = \left[\alpha_f + 2\ \dot{w}_f\ K_f\right] \frac{P_{ox}}{\dot{w}_{ox}} \quad (27)$$

$$B_3 = \alpha_{ox}\ \dot{w}_f^2\ \frac{K_f}{\dot{w}_{ox}} \quad (28)$$

$$B_4 = \left[\alpha_f\ \dot{w}_{ox}^2 + 2\ \dot{w}_{ox}^2\ \dot{w}_f\ K_f\right] \frac{K_{ox}}{\dot{w}_{ox}} \quad (29)$$

$$B_5 = \alpha_{ox}\ (\dot{w}_{ox} + \dot{w}_f) \frac{\alpha_f}{\dot{w}_{ox}} \quad (30)$$

$$B_6 = -\left[\alpha_f\ (\dot{w}_{ox} + \dot{w}_f) + 2\ \dot{w}_f^2\ K_f + 2\dot{w}_f\ \dot{w}_{ox}\ K_f\right] \frac{\alpha_{ox}}{\dot{w}_{ox}} \quad (31)$$

$$C = 2\ \alpha_{ox}\ \dot{w}_f\ K_f + 2\ \alpha_f\ \dot{w}_{ox}\ K_{ox} + 4\ \dot{w}_f\ \dot{w}_{ox}\ K_f\ K_{ox} \quad (32)$$

and, for convenience in notation,

$$K_f = K_{mf}\ \rho_f^{-1} + K_{sf}\ \rho_f^{-1} \quad (33)$$

$$K_{ox} = K_{mox}\ \rho_{ox}^{-1} + K_{sox}\ \rho_{ox}^{-1} \quad (34)$$

All quantities appearing in Eqs. (18) through (34) are known, and the equations are practically applicable. A similar, but much more complex, equation including the interaction of all three parts of the system can be derived; however, since the tank pressures are expected to change very little, the added complexity is not warranted.

The above equations are perfectly general and are applicable to all motor feed system combinations in which the tank-pressure variations are small.

A direct application of the equations is useful in correcting for mixture-ratio changes due to the varying static heads. This is a serious problem for a low pressure system. In the *Juno IVA* version the static head change during flight causes a mixture-ratio variation of approximately 5%; hence, a correction for the static head must be made.

The static head is equivalent to a small increase in the tank pressure. Hence, the above equations can be used to compute the changes in the propellant-flow rates due to the static head. If the changes in the flow rates are integrated over the time interval of firing, the change in total propellant consumed is obtained. An equal and opposite change in the weight of propellant consumed is then produced by varying the system constants, K_{ox} and K_f. In this manner new system constants are obtained which produce the desired in-flight mixture ratio. The method will here be applied to *Juno IVA*.

The operating conditions for *Juno IVA* are given in the following tabulation:

Chamber pressure, P_c	150 psia
Tank pressures, $P_{ox} = P_f$	250 psia
Apparent chamber pressure as seen by the oxidizer, P_{cox}	180 psia
Apparent chamber pressure as seen by the fuel, P_{cf}	175 psia
Average mixture ratio, r	1.0
Oxidizer flow rate, $\dot{w}_{ox}$	10.0 lb/sec
Fuel flow rate, $\dot{w}_f$	10.0 lb/sec
Burning time	450 sec

These values require:

$K_{ox} = 0.70$ $\quad$ $K_f = 0.75$

$\alpha_{ox} = 9.0$ $\quad$ $\alpha_f = 8.75$

Substitution of the above quantities into Eqs. (19) through (32) yields the constants:

$A_1 = 575$ $\quad$ $B_1 = -225$

$A_2 = -219$ $\quad$ $B_2 = 594$

$A_3 = -172.5$ $\quad$ $B_3 = 67.5$

$A_4 = 61.2$ $\quad$ $B_4 = -166$

$A_5 = -402$ $\quad$ $B_5 = 157.5$

$A_6 = 157.5$ $\quad$ $B_6 = -427$

$C = 467.5$

The static head at the injector is given by:

$$\Delta P = z a \rho \quad (35)$$

where z is the height of the propellant above the injector, a is the acceleration of the missile, and ρ is the density of the propellant.

For *Juno IVA* the acceleration as a function of time, t, is:

$$a = \frac{6{,}000}{11{,}349 - 20t} \text{ ft sec}^{-2} \qquad (36)$$

The height of the propellants above the injector is, of course, determined by the missile structure. The latest configuration of *Juno IVA* consists of spherical fuel and oxidizer tanks having diameters of 63 and 56.5 in., respectively. The distance between the centers of the tanks is 72 in., and the center of the fuel (which is below the oxidizer tank) is located 46 in. from the injector.

For this configuration the static heads are given by:

$$\Delta P_f = 13{,}600 \frac{1.28 - \frac{t}{450}}{11{,}349 - 20t} \text{ psi} \qquad (37)$$

and

$$\Delta P_{ox} = 17{,}650 \frac{2.59 - \frac{t}{450}}{11{,}349 - 20t} \text{ psi} \qquad (38)$$

For the sake of simplicity, the height of the propellants in the tanks was assumed to be a linear function of time. This is not exactly true; however, the deviation from linearity in no case amounts to more than 0.1 psi. Also, a small correction for the density change of the fuel in the motor cooling passages is included.

Equations (37) and (38) can now be substituted into Eqs. (18) and (19). By setting $\Delta\alpha_f = \Delta\alpha_{ox} = 0$, these equations may be integrated over the operating time (450 sec) to give the change in the total propellant consumption as a function of ΔK_f and ΔK_{ox} (these quantities are considered constant with respect to time). Since no change in oxidizer and fuel consumption from the design values is desired, both of these quantities must be set equal to zero. Two equations with ΔK_f and ΔK_{ox} as unknowns result. The solution for the case in question is:

$$\Delta K_f = 0.0155$$

$$\Delta K_{ox} = 0.0606$$

The new system constants therefore become:

$$K_f = 0.7655$$

$$K_{ox} = 0.7606$$

The new set of influence coefficients, based on these values, is given below:

$$A_1 = 605 \qquad B_1 = -225$$

$$A_2 = -219 \qquad B_2 = 602$$

$$A_3 = -185 \qquad B_3 = 68.9$$

$$A_4 = 66.6 \qquad B_4 = -183.5$$

$$A_5 = -423 \qquad B_5 = 157.5$$

$$A_6 = 157.5 \qquad B_6 = -433$$

$$C = 504$$

The substitution of these values into Eqs. (18) and (19) yields:

$$\frac{\Delta \dot{w}_f}{\dot{w}_f} = 1.20 \frac{\Delta P_f}{P_f} - 0.434 \frac{\Delta P_{ox}}{P_{ox}} - 0.367 \frac{\Delta K_f}{K_f} + 0.123 \frac{\Delta K_{ox}}{K_{ox}} \qquad (39)$$

$$- 0.840 \frac{\Delta \alpha_f}{\alpha_f} + 0.312 \frac{\Delta \alpha_{ox}}{\alpha_{ox}}$$

$$\frac{\Delta \dot{w}_{ox}}{\dot{w}_{ox}} = - 0.446 \frac{\Delta P_f}{P_f} + 1.196 \frac{\Delta P_{ox}}{P_{ox}} + 0.1365 \frac{\Delta K_f}{K_f}$$

$$- 0.364 \frac{\Delta K_{ox}}{K_{ox}} + 0.312 \frac{\Delta \alpha_f}{\alpha_f} - 0.859 \frac{\Delta \alpha_{ox}}{\alpha_{ox}} \qquad (40)$$

Equations (39) and (40) show the effect of changes in the system parameters on the propellant flow rates for the flight model of *Juno IVA* having the configuration described above. In these expressions, ΔP_f and ΔP_{ox} now refer to variations other than those due to changes in static head. The correction for the static head is accomplished by changing the over-all system constants, K_f and K_{ox}, by the amounts indicated above. This may be accomplished by adjusting trim orifices in the two propellant lines. Alternatively, a trim orifice may be included in only one of the propellant lines, but then the tank-supply pressure must be varied. A slightly different analysis is required in this case. For a different missile configuration or for a missile with grossly different system parameters, a new analysis must be performed starting with Eqs. (18) through (34). The correction for static head is then carried out as outlined above.

e. Expected accuracy. Based on the experimental results obtained to date, an estimate was made of the accuracy to which the expected performance can be predicted. Also an estimate was made of the expected in-flight performance. These results are presented in Table 6.

f. Growth potential. During the course of the development of the *Juno IV* propulsion system, two analyses were

made to indicate the possible growth potential of this vehicle. The absolute magnitude of the values given for gross weight, velocity increment, etc., reflect only the values in use at the time the analysis was made and should not be considered as final results. However, the relative values of payload weights should be valid and indicate approximate payload growth potential.

The first analysis was made to estimate the relative circumlunar payload increases obtainable from propellant substitution in the third stage only of a three-stage vehicle. The results of this study are as follows:

Table 6. Expected Development and In-Flight Variations of System Performance Parameters—System B, Gimbal Motor Control and Heated Helium Pressurization

Parameter	Expected Development Variation %	Expected In-Flight Performance Variation %
Characteristic exhaust velocity, c^*, ft/sec	5600 ± 1	
Thrust coefficient, C_F (uncertainty due to difference between equilibrium and frozen flow)	$1.785 \begin{smallmatrix}+0.9\\-0.0\end{smallmatrix}$	
C_L (includes all losses such as those due to divergence, boundary layer, growth, etc.)	0.965 ± 1	1
Specific impulse, I_{sp}, sec	$300 \begin{smallmatrix}+2.9\\-2.0\end{smallmatrix}$	1
Throat area, A_t, in.^{2}	23.05 ± 0.5	—
Average fuel flow rate, $\dot{w}_F$, lb/sec	10.0 ± 2.4	1.5
Average oxidizer flow rate, $\dot{w}_{ox}$, lb/sec	10.0 ± 1.8	1.0
Average mixture ratio, r	1.00 ± 4.2	2.5
Average chamber pressure, P_c, psia	$150 \begin{smallmatrix}+1.9\\-3.7\end{smallmatrix}$	1.7
Average thrust, F, lb	$6000 \begin{smallmatrix}+3.7\\-2.9\end{smallmatrix}$	1.7
Burning time, sec	$450 \begin{smallmatrix}+3.7\\-2.9\end{smallmatrix}$	1.7

W_3 = third-stage gross weight = 4739 lb

ΔV_3 = third-stage gravitationless velocity increment 16,464 ft/sec

W_{p3} = third-stage propellant weight = 3911 lb

W_D = dry weight of third stage = 828 lb

The nonpayload dry weight (i.e., propulsion system plus structure) is given by the following relation:

$$W_D - W_{PAY} = 162 + 0.0822\ W_{P3} \tag{41}$$

where the constant 0.0822 is based on an average propellant density ($\bar{\rho}$) of 1.185 gm/cm^3 and is inversely proportional to $\bar{\rho}$. Equation (41) may be written in its more general form:

$$W_D - W_{PAY} = K_1 + K_2\ W_{P1} \tag{42}$$

where

$$K_2 = \frac{0.0974}{\bar{\rho}}$$

For a helium pressurized N_2O_4-N_2H_4 system having a 4739-lb gross weight, operating at 150 psia chamber pressure, and a mixture ratio of 1.0, $K_1 = 162$ and $K_2 = 0.0822$.

The extent that payload is affected by substituting a different propellant into this third stage was determined. This imaginary propellant substitution is performed in such a manner as to keep the same W_3 and ΔV_3. Thus the results are valid, provided the first and second stages (O_2-N_2H_4 *Jupiter* first stage and O_2-RP modified *Hermes* second stage) are not subsequently modified to any great extent.

It was assumed that general form of Eq. (42), which accounts for the increase in W_D due to variations in propellant density, was applicable for all the propellant systems considered. Thus:

$$W_D = 162 + \frac{0.0974}{\bar{\rho}} W_P + W_{PAY} \tag{43}$$

(44)

$$W_{PAY} = 4600 - (W_D + W_{P3}) = 4438 - \left(1 + \frac{0.0974}{\bar{\rho}}\right) W_P$$

The I_{sp} values used to calculate the value of W_p required for each propellant combination were obtained by applying the ratio of sea-level theoretical equilibrium I_{sp} values at $P_c = 300$ to the value of 293 sec,[2] the effective vacuum velocity of the N_2O_4-N_2H_4 system. The propel-

[2]This value includes a 5-sec reduction from the main thrust chamber I_{sp} to account for propellant consumption in control motors. If motor gimbaling is used then this number will be slightly greater but K_1 might also change.

lant systems considered and the results of the analysis are given in Table 7.

It can be seen from the table that payload increases of the order of two or more can be obtained by using elemental fluorine with either N_2H_4 or H_2. Payload increases of approximately 20% can be achieved by the use of O_2-N_2H_4 or ClF_3-N_2H_4.

The second analysis was performed to determine the increase in circumlunar payload which might be expected from certain propellant substitutions in all three stages of a *Juno* IV vehicle. Six 3-stage vehicles were considered. With the exception of the first stage of the first proposed vehicle, all of the stages of each vehicle use N_2H_4 as the fuel.

The *Jupiter* was used for the first stage of all six combinations. For five of these six, it was assumed that the *Jupiter* could be operated on O_2-N_2H_4 instead of O_2-RP without any significant change in the weight of the first-stage hardware. The gross weight of all six vehicles was held constant at 135,000 lb. Thus, by substituting the O_2-N_2H_4 into stage one, the higher I_{sp} obtained reduces the first-stage propellant requirements and permits an equivalent increase in the weight of the upper stages. The gravitationless velocity increments for each of the three stages were preserved in all six vehicles; these values are 11,700 ft/sec at first-stage burnout, 24,360 ft/sec at second-stage burnout, and 40,320 ft/sec at third-stage burnout.

A tabulation of the systems considered, as well as the results of the analysis, is presented in Table 8.

All of the third-stages were assumed to be of the heated-helium pressurized type having a third-stage gross weight W_3 given by

$$W_3 = \left(1 + \frac{0.1316}{\bar{\rho}_3}\right) W_{P3} + 235\ W_{PAY} \qquad (45)$$

where W_{P3} is the third stage propellant weight, $\bar{\rho}_3$ is the average propellant density in the third stage, and W_{pay} is the payload.

All of the second stages were assumed to be pressurized on the fuel side by gas-generator gases and by heated helium on the oxidizer side. The formula used for the gross weight of the second stages was

$$W_2 = \left(1 + \frac{0.0935}{\bar{\rho}_2}\right) W_{P2} + 1726 + W_3 \qquad (46)$$

The I_{sp} values chosen are based on the assumption that it will be possible to develop motors having equal values of nozzle expansion ratio ($\epsilon = 20$ for third stage and $\epsilon = 25$ for second stage) for each of the propellant combinations considered. This amounts to assuming that no reduction in heat-transfer area from that which exists in the N_2O_4-N_2H_4 motor will be required in order to successfully cool the ClF_3 and the F_2 motors.

The use of the scaling formulas given in Eqs. (45) and (46) implies the assumption that it will be possible

Table 7. Relative Circumlunar Payloads Obtainable from Propellant Substitution in Third Stage

Propellant	Sea-Level I_{sp} at P_c 300	$R(lb_0/lb_f)$	ρ_{ox}	ρ_f	$\bar{\rho}$	I_{sp} at Altitude	v^*	K_2	W_p	W_D	W_D-W_{pay}	W_{pay}
N_2O_4-N_2H_4	257	1.00	1.44	1.005	1.185	293	0.8263	0.0822	3911	328	484	344
N_2O_4-N_2H_4	258	1.25	1.44	1.005	1.208	294	0.8251	0.0806	3908	331	477	354
F_2-H_2	365	5.6	1.51	0.07	0.367	416	0.7087	0.2653	3359	1380	1053	327
F_2-H_2	348	18.85	1.51	0.07	0.742	397	0.7253	0.1313	3436	1303	613	690
F_2-H_2	356	11.5	1.51	0.07	0.570	406	0.7173	0.1710	3398	1341	743	598
F_2-N_2H_4	315	2.13	1.51	1.005	1.301	359	0.7604	0.0748	3603	1136	432	704
F_2-N_2H_4-H_2O	288	1.52	1.51	1.03	1.274	328	0.7908	0.0765	3748	991	449	542
F_2-36.3% NH_3 -63.7% N_2H_4	313	2.6	1.51	0.855	1.246	357	0.7622	0.0782	3611	1128	444	684
O_2-H_2	349	3.18	1.14	0.07	0.245	398	0.7244	0.3976	3432	1307	1526	negative
O_2-N_2H_4	274	0.85	1.14	1.005	1.062	312	0.8068	0.0917	3822	917	513	404
Cl F_3-N_2H_4	258	2.6	1.80	1.005	1.475	294	0.8251	0.0660	3908	831	420	411
O_2-H_2	339	5.23	1.14	0.07	0.332	386	0.7352	0.293	3485	1254	1183	71

*Note: $v = \left[1 - \exp\left(\frac{-512.3}{I_{sp}}\right)\right]$

to develop a propellant-transfer system for the halogen systems based on heated helium and N_2H_4 gas generation. Much more analytical and experimental work will be required in order to establish the validity of both the I_{sp} and the weight-scaling-laws assumption.

Keeping the above reservations in mind when interpreting the data, the discussion indicates the considerable growth potential available in circumlunar payload (from 320 to 1490 lb) by substitution of the high-energy fuels and oxidizers in the various stages of this vehicle. This improvement can be made in a stepwise manner as these high-energy-propellant combinations are brought to operational status.

C. Injector Design

1. SPLASH-PLATE TYPE OF INJECTOR

a. Basis for selection of injector type. The basic injector selected for development consisted of a number of doublet elements of oxidizer on fuel impinging on a splash ring. The selection of this injector-type for N_2O_4-N_2H_4 propellant combination was based on information obtained in previous research programs using these highly reactive propellants. Because of extremely rapid reactivity on contact, portions of the fuel and oxidizer were blown apart so that a uniform mixture-ratio distribution could not be obtained with conventional impinging streams. A schematic diagram illustrating this behavior is shown on the right-hand side of Fig. 14. Injectors composed of such a ring of doublets produced very low performance at several thrust levels. In addition, an injector of this type sustained a tangential mode combustion instability at the 6,000-lb-thrust level.

The use of a splash plate with this propellant combination produces a secondary mixing region of the partially vaporized products of the initial reaction as shown on the left-hand side of Fig. 14. In addition, the plate serves to force large-scale recirculation of the combustion gases which anchor the flame zone to the lip of the plate. Since a large amount of self-vaporization occurs behind the splash plate due to the initial nonflame reactions, the propellants enter the main combustion zone as a compressible fluid at fairly high velocity. The mass and mixture-ratio distribution are, therefore, quite uniform in a circumferential direction. As a result, there is little chance for tangential instability to become established.

b. Plan of development. The development program was to be carried out in two steps. First, a series of research injectors would be tested in order to establish the best orifice pattern, impingment angle, momentum ratio, and stream hydraulic characteristics. In addition, these research injectors would be used to test the effect of splash-plate opening area, face angle, and axial position. Second, flight-weight injectors would be built having N_2O_4-cooled splash plates and incorporating the best configuration of the research models as determined experimentally.

A number of uncooled chambers and nozzles would be used for short-duration testing, and water-cooled chambers and nozzles would be used for evaluating over-all heat-transfer characteristics for various injector configurations. All of the injectors have been designed so that they can be used with the light-weight motors (described in another Section of this Report). Only the best injector patterns would be tested with regenerative cooling and under vacuum exit conditions.

c. Description of injectors. The first research injector (research injector 1) had a fixed impingment included angle of 55 deg and contained 64 holes for removable, face-sealing orifices. A number of patterns using 16 oxidizer and 16 fuel orifices could be tried (the remaining holes were plugged). The various patterns which were tried are shown in the schematic drawings in Fig. 15. The first series of tests with this injector were made with

Table 8. Relative Circumlunar Payloads Obtainable From Propellant Substitution in Three-Stage Vehicle

Stage 1	O_2-RP-1 I_{sp} = 291*	O_2-N_2H_4 I_{sp} = 314**	O_2-N_2H_4 I_{sp} = 314**	O_2-N_2H_4 I_{sp} = 314**	O_2-N_2H_4 I_{sp} = 314**	O_2-N_2H_4 I_{sp} = 314**
Stage 2	N_2O_4-N_2H_4 I_{sp} = 304	N_2O_4-N_2H_4 I_{sp} = 304	N_2O_4-N_2H_4 I_{sp} = 304	ClF_3-N_2H_4 I_{sp} = 305	ClF_3-N_2H_4 I_{sp} = 305	F_2-N_2H_4 I_{sp} = 372
Stage 3	N_2O_4-N_2H_4 I_{sp} = 301	N_2O_4-N_2H_4 I_{sp} = 301	ClF_3-N_2H_4 I_{sp} = 302	ClF_3-N_2H_4 I_{sp} = 302	F_2-N_2H_4 I_{sp} = 369	F_2-N_2H_4 I_{sp} = 369
Circumlunar Payload	320 lb	403 lb	524 lb	582 lb	1009 lb	1490 lb

*Includes 2.0% gas-generator penalty for bipropellant gas generator.
**Includes 0.8% gas-generator penalty for N_2H_4 gas generator.

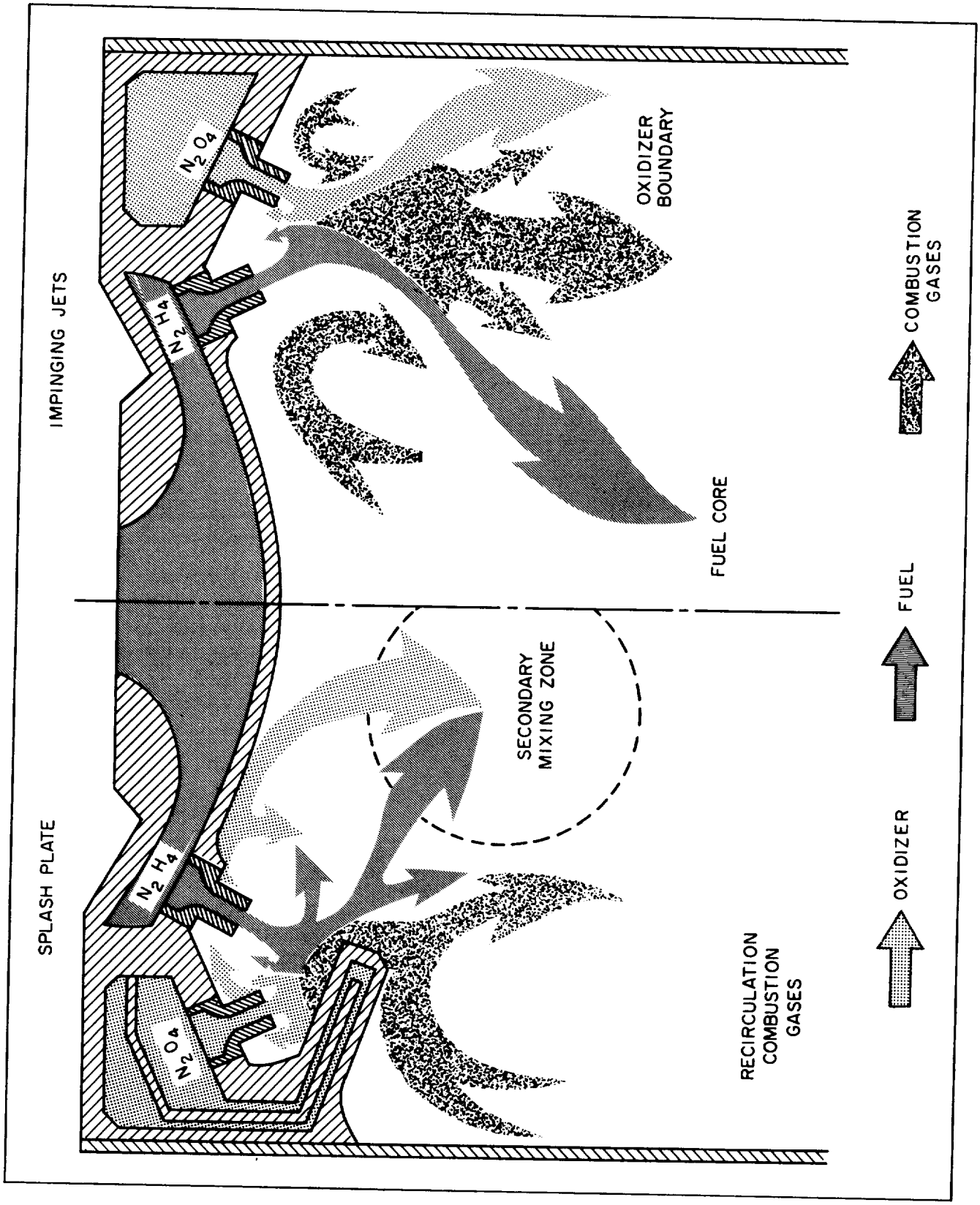

Fig. 14. Schematic Diagram of Two Injector Designs Using N_2O_4-N_2H_4

short orifices (approximately one diameter long). It was found that screens at the orifice entrance were required in order to stabilize, to some extent, the resulting streams. A longer (2.5 diameter) set of orifices was also made for this injector, and more stable streams were produced.

A more versatile research injector has been built (research injector 2) which has removable face-plates and orifices so that various impingment distances and impingment angles can be tried. The orifices for these injectors have a much larger screen entry area in order to decrease the injector pressure drop. Also, injector 2 manifold has been modified to aid the stream stability by better control of liquid velocity at the entrance to the orifice. In addition to the various configurations shown in Fig. 15, the research injector 2 will be used to vary the stream momentum ratios and velocities in order to optimize the combustion efficiency and stability.

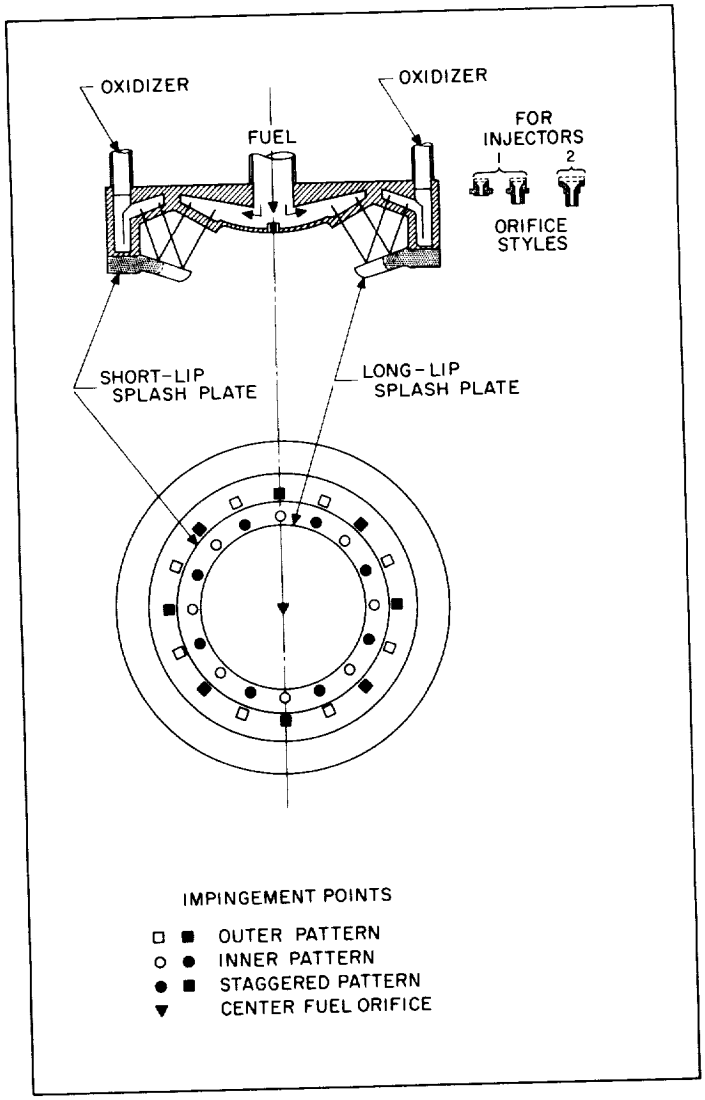

Fig. 15. Schematic Diagram of Splash-Plate Injector Configurations

d. Propellant valve and feed system. The propellant feed system is based on axially symmetrical flow pattern throughout. An axially-in-line duo-ball valve unit has been designed and is shown in Fig. 16. The balls, seals, and valve-stems are parts of a 1¼-in. Jamesbury duo-seal ball valve. These valves have been operated with no difficulty for nearly 100 motor firings. One of the 1¼-in. valves was also tested successfully at 325°F with water, so that no problem is anticipated in operation with hot hydrazine. The oxidizer will enter the upper ball valve through two opposed inlets, which in turn are fed by two ¾-in. flexible teflon hoses. One of these lines is shown in the upper right-hand side of Fig. 16. Below the valve the oxidizer is distributed into four ⅜-in. tubes located 90 deg apart. The N_2O_4 flows from these tubes into a collector manifold, then through the splash-plate, and finally through the outer row of orifices of the injector.

The fuel enters the upper manifold of the combustion chamber through four equally spaced flexible hoses, one of which is shown schematically on the right hand side of Fig. 16. From the upper chamber manifold the fuel flows axially down the chamber and nozzle passages to a lower manifold, and then returns through four ⅜-in tubes to the lower ball valve.

The dual-ball valve shown in Fig. 16 has not yet been fabricated. However, all motor tests have used two separate Jamesbury ball valves axially aligned with a feed system closely simulating that design.

The valves will be operated by means of a rotary actuator (Fig. 17) attached directly to the oxidizer valve and linked to the fuel valve as shown on the left-hand side of Fig. 16. The linkage is so designed that the oxidizer valve opens nearly halfway before the fuel valve starts to open. By adjusting the total actuating time, an oxidizer lead into the chamber can be obtained. Similarly, during shutdown, the fuel valve will be fully closed while the oxidizer valve is still one-third open. A small ball-valve is incorporated into the actuator, shown in Fig. 17, which will purge the fuel injector manifold so that all fuel is gone before the oxidizer has stopped flowing.

e. Performance results. The first series of tests was made to determine the best over-all orifice pattern on

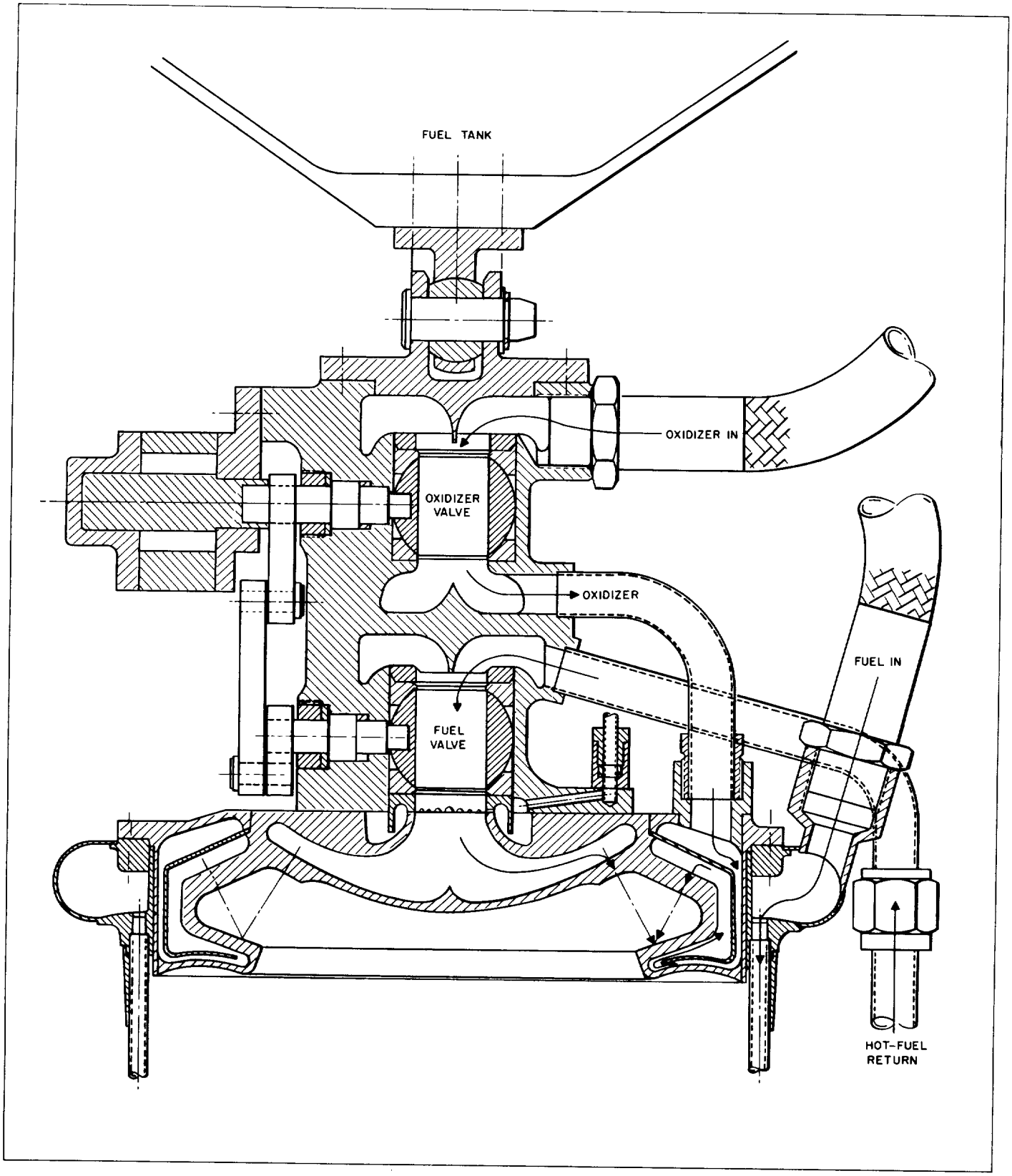

Fig. 16. Propellant Feed System and Ball Valves

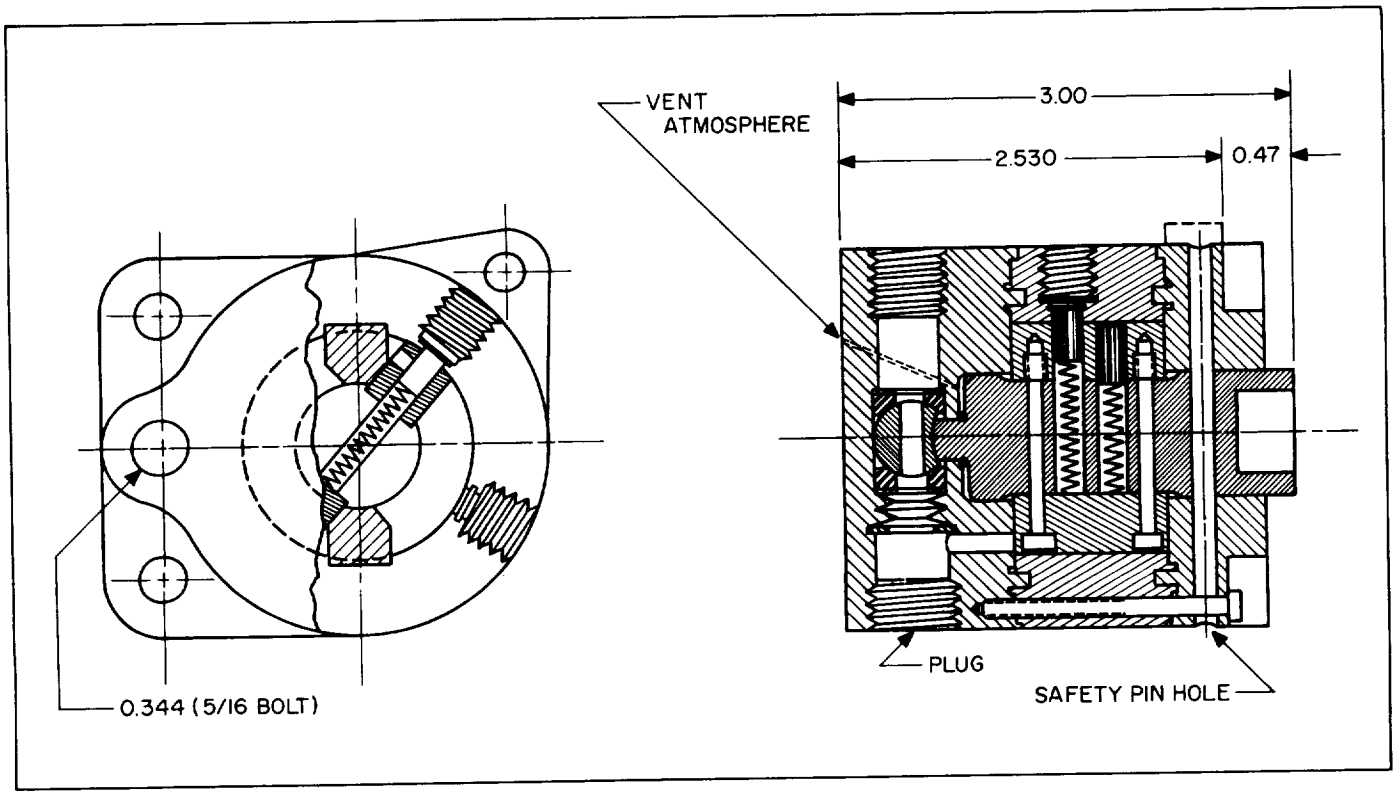

Fig. 17. Rotary Actuator for Main Propellant Valves

which to concentrate the devlopment program. The following combinations (shown schematically in Fig. 15) were tried:

1. The outer row of oxidizer orifices and outer row of fuel orifices with the short-lip splash plate. Data given in part A of Table 9 for an L^* of 39 in. are plotted in Fig. 18. Results for this pattern with an L^* of 24 in. are given in part D of Table 9 and shown in Fig. 19.

2. The inner row of oxidizer orifices and inner row of fuel orifices with the long-lip splash plate. These data are presented in Table 9 for an L^* of 24 in., and are compared with the outer row pattern in Fig. 19.

3. A staggered orifice pattern having eight outer row doublets and eight inner row doublets. Data are given in part B of Table 9 for a short-lip splash plate (intercepting only the outer eight pair) for an L^* of 39 in.

4. Results for the staggered pattern with a long-lip plate (intercepting all of the streams) are presented in Table 9 for $L^* = 39$ in. Data for the two staggered patterns are compared in Fig. 20.

All of the tests shown in Figs. 18, 19, 20 were made with research injector 1, using the short orifices shown in Fig. 18. Inspection of the water flow pattern with these orifices showed some unstable behavior in the liquid streams. A new set of longer orifices was used with injector 1 for the series of tests reported in part F of Table 9 and shown in Fig. 21. In these tests, distortion of an oxidizer manifold deflector plate after repair welding caused some of the oxidizer streams to flare out. It is possible that this flaring had some effect on the higher performance with these new jets by allowing a better penetration of the stable fuel jets into the outer region of the splash plate.

The staggered orifice pattern with the short-lip splash plate has shown some burning of the injector face, and with the long lip plate, this burning has been quite severe. Since the pressure drop across the long-lip plate was also very high, it was decided to drop this pattern from development, even though it appeared to have high performance. The performance with the short-lip plate

Table 9. Experimental Performance of 6,000-lb-Thrust Motor With N_2O_4-N_2H_4

Orifice Pattern	Mixture Ratio	p_c psia	c^* ft/sec	ΔP^1 psia	Remarks
A: 14-in. long chamber, short-lip splash-plate, outer row of orifices only (ΔP = approximate pressure drop across splash-plate) L^* = 39 in.	0.85	139	5454	—	
	1.04	153	5525	20	
	1.07	150	5460	18	
	1.21	147	5340	20	
	1.03	153	5487	19	1.5% fuel through center of injector face
	1.12	147	5385	19	1.5% fuel through center of injector face
B: 14-in.-long chamber, short-lip splash-plate, staggered orifice pattern, 8 outer pair, 8 inner pair L^* = 39 in.	0.91	153	5510	16	
	0.98	153	5530	17	
	1.03	154	5520	16	
	1.08	146	5435	16	
	1.09	154	5460	18	
	1.10	149	5426	14	
	0.98	154	5530	17	3% fuel through center of injector face
	1.05	153	5470	18	3% fuel through center of injector face
C: 14-in.-long chamber, long-lip splash-plate, staggered orifice pattern, 8 outer pair, 8 inner pair L^* = 39 in.	1.06	144	5545	56	3% fuel through center of injector face
	1.08	145	5545	—	3% fuel through center of injector face
	0.88	142	5540	56	
	0.89	141	5560	54	
	0.97	142	5560	54	
	0.98	141	5584	57	
	1.07	143	5535	57	
	1.20	136	5375	48	
D: 8-in.-long chamber, short-lip splash-plate, outer row of orifices only L^* = 24 in.	0.77	144	5160	14	
	0.82	146	5230	12	
	0.83	146	5250	17	
	0.85	147	5285	12	
	0.88	146	5260	19	
	1.05	148	5280	—	
	1.07	148	5275	—	
	0.95	154	5250	8	3% fuel through center of injector face
	1.03	148	5390	—	3% fuel through center of injector face
	1.08	153	5350	11	3% fuel through center of injector face
	1.13	156	5379	8	3% fuel through center of injector face
	1.34	127	4997	—	3% fuel through center of injector face
E: 8-in.-long chamber, long-lip splash-plate, inner row of orifices only L^* = 24 in.	0.86	144	5230	24	
	0.99	144	5180	22	
	1.03	143	5150	26	
	1.04	143	5135	—	
	0.93	146	5340	30	3% fuel through center of injector face
	0.99	146	5282	30	3% fuel through center of injector face
	1.04	145	5185	24	3% fuel through center of injector face
F: 14-in.-long chamber, short-lip splash-plate, outer row of new long orifices, L^* = 39 in.	0.72	151	5285	21	
	0.80	152	5455	29	
	0.84	155	5515	—	
	0.91	158	5600	20	
	0.91	153	5585	21	
	0.92	150	5630	28	
	0.82	152	5535	23	3% fuel through center of injector face
	0.85	153	5540	—	3% fuel through center of injector face
	0.95	150	5665	24	3% fuel through center of injector face
	1.02	152	5540	23	3% fuel through center of injector face
	0.91	154	5585	17	5% fuel through center of injector face
	1.01	152	5500	19	5% fuel through center of injector face
	1.06	152	5440	19	5% fuel through center of injector face

[1] Pressure drop across splash plate.

and staggered orifice pattern was about equal to that of the outer row pattern. For these reasons, the outer row pattern with a short-lip plate was selected for further development.

A series of tests was carried out with the research injector 2, using the outer-row configuration. This injector has produced quite high performance, but it also evidences a somewhat rough over-all combustion accompanied by a longitudinal mode acoustic instability. The

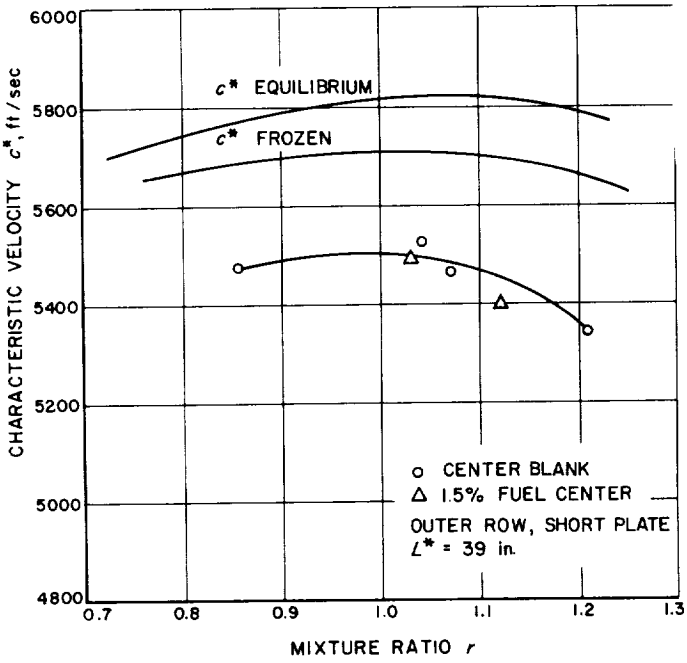

Fig. 18. Experimental Performance of 6,000-lb-Thrust Injector 1 With Short Orifices

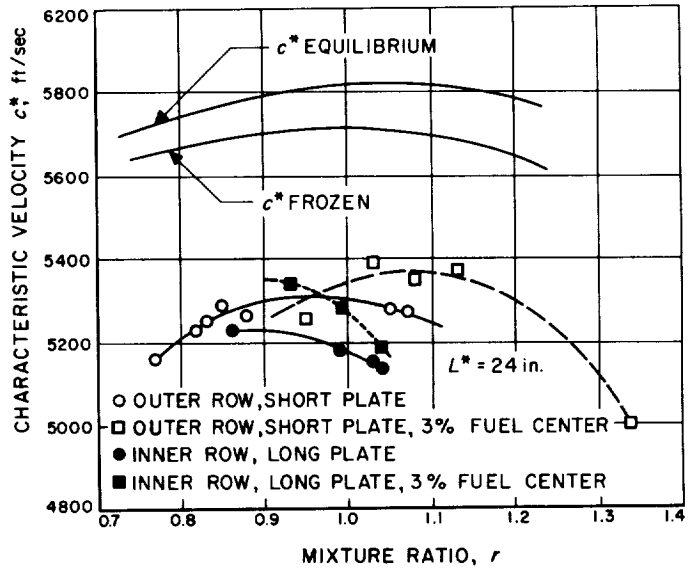

Fig. 19. Experimental Performance of 6,000-lb-Thrust Injector 1 With Short Orifices

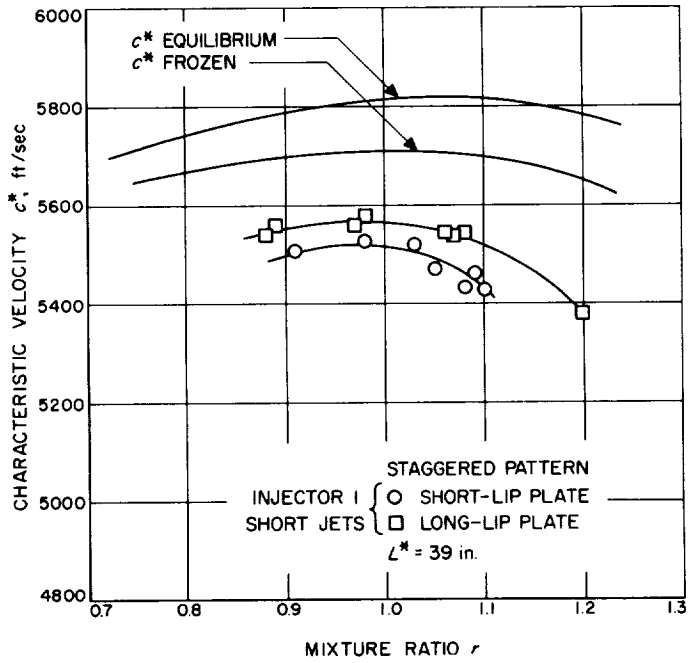

Fig. 20. Experimental Performance of 6,000-lb-Thrust Injector 1 With Staggered Pattern Using Short Orifices

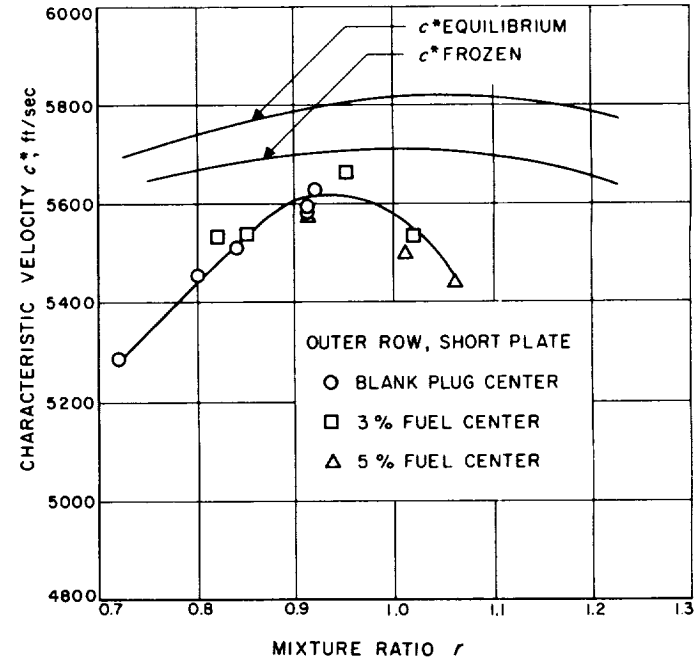

Fig. 21. Experimental Performance of 6,000-lb-Thrust Injector 1 Using Long Orifices

amplitude of this instability in the 39-in. L^* chamber is about 12 to 18 psi peak-to-peak. However, no injector damage has resulted from this instability, and heat-transfer measurements on a cooled chamber have indicated a normal heat loss based on theoretical values. The data for injector 2 are given in Table 10 and are compared with some data from injector 1 in Fig. 22. Further development of this new injector will be carried out to eliminate the "screech" and smooth the over-all combustion. Oxidizer jets having a controlled flare will be tried in order to determine if this is the controlling factor in the old injector which provided smoother operation. In addition, efforts will be made to decrease the pressure drop across the splash plate, which is higher with the new injector than for the injector 1.

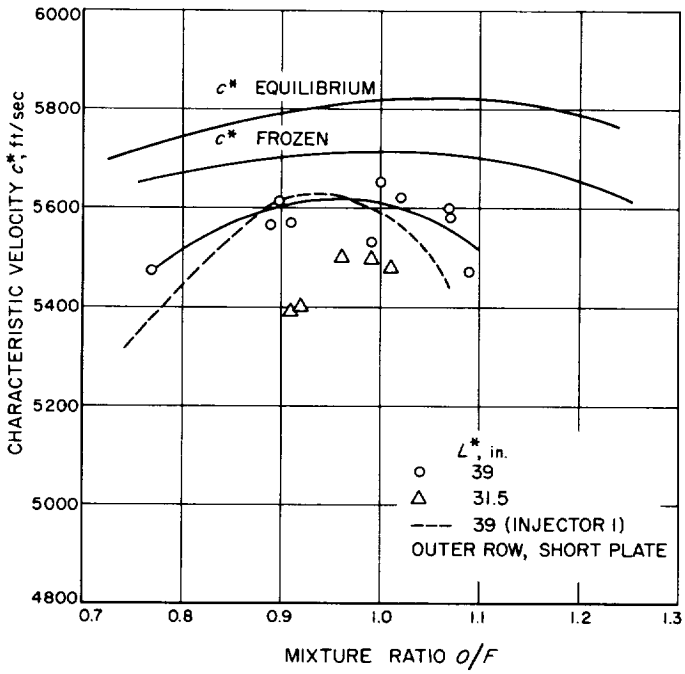

Fig. 22. Experimental Performance of 6,000-lb-Thrust Injector 2

2. ADVANCED INJECTORS

Concentric tube injectors have been considered for replacement of the splash-plate injector described previously. The advantages of concentric tubes over impinging streams with a splash plate are envisioned to be greater stability of the chamber pressure, lower injection pressures, reduced heat transfer to injector and combustion chamber, and possibly better performance.

The ideal concentric tube injector, at least from the fabrication point of view, is one employing a single element. At the present time, however, no 6,000-lb thrust single element has been developed. It is necessary, therefore, to incorporate several smaller elements into one injector. One requirement concerning the relative positions of these elements is symmetry, both geometrically and hydraulically. A highly symmetrical arrangement is obtainable wherein the distance of each element to all its nearest neighbors is a constant. This is accomplished by placing one element at the center of the injector and surrounding it by six elements at the corners of a hexagon centered about this element. Next, more elements are placed at all free corners of hexagons circumscribed about the outer six elements. Thus, two more units are added for each outer element, since three corners are already occupied and two corners are shared with nearest neighbors. Adding elements in this manner,

Table 10. Data for Injector 2

Orifice Pattern	Mixture Ratio	P_c psia	c^* ft/sec	ΔP[1] psia	Remarks
Injector 2, outer row of orifices, short-lip splash-plate	0.77	149	5475	27	
	0.89	151	5565	—	
	0.90	152	5615	35	recessed orifices
	0.91	151	5570	—	recessed orifices
L^* = 39 in.	0.99	152	5525	24	
	1.00	159	5655	—	
	1.02	152	5620	32	recessed orifices
	1.07	150	5600	27	
	1.07	161	5595	—	
	1.09	157	5470	—	
L^* = 31.5 in.	0.91	160	5390	33	
	0.92	160	5400	33	
	0.96	150	5500	33	orifices recessed into rear of face plate giving short free stream length to impingement
	0.99	154	5500	33	
	1.01	154	5480	32	

[1] ΔP = approximate pressure drop across the splash plate from oxidizer orifice region to P_c corrected.

symmetrical combinations of 1, 7, 19, 37, etc. units are obtained. For a resultant vacuum thrust of 6,000 lb, these combinations correspond to elements producing a vacuum thrust of 6,000, 860, 320, and 115 lb or a sea-level thrust of 4300, 610, 230, and 115 lb, respectively, at 150-psia chamber pressure. Since concentric tube elements of 40; 80; 200; and 800-lb thrust have already been tested successfully at the Laboratory, it was believed that two multi-element injectors, the 19-element injector based on the 200-lb thrust injector and the 7-element injector based on the 800-lb thrust injector, should be considered. While injectors having 37 or more units are conceptually feasible, it was believed that the complexities of fabrication and the close tolerances required made them impractical.

One element of the 19-element injector is shown schematically in Fig. 23. The fuel, supplied from the upper manifold, flows through the center tube and is dispersed into a radial sheet by the deflector shown. The oxidizer, supplied from the lower manifold, is admitted to the annulus around the center tube through tangential holes. In this manner, a tangential velocity is imparted to the oxidizer, and when it exits from the annulus, it forms the surface of the hyperboloid of revolution which intercepts the radial sheet of fuel. It has been found experimentally that performance and stability of the chamber pressure are greatly increased by extending the center tube to about ¼ to ½ in. forward of the injector face plate. The performance of a similar 200-lb element at 300 and 200 psia is shown in Fig. 24. Combustion was very smooth with chamber pressure variations amounting to approximately 2 to 3% of nominal chamber pressure.

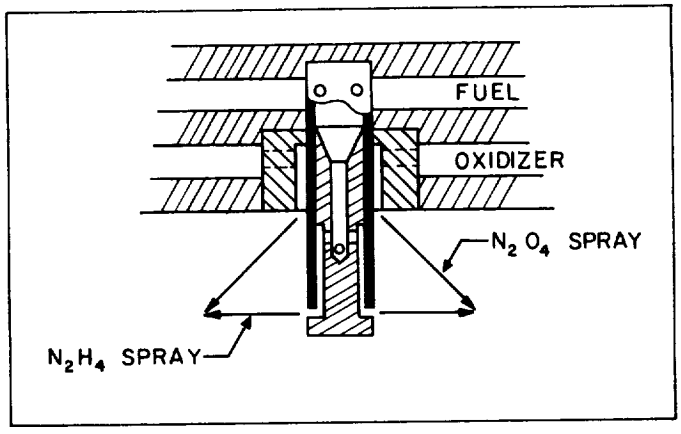

Fig. 23. Single Element of Concentric Tube Injector 316-lb Vacuum Thrust

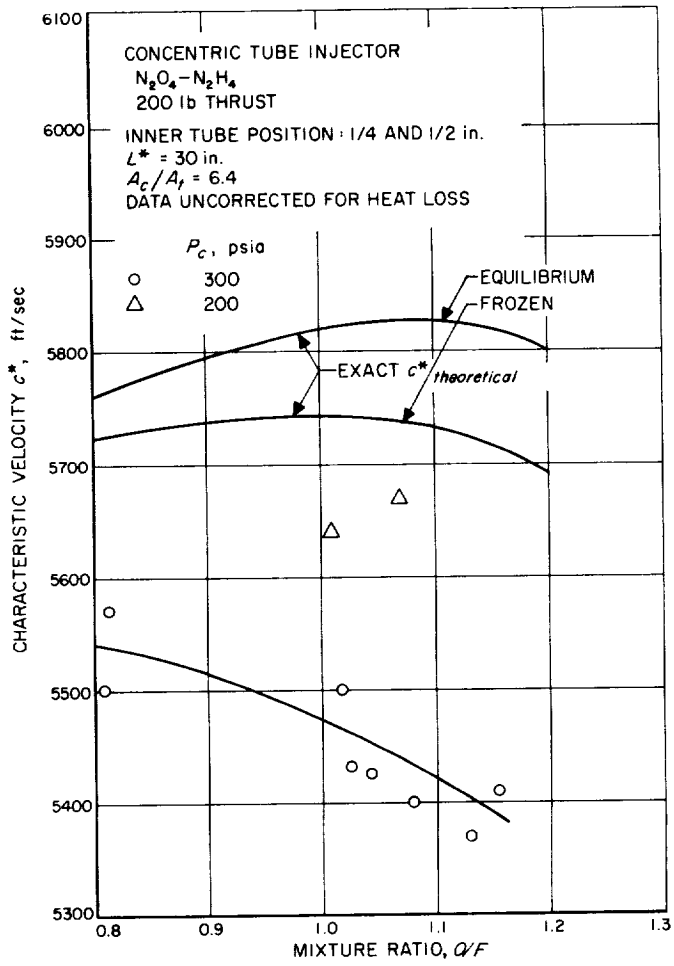

Fig. 24. Performance of 200-lb-Thrust Scale Concentric Tube Injector

The drop in performance with increasing mixture ratio is apparently due to lamination of the two propellant sheets, which results in large variations in local mixture ratio. Under these conditions the pockets of hydrazine formed decompose as a monopropellant, whereas the pockets of oxidizer undergo no combustion; hence a decrease in performance with increasing mixture ratio results. This problem can probably be eliminated by proper adjustment of the fuel and oxidizer momenta and film thicknesses.

It should be pointed out that the reported performance for the 200-lb-thrust element was measured in a 4-in. long chamber. In the 14-in.-long chamber, now contemplated for the 6000-lb thrust engine, these elements should perform much better. It should be possible to reduce the present 14-in. chamber length considerably without an appreciable drop in performance.

The schematic diagram of one element of the 7-element injector is shown in Fig. 25. The fuel, again supplied from the upper manifold, enters through the center tube and is dispersed into 32 streams by the serrations at the end of the tube. These streams are intercepted by a continuous annular sheet of oxidizer injected through the annulus surrounding the center tube. This arrangement allows good penetration of the fuel into the oxidizer and prevents the accumulation of large quantities of fuel, which can cause detonations in the chamber. It was borne out experimentally that the serration of the end of the center tube (in the manner described above) greatly increased the performance and stability over that obtainable with a continuous sheet of fuel. A summary of the performance of the injector in Fig. 25 at the 800-lb-thrust scale with 10- and 14-in.-long chambers is shown in Fig. 26. No change in performance at these two chamber lengths is apparent from the data. There is actually a slight improvement, which is, however, counterbalanced by increased heat losses. The drop in performance with increasing mixture ratio is probably due to the same mechanism as in the 200-lb-thrust scale. Work is presently in progress to increase the performance at high mixture ratios.

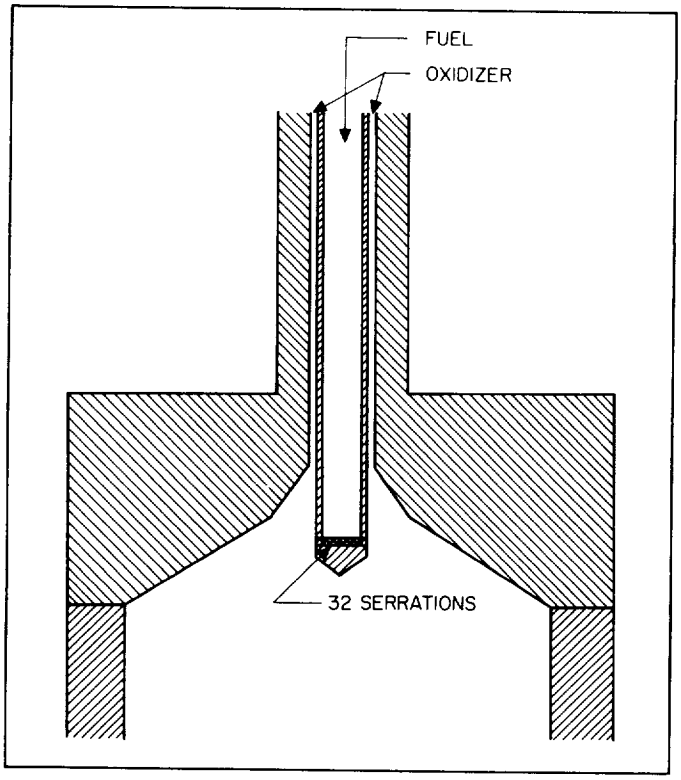

Fig. 25. Schematic Diagram of Seven-Element Injector

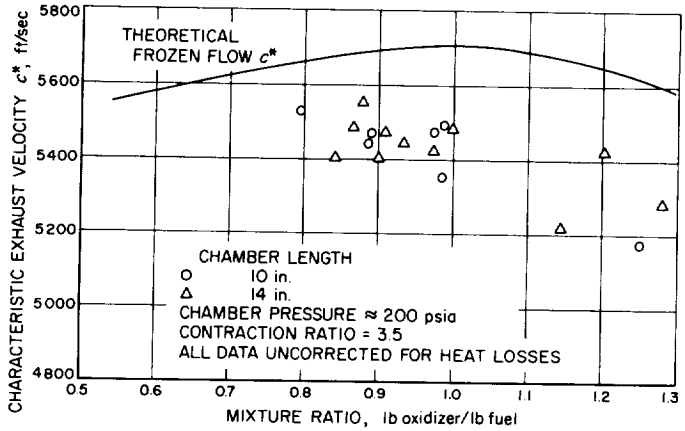

Fig. 26. Performance of 800-lb-Thrust Scale Concentric Tube Injector vs Mixture Ratio.

The valves and feed system used with the splash-plate injector can be adapted with only minor changes to give symmetrical hydraulic feed characteristics for both the 19- and the 7-element injectors. The purging mechanism at shutdown may also be the same as the one used for the splash-plate injector.

Heat-transfer measurements at the 40-lb-thrust scale have indicated that the heat transfer in the combustion chamber is about 30% lower than the value theoretically predicted. The cooling problem, therefore, appears to be less severe with concentric tube injectors. Heat transfer to the injector face plate also appears to be low enough to permit cooling by the oxidizer.

The main problems that have to be solved before the splash-plate injector may be replaced by a multi-element concentric tube injector are the interaction and stability of the several elements within one chamber. Plans are in progress to investigate this problem.

D. Thrust Chamber

1. DESIGN CRITERIA

The thrust chamber for the 6,000-lb-thrust engine was a completely new development, being expressly designed for its propellants, N_2O_4 as the oxidizer and N_2H_4 as the fuel and coolant. The engine development being made with the aid of extensive past and current JPL research on these propellants, has been motivated by the belief that these propellants constitute the best choice for a reliable, high performing, storable propellant combination.

To date one of the major deterrents to the widespread use of hydrazine as a bipropellant fuel has been the fact that as a monopropellant it has the thermodynamic potential for explosive thermal decomposition. Furthermore, some of the results of tests involving the limited use of hydrazine as a regenerative coolant in small motors have tended to substantiate dire predictions made on this basis. It is most important to note, however, that in these same programs hydrazine was also very successfully employed as a regenerative coolant during far more tests than those which ended in destructive explosions and that there were avoidable conditions which could plausibly be blamed for most of the explosions. This led to the conclusion that if the certain conditions which promote explosive thermal decomposition could be discovered and avoided, hydrazine should be capable of reliable utilization as a regenerative coolant. It therefore became the objective of one JPL program to determine these conditions. In brief it was found that (1) hydrazine must be kept away from materials and surfaces which are actively catalytic or readily reducible, (2) that the flow system must be designed such that there are no zones of local stagnation, (3) that the flow system must be kept clean of foreign material which might be catalytic, reactive, or cause stagnation, and (4) that sufficient coolant velocity for the particular local conditions of coolant bulk temperature and pressure must be provided to insure that the local value of the heat flux at the upper limit of nucleate boiling safely exceeds the local heat flux from the combustion gas to be expected at each station throughout the motor. These requirements, then, constituted the principal design criteria observed in the design and development of the 6,000-lb-thrust chamber.

In order to satisfy the first of these requirements, extensive literature surveying and compatibility testing were conducted and are reported in Ref. 2. In general it was found that most 300-series stainless steels, most aluminum alloys, and nickel were sufficiently compatible with hydrazine to be acceptable materials of construction for hydrazine-cooled thrust chambers. Thus, none of the materials normally selected for thrust chambers, except mild steels and ferritic stainless steels, was excluded from potential use. In areas of uncertainty, such as with certain braze alloys, specific tests were made to determine compatibility.

In order to obtain the necessary data to be able to design to meet the last requirement, extensive tests of the boiling-heat-transfer characteristics of hydrazine were made using electrically heated tube test sections. Hydrazine was forced through the tubes under various conditions similar to those to be expected in the thrust chamber with heat transfer being varied up to the burnout condition resulting from the transition from nucleate boiling to film boiling. It was found from these tests that hydrazine offers significantly better values of the upper limit of nucleate boiling than does any other liquid except water. The results of these tests have been reported in detail in Ref. 3. As pointed out in this Reference, the majority of the testing was conducted with round cross-section tubes with circumferentially uniform heat transfer. However, a few tests were made to determine whether or not several alternative passage configurations with heat transfer from one side only would perform similarly to the round tube. One rectangularly shaped configuration in particular (created by sheet metal seam welding and subsequent hydroforming), had a characteristic re-entrant corner at the edges of the passages which was found to cause burnout to occur at heat fluxes roughly half of the values measured under similar flow conditions in a round tube. It was found that a similar rectangularly shaped passage formed by electroforming, but with filleted corners, performed similarly to the round tubes. Thus, certain coolant-passage design criteria were established by these tests.

Other tests were made to determine the distribution of local heat flux to the wall from the combustion gases using moderate-thrust scale motors which were constructed of numerous axially short sections each of which was individually water cooled. The data from these tests were found to be consistently only a few percent lower than analytical predictions, thereby lending confidence to the analytical methods available for designing the cooling for a thrust chamber using these propellants.

The results of design analysis revealed that the thrust chamber should be designed for single pass coolant flow from injector toward nozzle exit to be able to take advantage of the better cooling characteristics of the cooler hydrazine in the injector region where heat fluxes are high and predictions are uncertain due to combustion-dominated flow (see Ref. 4). Provision for the fuel return to the injector is through four external tubes. The predicted minimum local ratio between limiting cooling heat flux and heat flux to the wall is located at the throat. The ratio increases substantially on either side of the throat. For a small low chamber pressure engine such as the

6,000-lb-thrust engine an adequate cooling margin is easily achieved with very low cooling velocities and low pressure drop. The cooling problem in such an engine arises from the bulk temperature rise of the small coolant flow. In this thrust chamber, even with the favorably low-mixture-ratio characteristic of the propellant combination, the coolant available was just sufficient to cool the combustion chamber and a conical expansion nozzle expanded out to 20:1 area ratio and still maintain the exit coolant bulk temperature below an acceptable maximum value, 50°F below saturation temperature. Actually from an area ratio optimization viewpoint, it would have been preferable to expand out to nearly 25:1, hence the lower area ratio constitutes a compromise to the cooling requirements. However, because of the flat nature of the curve, the payload sacrifice thus incurred was only a few percent.

An analytical investigation was made of the possible effect on the cooling problem resulting from the use of expansion shapes other than the conventional 15-deg cone. It was found that a contoured nozzle shaped according to method of characteristics computations could be selected such that, giving the same thrust coefficient as the 15-deg cone, its total heat transfer load would be 7% less, its length would be 20% less, and its weight about 8% less than that of the 15-deg conical nozzle. For this reason such a contour nozzle was selected for the 6,000-lb-thrust chamber. It was found that at some sacrifice in C_F, even greater savings in total heat transfer, length, and weight could be accomplished. It was also found that up to about 1% could be gained in C_F by selecting another contour of the family studied, but with the cost of total heat transfer, length, and weight somewhat greater than even the 15-deg cone. The details of the contour calculations and the results of analysis of thrust coefficient, heat transfer, length, and weight are given in Ref. 5.

In addition to these basic design requirements several other details of the engine design were found to affect thrust-chamber cooling design. The question of whether or not to use monopropellant hydrazine motors rather than gimbals for thrust vector control strongly influenced the hydrazine flow rate available for cooling since the combustion requirements were such that it was desirable to maintain a near-unity mixture ratio in the main thrust chamber. It was finally decided to use gimbals for reasons discussed in Section B-3 of this Report. Thus, the lower flow rate was available for cooling, imposing the expansion area ratio limitations mentioned above. The choice of gimbals also resulted in aggravating the engine shutdown problem since the steering motor flow would ordinarily be maintained after engine shutoff, thus, providing a means of removing the heat stored in the motor walls during steady state operation. Without the sustained flow this heat must be absorbed by the stagnant hydrazine locked up in the thrust chamber at shutdown. Although stagnant hydrazine does have some capacity for safely absorbing such heat, it is limited by its so-called auto-ignition temperature. Unfortunately, this temperature is not a specific physical property of hydrazine, but varies largely with the manner in which it is measured. Values varying all the way from about 400 to 600°F have been reported in the literature. It was found in the analysis of the shutoff conditions for the several thrust chamber designs under consideration that the equilibrium temperature in the locked up hydrazine could be maintained below 400°F, but not very far below. Whether or not such conditions would be reliably safe from explosive thermal decomposition on shutdown is not clear. For this reason serious consideration was being given to a system which would provide a short duration by-pass flow through the cooling passage back to the tank upon shutdown.

2. TUBE WALL

In making the selection of a type of thrust chamber construction for the initial development phases of the 6,000-lb-thrust engine the most important criterion was the estimated length of time to produce the first successful units. For this reason, types of construction requiring complex three-dimensional dies, types having cooling-passage configurations which might cause problems with hydrazine cooling, and types critically dependent on high-quality brazing or other questionable fabrication techniques were all rejected for the initial thrust-chamber development. The one type that seemed to offer the best compromise to the needs of this engine and time scale was a tube-wall type. There were, however, several objections to the conventional tube-wall type: (1) requirement of complex three-dimensional forming dies, (2) passage configurations having tight corners, (3) and the necessity of splitting tubes to accommodate the large expansion-area ratio desired. In particular, the transition from one tube to two or more tubes is difficult to accomplish without creating some stagnant zone. Each of these difficulties could be circumvented by one particular type of tube-wall construction, however, one

using tubes which are kept round in cross section over the full length of the motor, with the local diameter formed to the appropriate size at each station. A process for accomplishing the necessary tube forming had been worked on with considerable success by the Le Fiell Manufacturing Company of Los Angeles using a combination of spinning and drawing. Based on what they had already demonstrated to be possible with their process there seemed little doubt that the tubes needed for the 6,000-lb-thrust chamber could be produced rapidly. Thus the round-tube wall thrust chamber was selected for the primary thrust chamber development effort.

The specific thrust chamber configuration was the result of a heat transfer and cooling design analysis which proceeded about as follows: Calculation of the distribution of local heat flux was made considering convection to be the dominant mode, and accounting for increased heat flux due to equilibrium recombination methods described in Refs. 4 and 6 were used in making the calculations. The local thrust-chamber diameters were determined from required throat area, desired combustion chamber contraction area ratio, and nozzle-expansion area ratio. The results of these calculations are plotted as q versus area ratio, A/A_* in Fig. 27. From the known quantity of coolant flow available and the calculations of local heat flux the distribution of local coolant bulk temperature was computed assuming a 100°F inlet temperature, and considering the effective heat-transfer area of each tube to be its projected area rather than its hemicylindrical area (a justification for this assumption is given in Ref. 3). Since the expected coolant passage pressure drop is just a few psi, the local pressure throughout the cooling passage was thus expected to be about equal to the pressure at the inlet to the injector, which in this case was about 225 lb/in^2. With the local coolant pressure and bulk temperature at the throat thus established and essentially fixed, the value of the heat flux at the upper limit of nucleate boiling q_{ul} (often called burnout) was thus directly determined by the coolant velocity that could be provided. In order to ensure compliance with the basic requirement that q_{ul} exceeds q, a ratio of about 1.6 at the throat was selected as being a proper margin to cover the various uncertainties involved. With the desired value of q_{ul} thus established, it was found from the results of Ref. 3 that a coolant velocity of about 20 ft/sec was needed. This requirement, together with that of necessary throat diameter, established the number and size of coolant tubes constituting the tube wall. Based on the minimum tube-wall thickness readily attainable from the tube spinning process being 0.016 in., it was found that 111 tubes with minimum diameters of 0.157 in. at the throat, maximum of 0.702 in. at the exit and 0.248 in. at the chamber was the proper configuration. Because of the coolant passage configuration characteristic of this type of thrust chamber the coolant velocity falls off in nearly inverse proportion to the local area ratio, as shown in the coolant velocity distribution also presented in Fig. 27. Even though the coolant velocity at the exit becomes less than 1 ft/sec the margin of q_{ul} over q is maintained about constant over the expansion region and increases to a comfortably high value in the combustion region where heat-flux prediction uncertainties are the largest. In Fig. 28 the results of pressure drop calculations show that the pressure drop in the tubes predicted from isothermal flow conditions is only about 2.5 lb/in.^{2}. Due to the effect of boiling, the pressure drop will probably be somewhere between 3 and 5 psi during actual regenerative cooling operation.

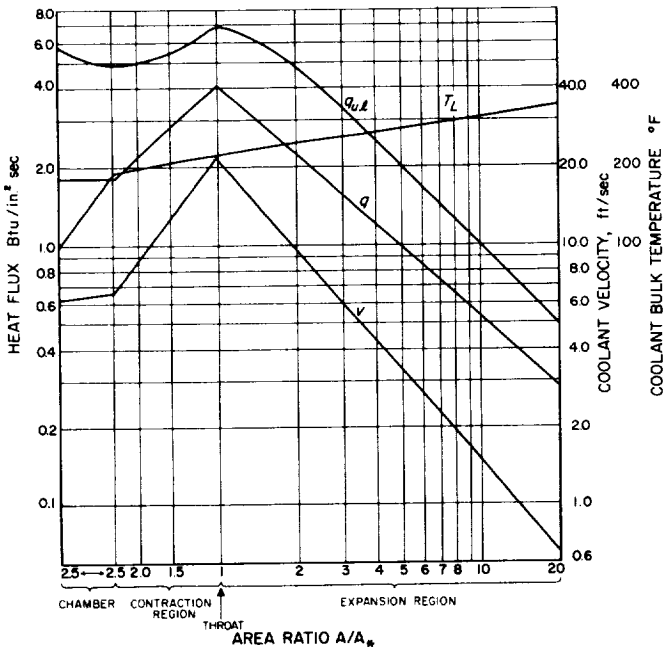

Fig. 27. q vs Area Ratio A/A*

As shown in the engine weight breakdown (Section IV-B-2a), the thrust chamber wet weight was about 95 lb, of which the tubes constituted 33 lb, and the propellant in the tubes, 20 lb. Thus all the other parts of the thrust chamber amounted to 42 additional lb. It was planned to seal between tubes by brazing with either nickel base

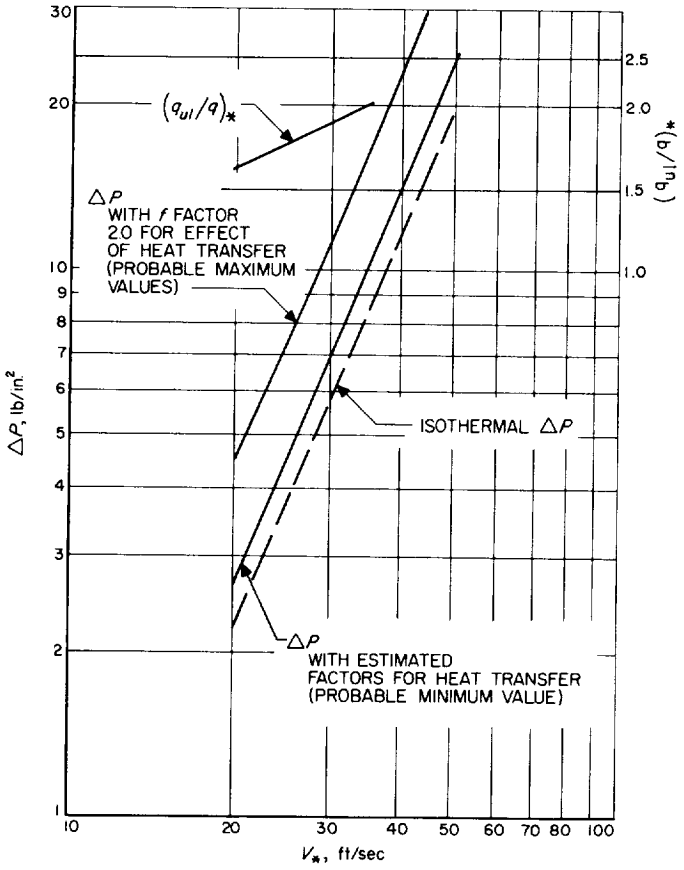

Fig. 28. Tube Wall Motor Pressure Drop as a Function of Throat Cooling Velocity

or silver base braze material, with an estimated weight of braze being 8 lb. To provide necessary hoop strength in the combustion zone and in the nozzle out to an expansion area ratio of about 3.5, the brazed tube bundle was to be wrapped with heat treated wire and then covered with an epoxy resin to protect the wire, requiring a total of about 4 lb. A series of 5 stiffening rings, weighing a total of about 5 lb, was to be distributed over the expansion cone beyond the extent of the wire wrap in order to provide some structural stiffness and resistance against vibration failures out in that region. The size and distribution of these rings was initially to be arbitrary, with the final design to be established from virbration measurements during preliminary engine testing. The weight of the manifolds and coolant return tubes was expected to be about 12 lb, with an additional 7 lb of propellant holdup. Finally, a skirt was to be placed at the nozzle exit to provide clear separation and prevent flow reattachment to the exit manifold which might cause cooling difficulties because of local stagnation and low velocity flow. All of these features, together with the over-all thrust-chamber configuration are illustrated in the thrust-chamber assembly drawing, Fig. 29.

A reasonably complete list of fabrication processes and time required to produce one of these spun-tube tube-wall thrust chambers is given in one of the last fabrication schedules to be drawn up, Table 11. From the schedule just about three months were expected to be required to complete each unit, with an initial production rate of about two per month. Of the numerous fabrication processes involved only two are worth discussing here, the tube spinning and the tube bundle brazing. The one major problem encountered in spinning the tubes was that numerous cracks appeared on the inside surface in the region of maximum reduction. The cracks varied all the way from a few which were quite deep, (nearly all the way through the wall) to numerous very shallow surface checks, depending upon the specific forming procedure used. This problem had not been previously encountered by the tube-spinning vendor in the spinning of tubes having less reduction and slightly greater minimum diameter, and hence was not expected. The problem received the full-time attention of people in the JPL materials group for nearly four months, during which time numerous potential causes were uncovered and means of correcting the situation attempted. Such difficulties as improper annealing between the several spinning processes, improper cleaning prior to annealing resulting in scaling and possible surface contamination, initial surface roughnesses being amplified by forming processes, galling due to die interference, as well as others, were discovered. Unfortunately because of the length of time required for the numerous processes, it took several weeks to see the result of each change. A few tubes were successfully produced by a combination of forming processes, one of which unfortunately had an unacceptably low production-rate capability. At the time the *Juno IV* program was stopped, these were the only tubes that had been produced that were free of cracks. It was the opinion of the materials group that the problem was not basic and would surely be solved by means of further refinements of the tube-forming process. Although there were some objections to using cracked tubes (due to possible vibration fatigue failure) heated tube tests made with tubes that were deeply cracked (although not all the way through) showed that this condition did not adversely affect the hydrazine q_{ul} value, as might be expected. Other ways of getting around the problem were also considered to be acceptable, such as spinning

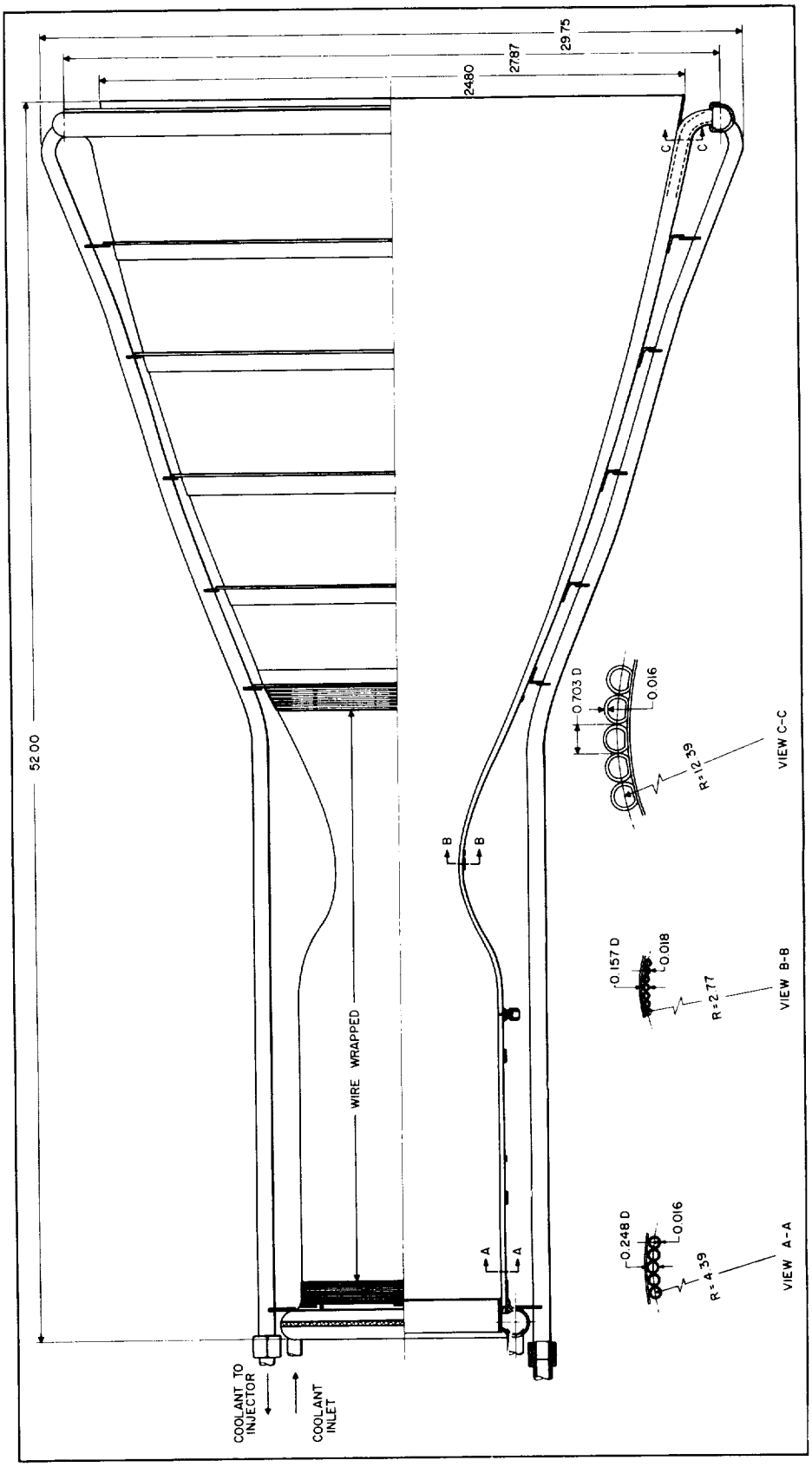

Fig. 29. Tube Wall Thrust Chamber Assembly

Table 11. Thrust Chamber Fabrication Schedule as of September 12, 1958

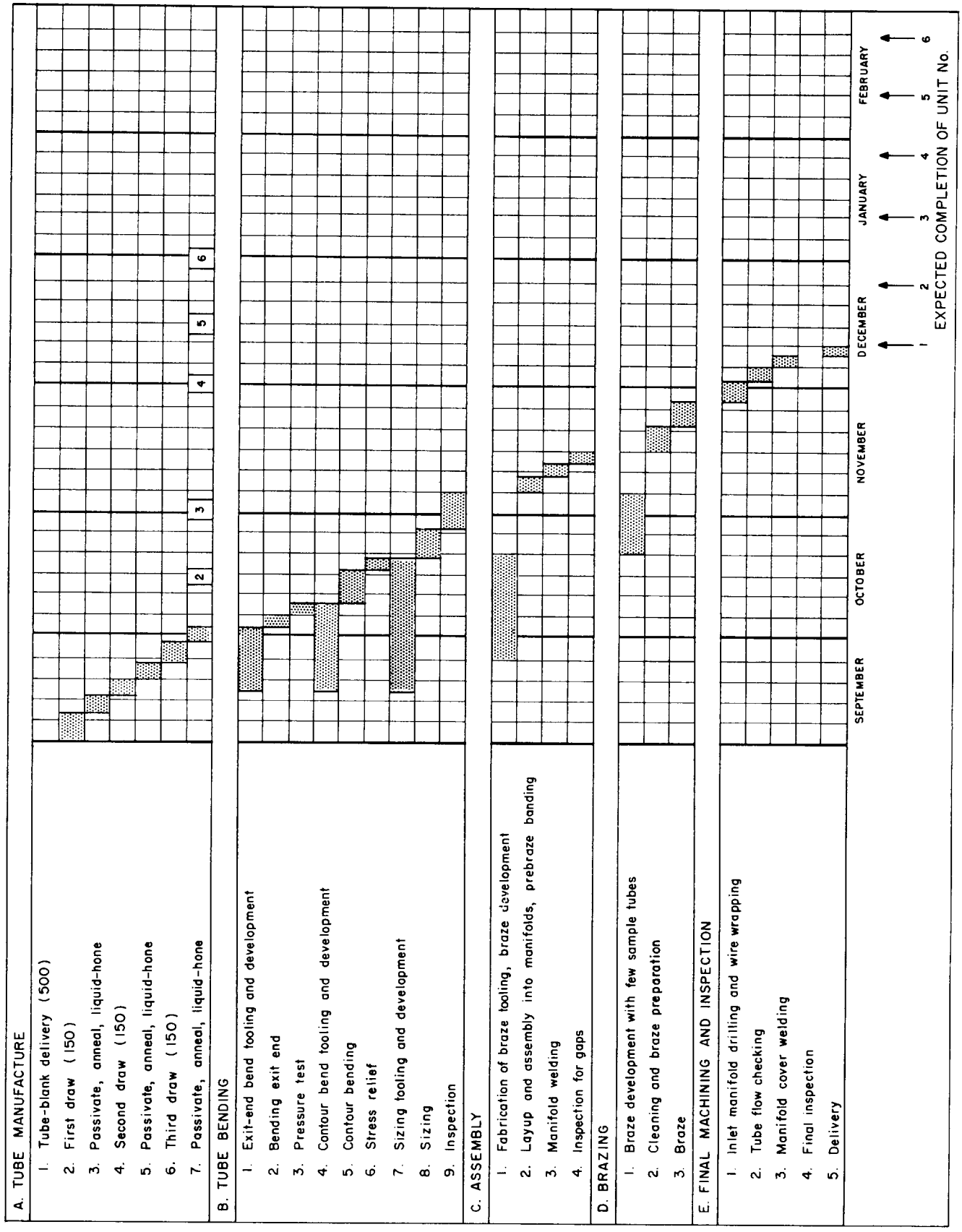

only down to 0.180-in. diameter, where the majority of the cracking started, and flattening the tubes down to 0.156 in. in the throat with a simple radial sector die. Flattening out of the tubes near the exit end to reduce the extent of the drawing was also considered acceptable but required a hoop compression ring to resist the tendency of the tubes to go back toward round due to coolant pressure.

The brazing problem connected with this thrust chamber was also given considerable effort. Although furnace nickel base brazing initially appeared to be the most desirable method of brazing, several problems and objections to this method were discovered. The main objection was that the perfection of furnace brazing would probably have consumed several of the first sets of tubes while problems of brazing tooling configuration, braze alloy placing, cleaning, atmosphere control, furnace cycle, etc., were being worked out for this thrust chamber. Furthermore, the use of nickel-base brazing required that the maximum gap between tubes after assembly into the bundle be less than 0.010 in. This would have also required some development time to achieve. Another objection raised was the fact that although the nickel-base braze alloys are quite strong, they tend to diffuse deeply into parent material causing severe embrittlement unless carefully controlled during brazing. Even under the best conditions, the braze is usually quite brittle. As an alternative, consideration was given to using silver-base braze alloys which could be applied by hand with a torch, thus avoiding many of the furnace braze problems that would require considerable development time. Test bundles were brazed with silver solder with acceptably low distortion. Silver solder melting temperatures were sufficiently high for the application. The major concern over the use of silver solder had been the lack of success that had been encountered using it in many research thrust chambers and injectors due to attack by the acid formed by the condensation of residual oxidizer vapor. It was not clear from this experience whether or not silver solder would stand up adequately as the braze material for the tube-wall thrust chamber. Because of the enumerated advantages of silver solder, a test program to evaluate it was to have been initiated about the time the program was terminated.

3. RIB THRUST CHAMBER

As mentioned previously the round-tube, tube-wall thrust chamber was selected because it was believed that it possessed the fewest heat transfer performance uncertainties and that it offered the best prospects of being successfully fabricated in the shortest time. However, it was recognized that it was a considerably heavier thrust chamber than could be built by any one of several alternate methods, principally because the individual tubes increased in diameter in direct proportion to the local nozzle diameter, thus resulting in considerable tube weight as well as propellant holdup weight. The obvious way around this particular problem, that of flattening the tubes into ellipses with minor diameters oriented radially with respect to the thrust chamber axis, was not considered acceptable because of the need for external restraining rings to prevent the tubes from deforming back to their natural round shape due to internal coolant pressure. Another more or less fundamental objection to all tube wall thrust chambers is the very tight tolerances required of each tube because of the problem of fitting together a necessarily large number of tubes with the attendant buildup of dimensional deviations. Consequently numerous alternate thrust-chamber construction methods were investigated concurrently with the development of the round-tube tube wall thrust chamber. Several showed promise but were found to have characteristically low q_{ul} values that were associated with resultant coolant-passage shapes. Others had fundamental fabrication problems that did not yield to the development effort that was expended. At least one, the channel-type developed by the Rocket Research Branch, NACA, Cleveland, looked exceedingly well suited to the 6,000-lb-thrust engine but required special tooling and special fabrication techniques that required greater engineering effort than was available.

Another method of thrust-chamber construction conceived during this investigation that showed great promise was adopted as the principal backup. As a means of identification, it has become known as the "welded-rib" type of thrust chamber. It consists of a thin 347 stainless steel sheet metal inner skin (0.016, actually the thinner, the better), formed to the desired thrust-chamber contour. On the outside of this skin is then spot welded numerous ribs which have been formed by rolling stainless steel wire into a rectangular cross section about 0.025 in. wide by 0.070 in. high. The ribs are spot welded to the inner skin about every ½ to ¾ in. by ordinary resistance-welding equipment adjusted to minimize expulsion in the weld region. The number of ribs required depends upon the span allowed between the ribs by stress con-

siderations. A thin layer of nickel-base braze alloy (in paste form) is applied the full length of each rib. The ribbed assembly is then wrapped with either round or flattened heat treatable stainless steel wire (17-7 PH or AM 350) under tension. Where it is necessary to hold down the wire to a rib locally to facilitate wrapping, spot welding is used. The outside of the wire wrap is then also coated with braze alloy, the manifold rings are tack welded in place, and the assembly is brazed. Finally the assembly goes through a heat-treat cycle, the individual channels are flow checked for blockage and the manifolds are sealed by welding, see Fig. 30.

There are several very attractive features of this method of construction, as well as several as yet unsolved fabrication problems. First, there is not a tight manufacturing tolerance in the whole process. The sheet metal spinning takes whatever shape and dimensions that are dictated by its spinning chuck and welding tooling. The wire ribs are not fabricated parts but are simply pieces cut off a long reel of specially rolled wire. The ribs are formed to the thrust chamber by the force exerted by the spot-welding machine. Even the precision required in locating the ribs on the skin is not particularly great. According to preliminary analytical studies of the problem, a position tolerance of about one rib thickness, 0.025 in., which is about 15% of the minimum span in present designs, should be more than adequate. The outer skin, of course, is automatically fitted tightly to the assembly by the wrapping process. The only really critical problem in the whole fabrication procedure is the brazing. There are several requirements that must be satisfied. First, continuous fillets must be formed between the inner sheet metal skin and the ribs and between the ribs and the outside wire wrap. This is necessary to eliminate pockets where hydrazine might be trapped, overheated and explode, and to develop strength between the three members so that pressure loads due to the coolant may be transmitted outward to the high-strength wire. The other requirement is that the braze must effect a seal between adjacent loops of wire constituting the outer wrap. Unfortunately these requirements preclude the use of torch brazing with silver solder. While these requirements may appear to be formidable, they are quite similar to the requirements of the brazing of the NACA channel type thrust chamber, which have been successfully accomplished through vacuum-brazing techniques.

The inner skin of a full expanded 6,000-lb-thrust chamber (having a conical, rather than contour, exit nozzle) has been completed using a combination of spinning in the throat region and rolling and welding in the chamber and exit cone. This chamber has also been ribbed, and is shown in Fig. 31. An investigation of the Floturning

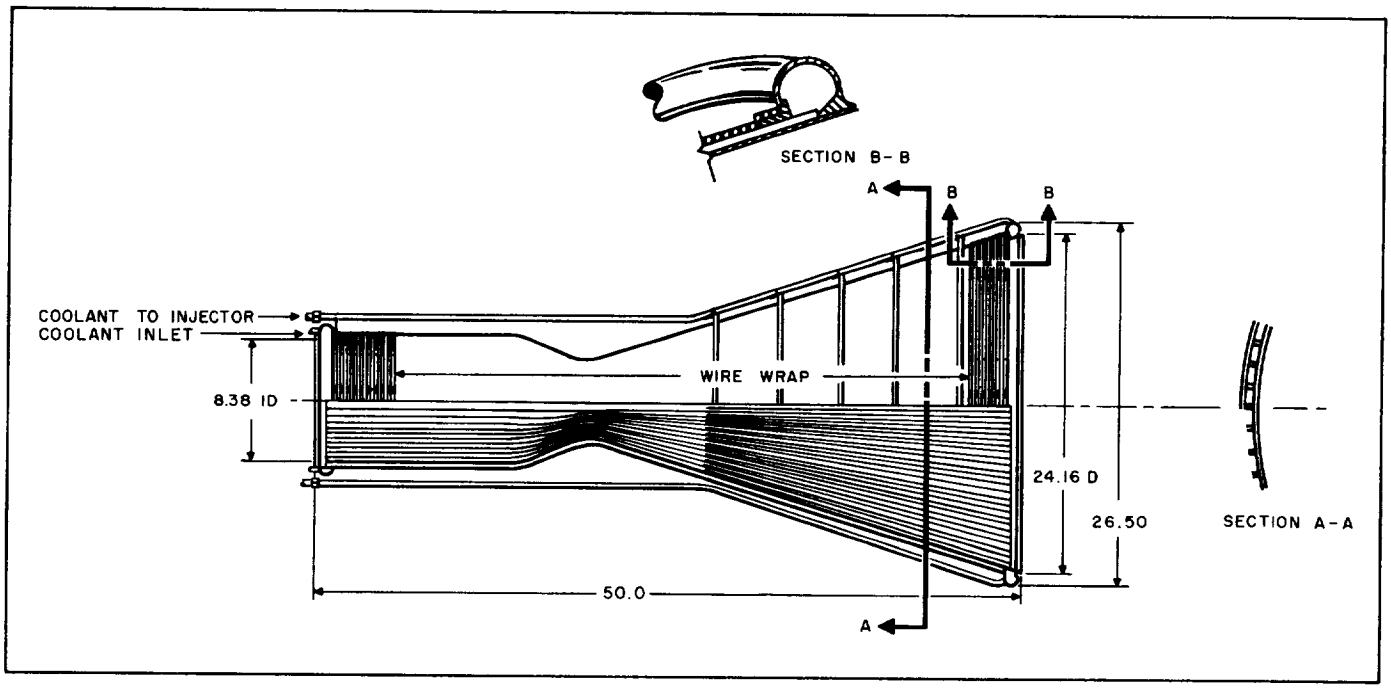

Fig. 30. Thrust Chamber, 6,000-lb-Thrust Rib Design

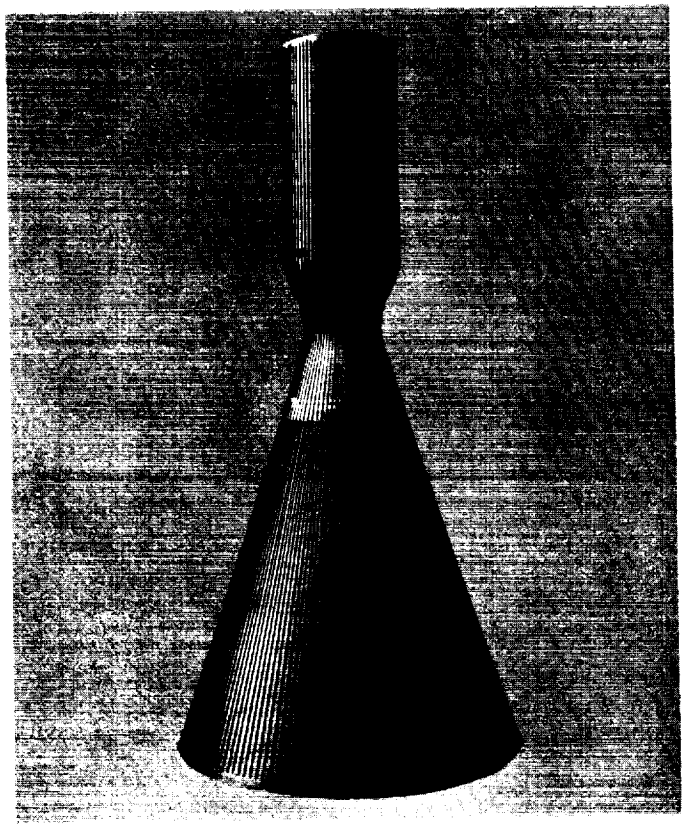

Fig. 31. Ribbed Liner, Welded Rib Thrust Chamber

process of Lodge and Shipley has shown that the inner skin can readily be produced with but one weld (at the throat) (instead of the present five) and with the contour-shaped exit nozzle. Future pieces will be made by this technique. The brazing has been under investigation using throat sections and thus far has only been partially successful using a hydrogen atmosphere. The braze test piece shown in Fig. 32, although successful in that the fillets were formed, had about a half dozen leaks between the wires.

In Table 12 a comparison between the weights of the round-tube tube wall and the welded-rib thrust chambers is given. The difference in weight, 42.2 lb out of 94.8 lb, is largely due to the fact that coolant-passage flow area is characteristically proportional to the square root of the local thrust chamber area ratio A/A_* rather than the first power as in the tube-wall type. This results in higher coolant velocities at each station away from the throat with resultant higher cooling margins (q_{ul} over q) (see Fig. 33) but also higher pressure drop. However, the pressure drop is still only about 10 to 15 psi which is acceptably low for this particular engine. Another weight saving is effected by the elimination of the heavy exit separation skirt and fairing required by the tube-wall design.

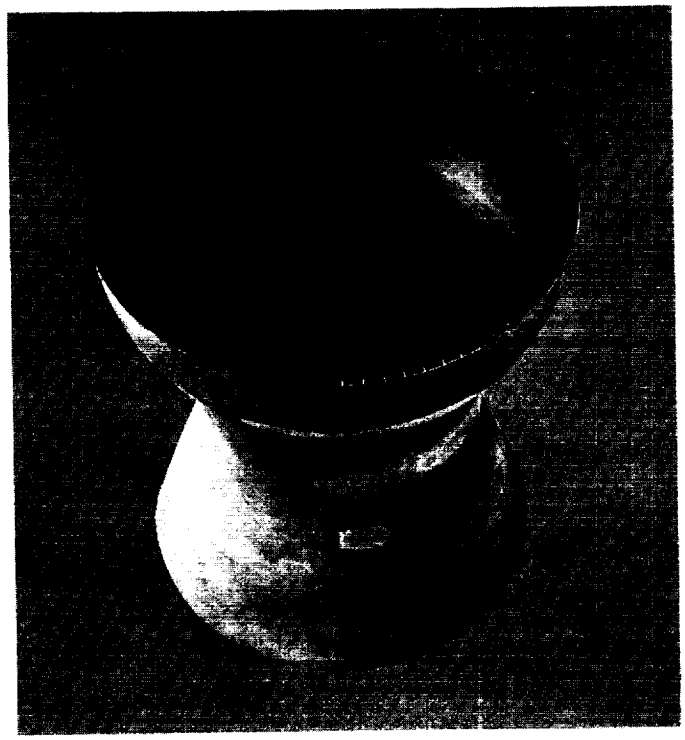

Fig. 32. Braze Test Piece, Welded Rib Thrust Chamber

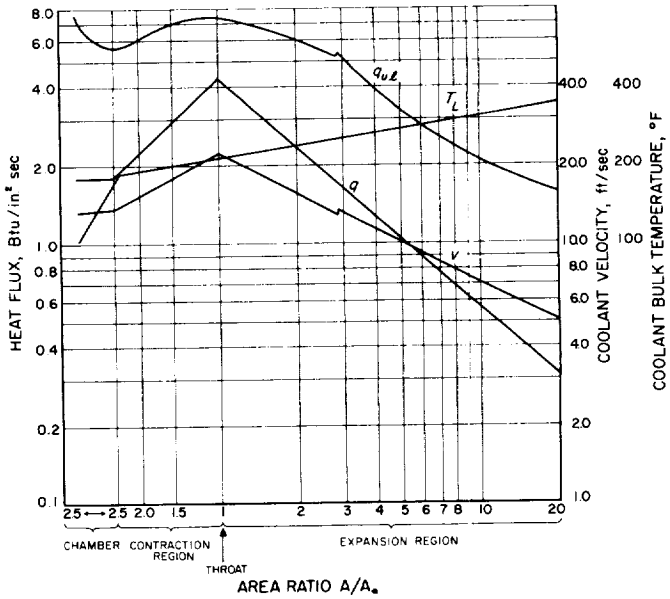

Fig. 33. Distribution of Heat Flux, Limiting Heat Flux, Coolant Velocity, Bulk Temperature for 6,000-lb-Thrust Chamber

Table 12. Comparison of Weight Breakdowns of Tube-Wall and Welded-Rib Thrust Chambers

Component		Thrust Chamber Weight, lb			
		Round-Tube Tube Wall		Welded Rib	
Tubes (111, 0.016 wall, 321 SS)		32.5			
Liner (0.016, 347 SS)	10.0				
Ribs (0.025 x 0.070, 347 SS)	3.0				
Wire wrap (0.032 round, 17-7 PH)	11.6			24.6	
Braze (25% filled, nickel-base braze)		8.0			
Nickel base				5.0	
Wire wrapping (injector to $A/A_* = 3.5$, 0.022)		4.4			
Stiffening rings		5.0		5.0	
Inlet manifold		3.0		3.0	
Exit manifold		5.4		3.2	
Coolant return tubes (4, 5/8 x 0.020)		3.0		3.0	
Exit skirt and fairing		6.8			
Thrust chamber dry weight			68.1		43.8
Propellant holdup					
in tube wall		19.7			
in rib wall				3.9	
in manifolds		4.9		2.8	
in coolant return tubes		2.1		2.1	
Total propellant holdup			26.7		8.8
Thrust chamber wet weight			94.8		52.6

E. Pressurization System

1. HELIUM SYSTEM

A simple feed system in which the propellants were displaced by gas under pressure was chosen for the first version of the 6,000-lb-thrust propulsion system. Later systems were to incorporate, first, heat exchangers to add heat to the helium gas and, finally, a gas generation system for displacing the fuel.

In the helium pressurization system the gas is stored in spheres at high pressure and flows through a pressure regulator into the propellant tanks. As the gas expands from the high-pressure spheres, it cools, and the cool gas absorbs heat from the sphere walls and the lines through which it flows. The amount of gas required depends on the amount of heat that the gas absorbs from its surroundings.

A simple formula for the volume of high-pressure gas required for a gas-pressure propellant system is

$$V_{gas} = V_{propellant} \times \Upsilon' \times \frac{P_{prop\ tank}}{(\Delta P)_{gas\ tank}}$$

where V_{gas} is the volume of the high pressure storage vessels

$V_{propellant}$ is the volume of the propellant tanks which are to be filled with gas

$P_{prop\ tank}$ is the pressure of the gas in the propellant tanks

$\Delta P_{gas\ tonk}$ is the change in pressure in the gas storage vessels

Υ' is an "effective" value of the ratio of specific heats of the gas

The value of Υ' depends on the amount of heat which the gas absorbs; it decreases as more heat is absorbed. A perfect gas in an adiabatic system would have $\Upsilon' = \Upsilon$. Helium is not a perfect gas, and experience indicates that there is an appreciable amount of heat absorbed by the gas from the tanks and lines of feed systems. The in-

clusion of a heat exchanger downstream from the regulator will further increase the amount of heat absorbed by the gas. However, not enough experimental information is available to predict an accurate value of γ' for the proposed system, so an approximate value was picked initially, with the intention of revising the number of spheres or the pressure to which they were charged after the prototype system has been tested.

The *Juno IVA* 6,000-lb-thrust propulsion system had the following given conditions:

$$V_{prop\ tank} = 130.6\ \text{ft}^3$$

$$P_{prop\ tank} = 250\ \text{psia}$$

$$(\Delta P)_{gas\ tank} = (3000 - 300) = 2700\ \text{psia}$$

$$'\gamma = 1.33\ \text{(assumed)}\ (\gamma_{avg} = 1.655\ \text{for helium gas at ambient temperature between 3000 psia and 300 psia})$$

from which:

$$V_{gas} = 130.6 \times 1.33 \times \frac{250}{2700} = 16.1\ \text{ft}^3$$

The gas is contained in 6 spherical vessels whose inside diameter is 21.5 in. and whose total volume is 16.1 cubic ft.

The gas-generation feed system consists of the following components:

1. Helium vessels
2. Pressure regulator
3. Pressure regulator dome loader
4. Pressure regulator dome loader supply valve
5. Heat exchanger
6. Line splitting "Y" fitting
7. Tank pressurizing line valves

These components are shown on the circuit diagram (Fig. 11). The specifications, and requirements, and the final status of the components of the helium pressurization system are discussed in Sec. IV-F.

2. GAS GENERATION SYSTEM

The 6,000-lb-thrust gas generation system has been described in general in Sec. IV-B-4 of this Report. As indicated, this system represents an alternate, materially lighter method of pressurizing the tanks of the 6,000-lb-thrust propulsion system. It is the purpose of this portion of the Report to describe in detail the components which constitute the hybrid gas-generation system.

The feasibility of developing a monopropellant-hydrazine generated gas pressurization system to pressurize and transfer anhydrous hydrazine is of course dependent upon the fact that this task can be conducted safely and with complete reliability. Theoretically, this should pose no difficulties, provided the gas and liquid temperatures involved are not excessive. In order to obtain a sound basis for the development project, an experimental program to pressurize liquid hydrazine with decomposition products at temperatures somewhat in excess of the design point, namely, 150°F was undertaken.

A series of fourteen tests were made utilizing a tank partially filled with anhydrous hydrazine. The test procedure consisted of (1) pressurizing the tank with decomposition products by statically back-pressurizing the tank while exhausting the decomposition products through a bypass, (2) passing the products over the surface of the liquid, (3) pumping the liquid hydrazine with the products, and (4) locking the decomposition products up in the tank with liquid hydrazine for long intervals. This procedure was repeated in each test at increasing temperature levels of the pressurizing gases up to a point at which the pressurizing gases were at an average of 200°F and the liquid hydrazine at 130°F. In no case was there any evidence of reaction between gas or liquid. The pressure level was quite smooth and very little pressure decay with time was noted, certainly no more than would be expected from the mere cooling of the gases.

a. Gas generator — decomposition chamber. The design of the catalytic decomposition chamber employed in this system is the result of an optimization study of the critical generator operating parameters. The exhaust products should be as low in temperature, and possess as low an average molecular weight as feasible while the chamber pressure should be as high as possible (high chamber pressure reduces the physical size of the catalytic reactor) consistent with the required tank pressure, system pressure losses, and component weights of the gas generator feed system. The operating parameters were determined to be: exhaust temperature, 1460°F, average molecular weight, 12.0 lb/mol, and average chamber pressure 407.5 psia.

The generant flow-rate, the remaining factor required to establish the size of the gas generator, was determined from the stage thrust level, engine mixture ratio, propellant tank pressure, and the effective temperature of the pressurizing gases in the propellant tank. These param-

eters were: thrust level, 6,000-lb, mixture ratio 1, tank pressure, 250 psia, and effective gas temperature 100°F.

The design of the catalytic decomposition chamber based upon these values and employing H-A-3 catalyst (Ref. 7) was found to be 1.8 in. in diameter and 7.8 in. in length. The entire generator including the injector, injector head, chamber body, catalyst, and miscellaneous parts was estimated to weigh 1.5 lb. At the termination of the program no complete flight model generators had been constructed; however, two models each of two prototypes, one for testing of the catalyst bed and one for bipropellant ignition tests, were fabricated. It was intended that the desirable features of each of these units would be incorporated in the flight models. The first prototype is described in JPL Sketch No. C-62479; the second, in JPL Sketch No. A-62480 through A-62485.

In order to verify that the design configuration of the catalyst bed fulfilled the initial design objectives, a prototype unit was tested with a continuous decomposition gas analysis system. The data from the analysis system made it possible to determine the percentage of ammonia dissociated which directly determined the exhaust gas temperature and average molecular weight. An exhaust temperature of 1460°F corresponds to an ammonia dissociation of 75%. A series of ten tests was made in which the gases were analyzed. As a further check on the analysis, a direct weight determination of ammonia present was made. The gas analysis indicated an average dissociation of 76.65%, while the direct weight determination gave 77.87%. From the close agreement, it would appear that the catalyst bed configuration performed quite satisfactorily.

b. Gas generator — ignition system. A number of methods exist for the ignition of monopropellant hydrazine; however, the design criteria of the 6,000-lb-thrust propulsion system indicated that the most suitable method would be to employ a bipropellant ignition system utilizing nitrogen tetroxide as the oxidizer. Two ignition systems were investigated. The first employed a cylinder with a piston being driven by a constant pressure source. The second employed a separate prepressurized cartridge loaded with nitrogen tetroxide which upon activation would blow down, exhausting the oxidizer. The initial ignition tests were made with a constant-pressure system employing smaller and smaller quantities of oxidizer to see where nonreliable ignitions occurred. It became evident from these tests that a very small quantity of oxidizer was necessary and that a piston system for this size operation was unnecessarily complicated. The development of the cartridge system was consequently undertaken and accomplished. The finalized system consisted of a cartridge of 16-cc capacity loaded with approximately two to three cc of nitrogen tetroxide and prepressurized with nitrogen to 600 psi. The cartridge was mounted on a valve which was timed to open simultaneously or with a 100-millisec lead of the generator fuel valve. The injection nozzle was sized to give a nominal mixture ratio of 0.10. A series of 31 tests was made with the cartridge system. In the last 26 of these tests a catalyst bed in the generator was utilized. All tests were quite successful. It was found that the cartridge took about 2 sec to blow down and that virtually full chamber pressure was obtained within 200 millisec of initial oxidizer injection.

c. Heat exchanger-hydrazine decomposition products to liquid nitrogen tetroxide. A detailed study of the heat exchanger to cool the hydrazine decomposition products was undertaken to arrive at an optimum heat-exchanger configuration. The operating parameters were chosen as follows: For the gas side the gas inlet temperature was assumed to be 1460°F; the gas outlet temperature, 150°F; the gas flow rate, 0.0832 lb/sec, and the allowable pressure drop up to 125 psi. For the liquid side the nitrogen tetroxide inlet temperature was assumed to be 75°F at a flow rate of 10 lb/sec, allowable pressure drop 10 psi or less. In addition to foregoing operating conditions, the anticipated propellant tank configuration materially influenced the design of the exchanger. The original 6,000-lb-thrust stage mission studies envisioned a single propellant tank shell with an internal diaphragm separating the propellants. In this configuration the only available location for the heat exchanger was inside the tank downcomer which itself was located inside the lower portion of the propellant tank. This condition dictated that the exchanger have the gas entrance and exit at the same end of the unit and be as small as possible in diameter with an allowable length of up to 30 in. Utilizing all of these criteria, a suitable design consisting of a single $\frac{3}{8}$-in. stainless steel tube of 0.035-in. wall thickness making six passes within a shell of 1.509-in. diameter was accomplished. The estimated weight of the unit including the downcomer weight was 3 lb. A proposed layout for such a unit was made under JPL Dwg. No. D-903-1328.

Negotiations were initiated with Aeroquip Corporation, to fabricate one such unit for test purposes. The

Aeroquip design differed somewhat from the JPL original layout principally because of tooling difficulties. Their design appears in Aeroquip Dwg. No. EX 15849. In addition to the Aeroquip unit and because of delivery delays on the part of Aeroquip an alternate fabrication of the exchanger was undertaken at the Laboratory. Neither unit had been completed at the termination of the *Juno IV* effort.

Soon after the initiation of fabrication of the heat exchanger, a decision was made to employ separate tanks for the propellants in the early versions of the 6,000-lb-thrust stage. It was anticipated that the later flights of the system would ultimately employ the single diaphram tank. Alternate designs of the heat exchanger were considered since its location in the early flights would be in an external downcomer. After some study, it was concluded that little if any weight saving was affected by having a design with gas inlet and outlets at opposite ends and that if the initial design was to be used at some time, it would be more desirable to obtain additional operating experience upon it rather than on another design.

Although the heat exchanger was never operated, a test apparatus was completely constructed. The apparatus consisted of two large nitrogen tetroxide reservoirs wherein the liquid tetroxide could be pumped from one tank to the other. Between the tanks was a section of line simulating the missile downcomer into which the heat exchanger was to be placed. A gas generator was also included to deliver decomposition products through the heat exchanger. It was expected that all operating parameters would be determined explicitly so that a high degree of confidence on the exchanger operation in the actual missile would exist.

d. Heat exchanger-hydrazine decomposition products to helium. The design of a heat exchanger to warm the helium pressurizing the oxidizer tank was somewhat difficult since the helium temperature could be expected to change continuously as the helium tanks blew down. The heat-exchanger design conditions were assumed as follows: Initial inlet temperature of helium, 80°F, minimum helium inlet temperature during operation, —130°F. This value was arrived at by assuming some heat pickup by the helium before it arrived at the heat exchanger. The maximum helium discharge temperature at the start of operation was assumed to be 200°F. Based upon these conditions, a simple design consisting of two concentric tubes consisting of a central $\frac{3}{8}$-in.-diameter, 0.025-in. wall thickness containing the hydrazine decomposition gases surrounded by a $\frac{9}{16}$-in. tube 0.035 in. wall through which the helium passes. The length of tube required for the unit was estimated to be 8 in. The estimated weight of the unit was 0.3 lb. Fabrication of the heat exchanger had not been initiated at the time of termination of the program.

e. Gas-generant tank. The supply tank for the hydrazine gas generant was assumed in the system design to be spherical in shape. The total weight of gas generant was calculated to be 38.3 lb, an adequate quantity to completely void the main propellant tanks including all reserves, etc. The design operating conditions for the tank were: tank operating pressure, 550 psia, tank volume (including 4% ullage), 1110 cubic in. The tank material was assumed to be aluminum alloy with an allowable strength of 40,000 psi. The tank was estimated to have an inside diameter of 12.8-in. and to weigh 3.5 to 4.0 lb. No detailed tank designs or negotiations with tank suppliers had been undertaken at the termination of the program.

f. Helium reservoir. A separate high-pressure helium source to transfer the gas generant was required in the fuel tank pressurization circuit. A separate tank differing from the main helium supply used to pressurize the oxidizer tank was necessary since the gas generator operated at a higher chamber pressure than the main engine and consequently the helium reservoirs had to blow down to different pressure levels. The helium reservoir was for the purposes of design considered to be a spherical aluminum alloy tank. The pertinent parameters were: Tank pressure, 3000 psia, effective specific heat ratio, 1.5, tank volume, 352 cubic in., allowable strength for the material, 40,000 psi. The tank was estimated to be 8 in. in internal diameter and to weigh 4.5 to 5.0 lb. No detailed tank designs or negotiations with vendors had been undertaken at the time of the project termination.

g. Control system. The complete exploitation of the advantages of the hybrid gas generation pressurization system in comparison with the compressed helium pressurization system depends to a large extent upon the ability of the control system to maintain close tolerances between the pressures in the fuel and oxidizer tanks. The 6,000-lb-thrust stage, as it was conceived, did not possess any sort of propellant utilization system, thus the control of mixture ratio and the minimization of tank propellant residuals was solely a case of equalization of the pro-

pellant flow rates by suitable regulation of the pressurization gases in the propellant tanks. It is interesting to note that a 1-psi difference in pressure levels could mean a waste of approximately 50 lb of propellant. In the compressed helium system this close control was accomplished by utilizing a common pressure regulator to supply both tanks. In the hybrid gas generation system, the pressurizing gas sources for the fuel and oxidizer tank are separate and contain their own regulating valves. Consequently, some means must be employed, in lieu of a true propellant utilization system, to accurately maintain pressure levels between the two tanks.

A number of control systems was investigated. Of the systems considered, three were determined to possess the capabilities of being accomplished within the project time scale. One system consisted principally of supplying a close regulation system on the gas-generation system and a coarse regulation system of the oxidizer tank helium pressurization system. The pressures of both systems were compared by being routed through a pressure equalization device which was expected to maintain the oxidizer side to within $\pm$ ¼ psi to $\pm$ ½ psi of the fuel-side system. Design and fabrication of the pressure regulators and pressure equalizer was under negotiation with Robertshaw-Fulton Company at the termination of the *Juno IV* project.

The second system visualized the use of an accurately regulated gas-generation circuit but incorporating a helium pressure regulator to control the oxidizer tank pressure with the regulator dome pressure being supplied by the pressure of the liquid hydrazine in the fuel tank. This system was to be designed and fabricated by the Laboratory. Components were only in the design stage when the program was cancelled.

The third system consisted of, again, a closely related gas-generation circuit with an on-off-valve and a paralleled bypass line in the oxidizer pressurization circuit. A sensitive pressure switch was to be mounted between the tanks which would cause the on-off valve to actuate to hold the oxidizer tank in close tolerance to the fuel tank. All components of this rather simple system were available on the Laboratory but had not been used at the termination of the *Juno IV* effort.

F. Components of the 6,000-Lb-Thrust Stage

This section is devoted to a discussion of the specifications and performance requirements of a number of the components of the 6,000-lb-thrust propulsion system which are not closely associated with one of the subsystems. The main propellant valves and their actuator and the heat exchanger are not included in this discussion.

1. OXIDIZER AND FUEL FILL AND DRAIN MANUAL DISCONNECTS (1)[3] (5)

These are the fittings through which the propellants are introduced into the system. The disconnects are located at the low points in their respective circuits; the oxidizer disconnect at the inlet port to the main oxidizer valve, and the fuel disconnect at the exit manifold of the motor.

The disconnects are required to withstand 300-psi pressure and to disconnect manually without spilling more than a few drops of propellant. Relatively standard types of hydraulic disconnect couplings equipped with seals of appropriate materials were adjudged satisfactory, and nominal ½-in. tube line size was chosen.

Wiggins and Aeroquip manual disconnects were evaluated. Both withstood immersion in hydrazine for periods of several days; however, the Aeroquip disconnect became difficult to operate after the lubricant was removed, while the Wiggins disconnect was relatively unaffected.

Seal materials suitable for use in hydrazine include the neoprene, butyl, and buna formulations used for hydraulic oils and normally furnished in the disconnect fittings.

Seal materials compatible with nitrogen tetroxide are Teflon, Kel-F, Polythene, and some formulations of the fluorosilicone rubber, LS-53. The first three, while suitable for use with N_2H_4, are not elastomers, and the LS-53 is not suitable for use in N_2H_4. There is, therefore, no elastomer which can be used in both propellants.

Testing of the disconnects was not carried out to the point of equipping them with seals compatible with N_2O_4.

2. OXIDIZER AND FUEL VENT REMOTE DISCONNECTS (3) (4)

These disconnects are located at the outer shell of the vehicle near the tops of the propellant tanks. Gas displaced from the propellant tanks during the filling operation is vented through them, and they are used for

[3]Numbers in parentheses refer to component numbers on Fig. 11.

preflight prepressurization of the propellant tanks. These disconnects remain attached until the last moment before takeoff, and then are decoupled automatically or as a result of a signal from the control center. The same requirements of seal-material compatibility apply to these disconnects as to the manual disconnects discussed previously.

The Wiggins manual disconnects can be operated remotely by pulling on the outer sleeve, so that a simple cord attached to a boom which tilted back could provide automatic decoupling of these disconnects.

Wiggins and Robertshaw Fulton were actively at work designing solenoid-actuated disconnects which could be actuated from the control center. Each of these was to have a lanyard over-ride. Wiggins had not produced a final design. Robertshaw Fulton had furnished copies of their Drawing 1908-29101. The major requirements of these disconnects are:

1. Tight shutoff.
2. Light weight of part remaining with vehicle.
3. Low spillage during separation.
4. Minimum reaction force when separated.

The problem of limiting the total reaction on the vehicle when several remote disconnects are actuated simultaneously just at the instant of takeoff appears to be of great importance. Robertshaw Fulton had started construction of a fixture with which to measure disconnect reaction forces at the time the contract was cancelled.

3. ENGINE-FUEL BLEED VALVE (7)

The branch of the fuel circuit between the lower motor manifold and the fuel valve above the motor must be bled of entrapped air during the fuel filling operation. A small manually operated valve will be satisfactory for this operation. No specific supplier had been chosen.

4. PROPELLANT-TANK PRESSURIZATION VALVES (9) (10)

The tanks are pressurized through ¾-in. ball valves which mount on the tops of the tanks. These ball valves incorporate a 90 deg bend in the discharge fitting, ending in the tank mounting flange. In this manner the vertical distance occupied by the valve and its inlet line is held to a minimum. The valves must hold 300 psi and seal in both directions. The elbow on the discharge side incorporates a side outlet which leads to the vent and prepressurization remote disconnect.

Clary has submitted a proposal with Drawing No. 523504A and had started production at the time the contract was cancelled. Robertshaw Fulton had submitted preliminary proposal drawings, but was intending to make important changes before seeking final approval. Both valves incorporate actuating systems designed to operate with nitrogen gas at 1500 to 3000 psi.

5. HELIUM REGULATOR AND DOME LOADER (13) (18)

The regulator supplies nearly constant pressure gas to displace the propellant from the tanks. The flow requirement is 0.29 ft^3/sec at 250 psi while the upstream pressure blows down to 300 psi from an initial value of 3000 psi. In order to meet the trajectory and guidance requirements, it was necessary that the thrust program of the vehicle be quite reproducible and predictable, even though a moderate change in thrust from beginning to end of the cycle was permissible. An over-all limit of $\pm$ 5 psi from the nominal value, with a reproducibility at any point in the blowdown of $\pm$ 1 psi were established as regulator performance requirements. Ambient temperature limits are 40 to 90°F. The regulator is used as a main line valve; therefore the seat must hold almost leaktight against 3000 psi helium when the dome is vented. To protect against an allowable leakage of 1 cc/min, a small relief valve set at about 270 psi is installed in the line between the regulator and the tank pressurizing valves.

The regulator is controlled by a dome loader that is made to hold the dome pressure to a given value or to adjust the dome pressure so as to hold the regulated pressure or the pressure at some point in the discharge line at a given value. The lines leading into and out of the regulator are sized by the requirement for minimum system pressure drop. If the helium emerges from the heat exchanger at 0°F and 250 psi, the density is

$$\rho = \frac{P}{RT} = \frac{250 \times 144}{386 \times 460} = 0.203 \text{ lb/ft}^3$$

and the total mass flow is $W = \rho Q = 0.203 \times 0.29 =$ 0.059 lb/sec of helium.

The dynamic pressure or velocity head in a line is

$$q = \frac{1}{2} \rho V^2 \text{ or } \frac{1}{2} \frac{w^2}{\sigma A^2}$$

At the inlet to the regulator at the end of blowdown to 300 psi, the temperature will probably not be more than 0°F, corresponding to a density of 0.244 lb/ft^3. A ½-in. tube having an inside diameter of 0.402 in. and a passage area of 0.1272 in.^{2} is used at this position, and the corresponding dynamic pressure is 1.96 psi. In a similar manner the dynamic pressure in a ¾-in-diameter tube carrying the gas to the fuel tank at a flow rate of 0.160 ft^3/sec is found to be 0.089 psi.

The regulator is to have a ½-in. tube inlet, a ¾-in. tube outlet to the heat exchanger. The line splits to two parallel ¾-in. tube lines, one leading to each tank, downstream from the heat exchanger.

Clary had submitted a design and made and delivered one regulator and one dome loader. The design was adaptable to "remote" or downstream sensing, and they reported that it had operated satisfactorily in preliminary tests with nitrogen gas. No evaluation tests have been completed at JPL.

Robertshaw Fulton had submitted designs for a standard regulator and for a modified version adapted for downstream sensing. They had submitted a design for a two-stage dome-loading regulator, and discussions were in progress on the design of a dome loader which would be adaptable to downstream sensing.

6. RELIEF VALVE (16)

The relief valve between the regulator and the tank pressurizing valves was intended to take care of any slight leakage which might occur through the regulator seat. It was to be set to relieve between the operating regulated pressure and the maximum allowable tank pressure, approximately at 270 psia. Two standard models of relief valve had been ordered from Pneu-Hydro Company (two each), and Clary had promised to submit a proposal in the near future.

7. DOME-LOADER CONTROL VALVE (17)

The dome-loader control valve admits high pressure gas to the dome loader, which in turn pressurizes the dome of the main regulator, thus admitting regulated pressure helium to the lines leading to the propellant tanks. At shutoff this valve is closed, and the dome loader circuit vents down through a small bleed to the atmosphere.

This function could be performed by a combination of a normally open and a normally closed explosive valve. Ten each of normally open and normally closed CONAX explosive valves had been ordered and received.

Repeatable operation could be achieved by using a solenoid valve for this function; test-cell operations would also be facilitated. A requirement for the solenoid valve is that it be turned on and off by a short pulse of current and that it maintain its position without requiring any "holding current." This eliminates long-time current drain on the batteries of the vehicle.

No orders had been placed for solenoid valves. Possible suppliers are Robertshaw Fulton, Eckel, Graves, and Pneu-Hydro.

8. NITROGEN FILL VALVE (19)

This is to be a ¼-in.-size manually operated valve. It is used for charging the small sphere which holds the nitrogen used to actuate the tank pressurizing valves and propellant valves and to flush the fuel manifold. After the valve is closed and the fill line disconnected, the inlet port should be capped to prevent leakage.

A stock valve such as is used in high-pressure aircraft hydraulic systems, in ⅛- or ¼-in. tube size, should be satisfactory. No vendors had been contacted.

9. ACTUATOR OPENING VALVE (20) (2)

This valve admits high-pressure nitrogen to the actuating cylinders to open the tank pressurization valves and the main propellant valves. It is closed after the actuation has been accomplished, to enable the pressure in the actuating cylinders to bleed down, in preparation for the closing stroke.

A combination of normally open and normally closed explosive valves or an on-off solenoid valve which does not require continuous holding current can be used for this application, as for the dome loader valve application, but the capacity of the valve must be larger. A valve with through ports equivalent to ¼-in. tube size will probably be satisfactory. No vendor had been selected. Robertshaw Fulton, Graves, Eckel, and Pneu-Hydro are possibilities.

10. ACTUATOR CLOSING VALVE (25)

This is the same as the opening valve, but used for shutoff.

11. OXIDIZER TRIM ORIFICE (26)

This is an orifice inserted in the oxidizer line to adjust the hydraulic resistance so that the propellant mixture

ratio will be as desired. No preparations had been made beyond ensuring that the circuit and layout provided access to a straight piece of line in which the orifice and its housing could be inserted.

12. GAS-FLOW DIVIDER (29)

The helium from the regulator passes through the heat exchanger and then to a divider where the flow is split into two equal pressure streams, one going to each tank. This divider will have to be made to fit the structure and line fittings used. Nothing had been built.

13. PROPELLANT-TANK BURST DIAPHRAGMS (30) (31)

Burst diaphragm fittings with balanced opposed discharge are mounted in the lines leading from each tank. Their function is to relieve pressure buildup in the tanks if it should become excessive. The most likely cause of pressure buildup is warming of the tanks from radiation during coasting after motor operation has ceased. Such pressure buildup would be slow, and a small burst diaphragm would be sufficient. It was proposed to design and fabricate these parts at JPL.

14. GAS DIFFUSER

Pressurizing gas enters the tanks through the diffuser, which breaks up the gas stream so that it does not penetrate the liquid interface. A cylinder 3 in. long and 1 in. in diameter, with the end opposite the inlet closed and walls having 20% open area (screen) will have a very low pressure drop and will distribute the flow radially over the surface of the liquid.

G. Results of Special Tests

1. HEAT-TRANSFER MEASUREMENTS

The accurate prediction of rates of heat transfer to the walls of a rocket motor is a critical factor in the thrust-chamber design. Since insufficient experimental data were available to verify analytical prediction methods for heat-transfer rates to a motor of low contraction area ratio, it was decided to perform several tests in a heat-transfer research motor to obtain such data.

A sectionally cooled rocket motor, JPL Drawing Number J903-1238, was operated in five tests to determine local rates of heat transfer to the motor walls at a chamber pressure of 150 psia (a photograph of the motor is shown in Fig. 34). Propellants were nitrogen tetroxide and hydrazine at a mixture ratio of 0.9, and the operating

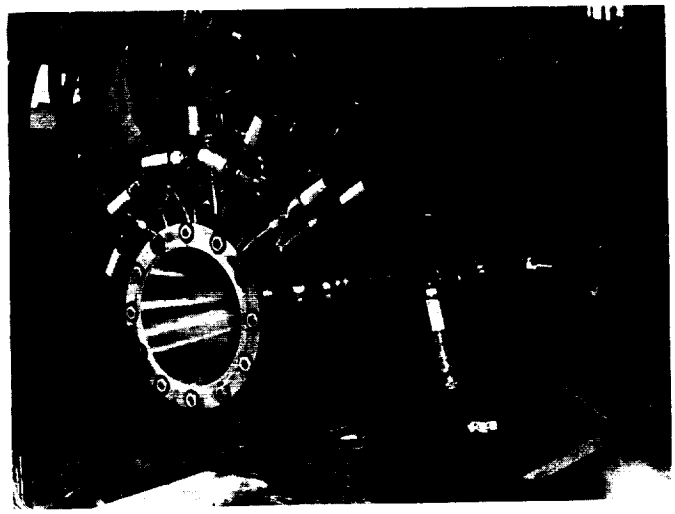

Fig. 34. Sectionally Cooled Motor

thrust level of the motor was approximately 2000 lb. The results of these tests are adaptable to the design of a flight-weight rocket motor operating under similar conditions.

The test motor consisted of ten chamber sections of 1-in. width and 16 nozzle sections of ½-in. and ¾-in. widths, with all the sections fitting tightly upon final assembly. Each section was provided with a cooling passage beneath the inner wall, a cavitating venturi flow meter, and a differential thermocouple to indicate temperature rise of the water coolant. Measurements of width and inner diameter of each section yielded the surface area exposed to the rocket gas flow, and the calorimetric measurement of enthalpy rise of the water coolant yielded the total heat-transfer rate to each section. From the surface area and total heat-transfer rate the average heat flux per unit area was calculated.

The injector installed in the test motor was a splash-plate injector with fourteen orifice pairs of fixed size and an integral uncooled splash plate, JPL Drawing No. 5-4273A. The injector was designed for higher chamber pressure, lower thrust operation, consequently it was operated at an unusually high splash-plate pressure drop under present test conditions, resulting in unusually high performance.

Chamber pressure was measured through a tap located at the nozzle entrance, using a pressure transducer gauge.

Physical dimensions of the motor were as follows: chamber diameter, 5 in ; throat diameter, 3.9 in.; nozzle exit diameter, 7.442 in., L^*, 20.4 in.; contraction area ratio, 1.64.

The duration of motor test runs was set at 8 sec, which was sufficient for thermal equilibrium of the calorimetric system. A 50-millisec oxidizer lead was provided to ensure smooth starting of the motor. The 8-sec duration was timed electrically, and the motor was shut off, automatically followed by an immediate nitrogen and water flush of the propellant lines and motor. After the shutoff, the motor was again flushed with water and inspected for damage.

Table 13 indicates the operational data obtained during the runs. The chamber pressure shown is corrected to nozzle entrance stagnation conditions.

Table 13. Operational Data Obtained During Runs 540 Through 544

Run No.	P_c, psia	r	c^*, $\frac{ft}{sec}$
540	148	0.911	5580
541	147	0.930	5620
542	149	0.929	5740
543	147	0.918	5610
544	148	1.020	5680

The high-performance level, or c*, in these tests was useful for observing the upper limit heat-transfer rates to the motor walls that might be expected. This was achieved by use of high-pressure-drop injector orifices which resulted in increased propellant stream breakup and improved combustion.

Figure 35, shows the heat-flux distribution indicated in runs 540 through 543. For comparison, the analytical prediction of heat flux for these conditions is also shown. A good agreement is seen to exist between the experimental data and the analytical prediction. Figure 36 shows the heat flux measured in run 544. These data are shown separately due to several rather significant coolant leaks which were discovered subsequent to this run, rendering the results of calorimetric measurements questionable.

Tests 540-543 show that, from a preliminary standpoint, the analytical prediction method currently in use is valid for the operating conditions considered. Additional testing of this nature is required, however, in order to verify the results indicated.

2. DIFFUSER TEST

Development of an exhaust diffuser has nearly been completed that will permit testing of the 6,000-lb-thrust

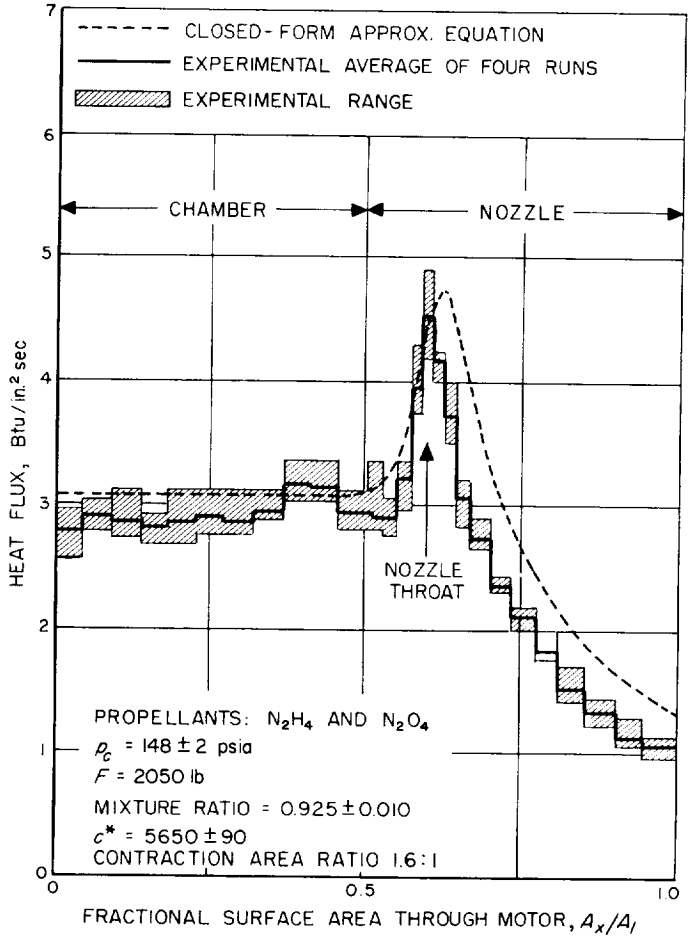

Fig. 35. Summary of Test Data for Runs 540-543 With Sectionally Cooled Motor

nozzle at ground level without separation while operating at design chamber pressure. Tests are in progress on the 1/10-scale model using N_2O_4-N_2H_4, and it is recommended that these be completed since the results have been requested by numerous individuals from the Laboratory, and other concerns as well. The configuration being used includes straight, converging, and diverging ducts similar to a wind-tunnel second throat as shown in Fig. 37. So far this arrangement has been found to give the best performance. The step at the nozzle-exit simulates a flared exit section on the full-scale nozzle created by the coolant manifold.

Results of the experiments conducted, using decomposition products of N_2H_4, are shown in Figs. 38 and 39. An N_2H_4 gas generator was used to supply the working fluid for preliminary testing, since this permitted a more rapid determination of an optimum configuration than did testing with bipropellant gases. Numerous diffuser

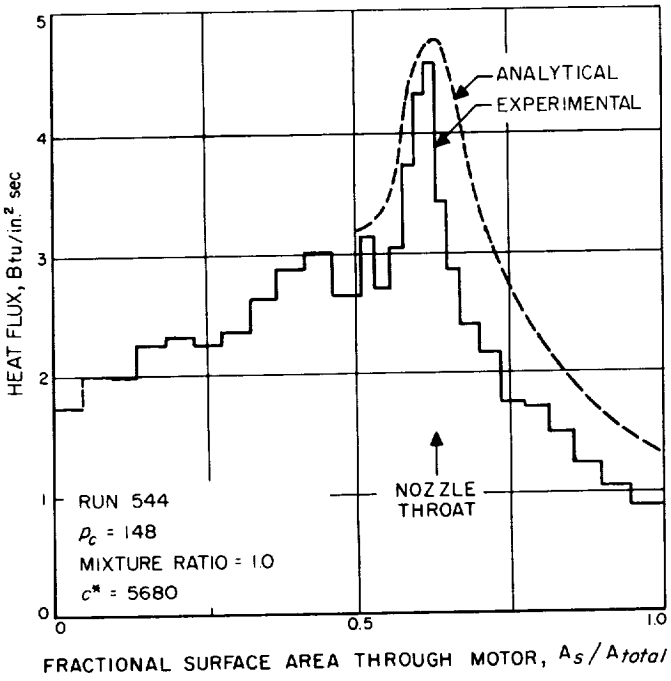

Fig. 36. Test Data for Run 554 With Sectionally Cooled Motor

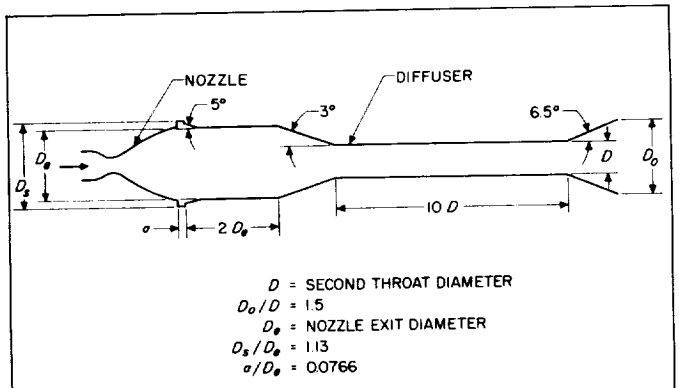

Fig. 37. Nozzle Exhaust Diffuser

arrangements were tested; however, the results shown in Figs. 38 and 39 are for the proposed design only. It should be noted in Fig. 38 that a nozzle-exit pressure of 0.7 psia was obtained at a minimum chamber pressure of 150 psia. Under these conditions the nozzle was flowing full. To arrive at this operating condition it was first necessary to swallow the normal shock through the second throat at a chamber pressure between 219 and 239 psia and then to reduce the chamber pressure to 150 psia. When the chamber pressure was reduced below 150 psia, the normal shock returned to the nozzle and the flow separated. Figure 39 shows that the minimum length of the second throat is approximately ten diameters for a minimum chamber pressure of 150 psia.

It will be necessary to try several throat diameters to find the optimum one for bipropellant operation. Second throat diameter is dependent upon a mean gas specific heat ratio which is different for the N_2O_4-N_2H_4 bipropellant gases than for the decomposed products of N_2H_4. Two second throat sizes have been tested on the bipropellant stand. The shock could not be pushed through the second throat of the smaller diameter. For the larger diameter throat, the normal shock was swallowed at a chamber pressure of 235 psia. After the minimum throat size has been established, tests should be performed in which chamber pressure is reduced during operation to determine the minimum value for a full flowing nozzle just as was done with monopropellant N_2H_4 gases.

Diffuser cooling has been accomplished by external water sprays. Although such cooling has been adequate, several hot spots have appeared along the second throat section and have moved when the location of the normal shock was changed by varying chamber pressure. To observe this condition more closely, a lucite tube will be used as an outer coolant jacket of the second throat section so that the inner diffuser tube can be submerged in a bath of water. Provisions will be made for coolant circulation, should it be required.

The full-scale diffuser has been designed as a double wall unit using water bath cooling with provisions made for forced convection cooling if found to be necessary.

3. WATER HAMMER

In conjunction with the design of the 6,000-lb-thrust engine an investigation of some hydraulic transients of its liquid feed system was carried out. The purpose of this investigation was to determine the following:

1. The increase in pressure (water-hammer) at the propellant valve as a function of valve closing time for no pressure relief, pressure relief to the gas side of the propellant tank, and dumping propellant at a programmed rate.
2. The mass of fuel that can be returned to the propellant tank by utilizing the kinetic energy of the fluid flowing in the conduits.
3. Maximum water-hammer pressure following instantaneous propellant-valve opening.

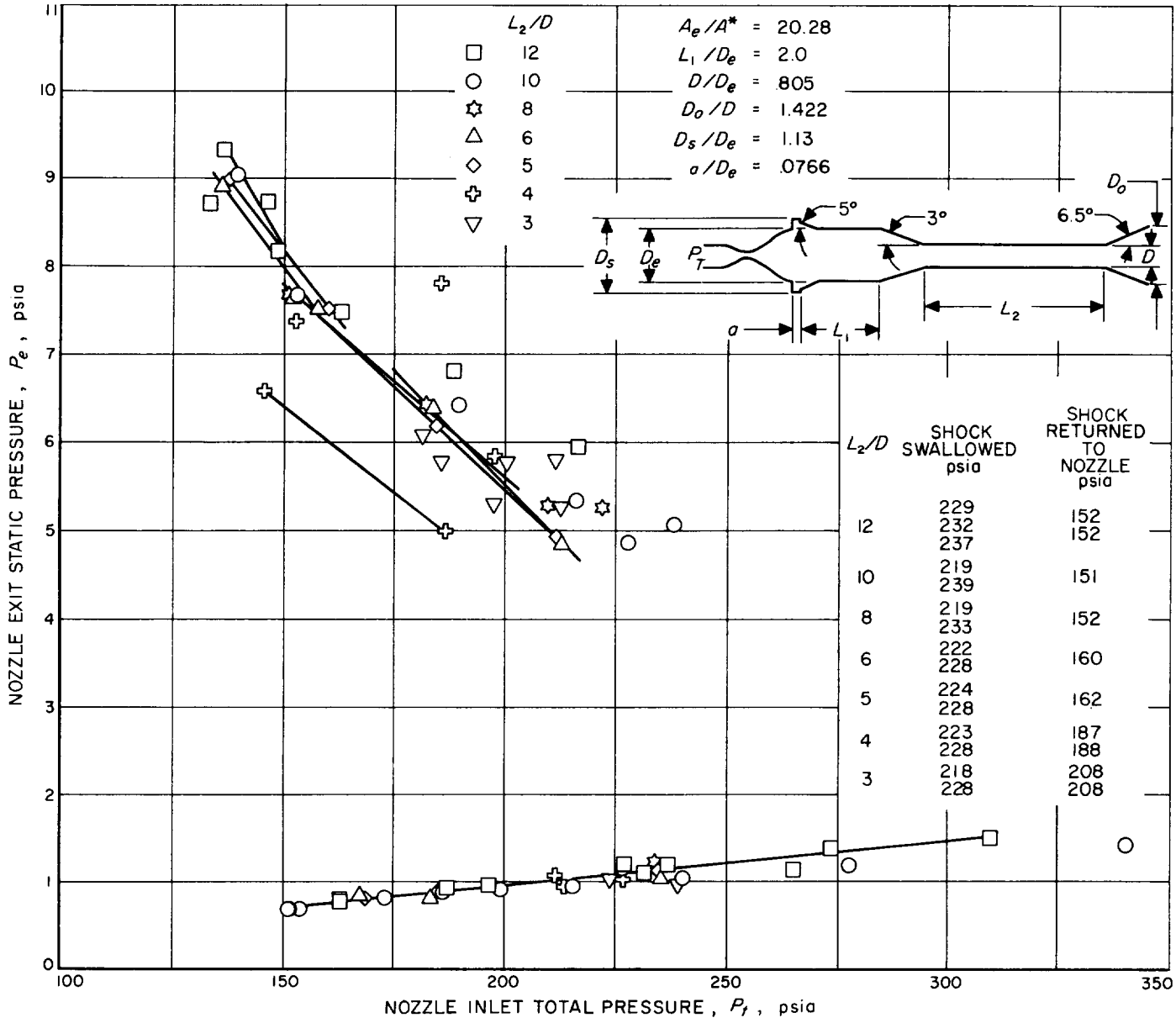

Fig. 38. Exit Diffuser Performance.

Calculations and tests for the fuel system were carried out by substituting for the compound conduits a simple conduit of equivalent hydraulic characteristics determined from the usual relations. This artifice for comparatively slow rates of valve closing is reasonably accurate; however, for rapid valve closing, and particularly those approaching instantaneous closing, there is a marked discrepancy between the magnitude of the water-hammer pressure measured and that computed for the simple equivalent system. In these cases it is necessary to make more accurate determinations, taking full account of the partial reflections at points in the conduit where the wave velocity changes.

For the oxidizer feed system no calculations or tests were carried out because this portion of the feed system had not been frozen into the design.

Results of the calculations and tests of water-hammer pressure as a function of valve closing time are shown in Fig. 40. From Fig. 40 it is seen that there is no difference between the data for no pressure relief and for pressure relief. The reason that the pressure relief valves

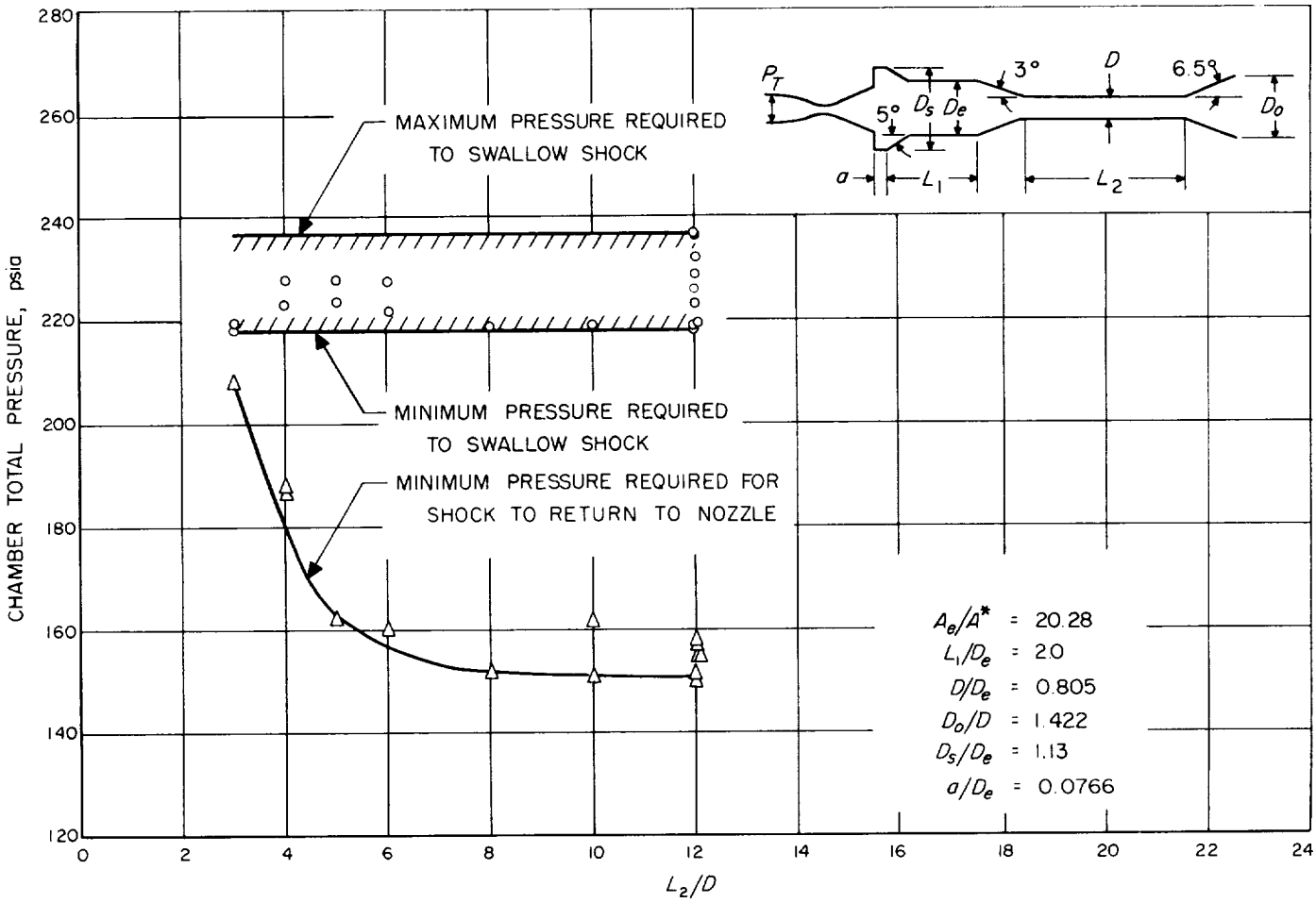

Fig. 39. Chamber Total Pressure vs L_2/D

used did not do their job was that the inertia of the valve and spring was so large that the relief valve acted as a dead-end and reflected the front of the surge wave instead of absorbing it. However, special types of surge suppressors or relief devices of low inertia characteristics can be made to relieve the water-hammer pressure. Also from Fig. 40, it is seen that dumping of propellant at a programmed rate does a good job of pressure relief.

The mass of fuel that can be returned to the tank utilizing the kinetic energy of the fluid in the fuel feed system was measured to be about ½ lb of fuel for a valve closing time of about 15 millisec. The total mass of fluid that it is possible to return to the tank is directly dependent on the valve closing time.

Maximum water-hammer pressure following instantaneous valve opening was computed to be about 14% of tank pressure. Measurements of water-hammer pressure for valve opening of four millisec agreed fairly well with that value. Additionally, the tests showed that larger values of water hammer could be obtained if the injector manifold volume was large enough so that the time required to fill this manifold would allow transient fluid velocity at the valve to be appreciably above steady-state velocity. The amount of water hammer obtained under these conditions would be the difference in velocity between steady-state flow and the maximum transient velocity of the system.

4. MONOPROPELLANT-HYDRAZINE CONTROL MOTORS

In the original concept of the 6,000-lb-thrust propulsion system consideration was given to the use of multiple, small monopropellant-hydrazine control motors to provide attitude and vernier control. Preliminary studies had indicated that such a system was competitive in weight with the alternate system of gimbaling the main engine

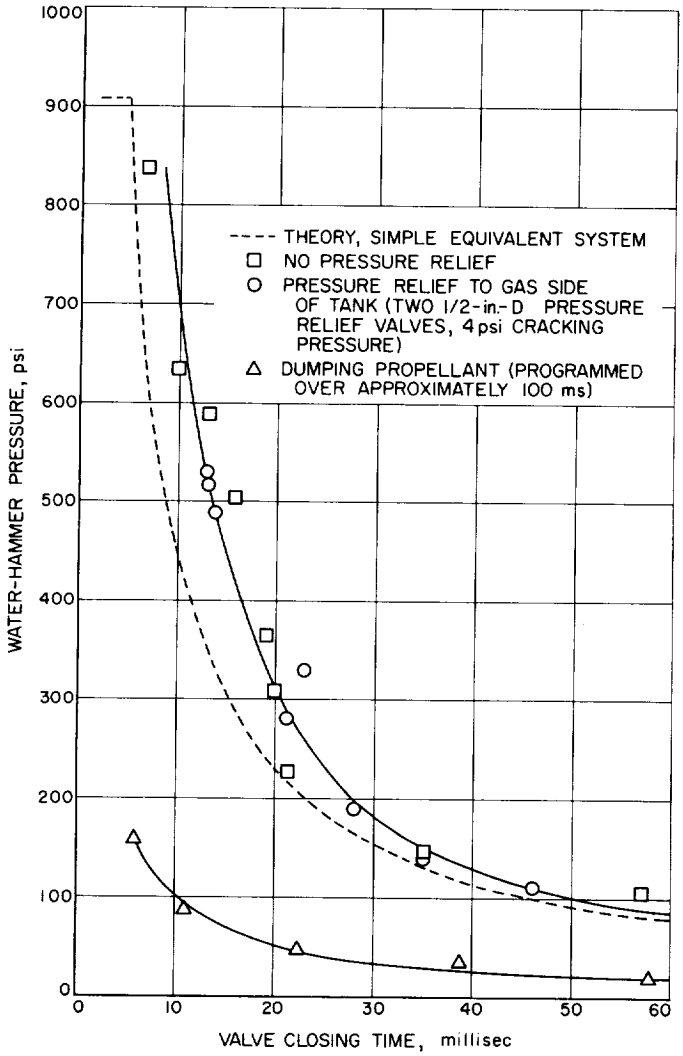

Fig. 40. Water-Hammer Pressure vs Valve Closing Time

plus the use of roll control jets. The use of monopropellant-steering motors, in addition to supplying attitude control, was expected to alleviate the anticipated problem surrounding main engine cutoff with the regenerative cooling passages full of hot hydrazine and to increase the propulsion system capabilities by improving the cooling of the main engine, furnishing very accurate velocity cutoff control, minimizing propellant holdup by allowing for monopropellant runout, and making restart in nongravity fields readily possible. Circumventing the shutdown problem was to be accomplished by supplying as feed to the monopropellant motors a portion of the regeneratively heated hydrazine from the cooling passages of the main thrust chamber.

Operationally the control motors were to be ignited slightly before the main engine, to operate concurrently with the main engine supplying attitude control, and then continue to operate for some period after main engine cutoff to allow the already regeneratively heated hydrazine in the cooling passages to be purged. The length of operation after main engine termination would be dependent upon the desire for velocity control and/or monopropellant runout. Furthermore, because the hydrazine in the main engine could be isolated from the main propellant tank by a check valve, it would be possible to restart the steering motors in a gravity free field. Operation of the steering motors for a short period of time would cause the propellants to settle to the bottom of the main tanks so that ignition of the main engine could be readily achieved. An interesting side effect is that, since the steering motors operate on hot hydrazine, an increase in their monopropellant performance could be expected.

In order to investigate the feasibility of operating a monopropellant-hydrazine motor on heated propellant, a test apparatus was constructed where the fuel to the gas generator could be preheated. The test procedure consisted of (1) igniting the monopropellant motor and operating an ambient temperature propellant until stable operation and performance data were obtained, (2) heating the propellant through the use of four dc welding machines which generated a high amperage current through an isolated section of the feed line, (3) raising the bulk temperature of the propellant in 50-deg increments from ambient to the desired operating condition, and (4) obtaining a set of performance data at each temperature level.

The operating parameters chosen for motor chamber pressure and steady-state propellant feed temperature were 100 psia and 320°F, respectively; these values were determined as being representative of the conditions which were to be encountered in a flight system. A series of seven tests was made. In this series of tests the foregoing conditions were reached with no adverse effects being encountered. Consequently, the temperature level was raised above 320°F to determine the upper limit of motor operation and whether this limit would coincide with the saturation temperature of hydrazine at the motor operating pressure. These tests demonstrated the following: (1) Decomposition of the monopropellant became more smooth as the feed temperature was raised. (2) The

characteristic exhaust velocity increased directly with the addition of heat, (There was a 7½% increase at 320°F over the ambient condition of 75°F.)/(3) Excellent operation was maintained up to the saturation temperature. When this point was reached, an explosion occurred in the injector spray jet. In these tests the saturation temperature was 383°F. The explosion occurred when the hydrazine was heated to 378.5°F.

A series of system designs was made of various control motor configurations and some experimental work was conducted. Initially it was desired that the 6,000-lb-thrust propulsion system not possess any in-flight restart capability. On this basis it was determined that a motor configuration should be selected employing type H-OU-55 hydrazine decomposition catalyst which is capable of a single spontaneous ignition. The first design study undertaken involved the use of four motors spaced at 90-deg intervals about the missile. The design parameters and motor configuration were estimated to be as follows:

$F = 90$ lb

$\overline{P}_c = 150$ psia

$c^* = 4270$ ft/sec

$I_{sp} = 234.5$ sec

$\epsilon = 50{:}1$

$\alpha = 15$ deg

$\dot{w} = 0.384$ lb/sec

catalyst = H-OU-55

catalyst bed diameter = 4.5 in.

catalyst bed length = 2.7 in.

throat diameter = 0.658 in.

nozzle exhaust diameter = 4.65 in.

weight of one complete motor (injector, injector head, body, catalyst, convergent and divergent cones, etc.) = 3.01 lb

Before any fabrication of the 90-lb thrust motor could be undertaken, it was decided that a system employing three monopropellant motors spaced at 120 deg intervals about the missile and each having a thrust level of 120 lb was more desirable. The design of the overall missile system had become more definitive by this time, and it was evident that the values chosen for certain of the operating parameters for the 90-lb thrust motors would have to be altered. The design parameters for the larger size motor were as follows:

$F = 120$ lbs

$\overline{P}_c = 112.5$ psia

$c^* = 4250$ ft/sec

$I_{sp} = 231$ sec

$\epsilon = 50{:}1$

$\alpha = 15$ deg

$\dot{w} = 0.52$ lb/sec

catalyst = H-OU-55

catalyst bed diameter = 5.5 in.

catalyst bed length = 4.3 in.

throat diameter = 0.933 in.

nozzle exhaust diameter = 6.6 in.

ΔP across catalyst bed = 18.9 psi

ΔP across injector = 92 psi

weight of one complete motor = 6.7 lb

A heavyweight version of this motor configuration was fabricated from existing parts to provide the necessary catalyst-bed dimensions, and a test program was undertaken. At the time of design of this size motor, no operating experience with H-OU-55 catalyst at flow rates greater than 0.1 lb/sec was available. The critical condition in operating chambers with H-OU-55 had been found in the past to occur during the ignition phase. In view of this it was decided to conduct a series of tests, increasing the flow rate in increments until the 0.52 lb/sec flow was obtained. A series of fifteen tests was made. No real difficulties were encountered in raising the propellant flow rate to the desired condition. A total of twelve of the tests was made at 0.52 lb/sec. Good ignition was obtained in all but one test, in which partial quenching of the reaction occurred, necessitating a shutdown.

This condition of apparently random ignition failures, which had been noted in early programs but was thought to be corrected, raised some consternation regarding the basic reliability of the system and the possible need for further catalyst development. Chronologically at this point in the program the requirement for an in-flight restart capability of the propulsion system appeared to be imminent, and this condition coupled with the reliability considerations of the H-OU-55 catalyst led to a decision to redesign the steering motors to incorporate the better-known, but nonspontaneous H-7 catalyst with an

attendant bipropellant ignition system. The design parameters for this configuration steering motor were:

$F = 120$ lb

$\overline{P_c} = 117.5$ psia

$c^* = 4250$ ft/sec

$I_{sp} = 231$ sec

$\epsilon = 50{:}1$

$\alpha = 15$ deg

$\dot{w} = 0.52$ lb/sec

catalyst = H-7

catalyst bed diameter = 3.5 in.

catalyst bed length = 3.5 in.

throat diameter = 0.933 in.

nozzle exhaust diameter = 6.6 in.

ΔP across catalyst bed = 35 psi

ΔP across injector = 76 psi

weight of each complete motor (less ignition system) = 3.5 lb

Before any fabrication or testing of this motor configuration occurred a decision was made, based on over-all system considerations and the development time schedule, to go to a gimbal system for the main engine and to employ a roll control system located with the guidance package.

H. Structural Analysis of 6K Tube Wall Motor

1. LOADS

The value arrangement on the 6K motor is just forward of the injector, and therefore the fuel manifolds and the motor tubes are subject to full tank pressure prior to firing of the motor. During boost the motor is subject to a design acceleration of 5 g in addition to the pressure in the coolant passages. Very small side accelerations exist on the nozzle during launch due to its proximity to the missile's center of gravity.

When the fuel and oxidizer valves open, the injector manifolds receive a pressure surge load before flow through the orifices becomes steady. Upon ignition, another surge occurs in the manifolds which may reach 400 psia.

The chamber pressure under steady-state firing is 150 psia, dropping to about 85 psia at the throat and diminishing rapidly along the divergent nozzle such that sea level pressure exists approximately 5 in. aft of the throat ($A/A^* = 2.2$). The exit pressure is approximately 1 psia. This pressure distribution in the thrust chamber causes a tension load in the tubes at the inlet manifold of about 2400 lb.

The thrust load is carried from the injector through the valve structure to the gimbal. In addition to this 6 kips, the gimbal will react the actuator loads; the magnitude of this reaction will be dependent on final location and magnitude of the actuator force.

Dynamic effects from firing have not been evaluated to date. Much information on these loadings will come from the static-test-firing data.

2. STRUCTURAL ANALYSIS OF COMPONENTS

The gimbal and injector support structure has not been fully analyzed. However, several features are on the current layout because of stress considerations. To achieve the rigidity required to keep a safe level of motor natural frequency and to afford support to the injector, four wing flanges are used in addition to the valve housing structure. A one-plane bolted joint between the injector and the support structure simplifies machining and also assures that no residual clamping stresses will be present in the injector. The bolted joint allows for easy removal of the valve assembly for repair or replacement of parts.

A test injector has been designed with the objective of making it as near like the flight injector as could be anticipated. Pressure surge conditions and stiffness requirements led to altering the design to eliminate flat surfaces and to utilization of the wing flange support structure as well as the valve housing to support the injector thrust loads. A proposal for structural testing the injector has been prepared.

The inlet manifold distributes fuel to the thrust chamber tubes and also transfers tension and bending loads

to the injector through a bolted joint. The tension and bending loads are transmitted through the inner portion of the manifold. The outer portion of the toroid is of circular section and is very efficient for carrying the pressure loading to which it is subjected.

The motor chamber and nozzle consists of round tubes, a design well suited for carrying the pressure loads inherent with regenerative cooling. The chamber and throat section is wrapped with high strength wire to carry the chamber pressure transferred to it through the tubes.

The ends of the wire are securely attached to the motor and the whole wrap covered with epoxy or a synthetic rubber composition to protect the wires. No braze or solder bond to the tubes is used other than near the ends of the wire.

The pressure in the divergent nozzle drops so rapidly that wire wrap is unnecessary over most of its length. Instead rings or bands are spaced approximately 4 to 6 in. apart along this portion. These rings will serve to stiffen the motor against deformation from vibration loadings, as well as to support the pressure loads by hoop tension.

During static firing at sea level, an area of the nozzle from approximately 4 to 15 in. aft of the throat will experience an internal partial vacuum condition. The pressure will vary from zero to about —10 psig, resulting in a crushing load on the nozzle. Extra rings will be attached to the nozzle in this region to support these loads during sea level firing tests. The rings will then be removed for firing tests in the diffuser.

The local reinforcement required for the actuator connection to the motor is not yet firm. If the actuator is located on the skirt, the first stiffening ring aft of the throat will be used to distribute the actuator loads to the tubes. Should the actuator be attached to the wing flange structure forward of the injector, local reinforcement of this structure will be necessary.

Actuation causes bending loads which are carried by the tubes. The magnitude of the bending stress is dependent on the actuator location and prescribed motion. However, preliminary analysis shows that the bending stress at the throat section is of the order of only 1000 psi, assuming the actuator attach point forward of the throat. The natural frequency of the motor as a beam cantilevered at the injector is about 50 cps.

The tubes are heated over the inner surface between solder joints. The gas side reaches about 800°F and the liquid side 480°F. This nonuniform heating causes thermal stresses which have yet to be evaluated.

The exit manifold design is similar to the inlet manifold. The surface to which the tubes are welded is a channel for ease of fabrication. A piece with circular section and small radius completes the manifold. Pressure stresses are low.

V. MINIMUM WEIGHT INJECTION SYSTEM

A. Introduction

The JPL light-weight guidance system was entitled MING (Miniature Injection Guidance), and its function was to provide guidance and control for the upper stage or stages of a carrier to be used for the launching of earth satellites for space vehicles.

Since the time schedule for the use of the MING system in the *Juno IV* program was relatively short, no new basic development was to be attempted. Instead, elements and techniques from the already developed *Sergeant* guidance system were to be used. Thus, the components and techniques which comprise the MING system had already reached a high level of design maturity and had been tried and proven by flight experience. Also it should be noted that, from the point of view of reliability, the environmental levels imposed by the *Sergeant* were several times higher than those anticipated in the *Juno IV* system.

The MING system was to be fully self-contained, consisting of guidance, power, telemetry, and monitoring and control circuits for ground observation and control prior to takeoff. Since no aerodynamic forces are present in the higher stages of a launching vehicle, neither a full platform nor positional control would be required for the accuracies demanded by earth satellite or space-vehicle injection. For pitch guidance there was to be a single axis platform stabilized about the pitch axis of the vehicle on which there are mounted two accelerometers plus the stabilization gyro. The accelerometers used were to be the *Sergeant* Bell accelerometers, the gyro, the *Sergeant* miniature integrating gyro (MIG), and the single axis platform, the platform used in the *Sergeant* arming device. For path control and pitch a signal from the vertical accelerometer was to be integrated once and combined with the pitch angle from a pickoff from the platform, and the elevation program was to be obtained from a program device. This technique is identical to that currently employed in the *Sergeant*. For shutoff control the output of the horizontal accelerometer was to be integrated once and compared with a constant. Another MIG was to be used for roll control and yaw control was to be accomplished by a third MIG with an integrating loop around it. Certain initial conditions were to be taken from the guidance system in the booster stage.

A complete error analysis of this system was not performed; however, it appears that the over-all system error, including those errors contributed by the booster, would be less than one-half deg in orbital inclination and would be less than 50 miles (2-σ figures) in apogee-to-perigee distance.

A weight breakdown for the MING system is given in Table 14.

Table 14. Weight Breakdown of MING System

Component	MING Weight, lb
Single Axis Platform	11.8
Gyro	0.5
Two Bell Accelerometers	4.5
Platform Structure	5.0
Preamplifiers and Demodulators	0.5
Stabilization Amplifier	1.0
Heater Circuit	0.3
Attitude Sensors	3.6
Roll and Yaw Gyros	1.0
Rate Feedback Electronic	2.0
Temperature Control	.6
Program Device	25
Leveling and Mixing	1.5
Mixing Networks (Passive)	0.5
Amplifier	1.0
Yaw Computer	2.0
Shutoff Computer	15.0
Inverting Amplifier	5.0
Integrator	8.0
Zero Detector	2.0
Elevation Computer	8.0
Autopilot Amplifier	5.5
Signal Amplifiers (3)	2.5
Actuation Amplifiers (3)	3.0
Central Power System	44
Integrated dc	12
Ac Power	10
Power Transfer Switch	2
Batteries	20
Telemetering	88
Subcarrier Assembly	14
Transducers	9
RF and Power Supply	15
Cables	29
Antenna	10
Iso-amplifiers	11
Cables	30
Monitoring and Control	10
Nose Plug	7
Switching	2
Transducers and Iso-amplifiers	1
Guidance Component Brackets	5
Total Weight	249.4

B. Systems Analysis

The *Juno IVA* MING miniature Injection Guidance system was designed to inject a satellite into a nearly circular orbit with an apogee-to-perigee distance not to exceed 50 miles. In the *Juno IVA* MING system, information regarding the spatial behavior of the vehicle was to be obtained from a stabilized single-axis platform and a pair of yaw and roll gyros. The single-axis platform consists of a miniature integrating gyro (MIG) for maintaining stability and of two orthogonal accelerometers. The stabilized axis of the platform was to be so aligned with the pitch axis of the vehicle that the two accelerometers would be space stabilized in the trajectory plane. Roll and yaw maneuvers would displace the accelerometers slightly from the guidance plane but would not contribute any significant error.

Acceleration data from the accelerometers on the platform are fed into a guidance computer which is a linear, analog device. One portion of the computer is used to calculate a shutoff command for the second stage, whereas another portion of the computer provides pitch commands to the autopilot. In addition, signals from the platform and the two gyros regarding the attitude of the missile are fed to the autopilot. The MING system is activated shortly before burnout of the first stage by a guidance command from the first stage. The platform is initially aligned on the ground before firing and is uncaged at launch.

The MING system operates by constraining the vehicle to follow a precalculated path in space. Path guidance is accomplished by continuously comparing guidance signals with a stored precalculated program and nulling the resulting error. In azimuth, the vehicle is guided by gyro control only. Because of the lack of external forces acting on the vehicle, satisfactory guidance normal to the flight plane is possible without recourse to an additional space-stabilized accelerometer. To reduce the effects of thrust misalignments, integral control is employed in azimuth.

1. TRAJECTORIES AND PATH GUIDANCE ANALYSIS

A set of trajectory and guidance equations for *Juno* second stage has been simulated on the IBM 704 digital computer. The trajectory equations were limited to two dimensions and assumed a spherical, nonrotating earth. The guidance equations included pitch-angle control, "pitch" P velocity control, and shutoff velocity S control. Trajectory analysis involved selecting the standard trajectory and determining the noncritical P and critical S directions. In addition, pitch-gyro orientation for minimum gyro drift was determined. The definitions of these directions and the criteria under which they are determined are given in the following paragraphs.

The initial conditions for the second-stage standard trajectory were found by interpolating between sets of first-stage burnout conditions obtained from the Army Ballistic Missile Agency (ABMA). Several sets of interpolated initial conditions were inserted into the second-stage trajectory program and trial computations made until the desired injection conditions were obtained. The desired injection conditions are (1) vertical component of velocity equals zero, (2) altitude between 250 and 300 miles, and (3) speed as required for circular orbit. Plots of trajectory coordinates are shown in Figs. 41 through 44.

Upon obtaining the unguided standard trajectory, the guidance equations were inserted. These equations are as follows:

for path guidance

$$X = \bar{X} + k_2 (\dot{P}_m - \dot{P}_{ms}) \tag{1}$$

for shutoff control

$$V = -\dot{S}_m(t) + \dot{S}_m(t_f) \tag{2}$$

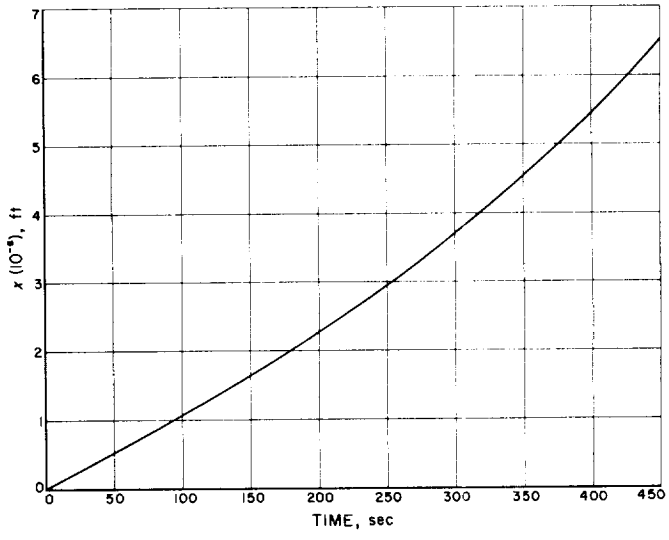

Fig. 41. Ground Range vs Time

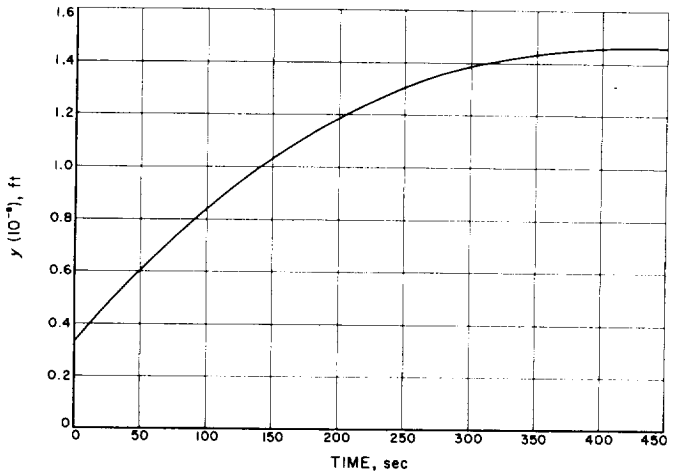

Fig. 42. Altitude vs Time.

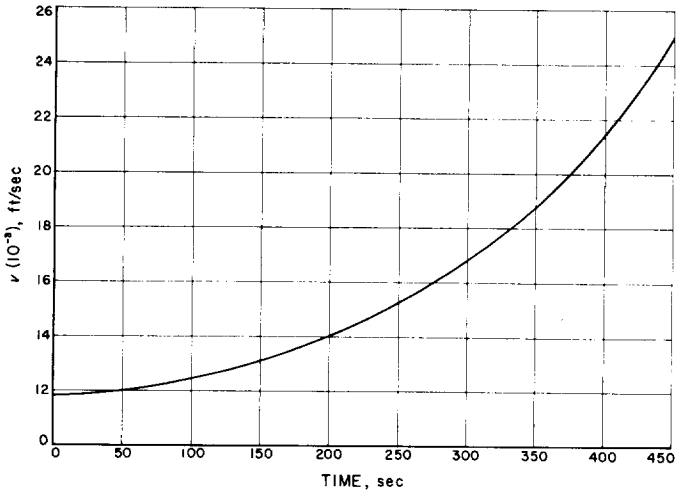

Fig. 43. Speed vs Time.

where

χ = body pitch angle referenced to local horizontal at second-stage ignition.

$\bar{\chi}$ = standard value of χ

k_2 = gain parameter

$\dot{P}_m$ = measured velocity in the $\dot{P}$ direction

$\dot{P}_{ms}$ = standard value of $\dot{P}_m$

V = output of shutoff computer; shutoff when $V = 0$

$\dot{S}_m(t)$ = measured velocity in S or critical, direction

$\dot{S}_m(t_1)$ = measured critical velocity at standard injection

The angles σ_p and σ_s define the P and S directions relative to the local horizontal at second-stage ignition. (See Fig. 45). The directions P and S are those into which the sensed accelerations are resolved in order to obtain guidance-error signals for path and shutoff control. These directions are determined by minimizing the coordinate errors at injection caused by motor performance during flight. The motor-performance errors considered were 1%

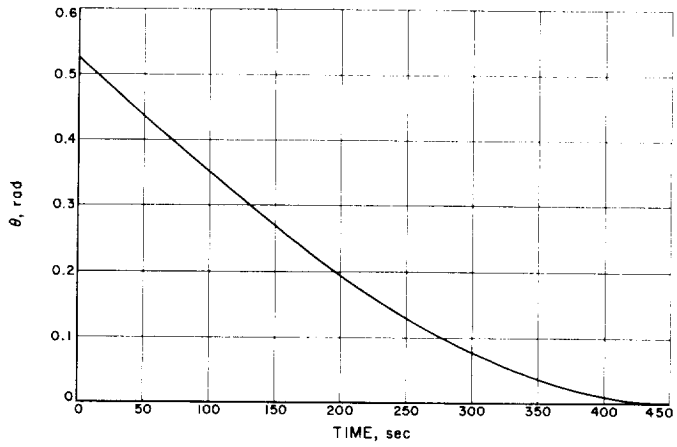

Fig. 44. Velocity Angle vs Time

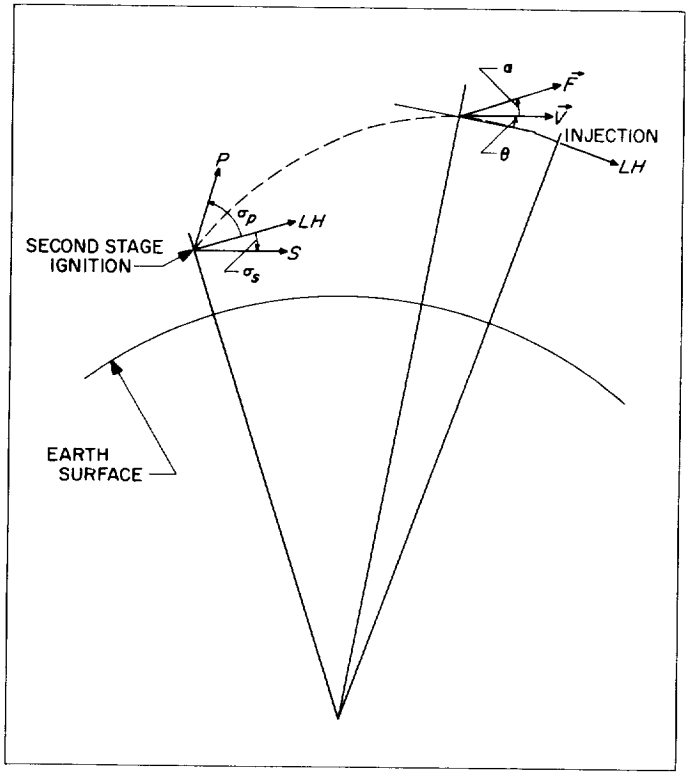

Fig. 45. Trajectory Coordinates

specific impulse and 1% flow-rate deviations. Figures 46 and 47 show the variation of errors at injection due to variation in the P and S directions. For the S direction, the minimum rms error in eccentricity of the orbit occurs at $\sigma_s = -6.3$ deg. For the P direction, the minimum error in path angle (there is a one-to-one correspondence of path angle and eccentricity errors) is a $\sigma_p = 64$ deg.

The pitch gyro orientation angle σ_g is determined by minimizing the following integral with respect to σ_g

$$D_T = K \int_0^{t_{co}} \frac{F}{m} \cos(\chi - \sigma_g)\, dt \qquad (3)$$

where D_T is the total-drift angle accumulated during burning. It was necessary to minimize D_T over both first-stage and second-stage burning since the gyro is uncaged at launch. The angle σ_g is measured counterclockwise from the horizontal at launch. For $\sigma_g = 115$ deg, D_T equals zero along the standard trajectory.

2. SHUTOFF SYSTEM

A functional diagram of the shutoff is presented in Fig. 48. A more detailed mechanization is shown in Fig. 49.

Two orthogonal accelerometers are space stabilized in the flight plane at an angle θ_L above the local horizontal at the launcher as shown in the diagram on Fig. 49. The outputs of these two accelerometers are resolved so as to yield an acceleration $\ddot{S}$ in the critical direction chosen to calculate shutoff. The resolved output of the critical mixing network is given by

$$\ddot{S}_m = \ddot{S} + g \sin\left(\sigma_s + \frac{x}{r_0}\right)$$

where σ_s is the angle of the critical direction above the local horizontal at launch, g is the magnitude of the gravity acceleration, and x/r_0 is a measure of the change in direction of the gravity vector due to a change in ground range x of the vehicle.

A constant, $\dot{S}_m(t_I)$, is installed as an initial condition on the shutoff integrator. This constant is determined from the standard trajectory and is inserted by a procedure of automatic calibration in which the component of gravity in the *noncritical* direction is integrated for a specified length of time while the vehicle is on the launcher. The output of the integrator is first nulled,

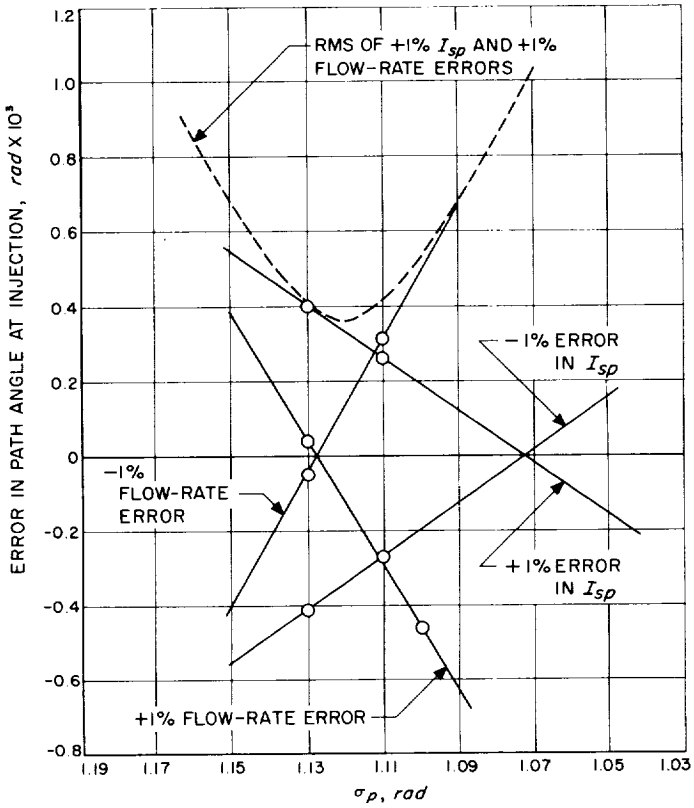

Fig. 46. Path-Angle Errors vs Elevation Guidance Direction

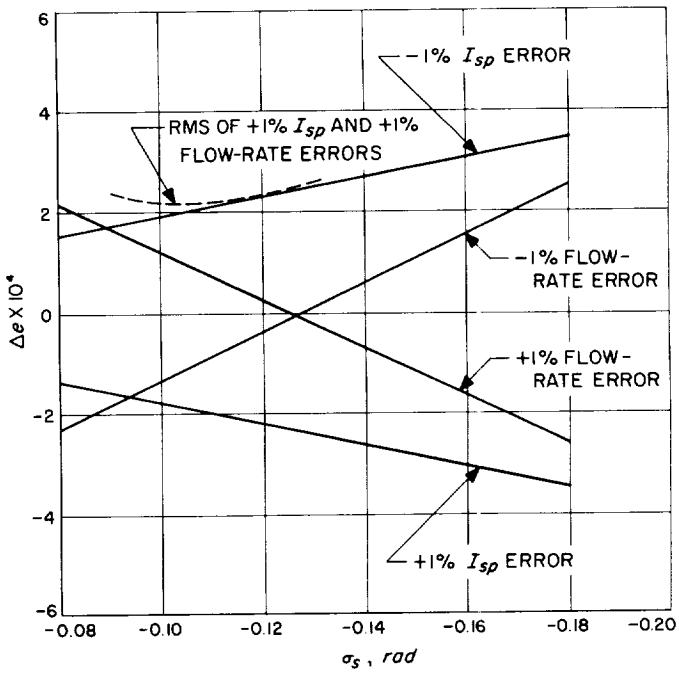

Fig. 47. Error in Eccentricity vs Critical Direction

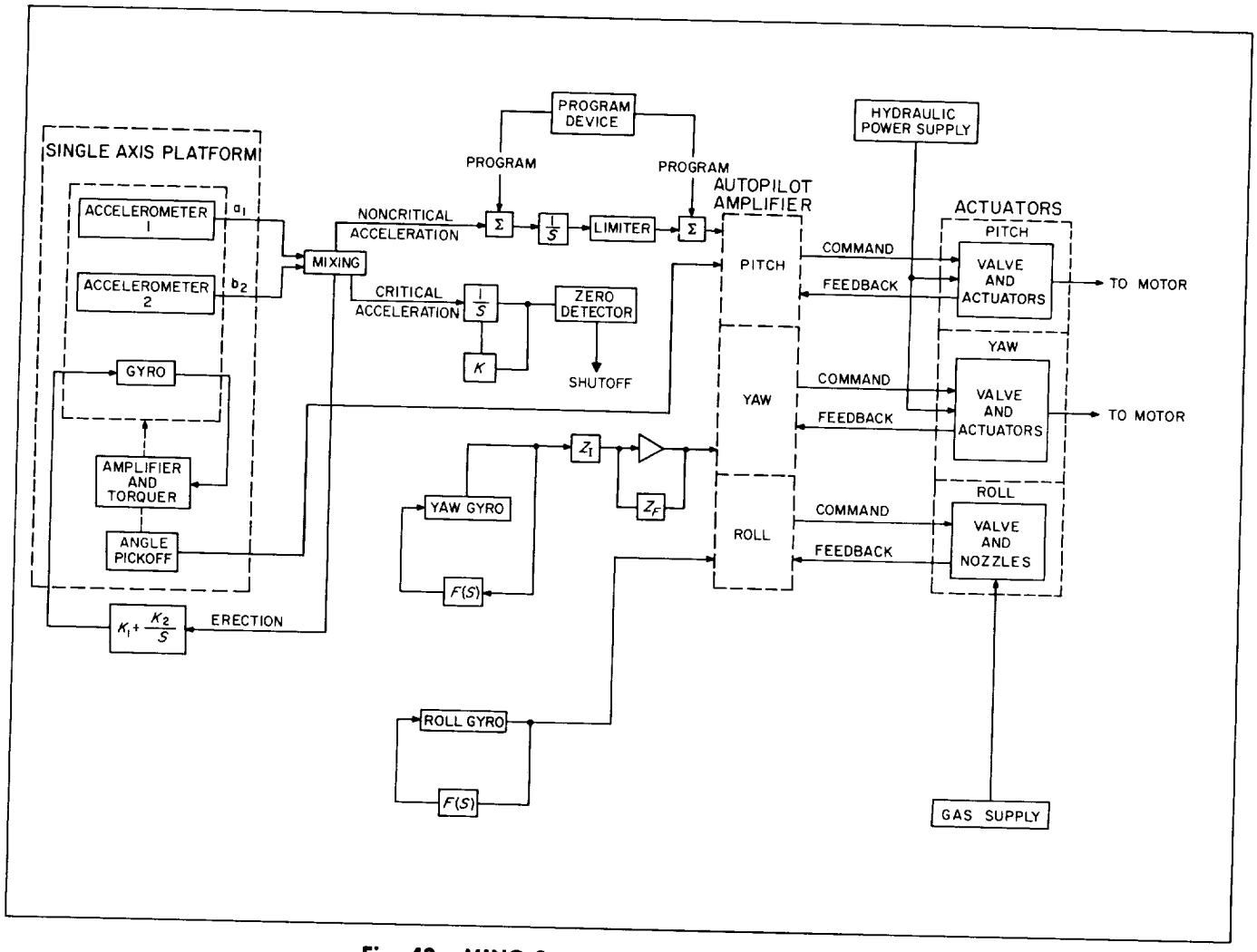

Fig. 48. MING System Functional Block Diagram

and then the critical component of gravity is applied to the first integrator for a period of time which is determined by dividing the shutoff constant $\dot{S}_m(t_I)$ by the sensed noncritical component of gravity at the launcher, $g \cos \sigma_s$. A typical value of calibration time is 600 sec. Any scale-factor error common to either the accelerometers, the mixing network, or the integrator is thus cancelled out. The exact sequence for the calibration and flight procedure is evident from observation of the mechanization diagram (Fig. 49). Since the sensed critical acceleration on the launcher is small, it is necessary to use the noncritical component of gravity for calibration in order to keep the calibration time short.

If the platform is erected to the desired angle by some means not dependent upon the accelerometers, an injection error is produced which is dependent upon the scale-factor difference, ΔK, between the accelerometers. By using the accelerometers to erect the platform in pitch in conjunction with the automatic calibration technique and by maintaining a particular relationship between the erection angle θ_L of the accelerometers with the local horizontal and the desired critical angle σ_s it is possible to eliminate the effects of first-order errors resulting from scale-factor differences between accelerometers. The effect of a scale-factor difference, then, is to slightly misalign the accelerometers in pitch. By making the erection angle obey the relationship $2\,\theta_L = \sigma_s + 90$ deg, the result of the above two effects, i.e., scale-factor difference and accelerometer misalignment, of course, will be to exactly cancel each other. A scale-factor difference between accelerometers will cause a scale-factor error in the shutoff system; however, this error is nulled by the

autocalibration. The effects of the elevation guidance system do require the accelerometers to have a scale-factor accuracy of a few tenths of a percent, however.

The shutoff first integrator integrates the in-flight accelerations so as to obtain the sensed velocity in the critical direction, $\dot{S}_m(t)$. A zero detector following the integrator detects when the integrated in-flight sensed velocity has reached a predetermined value, and at that time sends a shutoff command to the rocket motor. Figures 50 and 51 are graphs of the critical sensed acceleration $\ddot{S}_m(t)$ and of the critical sensed velocity $\dot{S}_m(t)$ as functions of time. A list of normalized accuracy requirements is shown in Table 15 for the shutoff system. The accuracies required are those which must be met such that that particular error would contribute approximately a 2-mile apogee-to-perigee error. The errors are divided into two categories, absolute errors and stability errors. Since some of the errors are cancelled or partially cancelled during the automatic calibration procedure, the effects of the errors will be different depending upon whether the error is present continuously (absolute errors) or whether the error appears after the calibration procedure (stability errors).

3. ELEVATION GUIDANCE SYSTEM

The second-stage vehicle is guided in pitch by a combination of attitude and guidance commands from the inertial guidance system. The guidance commands are proportional to inertial velocity deviations measured in a preset direction designated as the P direction in space. (See Figs. 48 and 49.)

The elevation guidance system consists of the two orthogonal accelerometers on the platform, an elevation-mixing network which resolves the two accelerometer outputs into the P direction, an elevation integrator, and a limiter following the integrator. The elevation program is composed of two parts. The first part of the program is basically the standard value of the sensed elevation guidance acceleration $\ddot{P}_{ms}(t)$, and the second part is the standard value of the inertial pitch angle $\bar{\chi}$ of the vehicle. The standard $\ddot{P}_{ms}(t)$ program plus the measured elevation acceleration $\ddot{P}_m(t)$ from the elevation-mixing network is fed into the elevation integrator where the signals are integrated to form an estimate of the velocity deviation in the elevation guidance direction. This velocity deviation is passed through a limiter (which is set to limit at approximately 20 ft/sec) to the autopilot where it is mixed with the pitch angle deviations to form the pitch command to the gimballed motor.

A major problem arises in the elevation guidance system because the MING system is required to function prior to booster cutoff. A large unpredictable velocity error occurs by allowing the first-stage rocket motor to burn to fuel depletion rather than by terminating the thrust at a predetermined command. To accept this perturbation, the elevation system measures the applied acceleration between the time the guidance command is sent to the second-stage MING system and the time of separation. The resulting integrated acceleration is compared with the standard value and is stored on the elevation integrator at separation. Before being stored, the velocity deviation is increased by approximately 30% so that the value stored on the elevation integrator represents about 1⅓ times the actual velocity deviation. This increase is necessary because the sensitivity of injection angle to elevation velocity perturbation is greatest at booster cutoff. The actual mechanization of the preliminary storage of the velocity deviations simply involves a change in gain of the elevation-mixing network at the time of separation.

A limiter following the integrator is provided because velocity deviations of the order of 400 ft/sec are expected at the initiation of second-stage guidance. Since a ratio of elevation-velocity gain to pitch-angle gain of approximately 0.005 rad/ft/sec is employed, a 400 ft/sec velocity error would call for an immediate pitch of the missile of approximately 2 rad or 120 deg in the absence of a limiter. In order to limit pitching of the missile, a limiter following the elevation integrator is included which slowly cancels any large velocity deviation, resulting in less severe requirements on the autopilot. A limit of 20 ft/sec results in a pitching of 0.1 rad, or about 6 deg. A velocity deviation of 400 ft/sec results in approximately 250 sec of limiting before the velocity deviation is nulled.

Figures 52 and 53 are graphs of the measured standard values of acceleration and velocity in the elevation-guidance direction. Figure 54 is a graph of the inertial pitch angle $\bar{\chi}$ of the vehicle. The direction in space in which the elevation guidance system was aligned was chosen so as to minimize the effects of second-stage motor-performance variations on the path angle at injection. The elevation guidance computer as presently

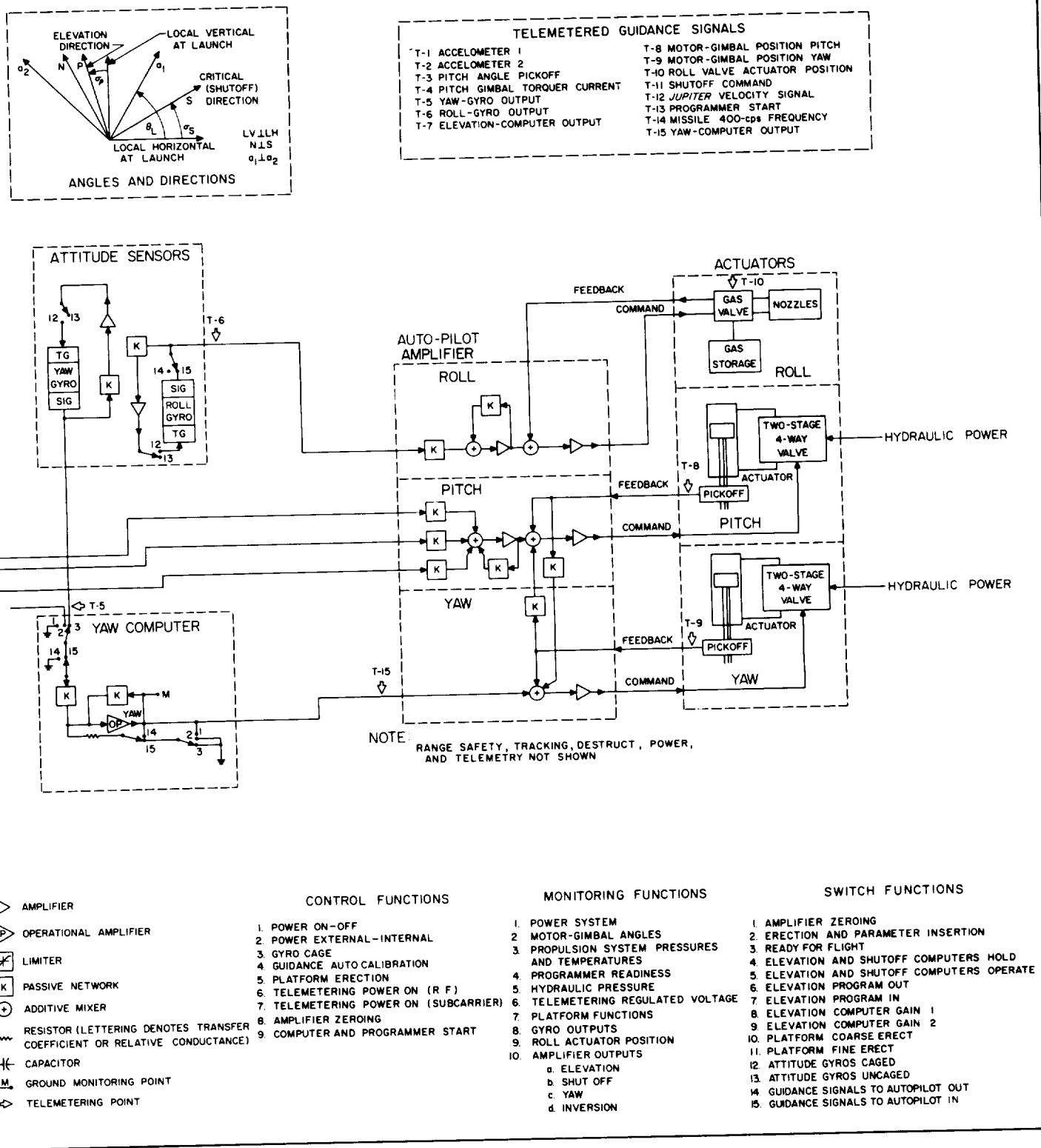

Fig. 49. MING System Mechanization Block Diagram

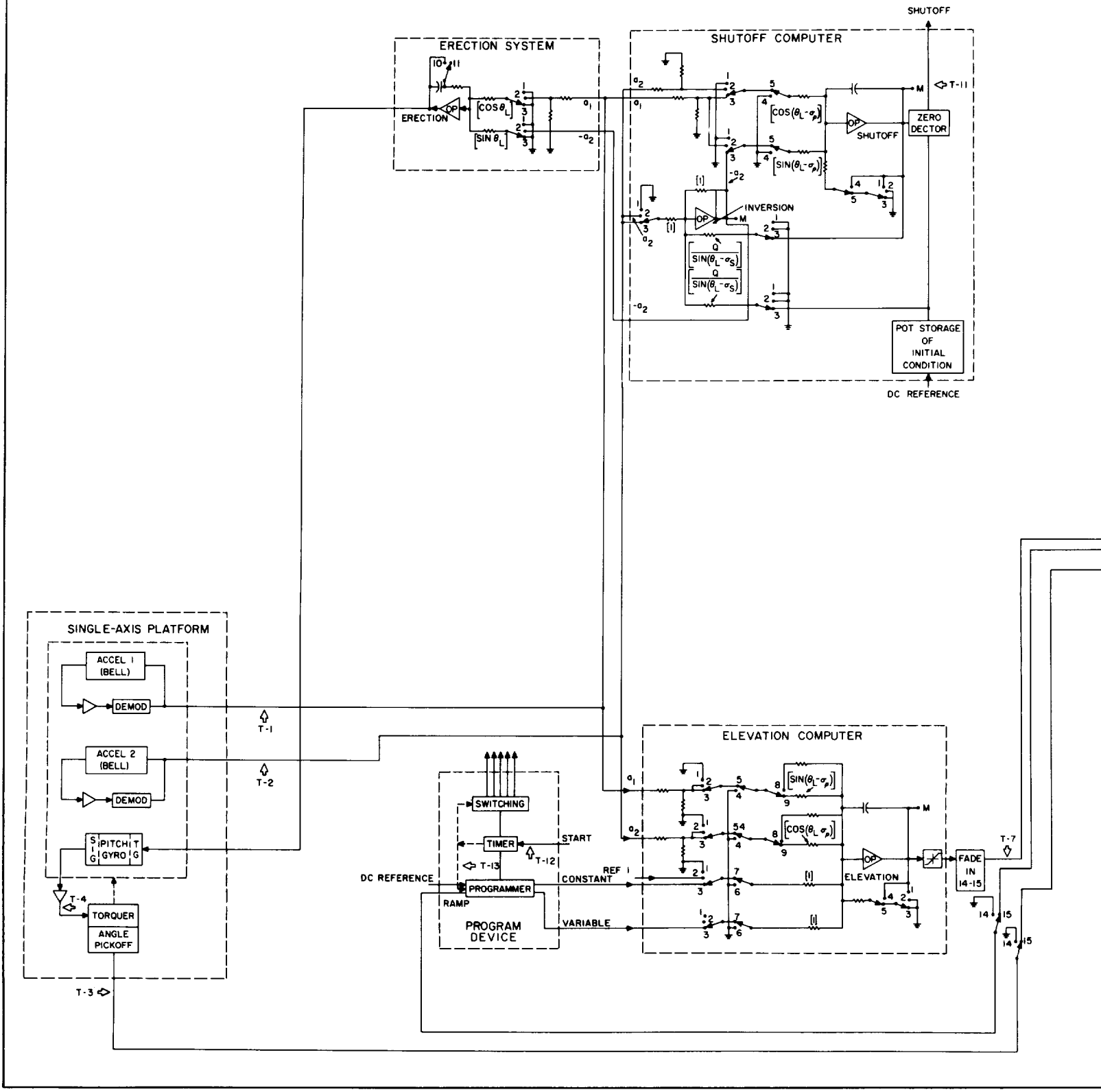

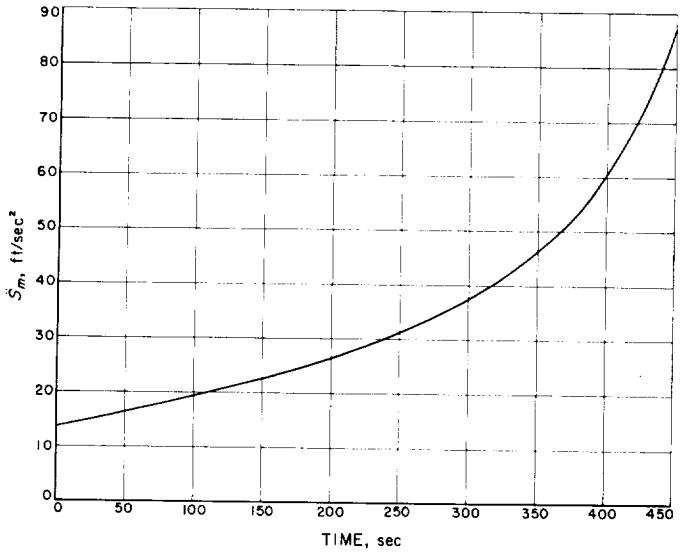

Fig. 50. Critical Sensed Acceleration vs Time

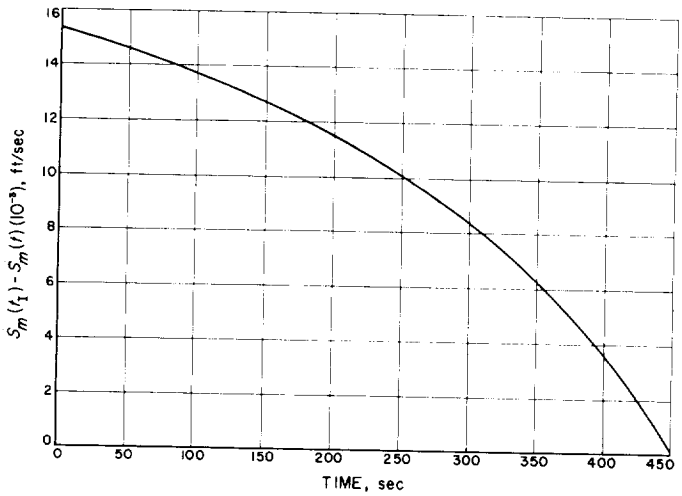

Fig. 51. Critical Sensed Velocity vs Time

proposed would result in a guidance accuracy of approximately $\pm 1\frac{1}{4}$ mil at injection for the path-angle error; approximately a 10-mile apogee-to-perigee error. Some of the normalized accuracy requirements for errors which would produce a 2-mile apogee-to-perigee error are noted in Table 16.

4. GUIDANCE PROGRAM

The elevation program contains the information defining the standard values of body-pitch angle and measurable velocities in the elevation-guidance direction. The method of introducing the program information into the guidance system is shown in Fig. 48.

Table 15. Shutoff System Error Coefficients for a Two-Mile Apogee-to-Perigee Error

Source of Error	Absolute Errors	Stability Errors
Accelerometers		
Null shift (a_1)	8.4×10^{-4} g	3.4×10^{-4} g
Null shift (a_2)	1.4×10^{-4} g	2.4×10^{-4} g
Scale factor (a_1)	None[1]	0.04%
Scale factor (a_2)	None[1]	0.04%
Critical mixing network	0.66% (ratio)	0.04%
Sign inversion	0.04%	0.04%
Integrator		
Null shift	24×10^{-4} g	2×10^{-4} g
Scale factor	none	0.02%
Calibration	0.10 sec	0.02%
Zero detector	3 ft/sec or 30 millisec delay	

[1]There are absolute accuracy requirements for the two accelerometers; however, these accuracy requirements are dictated by the elevation guidance system and are listed in Table 16.

Table 16. Elevation Guidance Error Coefficients for a Two-Mile Apogee-to-Perigee Error

Source of Error	Accuracy
Accelerometers	
Scale factor (a_1), %	0.06
Scale factor (a_2), %	0.08
Elevation mixing network, %	0.06
Elevation integrator	
Null shift, g	4×10^{-4}
Scale factor	none

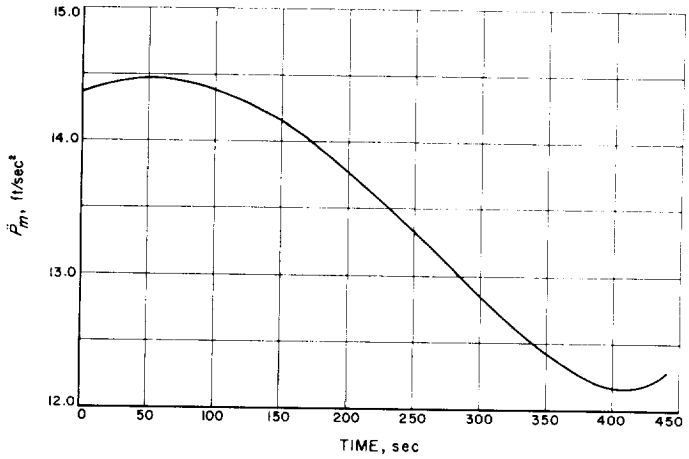

Fig. 52. Elevation Acceleration vs Time

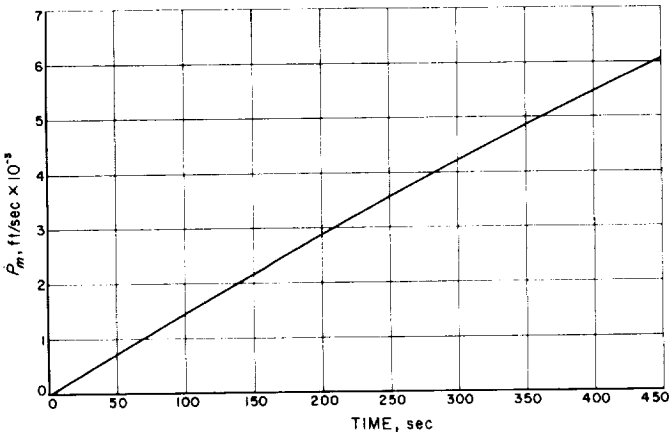

Fig. 53. Plot of P_m vs Time.

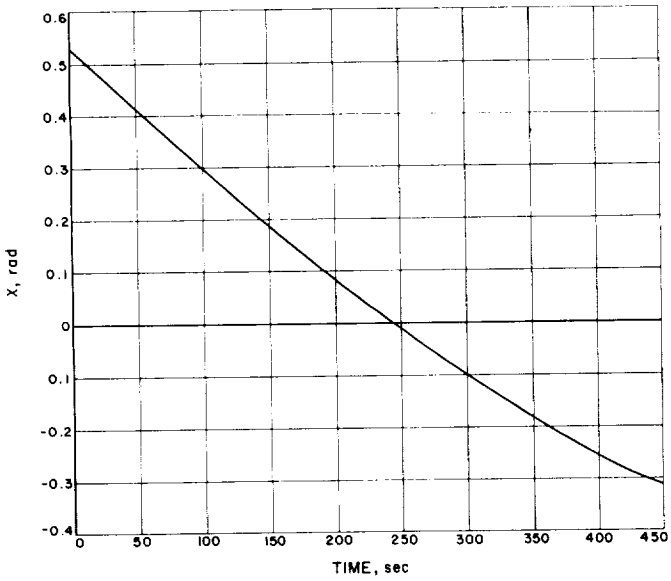

Fig. 54. Inertial Pitch Angle vs Time.

Because the output of the elevation integrator may be limited during the first portion of the trajectory, it is necessary to introduce the pitch-angle program directly into the autopilot during this period; this is the function of the signal shown in Fig. 48 at the right-hand side of the program device. The possibility of limiting also indicates that the standard value of measurable acceleration should be mixed with the actual measured value at the input to the integrator.

Mechanization of the program device and accuracy requirements on its components are eased without seriously compromising vehicle accuracy if the angle program following the limiter is a simple ramp signal that closely approximates the standard angle during the portion of flight when limiting is expected. The program information that is mixed with the noncritical acceleration is the sum of the standard value of this acceleration and the difference between the slope of the standard pitch angle and the slope of the ramp approximation that is introduced following the limiter.[4] For a typical trajectory, the acceleration program is the sum of a constant equal to about 12.4 ft/sec^2 and a nonlinear function of time that varies between 0 and 2 ft/sec^2. The accuracy requirements of program-device components are eased if the constant and variable portions of the acceleration program are generated separately. The latter portion is approximated in twelve steps each of 0.2-ft/sec^2 increments. Computations show that such a program is satisfactory from both guidance and control points of view.

The chronology summarized in Table 17 describes the events leading to separation and ignition of the MING stage when used in conjunction with the Jupiter as preceding stage. (In Table 17 events having the same number occur simultaneously.)

5. ERECTION SYSTEM

The erection system serves to orient the stable platform within the guidance plane. Signals representing misalignment from platform-mounted sensing elements (accelerometers) are received by the erection system, where they are operated upon and fed to the pitch gyro to cause appropriate torquing of the gimbal for nulling the misalignment. The erection system must be capable of aligning the platform to the specified accuracy and of maintaining the accuracy of the output signals throughout flight after the input signals have been disconnected.

If the accelerometers are to be erected to an angle of θ_L with the local horizontal, the accelerometer outputs are mixed so as to produce the horizontal acceleration at the launcher, which, of course, should be zero. The purpose of the erection system is to ensure that the mixed output signal from the accelerometers is zero when the erection procedure is complete. The torque signal fed to the gyro consists of the mixed accelerometer signal and its first integral. The output signal of the integrator at the end of the erection procedure should be proportional to constant platform drifts, including the earth's rate. This signal must remain relatively stable during the time from takeoff until the end of the flight.

[4] Errors may be reduced slightly if the difference in slopes is introduced only after the end of the period when limiting is expected.

Table 17. Sequence of Events at Separation From First Stage

Timing Sec	Event	Description
1.5 ±1.5[1]	1	1a signal sent from preceding stage indicating that a prescribed velocity has been reached. This signal is sent at the earliest time at which cutoff resulting from fuel depletion might occur.
		1b elevation and shutoff computers started with inputs from accelerometers only.
0.7	2	2 motor cutoff commanded as a result of fuel depletion.
0.2	3	3a signal sent from preceding stage indicating that its thrust has dropped to 10% of full value.
		3b ignition of MING-guided stage commanded.
		3c elevation program started and connected to elevation computer.
		3d Autopilot input fade-in begun.
0.04	4	4a thrust buildup begins.
		4b separation begins.
0.5 – 0.75[2]	5	5 thrust buildup complete.
	6	6a separation complete as exit plane of nozzle clears supporting structure of preceding stage.
		6b autopilot fade-in complete.

[1]Duration varies with motor performance
[2]Exact duration not yet determined

Of the several sources of error, the most prominent are mixing network errors and integrator stability errors. Normalized accuracy requirements are shown Table 18 for errors which would cause a 2-mile apogee-to-perigee error.

6. CONTROL SYSTEM

a. Introduction. Vehicle attitude stabilization would be a simple matter but for two characteristics of the upper stage: The main motor nozzle is swiveled to accomplish guidance and control, and the propellants are liquids. Both of these characteristics involve the movement of mass relative to the main airframe and must be included in a comprehensive stability analysis. Since the ignition of the upper stage occurs above any significant atmosphere, aerodynamic effects on stability are negligible.

Table 18. Erection Error Coefficients (for Two-Mile Apogee-Perigee Error)

Source of Error	Error
Erection mixing network	0 16%
Integrator drift (equivalent)	0.2 deg/hr or 1% of full scale per hour.

b. General considerations. The propellant mass which is considered to be sloshing (fundamental mode only) at midpowered flight of the upper stage consists of about 28% of the total mass at that time. The natural frequencies of the propellants at this time are between 0.6 and 0.7 cps. Midpowered flight is considered to be near the most critical time for stability.

The low propellant frequencies and the small amount of damping which is characteristic of sloshing propellants represent a potential stability problem. The propellant frequencies are in the same range as the vehicle natural frequency. It was decided to keep the vehicle undamped natural frequency in the vicinity of 0.5 cps and to attempt to stabilize the vehicle by means of propellant damping. Artificial damping by means of tank baffles or other methods can be used to augment natural damping.

Studies of the *Juno IVA* configuration indicate that this method of solution is adequate and that the vehicle can be stabilized for typical damping ratios obtained by means of tank baffles. The assumption of zero damping of the propellants gives an unstable vehicle, and this instability cannot be removed by any type of attitude control.

c. Summary of analysis. The stability analysis consisted of two methods of attack, a root-locus study and an analog-computer study. Spring-mass models representing the fundamental sloshing modes in each tank were supplied by the JPL structures groups, and thus the analysis problem considered in this section primarily involves dynamics investigations.

Both methods of attack included the effects of nozzle inertia. The analog-computer study simulated an actuator with torque output, whereas the root-locus study assumed a positioning actuator (infinite torque). Both studies were frozen-time investigations.

In the analog-computer study, step-function inputs to the autopilot were used to disturb the configuration at midpowered flight. The stability of the system was observed as a function of propellant damping. For zero propellant damping an unstable root with a damping ratio of — 0.019 to — 0.024 (time constant of 8 to 10 sec) was observed. Using the same control gains, the root-locus approach yielded a damping ratio of — 0.024. Propellant damping was added in the analog study, and neutral stability of the root in question was obtained with a propellant damping ratio of about + 0.02. A response obtained when the propellant damping was increased to + 0.05 appeared satisfactory.

A slight destabilizing effect was observed when Coulomb friction was added to the nozzle gimbal joint. This effect is not considered a significant problem, but requires further investigation. Attitude integral control has practically no effect on the stability of the root in question. The nozzle inertia also has very little effect on stability.

d. Control system. A block diagram of the *Juno IVA* control system is shown in Figure 55. Note that the system contains one platform and two gyros. The platform is a pitch single-axis device, which is used in the elevation guidance scheme and also supplies pitch angle. The two gyros for roll and yaw are single-degree-of-freedom, rate-integrating gyros which supply roll and yaw angles. Proposed mechanization for the compensation transfer functions makes use of operational amplifiers. Integral control in the yaw compensation appears to nullify the effects of yaw thrust misalignments and thus to maintain adequate path control. Integral control is not required in pitch, since elevation guidance is used.

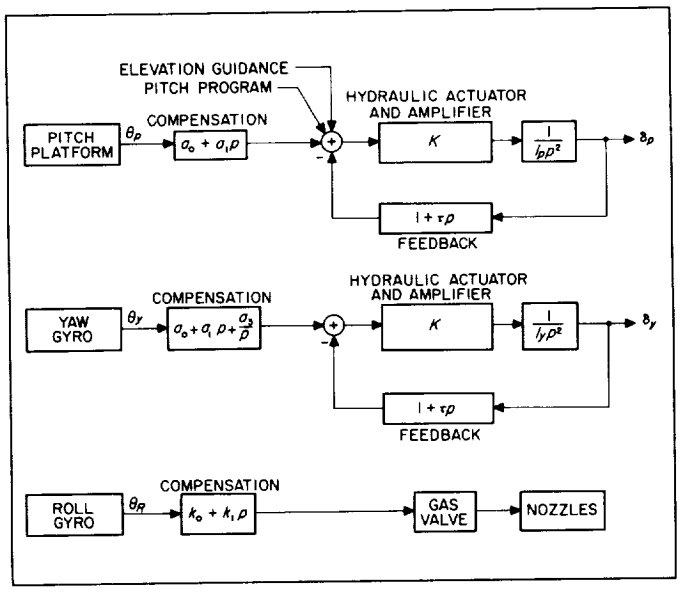

Fig. 55. Block Diagram of *Juno IVA* Control System

The following definitions of quantities are given for use in conjunction with Fig. 55.

θ_p = *pitch angles* δ_p = nozzle angle — pitch
θ_y = yaw angle; δ_y = nozzle angle — yaw
θ_R = roll angle
a_0, a_1, a_3, k_1, k_0 = control gains
a_0 = 1.0 deg/deg
a_1 = 0.45 deg/(deg/sec)
a_3 = 0.45 deg/(deg/sec)
K = gain factor for actuator and electronics 560 ft-lb/deg
τ = nozzle rate feedback time constant 0.032 sec
I_p, I_y = moments of inertia of motor nozzle about gimbal point (pitch and yaw, respectively)
$I_p = I_y = 32.5$ slug — ft²

The gains, K and τ, were chosen to give the actuator loop an undamped natural frequency of 5 cps and a damping ratio of 0.5. The control gains a_0, a_1, and a_3 give the vehicle an undamped natural frequency, which may vary between 0.4 and 0.6 cps, and a damping ratio, which may vary between 0.5 and 1.0 during upper-stage burning.

e. Conclusions. It is thus concluded that the *Juno IVA* second stage can be adequately stabilized if the damping of the propellants is 0.05 or greater. It would appear that some simple baffles would be required to achieve 0.05 damping.

C. Systems Development

1. PLATFORM.

(1) *Gyro Modification.* Roll and yaw sensing for the MING system is provided by modified single-axis gyros in a body-fixed application. The gyro selected was the Minneapolis-Honeywell miniature integrating gyro (MIG), which, because of its high internal fluid damping, provides low-frequency proportionality between input-

and output-axis displacements. The transformation ratio (output-axis displacement/input-axis displacement) of the present MIG is 6 to 1, with mechanical stops on the output axis of ±3 deg.

For the body-fixed application, the MIG was modified to allow a larger input-axis displacement by changing the stops on the output axis to ±7.7 deg (see Figs. 56 and 57) and by increasing the fluid viscosity for a transformation ratio of 3.5 to 1. The use of higher density fluid required increased temperature for neutral bouyancy. To ascertain this temperature, tests were conducted on the modified gyro after complete assembly. Although the tests could not show the exact condition of neutral bouyancy because of the minimum sensitivity to slight changes of temperature, operating temperature has been raised to 194°F ± 2. Normal operating temperature is 180°F ± 5. Gyro fluid filling procedure required changes to provide for the higher operating temperature.

Figure 56 shows one of the four milled-out sections of the MIG case. This process provided more freedom for the spin-motor flex leads and was necessary because of the increase in angular rotation of the gimbal from 3.0 to 7.7 deg.

Figure 57 shows the baffle plate to which the flex leads are soldered to the four short terminals. The two oblong holes directly opposite each other near the center determine the stop position. These were enlarged to provide for the increase in angular rotation. The four triangle shaped slots were also enlarged to accommodate the increase in angular rotation. The diameter of this plate is ¾ in.

Because of requirements for lower drift of the MIG, rework of the gyro included work to reduce mass unbalance and fixed-torque drift. Random short- and long-term variations in torque appear to be within allowable tolerances.

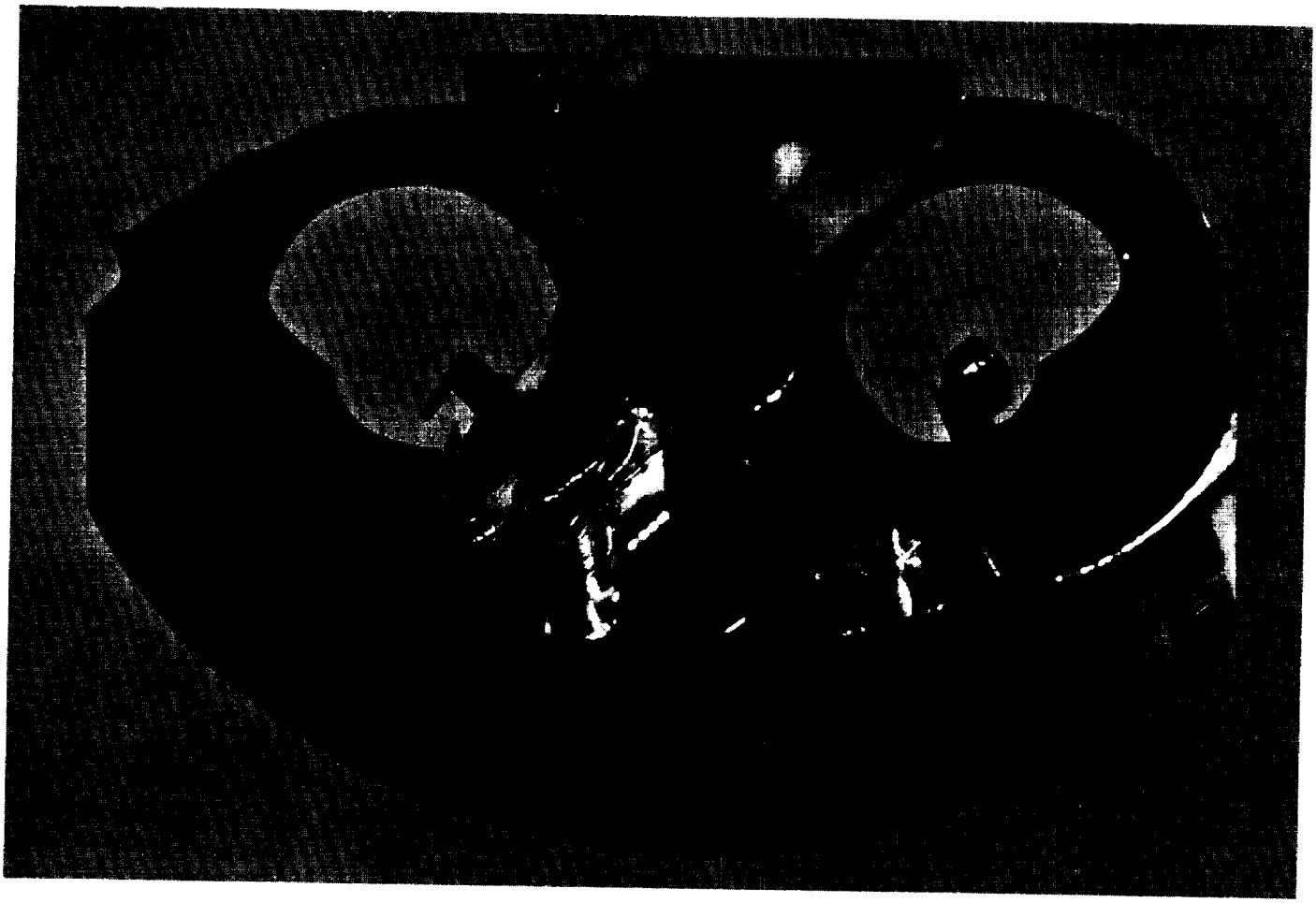

Fig. 56. MIG Case End Cap and Dualsyn Mount

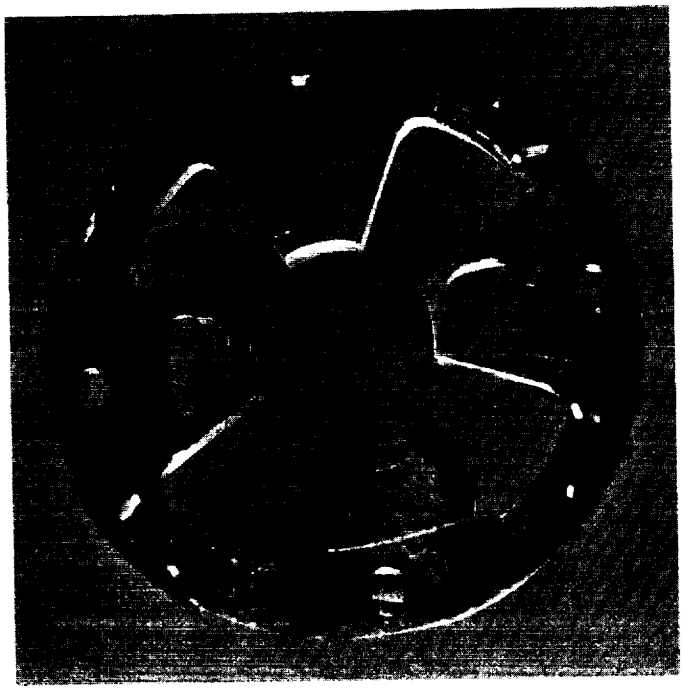

Fig. 57. MIG Baffle Plate

Electrical reaction torques within the dualsyn were to be reduced by reducing concentricity errors between the dualsyn rotor on the float and the dualsyn stator attached to the case. They should both be concentric with the precession-axis pivot and jewel. Measurement of these nonconcentricities has begun, and a fixture must be designed for radial adjustment of the dualsyn.

Reduction of mass unbalance required a more sensitive location of the balance weights. A special fixture has been designed and fabricated to detect extremely small motions of the gold-tab weights, thereby reducing mass unbalance drift to less than 0.2 deg/h/g.

Other features of the gyro which cause drift in a body-fixed system application are under investigation. In one instance, it is found that torques on the precession axis, caused by motion about the input axis, are approximately 20 deg/h/rad/sec. This must be expanded upon to determine the effective drift with a random velocity input to the gyro. Figures of drift due to noncommutativity of the single-axis gyro and drift due to cross-coupling motion must also be investigated.

(2) *Single-Axis Platform.* For guidance in the plane of the trajectory a single-axis platform is used, stabilizing about the pitch axis. Mounted on the pitch platform are two Bell Aircraft Company force-balance accelerometers for sensing linear accelerations in the pitch plane. These accelerometers generate guidance signals in order to control elevation and velocity of the vehicle. A standard MIG with improvements for reducing mass unbalance and reaction torques provides angular reference.

Figure 58 shows the *Juno IV* inertial package. The single-axis platform and two body-fixed gyros provide a self-contained set of reference coordinates, which tends to relieve the mounting tolerances for the inertial package, but at the expense of additional cross-coupling instability for the system. The entire system is approximately the size of an 8-in. cube.

2. COMPUTER.

(1) *Operational Description.* The MING computer performs three separate computing functions and provides a polarity reversal of the a_2 accelerometer signal for use in the erection of the single-degree-of-freedom platform. The computing functions performed by the guidance computer are motor shutoff computation, elevation guidance computation, and yaw-angle control computation.

The orientation of the pitch accelerometers is shown in Fig. 59, and a block diagram of the MING computer in Fig. 60. The shutoff computer mixes and integrates voltages proportional to the accelerations in the a_1 and a_2 directions to produce a voltage proportional to the velocity in the S direction, $\dot{S}_m(t)$. The $\dot{S}_m(t)$ voltage is then compared with a voltage proportional to V_0; when the sum of the $\dot{S}_m(t)$ and the V_0 voltages produces a null, the zero detector sends a motor shutoff command to the motor-control system.

The elevation-computer mixes and integrates the program voltage, the a_1 accelerometer voltage, and the a_2 accelerometer voltage. (See Fig. 60.) The elevation computer output and a voltage proportional to the measured pitch angle, $\chi(t)$, are mixed in the autopilot pitch amplifier to produce a pitch amplifier output signal porportional to

$$\left\{k_2\,[\dot{P}_m(t) - \dot{P}_{ms}(t)] + [\chi(t) - \chi(t)]\right\}$$

The autopilot maneuvers the missile in a manner that tends to null the pitch-amplifier output signal. By maneuvering the missile to maintain the null at the pitch amplifier output during controlled flight, the autopilot constrains the missile to fly the standard trajectory. The yaw computer operates on a yaw gyro signal that is proportional to the missile yaw angle. The yaw computer

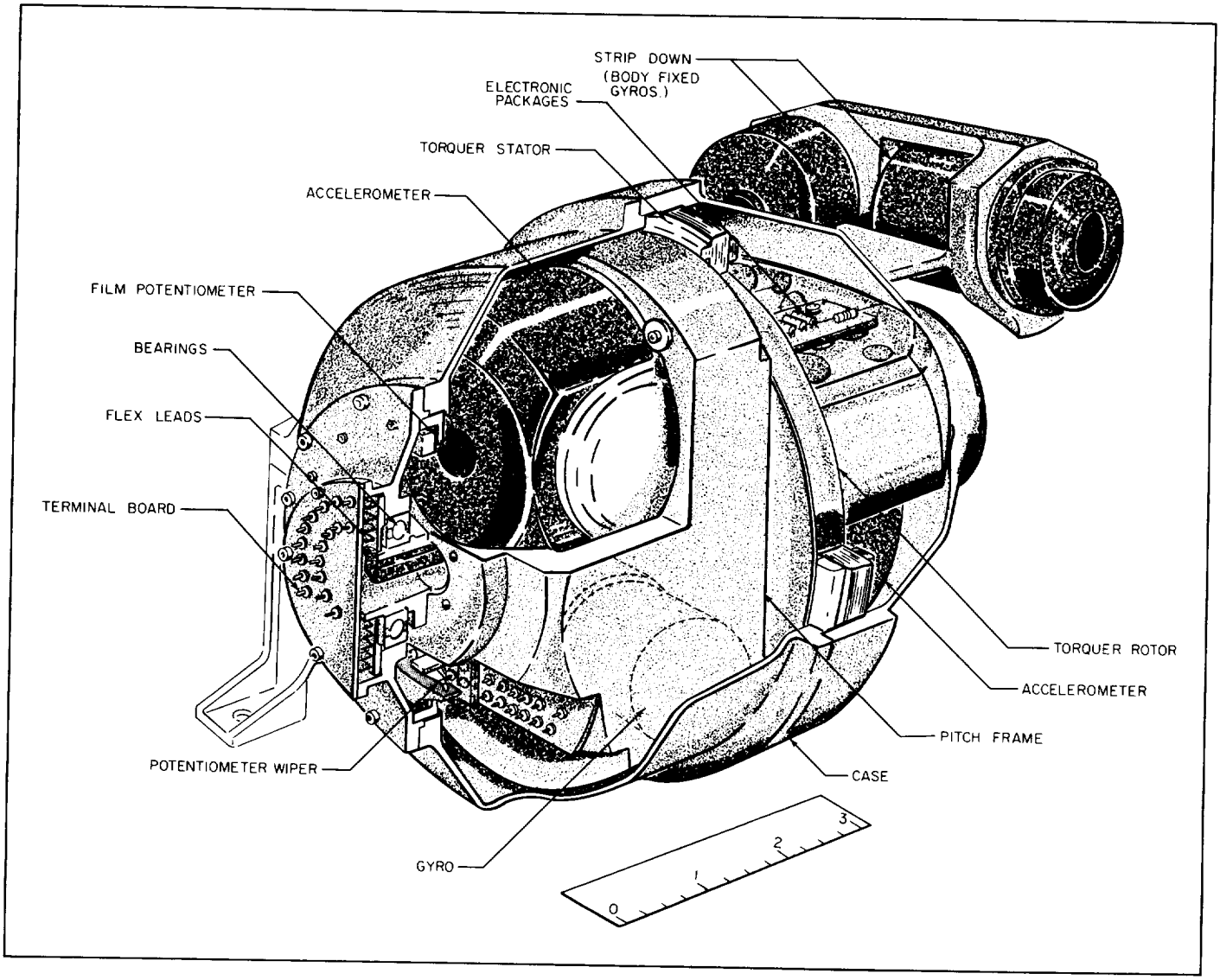

Fig. 58. *Juno IV* Inertial Package

output is supplied to the autopilot yaw amplifier. The autopilot maneuvers the missile to null the yaw angle. The transfer function of the yaw computer has not yet been specified.

(2) *Equipment Description.* An analog computer utilizing chopper-stabilized operational amplifier techniques has been proposed for the mechanization of the MING guidance computer. (See Fig. 61.)

Four operational amplifiers are required for the computer. The operational amplifier circuit is the same as that used in the *Sergeant* guidance computer and is capable of providing a maximum dc gain of 20×10^6. Under ideal conditions, i.e., several hours warmup, it has been possible to zero the *Sergeant* operational amplifiers to within ± 15 microv. A schematic diagram of the proposed operational amplifier circuit is shown in Fig. 62, and the operational amplifier packaged for full flight use in the *Sergeant* system is shown in Fig. 63.

The operational amplifiers are zeroed in the proposed system by a remotely controlled semi-automatic zeroing system. The zeroing system consists of one zeroing potentiometer and one miniature electric clutch per amplifier, a high-gain servo amplifier, and a size-10 servo gearmotor. The zeroing system is shown schematically in Fig. 61 and a schematic diagram of the high-gain servo amplifier is presented in Fig. 64. A flight version of a

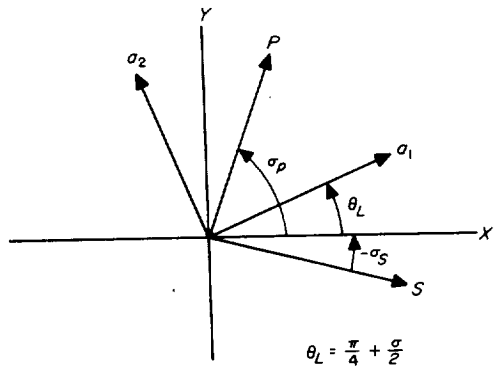

a_1 = direction of accelerometer 1 orientation

$\ddot{a}_1(t)$ = measured acceleration in the a_1 direction

a_2 = direction of accelerometer 2 orientation (a_1 and a_2 are orthogonal)

$\ddot{a}_2(t)$ = measured acceleration in the a_2 direction

k_2 = ratio of elevation guidance gain to pitch angle gain, equal to 0.005 rad/ft/sec

P = direction of elevation computation, elevation guidance direction

$\ddot{P}_{ms}(t)$ = measured acceleration in the P direction on the standard trajectory

$\ddot{P}_m(t)$ = measured acceleration in the P direction

S = direction of shutoff computation, critical direction

Fig. 59. Coordinate System of Pitch Accelerometers

similar zeroing system used to zero eight operational amplifiers is shown in Fig. 65.

A vacuum-tube relay amplifier can be utilized to accomplish the zero detection required in the shutoff computer. A schematic diagram of the proposed zero detector is shown in Fig. 66. The relay amplifier proposed has been packaged for flight in a configuration similar to that shown in Fig. 63. The sensitivity of the relay amplifier measured at the summing junction is 2 mv.

The V_0 initial condition voltage required in the shutoff computer is inserted into the zero detector from a reference potentiometer. (See Fig. 61.) In order to eliminate the effects of absolute-scale-factor errors between the $\dot{S}_m(t_s)$ and V_0 voltages, a semi-automatic calibration system is required to set the V_0 voltage on the potentiometer.

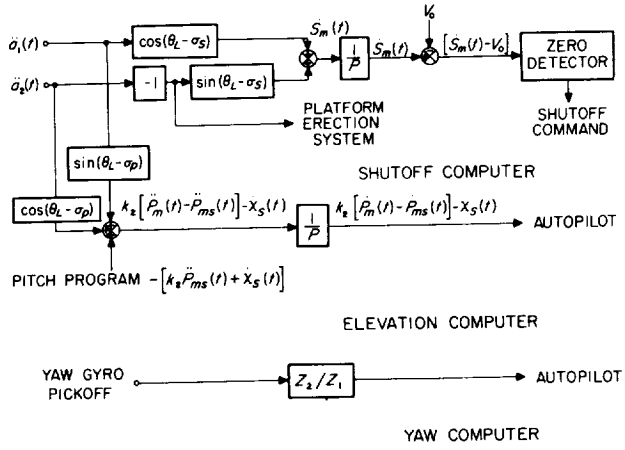

$\dot{S}_m(t)$ = measured velocity in the S direction

$\ddot{S}_m(t)$ = measured acceleration in the S direction

V_0 = measured velocity in the S direction on the standard trajectory at standard shutoff time $\dot{S}_{ms}(t_s)$

X,Y = earth referenced coordinate axes

θ_L = erection angle (angle between a_1 and the local horizontal at the launcher)

σ_s = critical angle (angle between S and the local horizontal at the launcher)

σ_p = angle between P and the local horizontal at the launcher

$\dot{\bar{\chi}}(t)$ = measured pitch-angle rate on the standard trajectory

$\bar{\chi}(t)$ = measured pitch angle on the standard trajectory

Fig. 60. Block Diagram of Elevation Computer

Voltage V_0 is set up by integrating the gravitational acceleration component in the N direction (see Fig. 59) for a period of time calculated to produce a voltage proportional to V_0 on the integrator capacitor. The voltage on the capacitor is then used as a reference input signal for a voltage transfer servo which sets the reference potentiometer. The voltage set on the reference potentiometer is of equal magnitude and of opposite polarity to the capacitor calibration voltage.

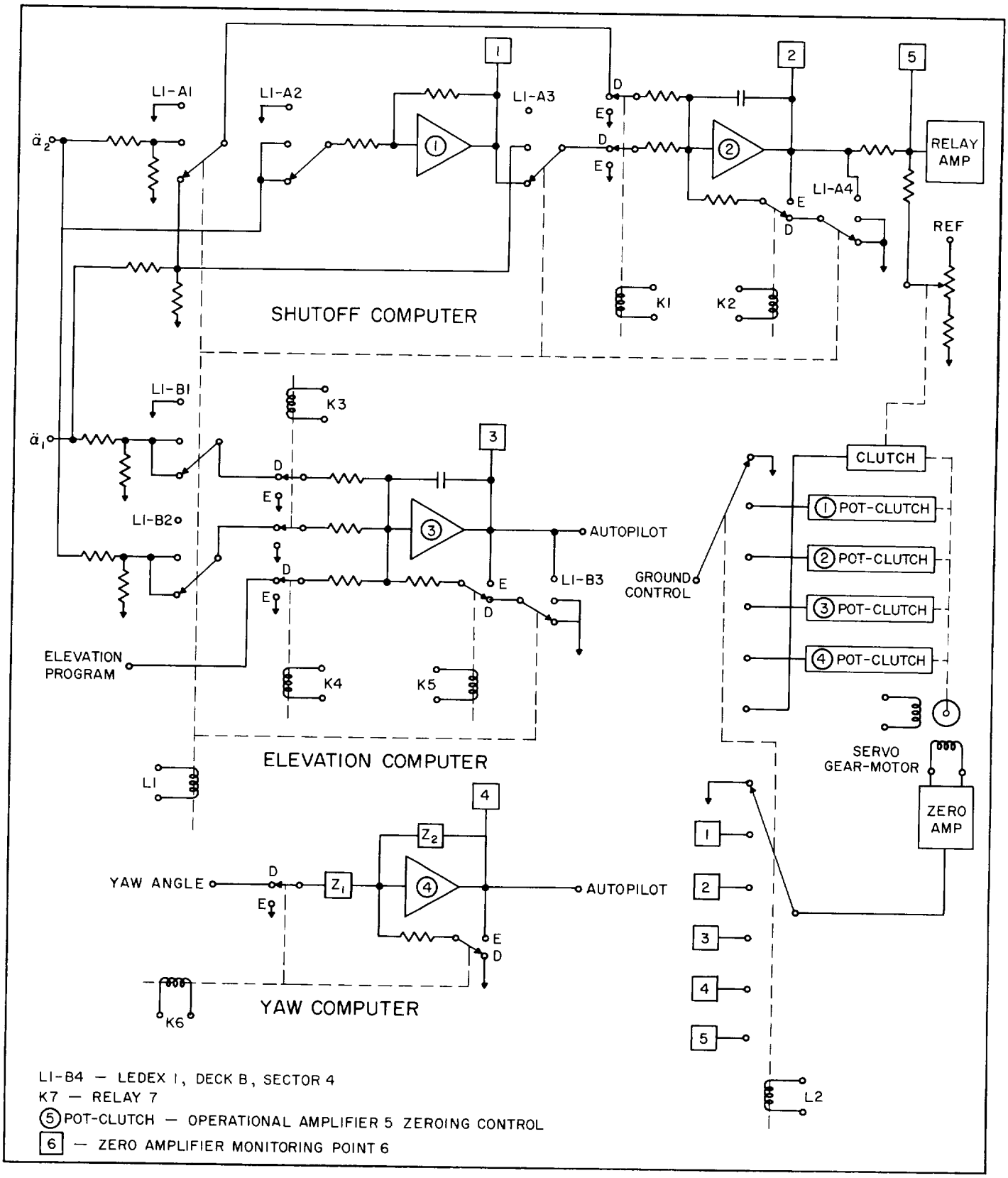

Fig. 61. MING Guidance Computer

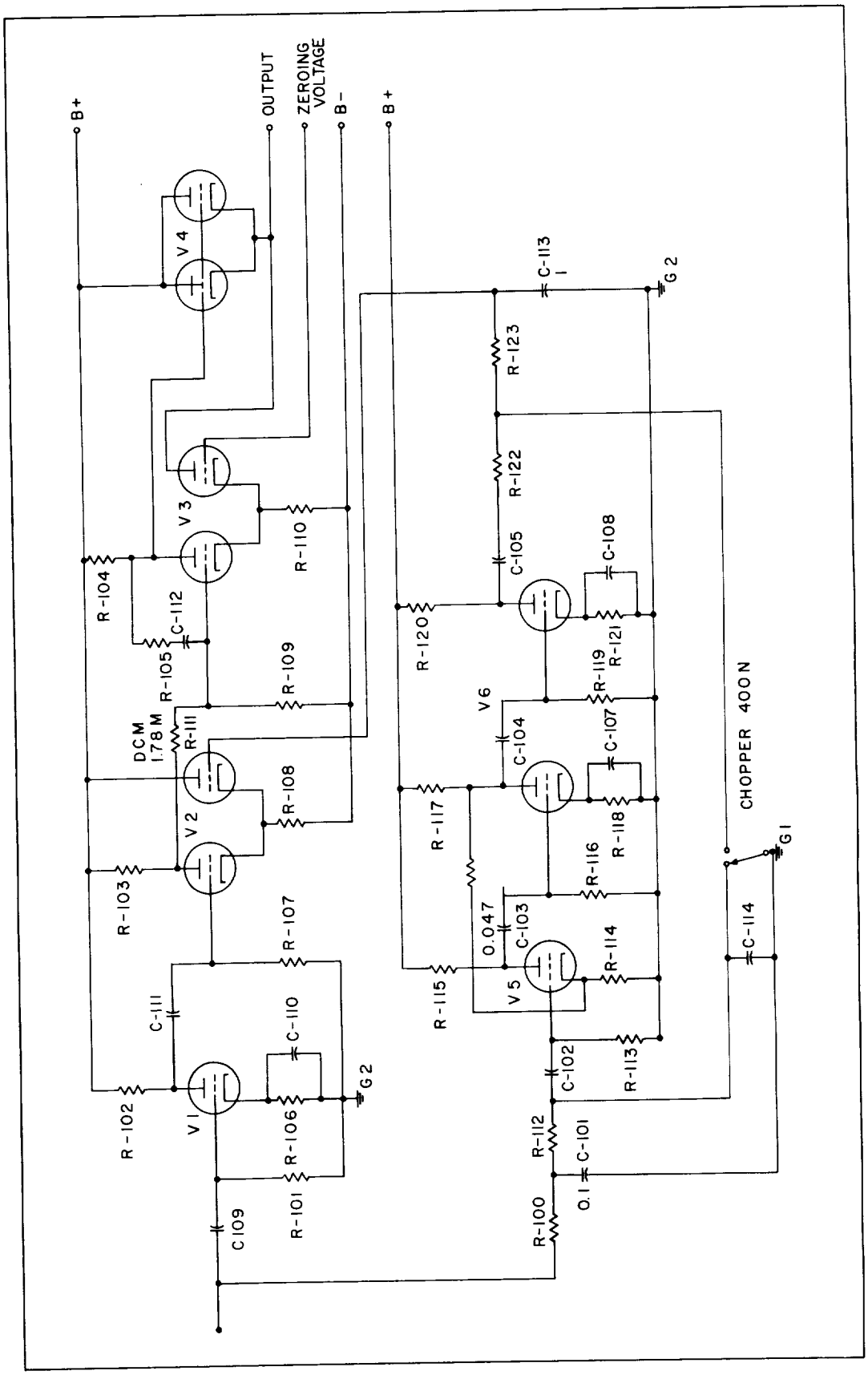

Fig. 62. Schematic Diagram of Operation Amplifier Circuit

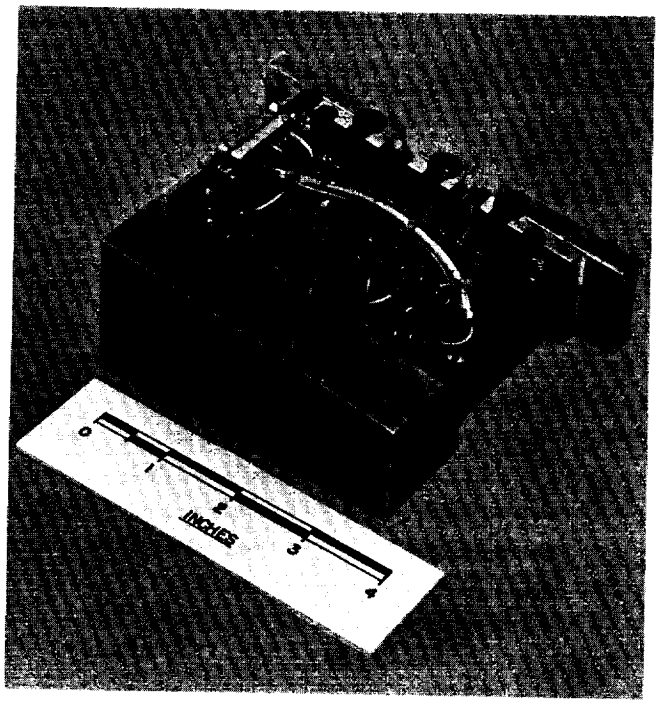

Fig. 63. Operational Amplifier Packaged for Flight

The switching required in the computer is accomplished by using multiple-deck Ledex switches and relays. The Ledex switches are used for ground programming, i.e., grounding accelerometer inputs and connecting bleeder resistors across integrator capacitors during zeroing of the operational amplifiers, selection of particular operational amplifier output and proper clutch for zeroing, reversing accelerometer inputs to provide the calibration signal for insertion of V_0, etc. The relay switches are used for switching during flight and for accurate start and stop of integration during insertion of V_0. The power required for switching the Ledexes and the inaccuracy of Ledex switching times prohibit their use for in-flight switching and for accurately controlled time-base functions. The energized and nonenergized positions of the relays are indicated by the letters E and D, respectively, at the contacts (see Fig. 61). The relay contact orientation shown was chosen to minimize the effects of contact voltages, absorption, and leakage.

The accuracy requirements of the guidance system make the accelerometer scale-factor tolerances very criti-

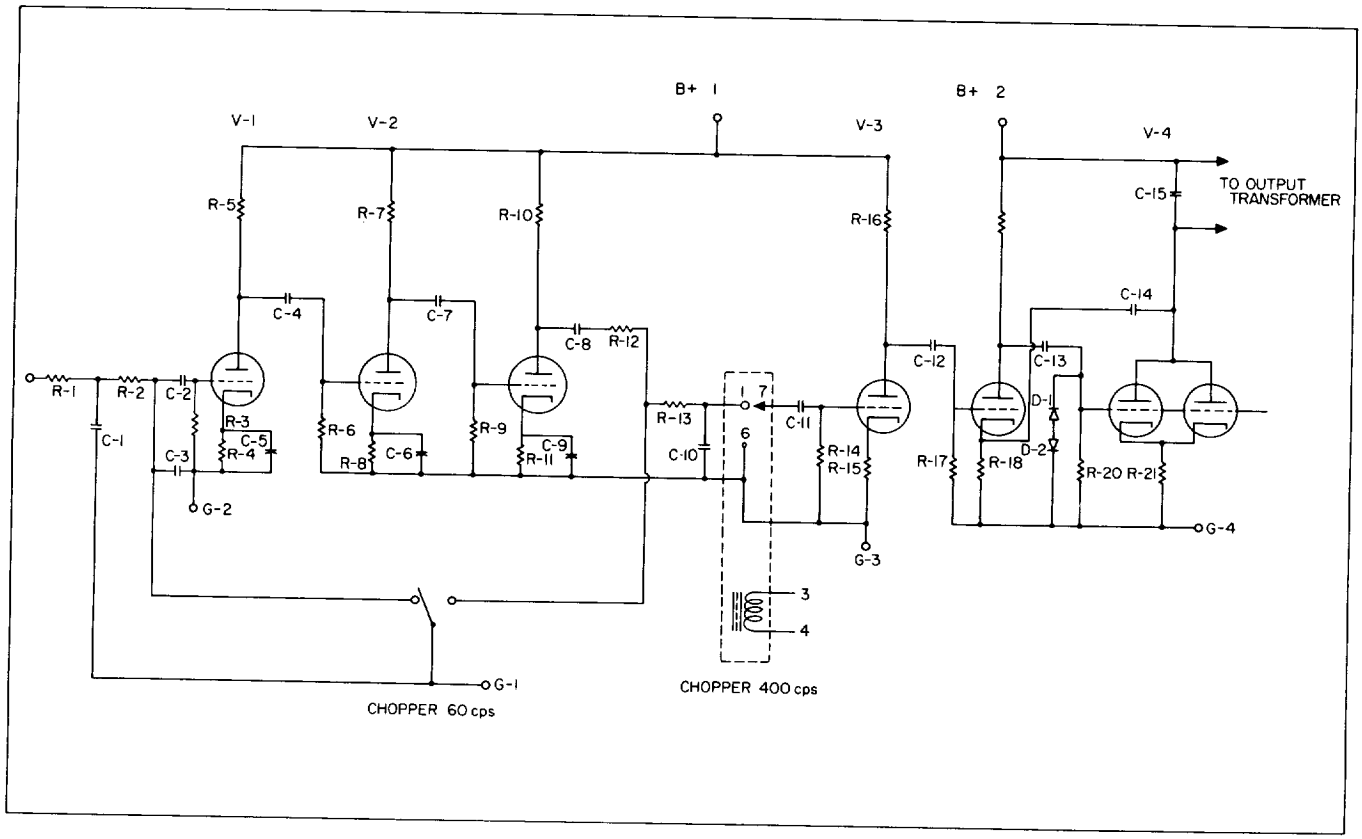

Fig. 64. Schematic Diagram of High-Gain Servo Amplifier

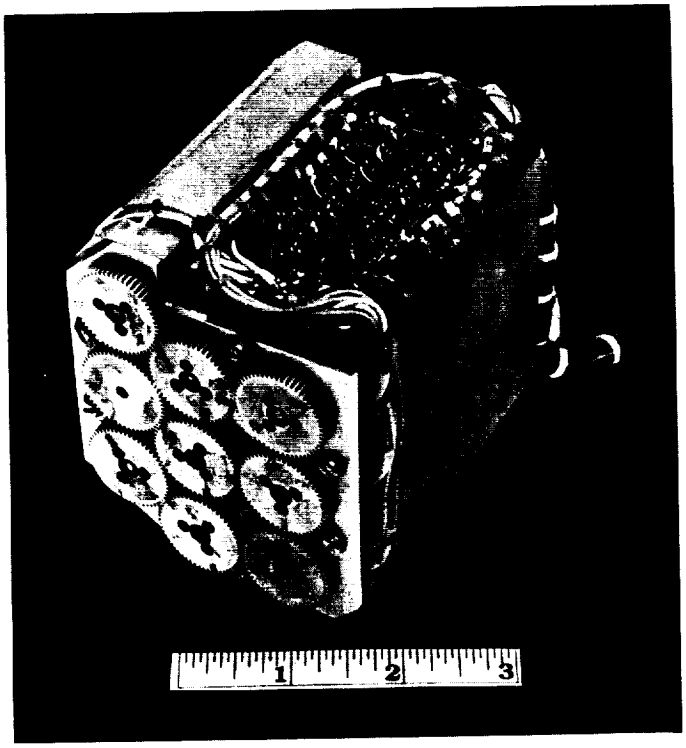

Fig. 65. Zeroing System

cal. The loading on the accelerometers must remain constant throughout erection, insertion of V_0, and flight in order to prevent accelerometer scale-factor changes. The changes in loading the accelerometers for the various Ledex positions corresponding to insertion of V_0 and flight are minimized by use of T input networks.

(3) *Preliminary Computer Error Analysis.* Table 19 presents the results of a very brief analysis which was made to determine what orbit eccentricity could be anticipated from known errors in the shutoff computer.

(4) *Computer Test Equipment.* A computer test set for the *Sergeant* flight computers (shown in Fig. 67) is capable of completely checking out a flight computer and can also insert parameters such as V_0. Similar test equipment would be required for the MING computer.

3. PROGRAM DEVICE.

Programming the pitch trajectory information for use in flight is provided by a magnetic tape recorder programmer. Elevation-acceleration and pitch-angular-rate information is stored on a magnetic tape which is started at the proper time. The tape readout is a series of pulses of sinusoidal signals which are amplified and used to drive a stepper motor which, in turn, drives the input to the

Table 19. Preliminary Computer Error Analysis

Source of Error	Error, Miles
Integrator absolute null uncertainty	3.5
Finite operational amplifier gain	2.6
Integrating capacitor stability, P.E., and absorption	1.6
Relay amplifier actuation uncertainty	1

elevation computer. The elevation computer compares the programmed information with the single-axis platform data from the accelerometers and gimbal-angle pickoff, and the error is a command to the autopilot.

Two different tape-drive mechanizations have been proposed, as shown in Figs. 68 and 69. Both require an accurate time base or frequency reference. The first of these (see Fig. 68) is a synchronous motor drive through a clutch-brake, the clutch being energized at the time of program start. Timing accuracy for this system is simply the accuracy of the 400-cps supply to the motor. Since the tape is driving continuously, approximately 60 ft of tape is required for adequate sensitivity of the magnetic head.

The second (see Fig. 69) and presently preferred, drive mechanism uses a rotary solenoid energized by a pulse source. The pulse source generates pulses at regular intervals, dependent on the program needs, and timing accuracy for the system is referred to a low-power frequency base within the pulse generator. The rotary solenoid drives through a torsion spring and escapement mechanism to the tape capstan. This type of drive requires only 1½ feet of magnetic tape and is adaptable to simplified ground control and to a rapid change of programming. Weights for the two systems are comparable, each system being approximately 10 lb.

This type of mechanization is the only one being considered for the *Juno IVA* program because it is capable of handling last-minute changes in the actual flight trajectory. If flight trajectories can be determined sufficiently in advance, other mechanizations can be considered which may reduce weight and complexity.

a. Description. In selecting the energy-source for *Juno IV*, design priority was established as follows: (1) simplicity and its inherent reliability and (2) minimum weight and size. A manually activated silver-zinc battery was selected to provide power. The character of the electrical loads can be divided into two groups: (1) power for actuators, such as hydraulic pumps, heaters,

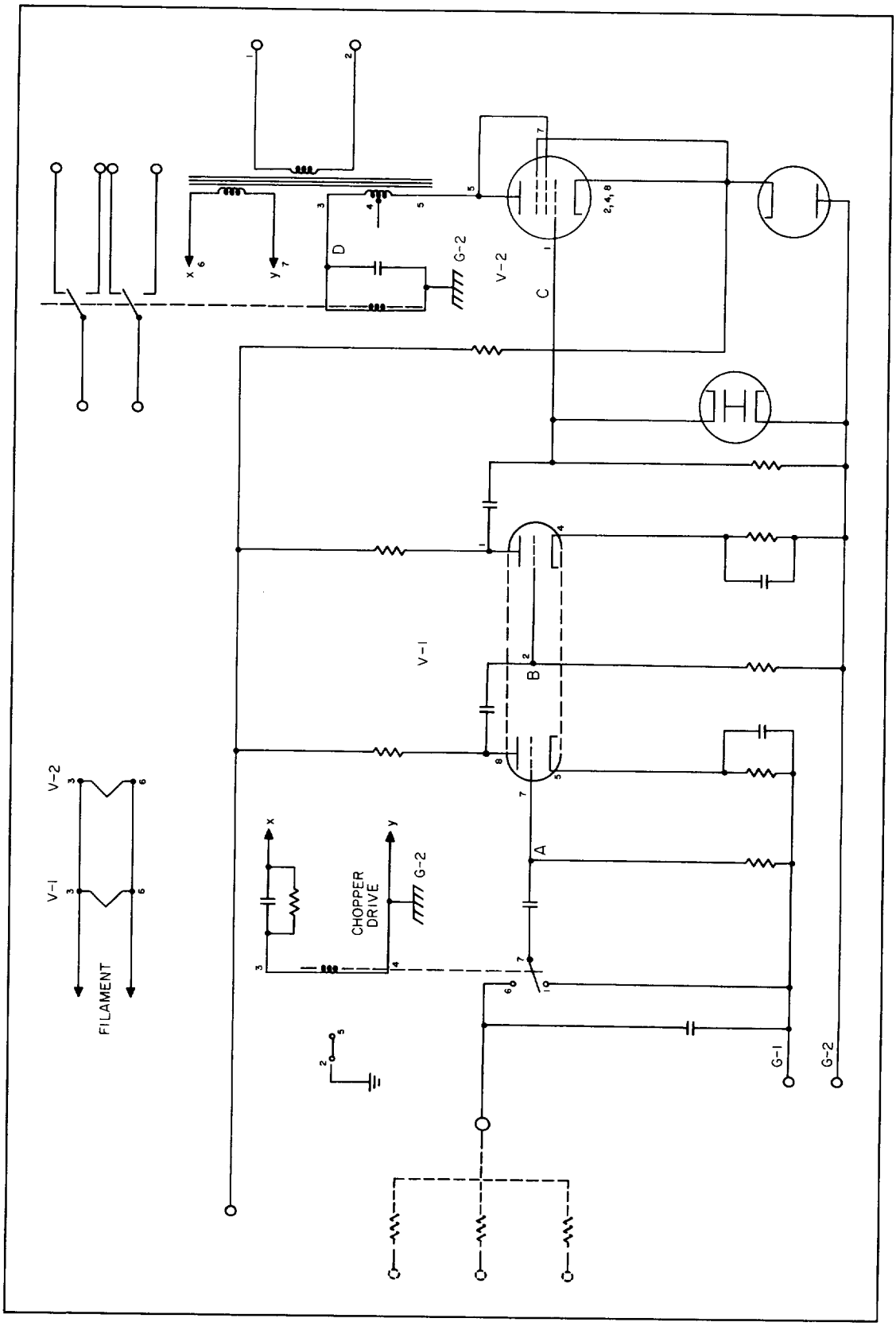

Fig. 66. Schematic Diagram of Vacuum-Tube Relay Amplifier Zero Detector

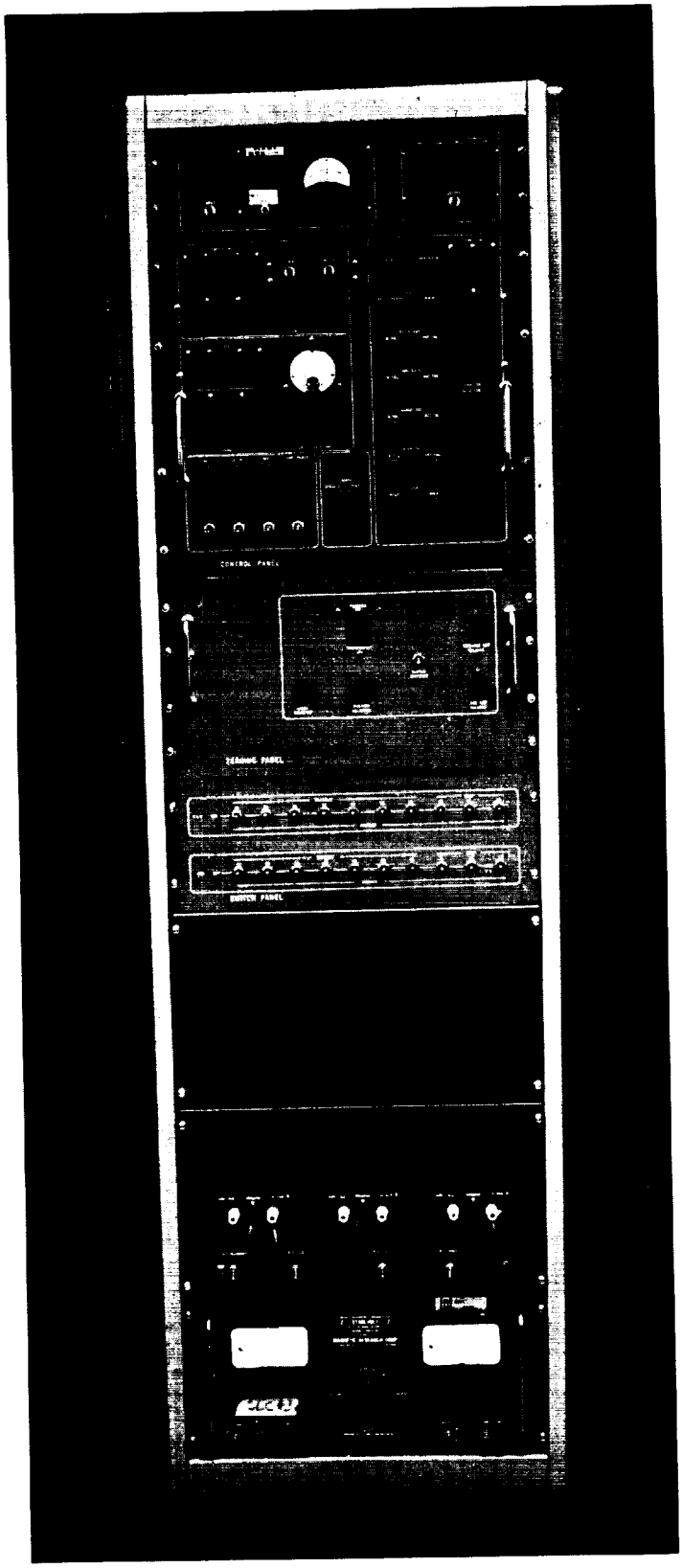

Fig. 67. Computer Test Set

and other loads all of which vary greatly and (2) guidance components whose loads are nearly constant and which require very good regulation. To accomplish these conflicting requirements, a system similar to that adopted for the *Sergeant* was proposed: That is, the use of one 28-v dc battery for the widely varying electrical loads and another electrically separate 28-v battery for the nonvarying loads to simplify the voltage regulator. (See block diagram, Fig. 70.)

The characteristics of the ac power required are shown in Table 20. Precision 400-cps power was needed to provide a very accurate time-base drive for the magnetic tape of the programmer. The precision frequency reference element was provided by a 3200-cps transistorized tuning-fork oscillator. A transistorized 8-to-1 binary countdown circuit provided a precision 400-cps signal to drive the two-phase power-switching transistors.

Precision dc power of $\pm$ 150, $\pm$ 65, and + 6.3 v was also required, as shown in Table 21. The 150-v dc was required to be accurate to 0.01% principally because of the shutoff-computer tolerance requirement. The total dc power required at all voltages was approximately 100 va. Again, a static inverter was selected to provide this power because it had the greatest reliability and the least weight. To achieve the very well-regulated voltage required for the shutoff computer, a dual-stage voltage regulator was employed.

b. Battery. A manually activated silver-zinc battery will be used to supply injection guidance power. Table 22, which presents a summary of injection power requirements, tabulates the total loads – 550 and 436 watts on the dual 28-v battery. The electrical loads on the batteries are of the following two types: One battery supplies the

Table 20. MING Power Requirements

Characteristic	General Injection Guidance ac Power	Accelerometer Excitation
Frequency, cps	400	8,400
Frequency accuracy (absolute) %	±0.01	±6
Phases	2 (90 deg ± 3 phase angle)	1
rms voltage, v	115 ± 5	115 ± 10
Total power, va	150	20
Load power factor	−0.7 to +1.1	−0.7 to +1.1
Total rms harmonics, %	5	10

Table 21. Injection Guidance dc Power Requirements

dc Voltage* v	Absolute Accuracy %	Stability for 4 hr at +30 to +130°F	Load Watts	Load Change % of Full Load	Ripple mv	Usage
±150	±0.10	±0.02	25 Each	90 to 100	2	Computer
±65	±0.5	—	30 Each	90 to 100	100	Platform
+6.3	±3	—	75 Total	80 to 100	100	Vacuum-tube filaments and relays

* Both plus and minus power supplies are required.

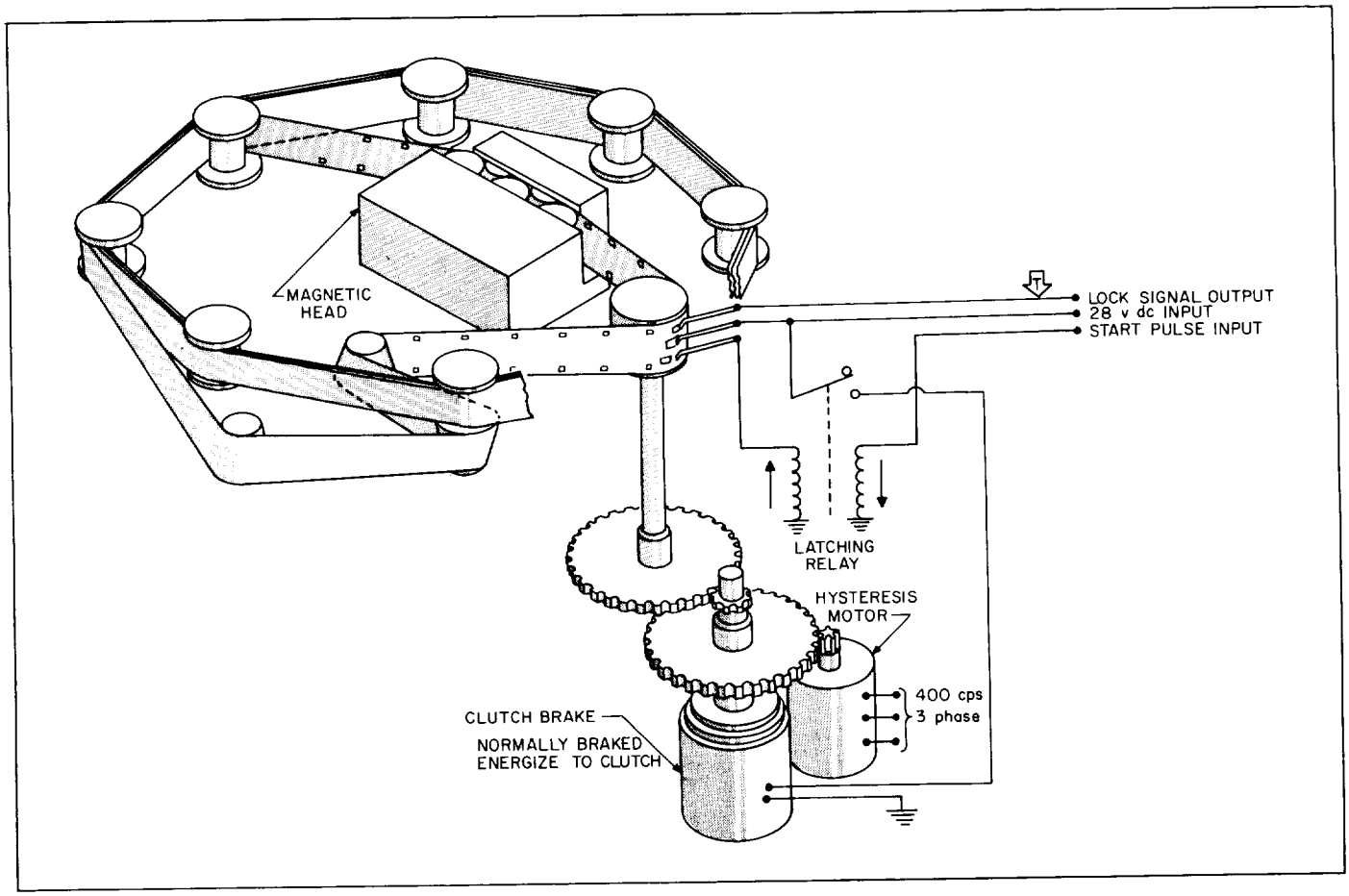

Fig. 68. Continuous Tape Drive Mechanism

power for the actuators and heaters whose load demand varies widely. The other dual battery supplies the power for guidance components whose loads are nearly constant and require very good regulation. The estimated wet weight of the dual battery is 7 lb and it has a volume of 300 cubic in.

c. Precision 400 cps power. A 3200-cps transistorized tuning-fork oscillator will provide a frequency signal accurate to 1 part in 10,000. This tuning-fork oscillator was initially developed for the *Sergeant* and has satisfactorily passed both *Sergeant* and *Juno IV* approval vibration tests with absolutely no permanent, or even transient,

Table 22. Summary of Injection Power Requirements in Watts

Guidance Component	Unregulated Power Direct From Battery 1 (28±4v)	Regulated dc Voltage Power			400 CPS 2 phase 115v	8,400 CPS 1 phase 115v	Total Power from Battery 2 (28v)
		Total ±150v	Total ±65v	Total +6.3v			
		Battery 2					
Platform	60	—	15	—	50	15	80
Attitude sensors	60	—	—	—	10	—	10
Program device	10	—	—	—	35	—	35
Leveling and mixing	—	—	2	—	—	—	2
Yaw computer	—	5	—	—	—	—	5
Shutoff computer	—	25	—	75	15@ 6.3v	—	115
Elevation computer	—	10	—	—	—	—	10
Autopilot amplifier and actuator	320	—	2	—	10	—	12
Telemetering	100	—	—	—	—	—	0
Payload spin motor	—	—	—	—	30	—	30
Subtotal	550	40	19	75	150	15	299
Power supply losses	0	8	4	15	100	10	137
Total guidance components	550	48	23	90	250	25	436

effect on the output frequency. A photograph of the 3200-cps tuning-fork oscillator and the 8-to-1 transistorized binary countdown module developed for the *Sergeant* is shown in Fig. 71. The precision 400-cps power supply is a two-phase system with 90-deg phase lag between the *A* and *B* phases. The precise determination of the 90-deg phase lag is easily accomplished by picking off signals in the 800-cps flip-flop.

d. 8400-cps power. Power of 8400 cps is provided for carrier excitation of Bell accelerometers. As shown in Table 20, the frequency and voltage of the 8400-cps power need not be extremely accurate. A conventional static converter using a 1-mil high-mu 80 core and DT-100 transistors provides sine wave 8400-cps power of 20 va. The 8400-cps power supply has been breadboarded and subjected to thermal environmental tests.

e. Precision D.C. power. As shown in Table 21, extremely accurate 150-v power must be provided to the guidance computer. This accurate dc voltage is provided by a two-stage voltage regulator. The first stage is of the nondissipative type. A static converter provides ac power to a variable pulse-width reactor. The width of the pulse of output power fed to a smoothing filter is regulated by a Zener-diode reference element. The second-stage regulator is a dissipative-type transistorized voltage regulator referenced to a 0.001% four-element Zener diode. One version of this precision dc supply has been developed for the *Sergeant* missile and is being regularly used in *Sergeant* flights. A prototype version redesigned to reduce size and weight has been breadboarded and is being subjected to thermal environmental tests. Other types of precision dc power supplies have been developed for other applications, such as the Dovap power supply, and could be adapted to the *Juno-IV* application.

f. Power transfer switch. A power-transfer switch was purchased for the *Sergeant* and is shown in Fig. 72. Limited life tests have been conducted on this power-transfer switch. A local manufacturer of such switches has been contacted and a substantially smaller power-transfer switch is on order. The current handling capacity required for *Juno-IV* is estimated to be 30 amps instead of the *Sergeant* 75 to 100 amps.

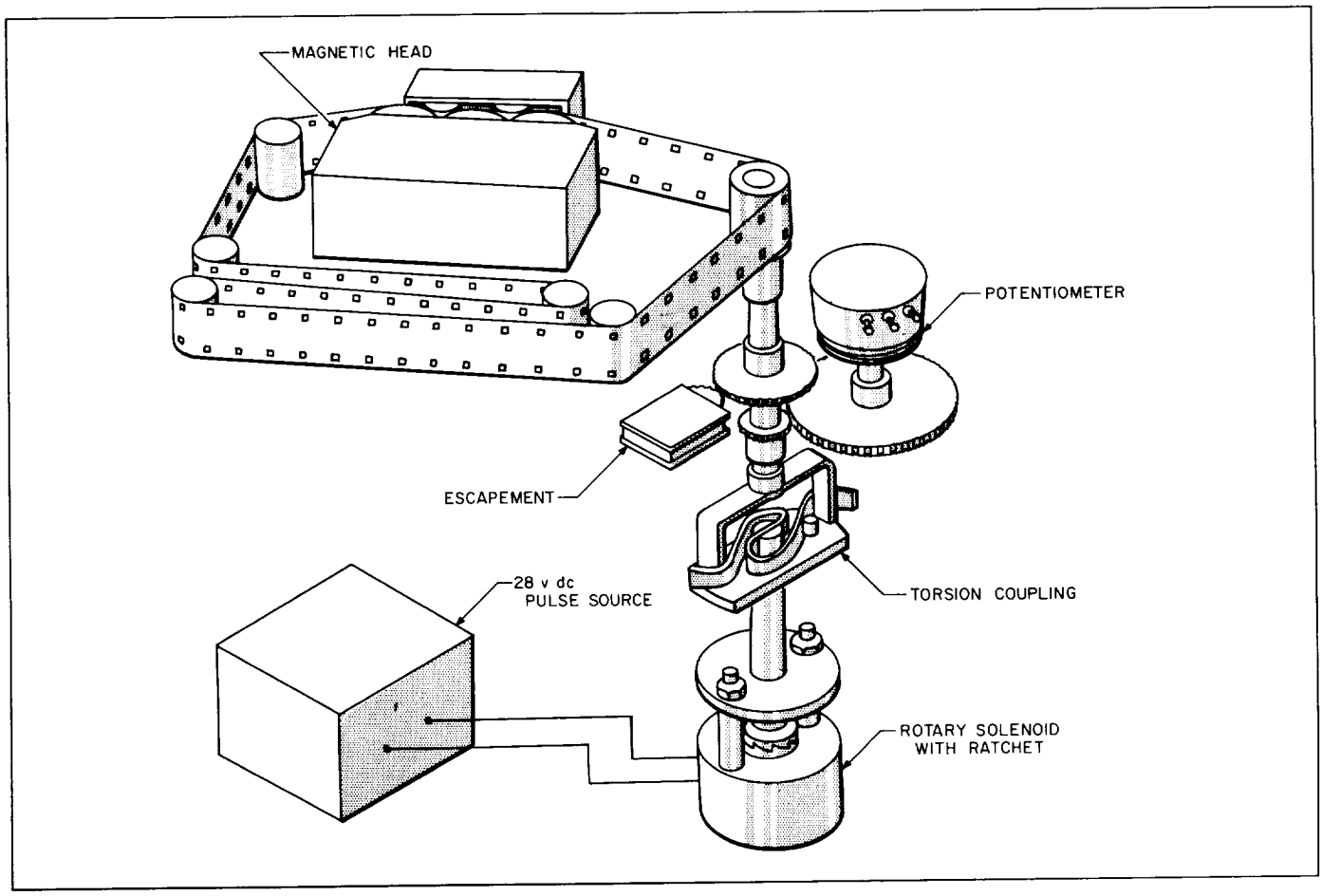

Fig. 69. Digital Tape Drive Mechanism

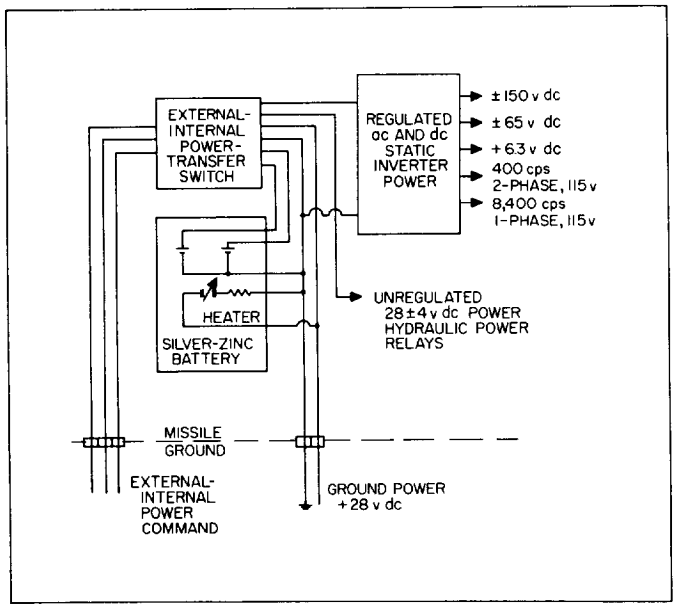

Fig. 70. Block Diagram of Voltage Regulator

Fig. 71. *Sergeant* Tuning Fork Oscillator

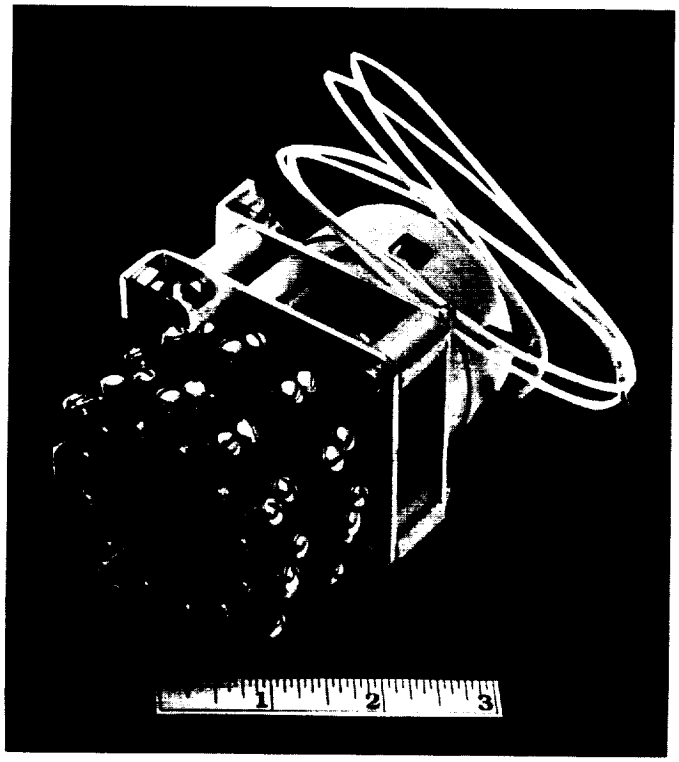

Fig. 72. Power-Transfer Switch.

4. HYDRAULIC SERVO ACTUATORS.

From the standpoints of weight and urgency of schedule, it appeared that hydraulic servo actuation would be required in pitch and yaw for the MING system. A contractor was found who had proven hydraulic component designs which closely matched the MING servo requirements for the 6000-lb-thrust, gimbaled motor. These requirements were determined to be as follows (see Fig. 73):

Mass load	110 lb
Maximum output	1500 in-lb/servo
Maximum amplitude	± 2 deg
Maximum rate	20 deg/sec
Maximum power	0.152 hp

Based on preliminary structural information, the contractor submitted a design proposal for an hydraulic actuator system which was to be mounted on the upper end of the motor in a self-contained manifold package weighing 6½ lb. This package was to be attached to the lower end of the fuel tank and was to be operated through two pairs of actuator arms in order to eliminate backlash and to minimize the effects of cross-coupling.

Unfortunately, it was found that the lower end of the fuel tank did not offer sufficient structural support for the dynamic and/or impact loads on the actuator arms. Design analysis and a test program would be required to ensure adequate mounting rigidity in the fuel tank.

The contractor was then asked to evaluate other mounting configurations at the lower end of the rocket motor, attaching the package through a long actuator arm to the skin of the missile, where sufficient structural support appeared feasible. The most desirable design here was indicated to be two separate, self-contained, double-acting actuator systems with a total weight of 18.5 lb. Careful assembly is required to prevent backlash, and cross-coupling is fairly large. Possibilities of damaging resonances in the long actuators or their uniball attachments would have to be carefully studied.

Test programs are now under way to determine adequate rigidity in a conical tank and to determine all of

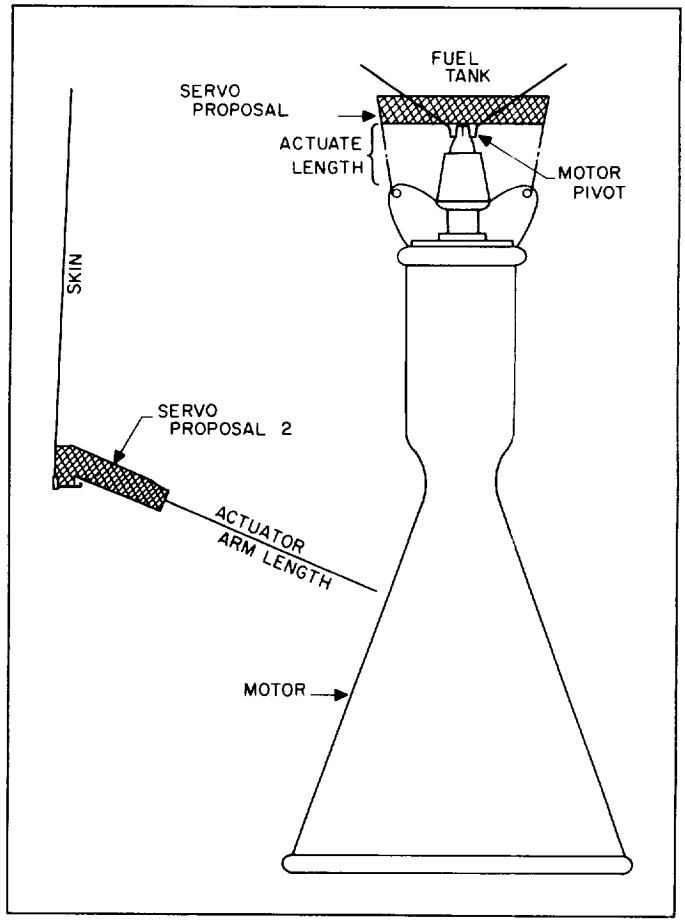

Fig. 73. *Juno IVA* Hydraulic Servo

the hydraulic servo characteristics pertinent to the problem.

D. System Evaluation

a. Purpose. The purpose of this system evaluation is to determine the performance of the MING system, and to explain nonstandard performance to an extent compatible with the available data.

b. Data. (1) Primary Data.

If a doppler transponder is carried in the second-stage vehicle, these data will be considered primary. If the final stage does not have a doppler transponder, but the booster stage does, the only primary data will be the position and velocity coordinates of the vehicle at second-stage ignition. (One-way doppler data will probably be available, but will be of doubtful value.) Thus no trajectory data would be available following second-stage ignition. However, the coordinates of the missile at its injection into orbit can be accurately determined from the detailed knowledge of the orbital parameters, which should be available some time following the flight. Therefore, an analysis is possible in which various perturbations caused by guidance or performance errors can be selected and computer-trajectory simulation studies performed, in an effort to obtain agreement between the simulated injection conditions based on the observed ignition conditions and an assumed set of errors, and the observed injection conditions.

There is no unique set of perturbations which will make the end points match, but the telemetered values of roll rate, yaw rate, pitch angle, and acceleration can be used in a qualitative way to determine a most plausible set. It should be pointed out that the ½-deg value of roll and yaw control system error corresponds to the 3σ values for the expected errors. Table 23 shows the expected 1σ value of doppler coordinates at ignition, assuming 75-point smoothing and raw-data errors of $\pm$ 100 ft rms. Also shown are the 1σ values of coordinates at injection as determined from the orbit parameters.

(2) Telemetered Data.

(a) Acceleration.

The accuracy of the accelerometer proposed for use in the MING System is 0.003% from 0 to 1g and 0.03% from 1 to 30g. If the accuracy of the telemetered values of the accelerometer outputs can be kept to approximately ½ ft/sec², while the accuracy of the telemetered value of pitch gyro output is held to 4 mils, the simulation of missile coordinates is greatly improved in its validity. The required accuracy in acceleration can be achieved only by switching range in the telemetering channel several times, and by calibrating at each switch. Table 24 shows a possible switching arrangement based on standard trajectory 0.307.

Table 23. Trajectory Accuracy

Item	$\frac{x}{\text{ft}}$	$\frac{y}{\text{ft}}$	$\frac{\dot{x}}{\text{ft/sec}}$	$\frac{\dot{y}}{\text{ft/sec}}$	$\frac{v}{\text{ft/sec}}$	θ rad
Doppler (at ignition)	17.5	17.5	2.78	2.78	7.34	0.00024
From orbit parameters	4.75×10^3	2.2×10^4	1	—	1	0.0020

Table 24. Telemetry of Accelerations

Full Scale	Range	Channel	Width	Switch	Probable Error	
g	ft/sec²	g	ft/sec²	Time from Second Stage Ignition	g	ft/sec²
a_1 Channel						
0.47 to 1.25	15.00 to 40.00	0.78	25	0	0.0156	0.5
1.15 to 1.93	37.00 to 62.00	0.78	25	390	0.0156	0.5
a_2 Channel						
0 to 0.78	0 to 25.00	0.78	25	0	0.0156	0.5
0.68 to 1.46	22. to 47.00	0.78	25	280	0.0156	0.5
1.35 to 2.13	43.50 to 68.50	0.78	25	390	0.0156	0.5
2.06 to 2.68	66.00 to 86.00	0.62	20	440	0.0124	0.4

(b) Pitch Angle.

The argument cited above applies to the pitch gimbal angle measurement. Table 25 shows a possible switching arrangement based on standard trajectory 0.307. The remaining measurements will be telemetered in the conventional manner. Figure 74 summarizes the quantities required, what they are used to evaluate, and how they are acquired.

Table 25. Pitch-Angle Measurement

Full Scale Range mils	Switch at Time From Second-Stage Ignition sec	Probable Error mils
0.370 to 0.570	—	4
0.180 to 0.380	70	4
0.010 to 0.190	210	4

E. Telemetry.

1. MEASUREMENTS

Telemetering measurements of the second-stage guidance and propulsion system are listed in the channel assignment shown in Table 26. Approximately half the channels are devoted to MING system measurements and the other half to propulsion and structural measurements. A standard FM/FM system using components developed for the *Sergeant* and *Jupiter* radio inertial guidance (RIG) program was planned. Commutation of temperatures, pressures, and some guidance functions was to be used wherever possible.

2. THE AIRBORNE SYSTEM

a. Introduction. The airborne telemetering system is composed essentially of two units, the subcarrier assembly and the RF system. Repackaging the standard flat JPL R&D system was necessary because of the curved mounting surfaces of the guidance compartment. Two methods of packaging the subcarrier housings, commutator, and power supply were proposed: (1) cut an existing curved *Sergeant R&D* chassis in half and bore holes for lightening, or (2) weld from aluminum a curved base assembly with standoff mounting posts for connectors mating with the subchassis. Both methods need further work to determine ability to maintain tolerances, ability to withstand vibration environment, operation problems, etc. Eight compartments were planned, one for the subcarrier power supply and switching, one for a four pole commutator, one for a mixer panel for transducer signal mixing, and five for circuit subchassis which house the plug-in modules.

The RF assembly, which includes the transmitter, RF power amplifier, high voltage and filament power supplies, was to be so housed in a pressurized container as to prevent high voltage breakdown at high altitudes. Typical components are shown in Figs. 75 and 76.

The revised weight estimates for the system are given in the following tabulation:

Subcarrier assembly	14 lb
Transducers	9 lb
RF assembly	15 lb
Cables	29 lb
Antenna	10 lb

b. Power supply. Since telemetering power is being supplied by the main guidance batteries, isolation of power return from telemetering signal return is necessary to prevent one source of ground loop problems. A dc-to-dc converter followed by a dual 20-v regulator both made by United Electrodynamics would be used. The combination is short-circuit-proof and provides all the regulated power needed by the subcarrier oscillators. The commutator motor, however, would be powered directly from the 28-v battery. It is also necessary to isolate the transmitter and RF power amplifier filaments from guidance battery power return. This is accomplished by again using a dc-to-dc converter mounted in the same housing as the remainder of the RF components.

In the event of central power failure, the telemetering system should not fail since it must be determined what happened, and why. Also the propulsion and structural data would be of interest. This back-up is provided for by the use of rechargeable Ni-Cad batteries floating across the 28-v line and blocked from discharging back into the source by diodes. The weight for 30 sec to 1 min of operation would be about 1.8 lb. Approximately 100 watts of 28-v dc power are required for the entire telemetering system.

c. Subcarrier oscillators. The JPL standard ICO made by either United Electrodynamics or American Missile Products was to be the basic subcarrier oscillator. Additional amplifiers or other circuits built into the standard modular form would precede the ICO when required.

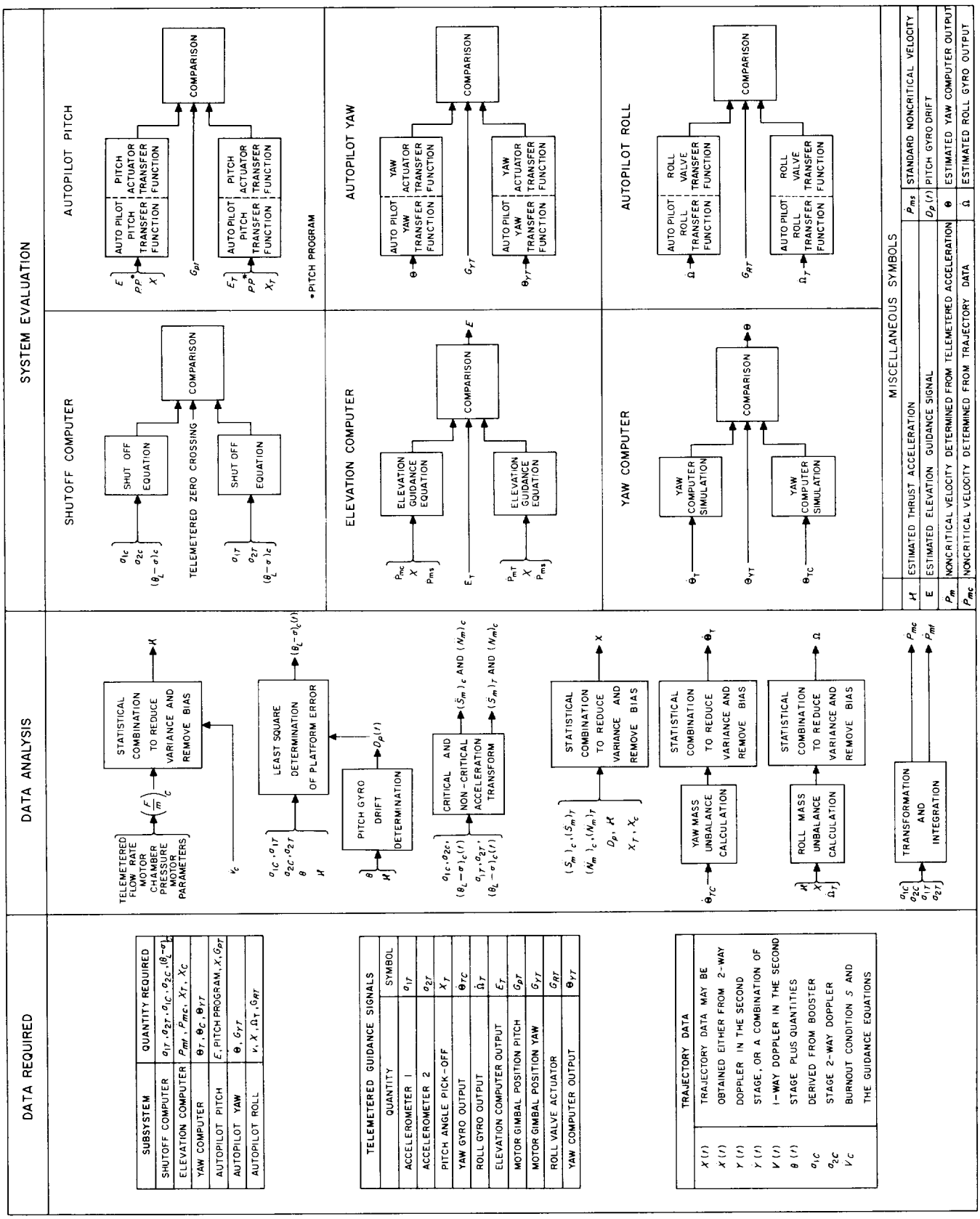

Fig. 74. Flow Chart of MING System Evaluation

Table 26. JPL Second-Stage Telemetering Channel Assignment

Channel	Measurement	Range	Frequency Response or Samples Per Second
1	Missile 400-cps frequency	400 ± 30 cps	
2	Accelerometer 1 output		
3	Accelerometer 2 output		
4	Pitch angle pickoff		
5	Yaw gyro output		
6	Commutated temperatures		
6a	Oxidizer temperature	40 to 100°F	½ S
6b	Fuel temperature in tank	40 to 100°F	½ S
6c	Fuel temperature in injector	80 to 400°F	½ S
6d	Helium supply temperature	— 200 to 400°F	½ S
6e, f	Helium tank temperature (2)	0 to 1000°F	1 S
6g, h	Motor temperature (2)	0 to 700°F	1 S
6j, k	Aft propellant tank temperature (2)	— 150 to 500°F	½ S
6l, m	Aft propellant tank temperature (2)	0 to 500°F	1 S
6p, q	Aft structure temperature (2)	0 to 1000°F	½ S
6r, s, t	Forward propellant tank temperature (3)	0 to 500°F	½ S
6u, v	Intertank structure temperature (2)	0 to 500°F	½ S
6 w, x	Servo actuator temperature (2)	0 to 500°F	½ S
7	Commutated pressures and positions		
7a	Helium tank pressure	0 to 3500 psig	½ S
7b	Helium regulated pressure	0 to 300 psig	½ S
7c	Fuel tank pressure	0 to 300 psig	½ S
7d	Oxidizer tank pressure	0 to 300 psig	½ S
7e	Nitrogen tank pressure	0 to 3500 psig	½ S
7f	Motor gimbal position, pitch		3 S
7g	Motor gimbal position, yaw		3 S
8	Separation angle		3 S
9	Commutated guidance signals		
9a	Pitch gimbal torquer current		
9b	Roll gyro output		
9c	Pitch autopilot input		
10	Events		
10-1	Propellant valve start open	blip	
10-2	Propellant valve full open	blip	
10-3	Pressurization valve full open	blip	
10-4	Range safety command	blip	
11	Motor chamber pressure	0 to 300 psig	300 cps
12	Oxidizer injection pressure	0 to 300 psig	300 cps
13	Fuel injection pressure	0 to 300 psig	300 cps
14	Roll valve actuator position		
15	Events		
15-1	Separation	blip	
15-2	Shutoff command	blip	
15-3	ABMA velocity signal	blip	
15-4	Programmer start	blip	
16	Vibration, guidance compartment		
17	Vibration, motor head		

d. Transducers. Pressure transducers (made by Farrell Engineering Company) having the subcarrier oscillator constructed integral with the gauge would be used. This transducer has been used in the *Sergeant* program for a considerable time and has given excellent results. The very corrosive fuel and oxidizer used present a problem with the O-ring and gauge materials. Additional development work is proceeding to obtain a satisfactory solution to this problem.

Temperature measurements are usually made by thermocouples, amplifying the very low voltage to a level sufficient to modulate a subcarrier oscillator. The use of a resistance-controlled oscillator (similar to the one used in the Deal program) coupled to thermistor elements has also been investigated. The RCO is a very simple, lightweight, stable device, and the thermistor probes themselves can be made very small. One problem with the probes is that special material must be used for the high-temperature measurements requested.

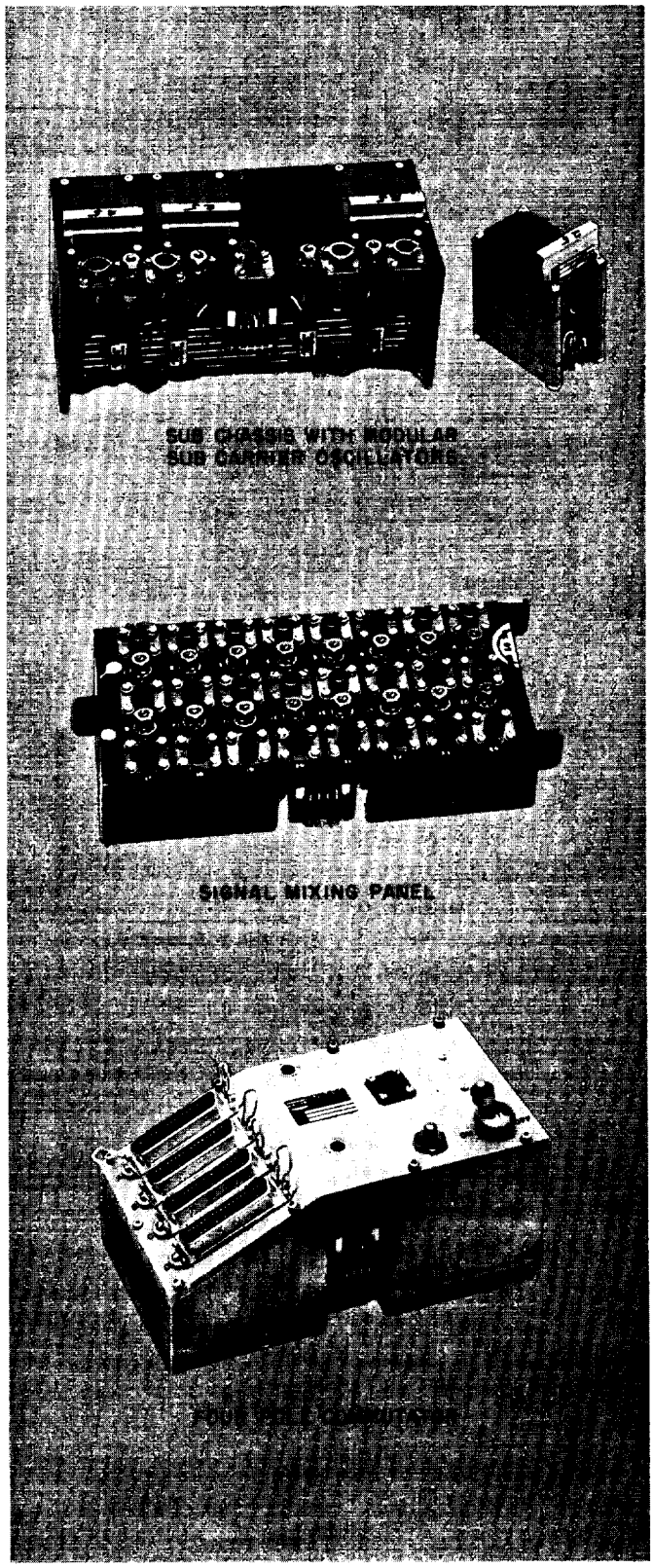

Fig. 75. Telemetering Components

Fig. 76. Telemetering Components

e. The R.F. System. Since the radio distance from the second stage to ground receiving sites may be in excess of 1000 miles, RF powers greater than the outputs of standard telemetering transmitters are required. Calculations show that 12 watts (which is available from a commercial power amplifier) is sufficient. The transmitter presently being used in *Sergeant* system is made by Radiation Incorporated, and the RF power amplifier selected is the one used in the *Jupiter* RIG tests, a Rheem model REL-09 which has a nominal 12-watt output with 2 watts of input and which does not require a blower for cooling.

Development work on a wide-band phase-locked loop receiver is continuing. Reduction and threshold by 28 db over conventional FM/FM telemetering systems has been achieved, and plans are being made for the construction of several receivers for field use. This improvement is realized for reception of standard telemetering frequencies and deviation ratios. These receivers would have been available for use at the Atlantic missile range and down-range sites for the *Juno IV* firings.

Telemetering antennas for the second stage were under development by the JPL Component Development Section. Although light-weight spike antennas were proposed, location, type, and mounting are still under investigation.

3. THE GROUND SYSTEM

a. Ground monitoring. A system was designed for ground monitoring of telemetering channels 6d, 7a, 7b, 7c, 7d, and 7e during fueling or anytime the vehicle was on the firing pad. The system, as shown in Fig. 77 would use the flight instrumentation on the stage, with provision for turning on the flight gauges without turning on the RF system. The data would be recorded on the Sanborn recorder, with four of the variables being also real time displayed on panel meters.

The missile equipment would consist of the pressure transducers, which include the subcarrier oscillators, one temperature transducer, isolation amplifiers, and associated cabling. The isolation amplifiers would be needed both to isolate the ground equipment from the telemetry equipment and to provide impedance matching to the lines to the blockhouse. The signals would be fed to the blockhouse by way of the first-stage tail plug.

The blockhouse equipment would occupy 72 in. of rack space and would consist of the discriminators, recorder, and calibration equipment, along with associated power supplies, etc.

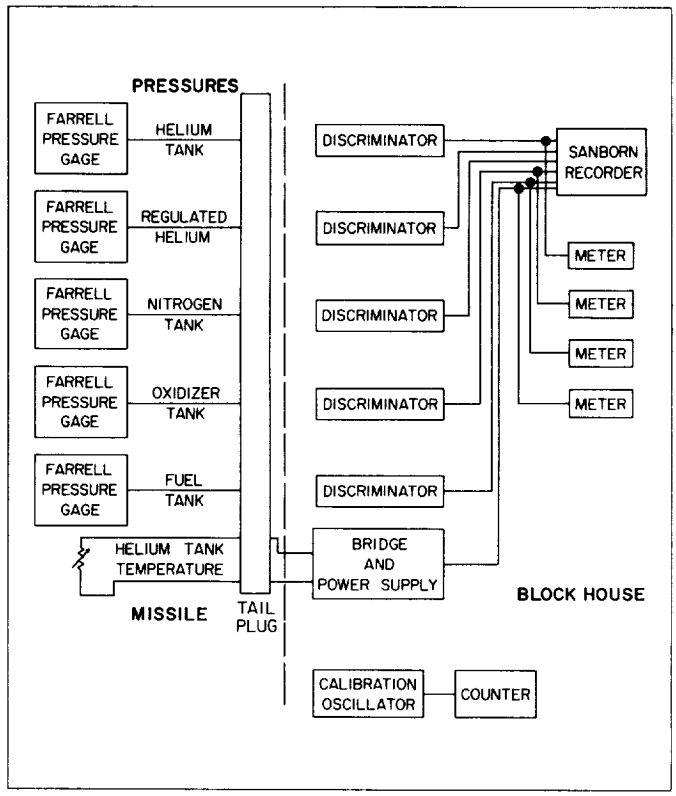

Fig. 77. Ground Monitoring Block Diagram

b. Test and calibration of airborne system. A test console for performing static calibrations of the telemetering system is being built into a suitcase for portable use and includes the necessary equipment to power, filter, and count the subcarrier frequencies as the inputs are varied for calibration purposes. Other equipment is for setting deviation levels and for selecting commutator segments. Dynamic tests and recordings of dummy runs would be handled by ABMA which has a complete dual data recording center. JPL use of this facility for these tests has been agreed to.

c. Flight recording. In Florida, a mobile recording and checkout station would be set up. Used in conjunction with the "suitcase console" for static checks, this station would be able to turn out real-time records of all tests and the flight. After the flight, "quick look" data reduction could be performed by this station.

Major equipment in this station would include a tape recorder, an oscillograph, a set of phase-locked loop discriminators, a phase-locked loop receiver, as well as a conventional receiver and various test equipment to maintain the station.

F. Tracking and Range Safety.

1. 960 MC/S TRANSPONDER

Standard range instrumentation at the Atlantic missile range (AMR) and Pacific missile range (PMR) is not adequate to evaluate the powered-flight performance of the proposed *Juno IV* vehicle for the following reasons: (1) The vehicle would be 1000 to 1500 miles down range and below the radio horizon from the launching area before burnout of the last stage, (2) A firing azimuth of northeast from AMR and south from PMR would require the installation and operation of new down-range stations — with a lead time longer than the schedule permitted for the first firing, (3) The weight and power consumption of standard flight equipment was not compatible with the minimum-weight guidance and instrumentation system of the *Juno IVA* vehicle. Consideration was given to the fact that the transmission from the payload package might be useful (as in the *Explorer* satellites) in evaluating vehicle performance; however, because the payload was not under the control of the vehicle development group and because it was not sufficiently well defined, it was believed that some instrumentation system not dependent on the payload was required.

A study was made to determine a satisfactory radio instrumentation system for the *Juno IV* vehicles. The results of the study are summarized in Table 27 and show that the *Juno IV* instrumentation system utilizes a major portion of the equipment of the *Juno II* program. The *Juno II* equipment consisted of one receiver and a 85-ft tracking antenna at Goldstone, one receiver and a 10-ft tracking antenna down range, one receiver at the launching area, and several converted *Microlock* receivers procured and operated by ABMA, Signal Corps, and BRL. The *Juno II* flight equipment was a crystal-controlled transmitter at 960 mc/sec.

The study indicated that the one-way Doppler system used for *Juno II* would not be satisfactory for *Juno IV;* therefore, it was planned to convert the *Juno II* transmitter into a transponder which received a signal at 880 mc/sec and converted it to 960 mc/sec (12/11 of 880) for retransmission. (See Fig. 78.) With the help of standard range instrumentation to fix a reference-point

Table 27. Summary of Tracking and Communications Equipment

Ground Equipment	Present Operation and Management	Geographical Location	Flight Equipment
JUNO II PROGRAM			
1 960-mc/sec TRAC(E) receiver and 85-ft tracking system	JPL	Goldstone, Calif.	960-mc/sec transmitter
1 960-mc/sec receiver and 10-ft tracking antenna system	JPL	Puerto Rico	
1 960-mc/sec converted *Microlock* receiver	JPL	Cape Canaveral, Fla.	
1 960-mc/sec converted *Microlock* receiver	ABMA	Cape Canaveral (formerly Gold Station, JPL)	
1 960-mc/sec Hallamore receiver	ABMA	Huntsville, Ala.	
1 960-mc/sec Hallamore receiver	Signal Corps	Florida or West Indies	
1 960-mc/sec Doploc receiver	BRL	Aberdeen, Md.	
JUNO IV PROGRAM			
1 960-mc/sec receiver and 880 mc/sec transmitter duplexed into 10-ft tracking antenna system	JPL	Down Range	UHF transponder receiving at 880 mc/sec and transmitting at 960 mc/sec
1 960-mc/sec converted *Microlock* receiver	JPL	AMR or PMR	
1 960-mc/sec converted *Microlock* receiver	ABMA	Cape Canaveral (formerly Gold Station, JPL)	
1 960-mc/sec Hallamore receiver	ABMA	Huntsville, Ala.	
1 960-mc/sec Hallamore receiver	Signal Corps	Florida or West Indies	
1 960-mc/sec Doploc receiver	BRL	Aberdeen, Md.	

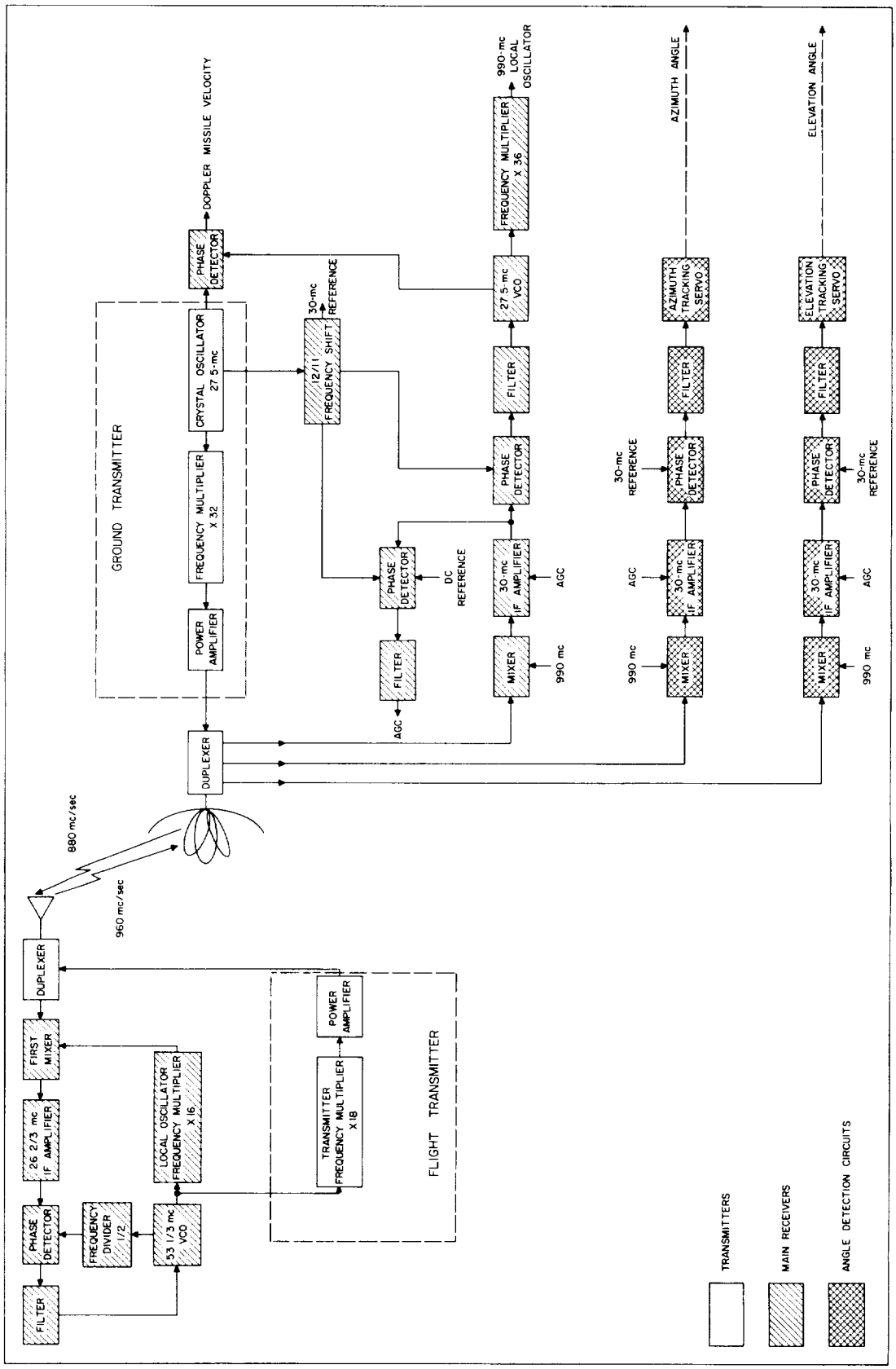

Fig. 78. Two-Way UHF Doppler System

position in space, this transponder would permit the integration of Doppler cycles to measure precise radial range. The transponder would permit the measurement of precise radial velocity and, with the use of the angle information, permit a reasonably accurate determination of position, velocity, and acceleration along the trajectory.

The ground-to-vehicle link would have included the addition of a ground transmitter to the *Juno II* down-range tracking station. This transmitter, as shown in Fig. 78, was to have been duplexed with the receiver and would have utilized the same 10-ft parabolic antenna. It was planned that the organizations operating the 960 mc/sec converted *Microlock* receivers would receive the *Juno IV* vehicle transmission in a manner similar to that for the *Juno II* program; however, there would be no transmitters at these sites, nor would a transmitter reference be sent to these stations in real time.

The radio tracking study was partially completed. No hardware was developed or procured during the *Juno IV* program.

2. RANGE SAFETY INERTIAL SYSTEM

a. Purpose and philosophy. The range safety protection is difficult for missile flights that use a relatively low trajectory, low thrust acceleration, and long burning times. The standard radar tracking techniques are applicable only while the radar has line-of-sight from the range-safety center to the vehicle. For some applications, the vehicle is well below the horizon relative to Patrick Air Force Base (PAFB) for an appreciable period of time during motor burning. Radar range safety surveillance would necessitate the use of radar well down-range from PAFB, a situation which would create communication problems. It is a common procedure in range safety to telemeter certain inertial signals, such as accelerometer and gyro outputs, to augment the radar data; however, complete reliance on telemetered inertial signals would not be satisfactory. Further, telemetering such signals is unnecessary. Computations and decisions can be done in the vehicle with great precision and reliability. (An airborne system to accomplish the range safety destruct decision is presented here.)

b. Functional description. The inertial range safety system (see Fig. 79) may be conveniently divided into four parts: angle sensors, safety bound sensors, majority decision device and associated circuitry, and the destructor.

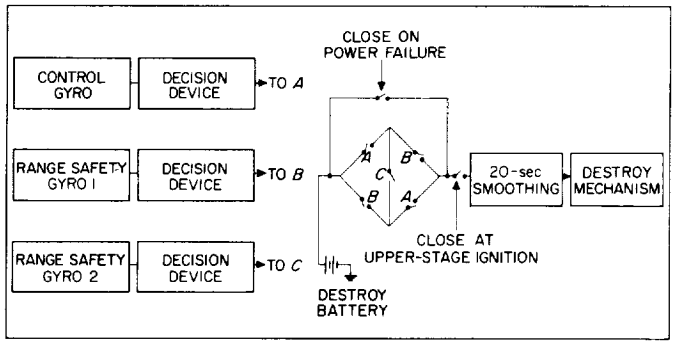

Fig. 79. Range Safety Inertial System

The angle sensors are three gyros. Two 2-degrees-of-freedom gyros, gyro 1 and gyro 2, which sense angular deflection about the yaw axis, and one guidance yaw gyro, a strapped-down single-degree-of-freedom gyro which senses angular deflection about the vehicle yaw axis. The output of each of these three gyros is fed into a yaw safety bound sensor, a decision device that sends a relay-closing command to the majority decision device if the output of its associated gyro exceeds the preset safety bound.

The majority decision device is a logic circuit which provides a closed path from the range safety destroy battery to the destructor in the event that it has received a relay-closing pulse from any two of the yaw safety bound sensors. In parallel with the majority decision device is a power failure fail-safe relay which provides a closed path between the range safety destroy battery and the destructor in the event of vehicle power failure. Between the majority decision device and the destructor, and in series with them, are two auxiliary elements. The first is the range safety system arming relay which closes at upper-stage ignition and opens at upper-stage shutoff. The second is a smoothing, or delay, element which acts as a low-pass filter preventing pulses shorter than some given duration from causing the output of the delay element to be large enough to trigger the destructor. This delay is necessary to eliminate the danger of unnecessarily destroying the vehicle as a result of system transients. The upper bound on the duration of the delay is that time of flight which at maximum acceleration in a 90-deg yaw attitude would put the vehicle in dangerous range of the East Coast at its completion. The delay time, for example, might be of the order of 20 sec. The destructor is the standard range safety destructor.

c. Range safety two-degree of freedom yaw gyros. The primary elements in the range safety all-inertial system

are a pair of 2-degrees-of-freedom gyros (of the Summers type). Range safety gyro 1 will be oriented with its spin axis perpendicular to the flight plane and with the angular-momentum vector of the spinner pointing to the right (easterly), and the inner gimbal axis will be oriented along the roll axis of the missile. The yaw angle will be measured relative to the outer gimbal and the airframe. The range safety gyro 2 will be oriented the same as gyro 1 except that the angular-momentum vector of the spinner will point to the left (westerly).

The orientation of the free gyros eliminates the drift about the yaw axis directly from mass unbalance (the chief contributor), since the thrust force is always perpendicular to the yaw axis. However, there is a drift about the roll axis caused by mass unbalance which is coupled into the yaw axis by virtue of the pitch motion of the vehicle. This effect (plus all other effects) gives a total error of less than 2½ deg for the 600 sec of operation. For purposes of analysis the 2½-deg error will be considered a two-σ number.

In order to reduce the possibility of human error, inherent in any range safety system, it is very important that gyros 1 and 2 be set to their reference independent both of the guidance gyro and of each other.

The orientation of the spin axes antiparallel helps to make the error effects independent. Such disturbances as missile banging at separation, virbration, etc., will not cause the two gyro to misorient together in some systematic way.

d. Guidance gyro. The third gyro used in the range safety inertial system is termed the yaw guidance system gyro. Since, in the proposed application, this will be a single-degree-of-freedom rate gyro (commonly called "strapped down" rate gyro). Since this gyro is a single-degree-of-freedom gyro, some difficulty is experienced if the missile has excessive rolling rates. Gyros 1 and 2 operate independently of roll angle or roll rate unless the vehicle rolls to 90 deg or more, in which case they would tumble, and the destroy signal would be sent.

The decision device and the safety bound sensors are basically relay circuits. Present reliability techniques render the probability of relay failure negligible.

e. Reliability discussion. From the standpoint of reliability, the important characteristic of this system is the use of three gyros to measure a single angle coordinate. In this application, monitoring this one coordinate is completely sufficient for the range safety problem. The range safety problem studied here assumes that the only potential danger is for the second-stage yaw angle to exceed some preset number, say ± 5 deg for an appreciable length of time. Detailed studies have shown that failures constrained to the standard trajectory plane are not cause for missile destruct.

The uses of the three gyros in this system differ. Two of the gyros are free, and the third controls the yaw heading of the vehicle. Thus, drifts of the control gyro are actually followed by the control system, i.e., for most types of errors in the control gyro the angle picked off will be near zero (depending on the yaw loop gain). The probability of the control gyro taking the missile out of the safety bound (± 5 deg) is estimated to be 1/100. Thus, for reliability studies of the range safety system, one must compute the probability of a failure of the two free gyros to be combined with the above event, i.e., it is desired to compute the probability of the range safety bounds being exceeded because of the control gyro but undetected by the free gyros. The probability P_{RSF} of the range safety system failing to destroy a missile outside the angle bounds, from the above type of failure is

$$P_{RSF} = \tfrac{1}{2}P_{CF}\ (\tfrac{1}{2}P_{1F} + \tfrac{1}{2}P_{2F} + \tfrac{1}{4}P_{1F}P_{2F})$$

where

P_{CF} = probability of the control gyro drifting in such a way as to lead the missile out of the bounds

P_{1F} = probability of gyro 1 having an error larger than the bound in either direction (thus the ½

P_{2F} = same as P_{1F} for gyro 2

The values of P_{1F} and P_{2F} are about 1/100.

Thus

$$P_{RSF} = \tfrac{1}{2} \times 10^{-4} = 1/20{,}000$$

a value less than normally required of a nuclear disaster.

The second general type of failure of the range safety system concerns those missiles that exceed the safety bound independent of the control gyro, e.g., a yaw actuator failure. In this case there are three essentially free gyros, two of which must fail to do their jobs in order to cause a range safety failure. Clearly, the probability of this is much smaller than that computed for case 1.

APPENDIX A

Summary of the Analysis on the *Juno IVA* Separation Utilizing an Energy-Storing Mechanical Device

I. OUTLINE OF THE PROBLEM

On August 27, 1958, separation of the two stages by the use of some mechanical, energy-storing mechanism was suggested. As an example, a sling-shot principle could be cited and helical springs, bungee cords, or Belleville spring could be employed. (See sketch A-1.)

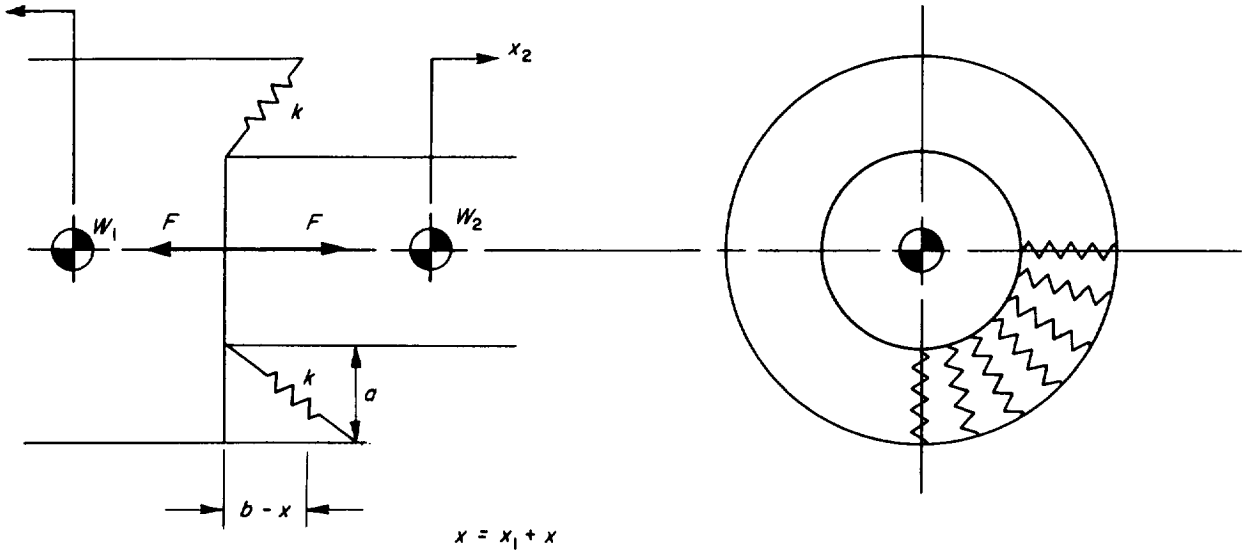

II. THE SCOPE OF THE PROJECT

It was decided that study of the items listed below would be emphasized.

1. Spring force-producing mechanism.
2. Locking and actuating mechanism.
3. Special features:
   a. Reliability.
   b. Self-compensating in the radial direction, axial motion of the two stages.
   c. Fairly easy handling.
   d. Safety.
4. Proposed sequence of events:
   a. Shutoff of Stage 1 motor.
   b. Separation and positive acceleration of stage 2.
   c. Ignition of Stage 2 motor.
5. Loading and checkout of the separation mechanism.
6. Transverse motion of the two stages during separation.
7. Separation mechanism attachment on Stage 2—axial loads on Stage 2 nozzle, etc.
8. Allowed overlap distance between the two stages.

III. EQUATIONS OF MOTION

As indicated in Sketch A-1, the equations of motion for the two stages at separation are:

$$\ddot{x}_1 = \frac{kg}{W_1}(b-x)\left[1 - \frac{a}{\sqrt{a^2+(b-x)^2}}\right]$$

$$\ddot{x}_2 = \frac{kg}{W_2}(b-x)\left[1 - \frac{a}{\sqrt{a^2+(b-x)^2}}\right]$$

Initial conditions: At $t = 0$, $x = x_1 = x_2 = \dot{x}_2 = \dot{x}_1 = 0$

The overlap distance is some distance required to separate, or $x = x_1 + x_2 = b$; thus

$$\ddot{x} = \ddot{x}_1 + \ddot{x}_2 = kg\ (b-x)$$

$$\left[1 - \frac{a}{\sqrt{a^2+(b-x)^2}}\right]\left[\frac{1}{W_1} + \frac{1}{W_2}\right]$$

where

k is the effective spring constant

W is the weight of the stages

b is the overlap distance

a is defined on Sketch A-1

g 32.2 ft/sec^2

Considering the absolute acceleration of the two stages, the following absolute relationship can be derived:

$$\ddot{x}_1 = \frac{W_2\,\ddot{x}}{W_1 + W_2}$$

$$\ddot{x}_2 = \frac{W_1\,\ddot{x}}{W_1 + W_2}$$

The above equations were solved and plotted for a number of different parameters and are illustrated in Fig. A-1.

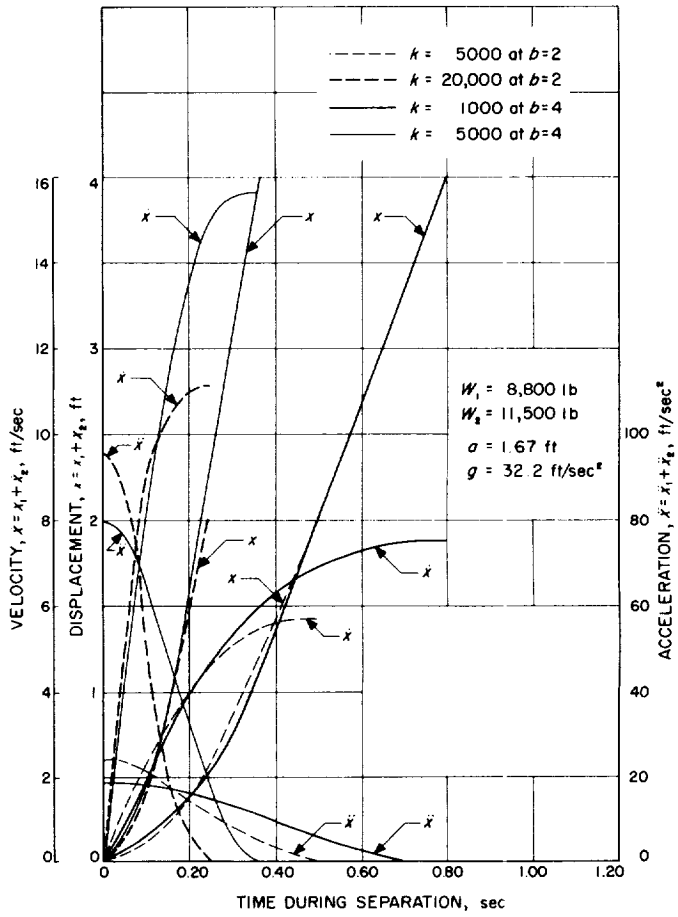

Fig. A-1. Equations of Motion Plotted for Different Parameters

IV. DISCUSSION

A. Results

1. The axial separation dynamics equations were solved, and some representative values are presented in Fig. A-1.

2. An attempt made to investigate angular motion through analytical expressions turned out to be too complicated for convenience. Thus, a conservative assumption was made taking a constant maximum value for the torque, $T = Fd$, with the following values:

$K = 10{,}000$ lb/ft

$b = 4$ ft

$a = 2$ ft

$d = \frac{1}{2}$ in.

$t = 0.3$ sec, separation time

$I_1 = 83{,}000$ slug ft^2

$I_2 = 4{,}800$ slug ft^2

α_1 and α_2 were calculated:

$$\alpha_1 = \frac{kdb}{2I_1}\left[1 - \frac{a}{\sqrt{a^2+b^2}}\right]t^2 = 0.0005 \text{ rad}$$

$$\alpha_2 = \frac{kdb}{2I_2}\left[1 - \frac{a}{\sqrt{a^2+b^2}}\right]t^2 = 0.0029 \text{ rad}$$

The angles swept are thus rather small and should not present a problem.

B. Belleville Spring

A possibility to utilize a Belleville spring was investigated. The analysis was made at a rather shallow level, mostly to demonstrate the possibility of using the spring, and realizing very strongly the assembly problems.

C. Areas Still to be Investigated

A number of areas still remaining to be investigated for a more thorough understanding of the problem following:

1. Complete analogue computer solutions for a given range of variable parameters with more realistic design values.
2. More detailed information on the bungee cord and the helical spring mechanics.
3. A thorough investigation of the structure around the joint of the two styles.
4. Choice between motor and special support structure for attachment of loading mechanism.
5. Minimum time interval with position acceleration required on stage 2 to get rid of the gas bungees in the fuel lines.
6. Actual, more accurate, test data on bungee cords and springs — load vs elongations plots.
7. Size of the doors in the missile to connect the springs or cords.
8. Need for adjustment devices to set the given initial spring tension in the system.
9. Effects of strain energy in the missile before and after separation.
10. Incorporate pitching rates in the rotational equations (α); consider translation.

D. General Comments

1. Two bungee cord manufacturers have been contacted. Both were east coast companies without adequate technical information agencies in existence (just distributors) on the west coast.
2. A number of helical spring manufacturers have been contacted in the Los Angeles area, and some of them were willing to engage in a specialized, closely controlled development project.
3. An approximate, conservative, axial thrust load value that the stage 2 motor can structurally take is 3,000 lb.
4. The problem seems to offer a number of attractive features and lends itself to a reasonable solution.

APPENDIX B

Summary of the Analysis on the *Juno IVA* Separation Dynamics Utilizing Stage 2 Thrust

I. INTRODUCTION

Separation dynamics of the *Juno IVA* vehicle was studied to determine the time and the radial clearance required during the separation of the two stages.

Several sketches utilized in this analysis are the overlap distance of the two stages (Fig. B-1), and two sketches defining different geometrical considerations (Fig. B-2). The two different geometrical configurations studied produced nearly the same results and thus are not considered separately. Only the first geometrical layout (where the centers of gravity of the two stages are displaced in the opposite directions (Fig. B-2a) is summarized in this Appendix).

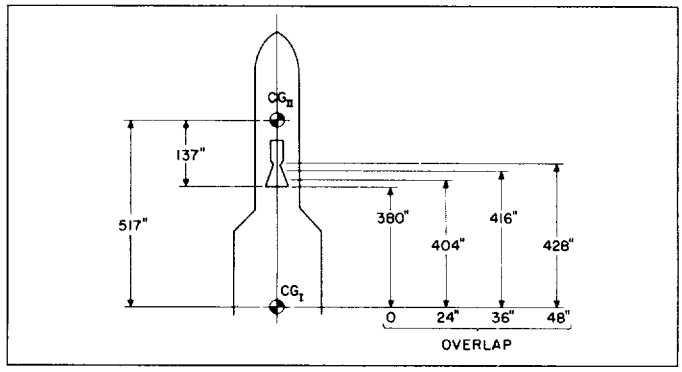

Fig. B-1. Rotational Lengths of the Two Stages as a Function of the Overlap Distance

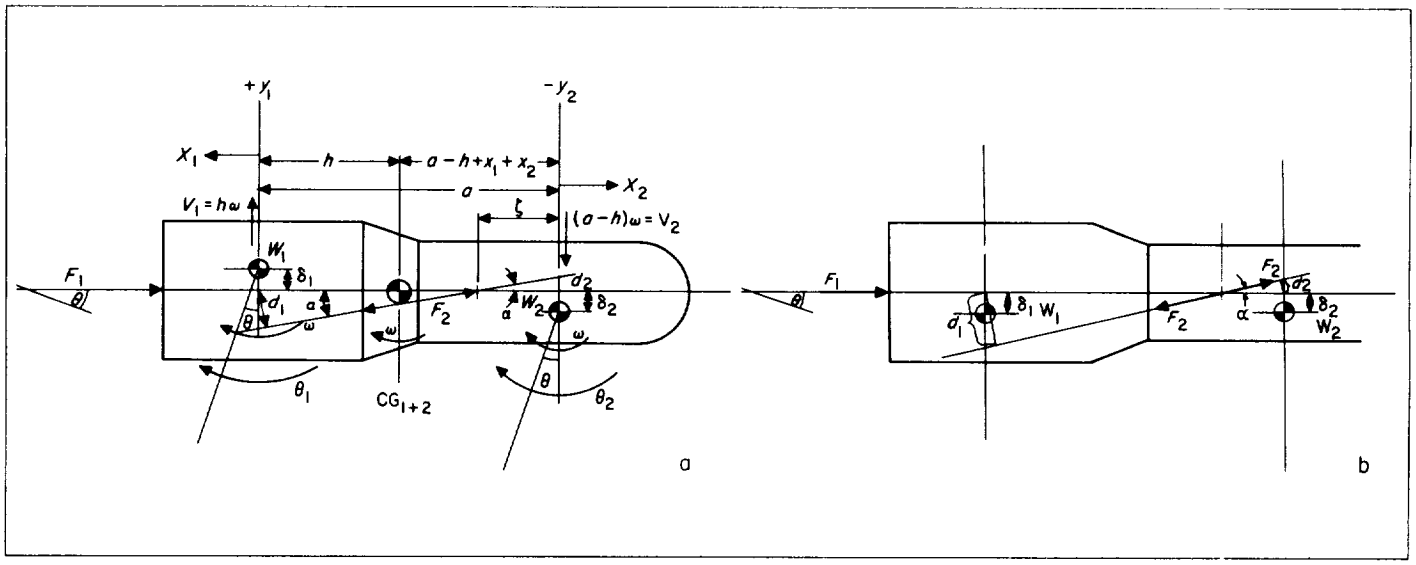

Fig. B-2. Geometrical Configurations

II. CONDITIONS AT SEPARATION

The following conditions were considered at separation:

W_1 = weight of stage 1 = 10,200 lb

W_2 = weight of stage 2 = 11,423 lb

I_1 = pitch moment of inertia of stage 1 = 83,000 slug-ft²

I_2 = pitch moment of inertia of stage 2
= 4,800 slug-ft²
center of gravity of stage 1 = 510 in.*
center of gravity of stage 2 = +7 in.*

ω = pitch rate at separation = 1 deg/sec

α = angular misalignment of stage 2 motor
= ¼ deg

δ_1 = radial displacement of the cg on stage 1
= ¼ in.

δ_2 = radial displacement of the cg on stage 2
= ¼ in.

$x_{1,2}$ = absolute axial displacement of the two stages

$\theta_{1,2}$ = absolute angular displacement of the two stages

a = distance between the cg of the two stages

b = distance from cg_2 to the point were the stage 2 motor is attached

$F_{1,2}$ = thrust of the two stages, lb

$V_{1,2}$ = translational velocity of the two stages, a function of ω and the distance between the individual and common cg

$Y_{1,2}$ = Radial displacement of the two stages

*This value refers to JOM 545342

A. Assumptions

1. Thrust of the two stages is a function of time and is defined on Figs. B-3 and B-4.
2. Stage 1 experiences full value of thrust from stage 2, F_2 throughout the separation.
3. Constant α throughout separation.
4. F_1 is directed through the geometrical center of stage 1.
5. F_2 is set with $\alpha - ¼$ deg throughout separation.
6. Throughout separation weights of the two stages remain constant.

B. Separation Equations Derived

$$\ddot{X}_1 = \frac{g}{W_1}\,[F_2 - F_1] + g \sin\theta_1$$

$$\ddot{X}_1 = \frac{F_2}{W_2} - g \sin\theta_2$$

$$\ddot{\theta}_1 = \frac{F_2}{I_1}[\alpha\,(X_1 + X_2 + a - b) + \delta_1] - \frac{F_1\,\delta_1}{I_1}$$

$$\ddot{\theta}_2 = \frac{F_2}{I_2}\,[b\,\alpha + \delta_2]$$

And initial conditions are, at

$t = 0$:

$$x_1 = x_2 = \dot{x}_1 = \dot{x}_2 = 0$$

$$\theta_1 = \theta_2 = 0$$

$$\dot{\theta}_1 = \dot{\theta}_2 = \omega$$

The term $g \sin\theta$ is rather small and $\sin\theta \approx \theta$ for small angles; $g\theta_2$ = small number ≈ 0, thus the equations solved were:

$$\ddot{x}_1 = \frac{g}{W_1}\,[F_2 - F_1]$$

$$\ddot{x}_2 = g\,\frac{F_2}{W_2} - g\,\theta_2$$

$$\ddot{\theta}_1 = \frac{F_2}{I_1}[\alpha\,(x_1 + x_2 + a - b) + \delta_1] - \frac{F_1\,\delta_1}{I_1}$$

$$\ddot{\theta}_2 = \frac{F_2}{I_2}[b\alpha + \delta_2]$$

The initial conditions remained the same as above.

The above Equations were solved for two different conditions:

1. A limiting case, where the thrusts on the two stages were such as to produce equal accelerations, with F_1 decaying and F_2 building up: $x_2 = x_1$.
2. Such a thrust combination value as to produce $\ddot{x}_2 > -\ddot{x}_1$.

The above two conditions safeguard against the undesirable situation of stage 1 "catching up" with and "bumping" into stage 2.

III. REPRESENTATIVE SOLUTIONS

Representative solutions are given in Fig. B-5, where overlap distance, individual rotation of the stages, and total radial clearance are plotted vs time required for separation.

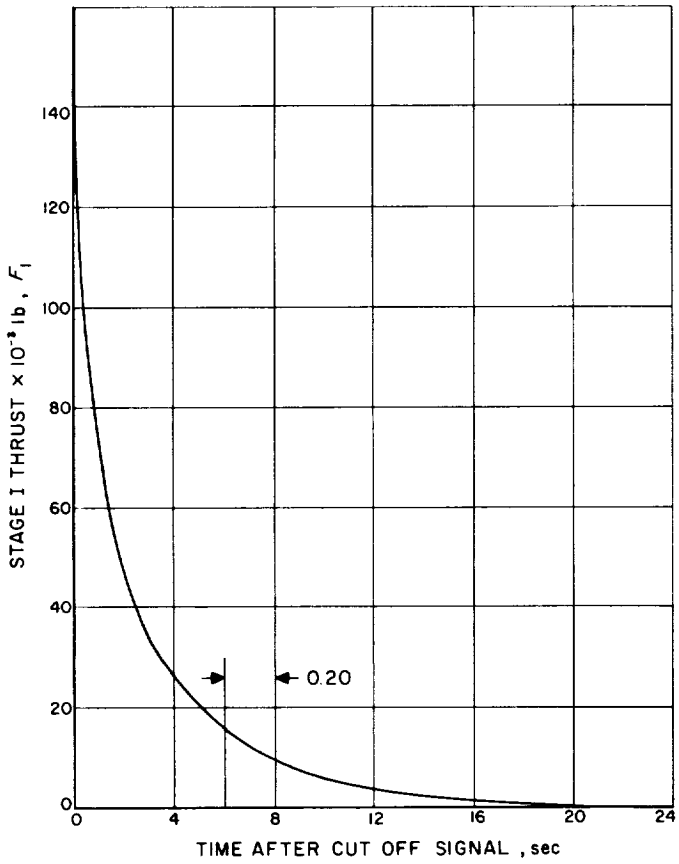

Fig. B-3. Stage 1 Thrust After Cutoff Signal.

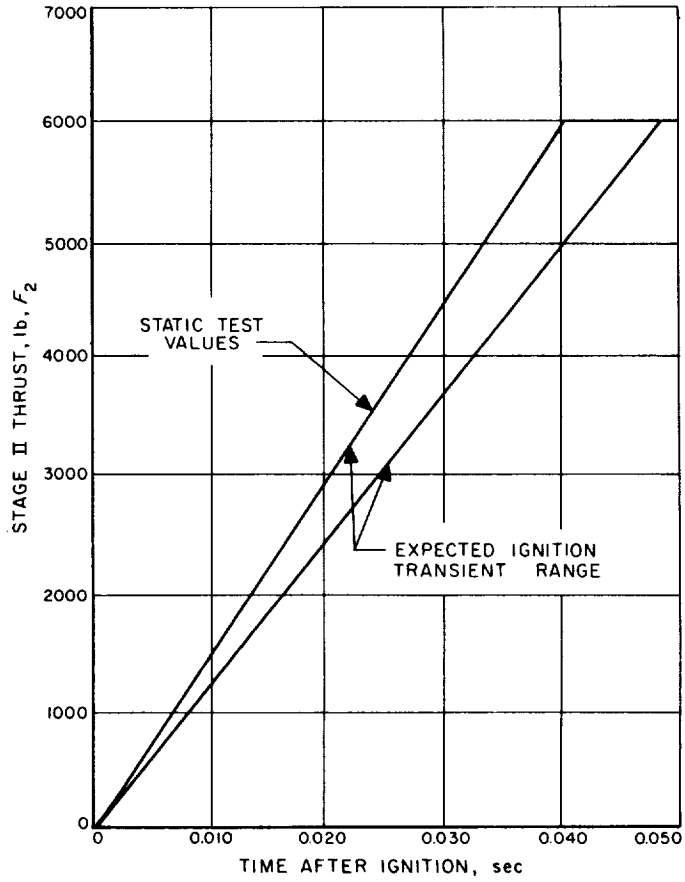

Fig. B-4. Stage 2 Thrust After Ignition.

IV. SUMMARY OF RESULTS

Discussion of results can be summarized in the following points:

1. Separation utilizing main motor thrust of stage 2 is quite feasible and can be accomplished in the time interval less than 1 sec.

2. Radial clearance required between the components of the two stages does not exceed 6 in. in the cases studied.

3. From the experience gained in the above analysis, hardly any major trouble areas could be expected. However, it should be borne in mind that the history of stored strain energy in the missile during separation has not been studied; a number of physical values assumed (such as the values of ω, α, etc.) are pure estimations; the action of F_2 on stage 1 is an unconfirmed assumption.

4. For an intelligent design a more complete analysis would be required.

5. The build up transient of F_2 is rather insignificant because of the short time involved.

6. The decay and the reproducibility of the decay of F_1 is of considerable importance and the shutoff of stage 1 should be controlled rather closely.

7. One obviously safe solution of the separation problem could be accomplished by disconnecting the stages at the full value of F_2 and some convenient, low value of F_1.

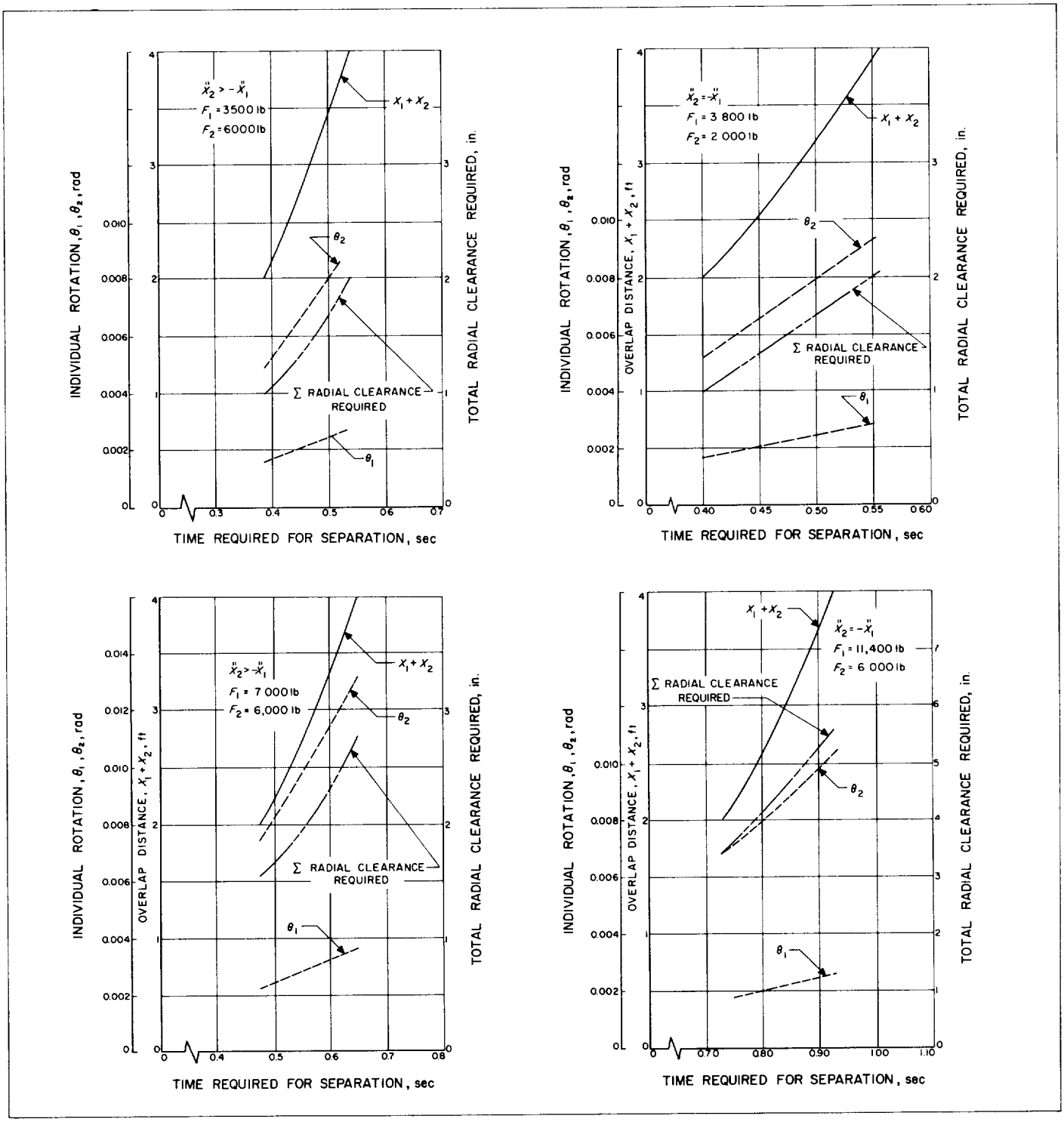

Fig. B-5. Representative Solutions for Time Required for Separation vs Rotation of Stages, Total Radial Clearance, and Overlap Distance.

APPENDIX C

Juno IV Propellant Tanks

The *Juno IV* second-stage propellant tanks were designed as pressure vessels, since the propulsion system was to use helium pressure or pressure from a gas-generation system rather than a pump to force the propellants from the tanks into the motor. The configurations considered were a single tank with a diaphragm separating the fuel and the oxidizer and a pair of tanks, one for fuel and one for oxidizer. The tanks should be as close to spherical as possible since a sphere is the lightest pressure vessel that can contain a given volume. A conical tank bottom is a necessary compromise in order to insure complete propellant drainage and also to provide a means of carrying the motor thrust since the tank is also used as the motor mount. The tank volume is fixed by the weight of propellant that must be carried and by an ullage volume large enough to prevent a temperature rise from causing a large pressure increase if the tank is sealed after it is filled.

Aluminum, rather than stainless steel was chosen as the tank material because a steel tank would require such a thin wall that maintaining reasonable tolerances would be very difficult, making the tank would be hard to fabricate. An increase in tolerance would be necessary if steel were used with a resultant weight increase. The 2014 aluminum alloy was chosen rather than the 7075 because difficulties have been reported with welding 7075 and because random strength brittle failures occur in it. The 2014 has been used in other programs and reports of similar difficulties with it were not known to us. However, since there are problems associated with welding the 2014 alloy, alternate tank using 6061 aluminum alloy was recommended because it is much easier to weld and despite its low strength.

The first configuration considered was a single tank with a diaphragm, the outside diameter of which was 70 in., making it compatible with an available 70-in.-diameter guidance compartment (Fig. C-1). The oxidizer, which has a higher vapor pressure than the fuel, was placed forward so that before pressurization the diaphragm would be in tension if the tanks were sealed after filling and no other precautions were taken. After pressurization, the diaphragm may be loaded by pressure from either side as a result of regulator fluctuation and must, therefore, be designed to withstand the maximum pressure that would cause buckling. A pressure of 20 psi was chosen for design purposes and this results in a spherical diaphragm with a radius of 42 in. and a thickness of 0.1 in. A lighter diaphragm could be used if the requirement for resisting a buckling pressure were removed. This could be done by placing the fuel forward and the oxidizer aft and requiring the fuel side of the tank to be filled and partially pressurized before adding the oxidizer. In addition, it would be necessary to operate the fuel side of the tank at a higher pressure than the oxidizer side to make sure that regulator fluctuation did not result in a buckling pressure on the diaphragm. This approach would be beneficial since the fuel is used as the motor coolant and requires a higher pressure than the oxidizer to compensate for the pressure drop in the motor coolant passages. In either case, discontinuity stresses at the tank-diaphragm joint might require the addition of a structural ring at the joint. A second reason for placing the oxidizer forward of the fuel is that, should an intertank leak develop, it is less dangerous for oxidizer to leak into the fuel than vice versa.

The second configuration considered was a double tank with the outside skirt diameter equal to 70 in. The advantages of this configuration were that there was no tank-diaphragm joint to be developed and that there was a smaller safety problem since a leak would permit fuel or oxidizer to leave a tank with only a remote chance of their mixing. A weight penalty, compared to the double tank with unrestricted diameter, of about 30 lb accompanies this configuration because of the rings needed to join the tanks and the skirt since the tanks are 7 and 13 in. smaller than the skirt.

The third configuration considered was the double tank with unrestricted diameter. This configuration has the same advantages as the one just described but does not suffer its weight penalty since the skirt can be attached to the tank through a doubler which needs no extra rings.

The weights of the double tank with unrestricted diameter and the single tank with a diameter of 70 in. are shown in Table C-1 and the tank layouts are shown in

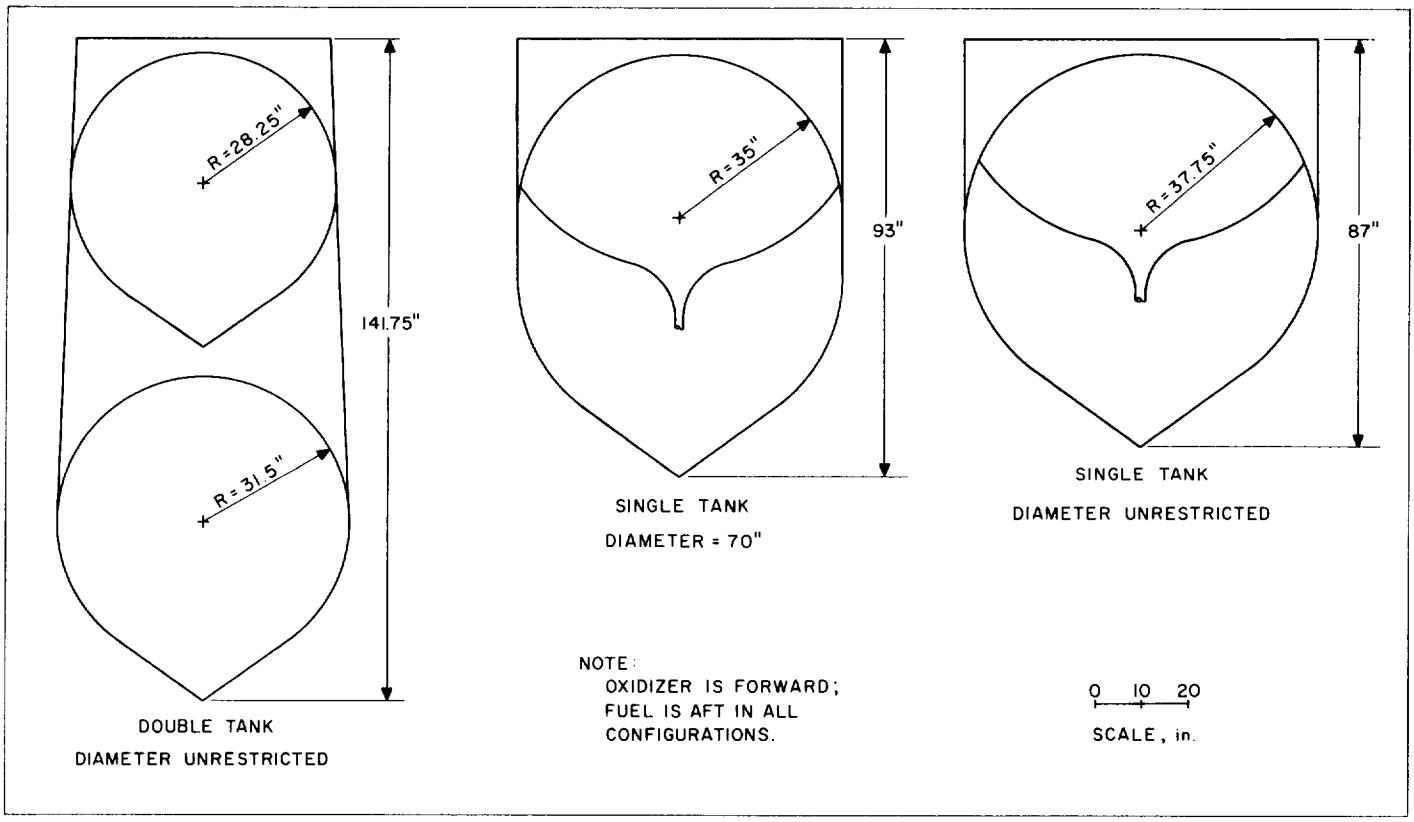

Fig. C-1. Tank Layouts

Fig. C-1. The extra length of the double tank configuration was not an excessively detrimental factor and, although the weight difference of 10 to 35 lb is in favor of the single-tank configuration, several factors (safety, ease of fabrication, and lack of a diaphragm and tank-diaphragm joint to develop) led to the decision to use the double tank with unrestricted diameter. These tanks would be made of 2014 aluminum, as mentioned earlier. Tanks made of 6061 aluminum would add 50 lb to the total weight shown in Table C-1. An increase in tank pressure to 265 or 280 psi would add 7 and 13 lb, respectively, to the oxidizer tank and 9 to 17 lb, respectively, to the fuel tank. These pressure increases on a 6061 aluminum tank would result in weight addition of 9, 15 lb and 11 and 21 lb, respectively.

When the *Juno IV* program was cancelled, spinning blank drawings and machine drawings for the two halves of the fuel and oxidizer tank were available. The details of the lower part of the bottom cone in each tank, assembly, and other tooling drawings were in preparation. Drawings were also being made for the equipment needed for a static test of the tank and skirt structure, and tests

Table C-1. Weights in Pounds of Tank Configurations[a]

1. Double tank (diameter unrestricted)			
Fuel tank	154		
Oxidizer tank	114	268	
10 in. of 0.1 in. doubler	22		
Center skirt (aluminum)	53		
Two rings	11	86	
5 in. of 0.1 in. doubler	11		
Forward skirt (magnesium)	12		
Two rings	21	44	
Total		398	(408)[b]
2. Single tank with diaphragm (diameter — 70 in.)			
Tank	270		
Diaphragm	53	323	
5 in. of 0.1 in. doubler	11		
Forward skirt (magnesium)	18		
Two rings	21	50	
Total		373	(388)[c]
3. Single tank with diaphragm (diameter unrestricted)			
Tank	231		
Diaphragm	53	284	
5 in. of 0.1 in. doubler	11		
Forward skirt (magnesium)	21		
Two rings	21	53	
Total		337	(352)[c]

[a]The following weights have not been included: complete aft skirts, rings and doubler, fuel lines, electrical cable.
[b]Includes 10 lb for extra propellant lines and electrical cable.
[c]Includes a ring at the tank-diaphragm joint.

were to be started on the loading method to be used for applying simulated logitudinal gravity loads to the tanks.

Weight and layout details are shown in Table C-1 and in Fig. C-1 for a single tank with a diaphragm and unrestricted diameter. These details are presented here to indicate that if development time is available to make a satisfactory diaphragm and tank-diaphragm joint and if configuration restrictions do not apply and if testing can demonstrate that safety is not a problem with this configuration, then a weight saving of 46 to 71 lb and a shortening of 55 in. in the propulsion system would be possible.

APPENDIX D

Skirt Design

The payload, guidance, tankage, and propulsion systems of the 6K stage are interconnected and supported by an external truncated conical shell or skirt. The skirt is conveniently described as consisting of three sections, aft skirt, center skirt, and forward skirt.

In order to find an optimum skirt design, several possible choices of construction were considered, including semi-monocoque, thin shell monocoque and corrugated thin shell monocoque construction. Since preliminary basic loads indicated that longitudinal loads would be high and aerodynamic heating would be relatively low, it appeared that a thin-walled corrugated-shell type of construction would have the highest strength-to-weight ratio. Furthermore, since this type of construction had been used in the *Jupiter* and Redstone programs, ABMA reports were available on the load-carrying characteristics of corrugated shells. It should be noted that detailed basic load analyses were being accomplished at the conclusion of the project which would justify or reject the above preliminary assumption.

Finally, a study was made on the strength-weight ratios for aluminum and magnesium sheet. This study indicated that aluminum would be a more efficient material for the skirt in all sections except possibly the forward section.

In order not to exceed the column buckling allowable of a single corrugation, ring stiffeners were positioned intermittently along the axis of the airframe. An optimum design (the current design is not necessarily optimum) would have the column-buckling stress equal to the crippling stress, equal to 1.33 times the design stress. The initial corrugation design was predicated on the optimization of the structure. Later changes in design loads and necessary geometrical configurations deviated from this optimum condition.

I. AFT SKIRT

The aft skirt extends between the separation joint (between stages 1 and 2) and the fuel tank. This skirt also supports the pressurization system, a series of 21 in.-diameter spheres hung between the two ring stiffeners located at the third points of the skirt.

The fixed tank diameters together with the fixed separation joint diameter of 70-in. required that a change in slope exist between the center skirt and aft skirt. This change in slope was accomplished by a kink joint at the fuel tank (station 65). This kink will introduce local stresses in the skin at station 65.

The preliminary stress analysis, including localized stresses resulting from the above local loads indicated that an 0.032 in. aluminum corrugation would be adequate.

II. CENTER SKIRT

The center skirt extends between the fuel tank and oxidizer tank.

Assembly of the tank piping required that accessibility be provided through this portion of the skirt. This was accomplished by the placement of two doors (approximately 16 by 23 in.) on opposite sides of the skirt between the two third point ring stiffeners.

The preliminary stress analysis indicated in this case that an 0.025 in. aluminum corrugation would be adequate.

III. FORWARD SKIRT

The forward skirt extends between the oxidizer tank and the payload and supports the MING guidance system.

The guidance system components are supported on the periphery of the skirt between two rings. The top ring also forms the payload attachment surface. Intercostals, spaced around the periphery, between the two rings, give the structure added strength and rigidity. The guidance packages are then hung from the rings and/or intercostals. All individual packages are screw attached, enabling them to be removed when necessary.

In order to meet the specifications outlined for the guidance system, it was necessary that the forward skirt be detachable from the oxidizer tank and center skirt. A screw joint served this purpose.

A stress analysis based on preliminary inertial loads indicated negligible stresses for this skirt. It was quite probable that aerodynamic loads in this region would be of considerable significance. Since aerodynamic loads were not available, an adequate stress analysis could not be performed for this skirt.

However, based on experience, it was felt that a 0.016-in. magnesium corrugation would be adequate for this skirt. It is to be noted that further analysis, based on critical load conditions, could result in changes in both the material and skin thickness.

IV. ATTACHMENT OF SKIRT TO TANK

The center and aft skirts are attached to the fuel tank, and the forward and center skirts are attached to the oxidizer tank through cylindrical aprons. These aprons, one each welded to the fuel and oxidizer tanks respectively, extend about 6 in. above and 6 in. below the tanks.

On the fuel tank, the skirts are riveted to the apron, the center skirt overlapping the aft skirt. The attachment on the oxidizer tank is similar, except that the forward skirt is attached with screws for easy removal.

APPENDIX E

Structural Design for Skirt-Supported Actuating System

Two actuating systems for the steering motor were proposed. One was to operate at the head end of the motor with actuators extended from the tip of the fuel tank and connected to the injector head of the motor. Problems in designing a supporting structure for this system such as stability of the thin wall tank, flexibility of the entire system, and the accessibility are of great concern. It was believed that it would be impossible to design and build a good, light-weight structure of this type that could meet all the requirements within the limited time schedule. An alternate system was proposed because of such difficulties.

The new system was to have actuators operating at the throat section of motor, with the other end of actuators connected to the end of the lower skirt. Preliminary structural design study of this type of actuation shows that a very favorable result can be accomplished within the limited time.

I. DESCRIPTION OF STRUCTURE

A relatively stiff ring to receive the end of the corrugated skin at the point of separation between stage 2 and the booster was designed for the purpose of resisting both rotational motion due to the eccentricity of the V-bent and radial motion due to the discontinuity of skirt at this point. With very little modification (i.e., simply by deepening the existing channel section) it can give a very satisfactory support for the actuators without paying an appreciable weight penalty. (See sketch E-1.)

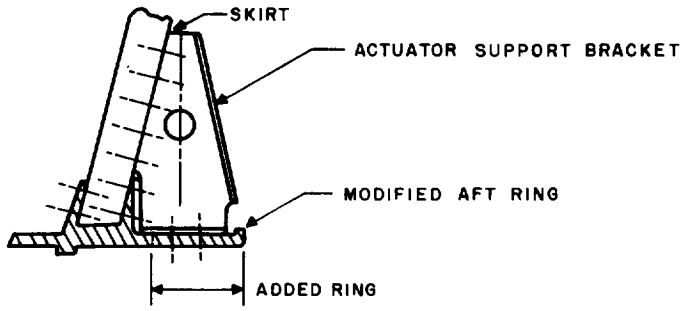

II. CONCLUSION OF DESIGN STUDY

1. With an addition of a 3-in. ring (weight about 5 lb) the natural frequency of supporting structure is up to about 30 cps.
2. For same structural weight, skirt support system gives a stiffer support than would be in the tank-end support system.
3. Cross talk between two actuators located 90 deg apart is more severe for this system than the other system (i.e., 3% vs 0.03%), but it is not unbearable.
4. Ovality of ring is not critical because the radial displacement of 0.015 in./g is only about 1% of the maximum piston travel.

III. STATUS OF DESIGN

1. An analytical study has been completed; it concludes that it is feasible to have actuators connected to the aft end of aft skirt.
2. Design information has been given to the Engineering Design Section; final drawings of ring and bracketry for actuators have not been drawn.
3. Actuator anchorage at the motor end has not been investigated thoroughly.

IV. ITEMS YET TO BE DONE

1. Design of bracketry near throat section of motor for actuator attachment has to be incorporated in the motor design.

V. COMMENTS

The members of Guidance group believed that this skirt-end supported actuating system would render a bigger, heavier and much more unreliable actuator design in comparison with the Tank-end, motor head design they had proposed previously. Since the inherent technical difficulty in the analytical analysis of the latter system appears to prevent a sophisticated design, it was suggested that a thorough design study as well as a test program be initiated in order that a future optimization of design may be accomplished.

APPENDIX F

Basic Loads Summary

I. BASIC LOADS

In order that a preliminary stress analysis of the *Juno IVA* airframe could be prepared, it was necessary to determine the critical applied loads.

It was possible that the critical loading conditions might consist of: inertial loads, maneuver loads, aerodynamic loads, ground handling loads and combinations of the above loads. The need for an immediate analysis of certain portions of the missile precluded the possibility of an accurate determination of all of these loads. Prior experience with similar missiles indicated that the design condition of maximum thrust at burnout of stage 1 with maximum motor gimbal angle would be a conservative design criterion for the major portion of the JPL 6K stage. The first preliminary basic loads analysis was based on this condition.

Ground handling loads were assumed to be noncritical as a basic design philosophy. It was felt that aerodynamic loads might be critical for certain portions of the JPL 6K stage, specifically the forward skirt or section of skirt between the payload and oxidizer tank. In view of this, an aerodynamic analysis was being prepared. This analysis had not reached any conclusions when the project was cancelled.

II. SUMMARY OF PRELIMINARY INERTIAL LOAD COMPUTATIONS

A design condition of maximum thrust at burnout of stage 1 with maximum motor gimbal was assumed critical for preliminary basic load computations.

The weight distribution shown in Fig. F-1 is based on the reference missile established by Appendix II, ABMA-JPL *Second Juno IV* Program Planning Conference Minutes dated 24, 25 September 1958, and ABMA drawing number GM 545342.

The total vehicle weight at burn-out stage 1 is 22052 lb. A maximum stage 1 vacuum thrust of 190,000 lb gives a design axial acceleration of 8.62 g.

Transverse accelerations based on a pitch moment of inertia of 5,267,679 lb-in.-sec^2 and stage 1 gimbal angle of 7 deg are given in Fig. F-2.

Axial loads, transverse shear, and bending moment based on the above basic inertial data are given in Figs. F-3, F-4, and F-5, respectively.

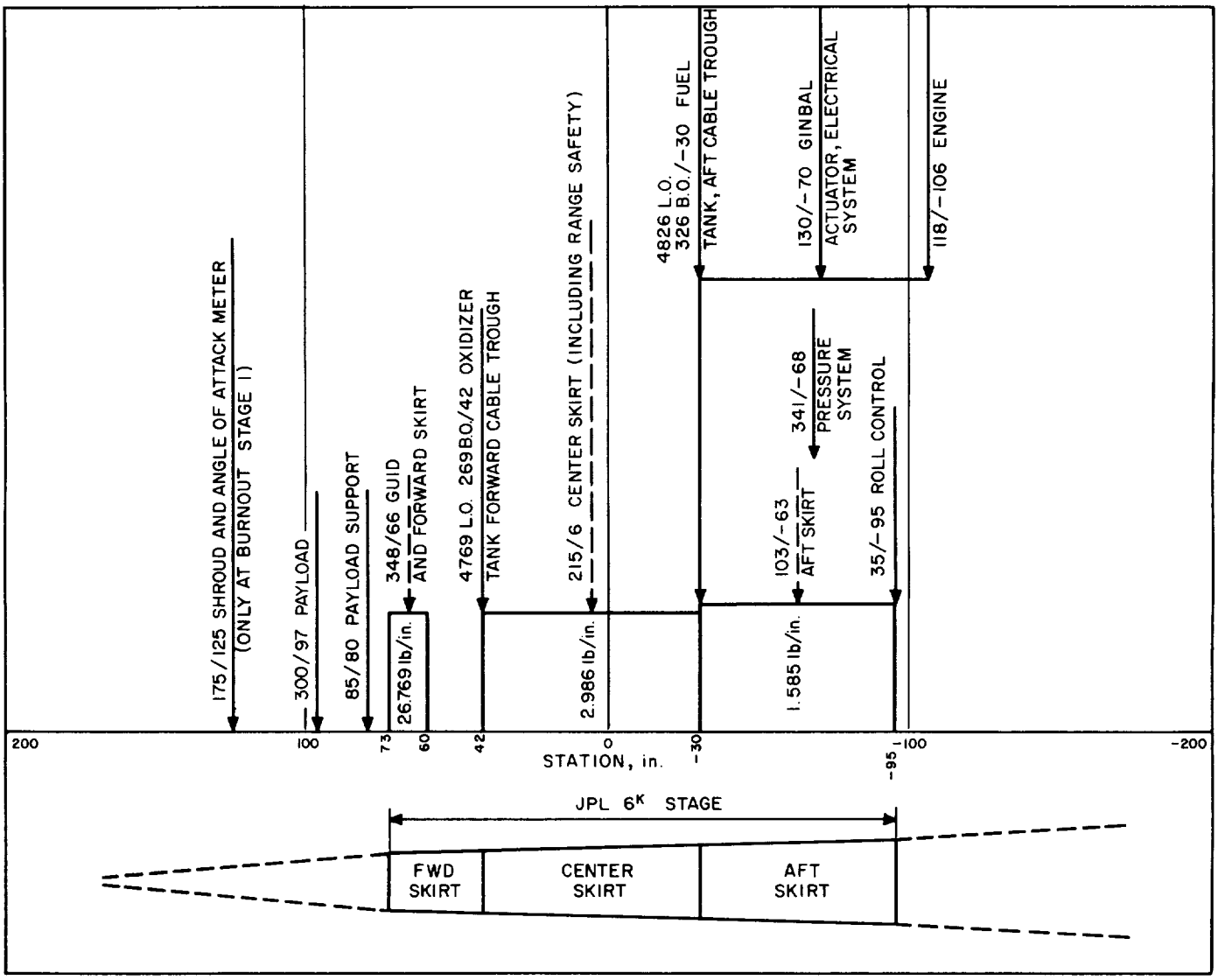

Fig. F-1. Weight Distribution vs Station

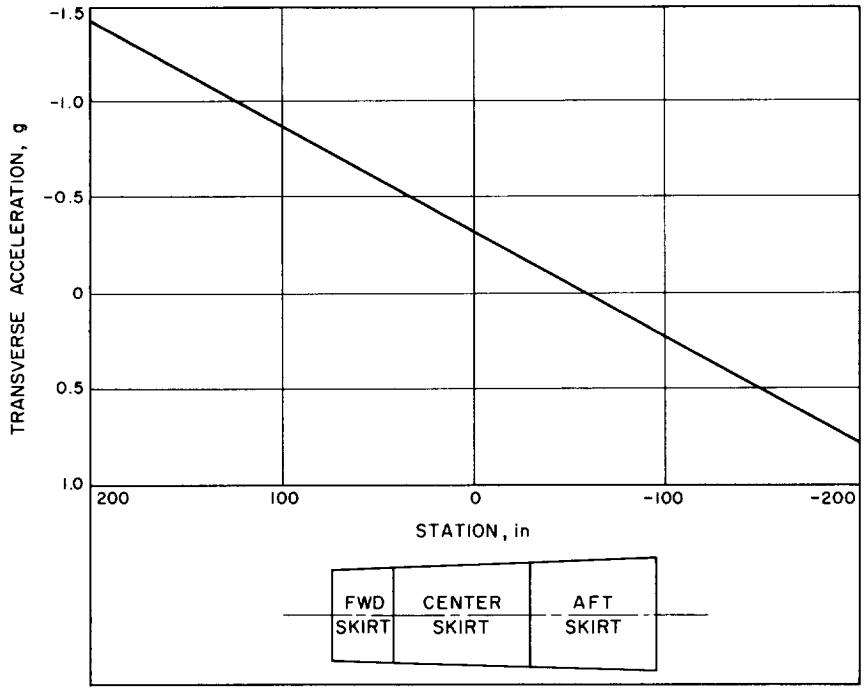

Fig. F-2. Transverse Acceleration vs Station

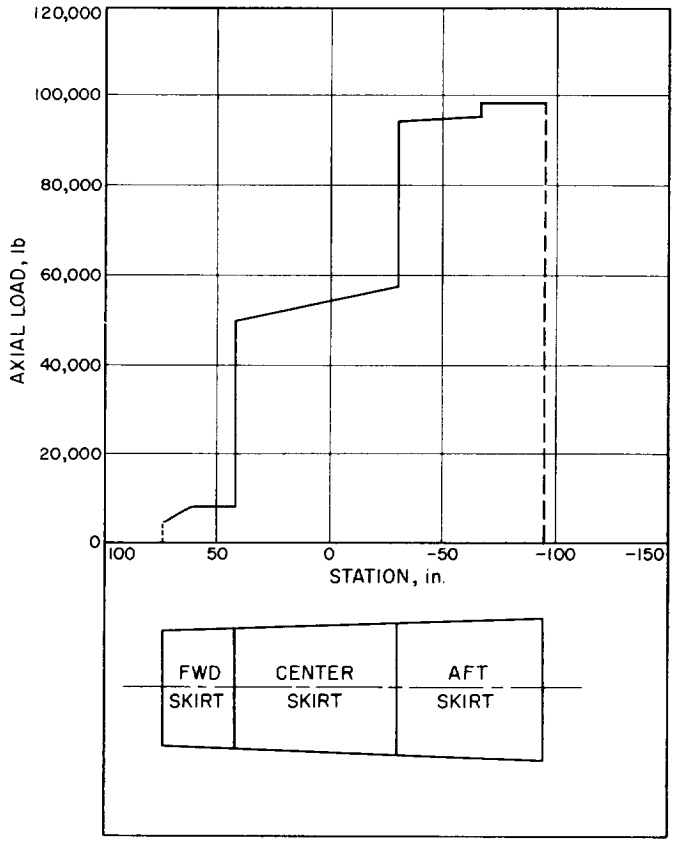

Fig. F-3. Axial Load vs Station

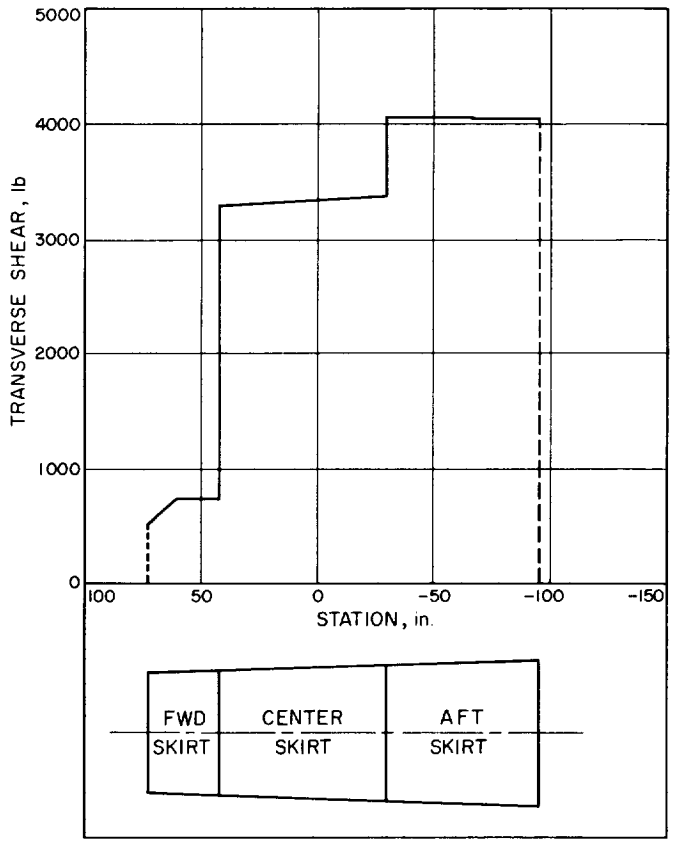

Fig. F-4. Transverse Shear vs Station

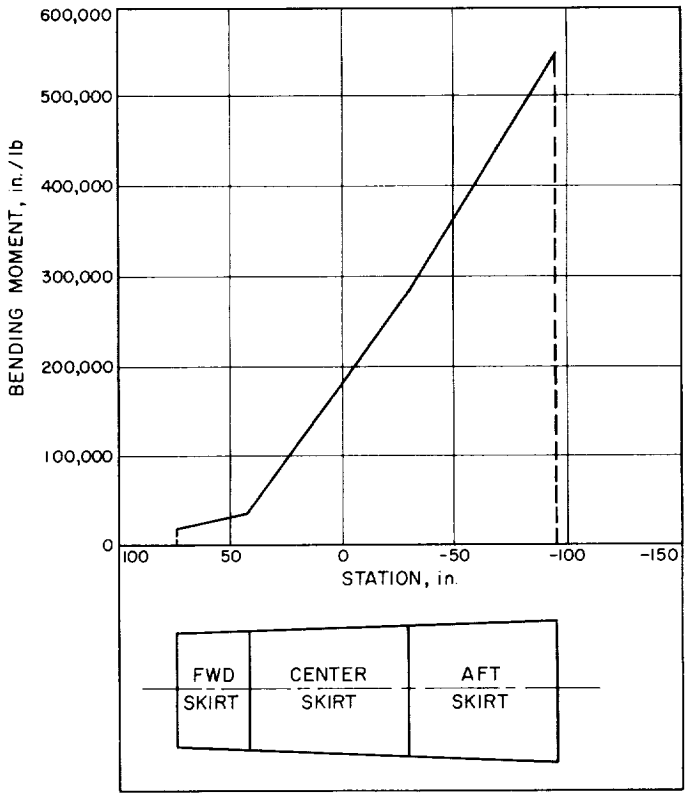

Fig. F-5. Bending Moment vs Station

APPENDIX G

I. PREFLIGHT OPERATION

Operation Analysis of the 45,000-lb-Thrust Propulsion System

A. *Fill preloaded components in missile building*

1. Load N_2O_4 generator start slug and install on missile.
2. Load four gas bottles with nitrogen to 3,000 psia, check for leaks, and install on missile.

B. *Fill oxidizer tank*

1. Make visual observation of main propellant valve (13)[1] to insure that the valves are in the closed position and that main propellant valve-lock pin is in normal position.
2. Connect vapor return line to oxidizer tank vent disconnect (3).
3. Remove oxidizer fill line cap (1) and connect fill line to oxidizer fill disconnect (2).
4. Fill oxidizer tank to required total weight. Monitor oxidizer tank pressure during and after fill.
5. Close remotely operated valve on vapor return line.
6. Establish that oxidizer fill line two-way valve is in closed position.

C. *Fill fuel tank*

1. Insert fuel vapor return line in fuel tank vent disconnect (6).
2. Remove fuel line fill cap (4) and connect fuel fill line to fuel fill disconnect (5).
3. Remove engine fuel bleed cap (7) and insert fuel bleed line. Provide clean collection equipment for overflow.
4. Start filling fuel. When solid column of fuel flows from engine fuel bleed, disconnect fuel bleed line and replace cap (7).
5. Save engine fuel bleed overflow for weighing.
6. Fill fuel system. Monitor fuel tank pressure during and after fill.
7. Complete filling of fuel tank to required total weight, taking account of the amount of overflow.
8. Close remotely operated valve on vapor return line.
9. Establish that fuel fill line two-way valve is in closed position.

D. *Fill generant tank*

1. Make visual observation of generant double valve (12) to insure that valve is in the closed position and that lock pin is in normal position.
2. Remove generant tank vent cap (8).
3. Insert generant vapor return line in generant vent disconnect (9).
4. Remove generant fill disconnect cap (10) and connect generant fill line to generant fill disconnect (11).
5. Remove generant bleed cap (25) and insert generant bleed line.
6. Utilizing a premetered gravity fill procedure, start filling generant tank.
7. When solid column of fuel flows from bleed port, disconnect generant bleed line and replace cap (25).
8. Finish filling generant tank.
9. Disconnect generant fill line from generant fill disconnect (11) and replace generant fill line cap (10) using new crush gasket.
10. Disconnect generant vapor return line from generant tank vent disconnect (9) and replace generant tank vent line cap (8) using new crush gasket.

[1]Numbers in parentheses refer to items shown in Fig. 3.

E. Disconnect propellant and generant vapor return lines and fill lines and connect helium charging lines

1. Disconnect oxidizer fill line from oxidizer fill disconnect (2) and replace oxidizer fill line cap (1) using new crush gasket.
2. Disconnect oxidizer vapor return line from oxidizer tank vent disconnect (3).
3. Disconnect fuel fill line from fuel fill disconnect (5) and replace fuel fill line cap (4) using new crush gasket.
4. Disconnect fuel vapor line from fuel tank vent disconnect (6).
5. Connect helium fill line to helium disconnect (14).
6. Connect helium fill line to helium disconnect (15).
7. Connect helium prepressurization lines to disconnects (3) and (6).

F. Arming of valve actuation systems

1. Visually inspect bleed indicator on closure side of generant valve actuator.
2. Remove generant valve lock pin.
3. Visually inspect bleed indicator on closure side of propellant valve actuator.
4. Remove main propellant lock pin.

Note: This is the final operation by personnel on the 45K stage. Further operations are remotely controlled.

G. Charging main helium and generant helium supply

1. Fill helium systems to 3,000 psia.
2. Monitor tank pressures in order to detect possible valve leaks.
3. Allow sufficient time for helium system to come to thermal equilibrium and recheck pressure.

H. Prepressurization of tank ullage

1. Fill tank ullages to tank design pressure and maintain until system comes to thermal equilibrium (oxidizer tank, then fuel tank)
2. Continuously monitor tank pressures during prepressurization.

Note: The 45K stage is ready for operation. Disconnects (3), (6), (14) and (15) are detached at lift-off.

II. FLIGHT OPERATION

A. Approximately 5 to 10 sec prior to 45K-stage ignition, normally closed explosive valve (16) is opened allowing prepressurization of generator system up to double valve (12).

B. At the appropriate point in the stage separation (to be established by type of separation employed), the fire signal explosively opens normally closed valve (17) pressurizing oxidizer tank, explosively opens gas bottle (18) actuating main propellant valve (13), and explosively opens gas bottle (19) actuating generant valve (12).

C. At appropriate shut-down signal, gas bottle (20) explosively opens, closing main propellant valve (13), and gas bottle (21) explosively opens, closing generant valve (12).

III. PREFLIGHT MALFUNCTION DETECTION AND REMEDIAL ACTION

A. Oxidizer system leak prior to fuel tank filling (visual detection)

1. If necessary, drain tank by reversing fill procedure and dissipate leakage by purging affected area with nitrogen, helium, or dry air.
2. Leakage at any point in the system requires remedial action before proceeding with the filling operation.
   a. Inspect equipment for corrosion or other leak causes. Replace affected components where necessary.
   b. Pressure-check system.
   Note: No leakage con be tolerated.

B. Fuel system leak (visual detection)

1. If necessary, drain tank and dissipate leakage by water flushing.
2. Leakage at any point in the system requires remedial action before proceeding with filling operation.
   a. Inspect equipment for corrosion or other leak causes. Replace affected components where necessary.
   b. Pressure-check system.
3. Evidence of heat generation or gas evolution in tank requires immediate evacuation of personnel. Reverse filling operation to drain tanks if fill lines are still connected.

C. Generant tank leak (visual detection)

1. If necessary, drain tank.
2. Dissipate leakage by water flushing.
3. Leakage at any point in the system requires remedial action before proceeding with filling operation.
   a. Inspect equipment for corrosion or other leak causes. Replace affected components where necessary.
   b. Pressure-check system.

D. Main propellant valve and/or generant valve failure

1. Check for visual leakage out of engine nozzle due to main propellant valve leak. If leakage is detected, drain propellant and replace valve.
2. If leakage of closure gas bottles (21) and/or (20) is detected, per items IF2 and IF5, blow down and replace defective bottle.
3. If gas bottle (18) has leaked into main propellant valve actuator, and step lock pin indicates pending valve motion, per item IF6, blow down and replace gas bottle.
4. If generant valve step lock pin shows pending valve motion, per item IF3, blow down and replace gas bottle (19).

E. Helium system leaks

1. If external leakage is noted, vent and take appropriate remedial action.
2. If oxidizer side explosive helium hold-up valve and regulator leak, manifest by buildup in oxidizer tank pressure, vent main helium system, vent oxidizer tank, vent fuel tank. Replace valve and regulator.
3. If generant explosive helium hold-up valve leaks and generant tank pressure exceeds design pressure, i.e. regulator fails to lock up, dump generant helium reservoir. Trapped helium downstream of regulator will bleed to atmosphere. If, however, regulator locks up satisfactorily, continue with normal countdown.

F. Prepressurization leaks

1. If oxidizer or fuel tank fails to hold pressure, blow tank down, blow down helium system, and pressure-check system in order to determine cause.

IV. INFLIGHT MALFUNCTION ANALYSIS

A. Check valves (3) and/or (6) fail to seal, oxidizer or fuel tank blow down, possible adverse starting transient and stage failure.

B. Check valve (14) and/or (15) fail to operate, helium blows down, stage fails.

C. Explosive valve (16) fails to open, stage fails to fire.

D. Helium generant regulator (22) malfunctions

1. Regulator fails to open, stage fails to fire.
2. Regulator bleed is plugged causing possible overpressurization of generant and fuel tanks.
3. Regulator regulates low, burning time increases giving possible error in trajectory pitch angle, p_c drops with possible reduced engine performance and/or engine cooling passages burnout.
4. Regulator regulates high, shorter burning time giving possible error in trajectory pitch angle, p_c increases, tank burst and stage fails if pressure is too high.
5. Regulator fails to close at thrust termination, generant tank is overpressurized and fails with possible fire as a consequence, ste pfails with a possibility of adverse affect on the subsequent stage if its is still nearby.

E. Gas generator malfunction

1. Generator fails to fire, stage fails.
   a. Double valve fails to open because explosive valve (19) fails to open or valve "hangup."
   b. N_2O_4 slug is not injected because of pressure leak in pressurized cartridge.

F. Explosive valve (17) fails to open, stage fails.

G. Helium oxidizer regulator (23) malfunctions

1. Regulator fails to open, stage fails.
2. Regulator regulates low, mixture ratio shifts with possible performance degradation, insufficient stage velocity increment may occur because of premature depletion of fuel.
3. Regulator regulates less than burst pressure of tank but greater than design pressure; mixture ratio shifts with possible performance degradation, insufficient stage velocity increment may occur because of premature depletion of oxidizer.
4. Regulator regulates to burst pressure; tank bursts destroying stage.
5. Regulator fails to lock up at main stage shutdown signal, oxidizer tank is overpressurized, and if sufficient helium remains in main helium supply to overpressure tank to burst pressure, step fails with possible adverse affect on the subsequent stage if it is still nearby.

H. Main propellant valve (13) fails to open, stage fails.

1. Explosive valve (18) fails to open.
2. Propellant valve "hangs up."

I. Main propellant valve (13) fails to close, stage runs to propellant depletion resulting in excess velocity increment of the stage and possible "burping" of engine.

1. Explosive valve (20) fails to open.
2. Propellant valve "hangs up."

J. Generant valve (12) fails to close, fuel tank is overpressurized with possible adverse affect on the subsequent stage if it is still nearby.

1. Explosive valve (21) fails to open.
2. Generant valve "hangs up."

APPENDIX H

Operation Analysis of the Heated Hybrid Pressurization System

I. NORMAL OPERATION

A. *Make sure all valves and actuators are in normal position*

B. *Fill oxidizer tank.*

1. Connect oxidizer tank vent and disconnect line to oxidizer vent disconnect (3).[1]
2. Remove oxidizer fill disconnect cap (2) and connect fill line to oxidizer fill disconnect (1).
3. Fill oxidizer tank to required total weight.
4. Remove oxidizer fill line from oxidizer fill disconnect (1) and replace oxidizer fill disconnect cap (2) using new crush gasket.
5. The oxidizer vent and pressurization line is left in place for use as a tank vent line, and for prelaunch pressurization of the oxidizer tank.

C. *Remove oxidizer ignition cartridge cap (28) and fill cartridge in gas-generator system. Replace cap.*

D. *Fill fuel tank*

1. Attach the fuel tank vent and pressurization system to fuel vent disconnect (4).
2. Remove fuel fill disconnect cap (6) and connect fuel fill line to fuel fill disconnect (5).
3. Remove engine fuel bleed cap (7) and insert disconnect opening device in engine fuel bleed disconnect (8). Provide clean collection equipment for overflow.
4. When solid column of fuel flows from engine fuel bleed disconnect (8), remove disconnect opening device and replace engine fuel bleed disconnect cap (7) using new crush washer.
5. Save engine fuel bleed overflow for weighing.
6. Fill fuel system. Continuously monitor fuel-tank pressure until helium system is charged. Unusual rise in fuel tank pressure indicates decomposition, and malfunction procedure must be followed.
7. Complete filling of fuel tank to required total weight, including amount of overflow.
8. Remove fuel fill line from fuel fill disconnect (5) and replace fuel fill line cap (6) using new crush washer.
9. Fuel tank vent and pressurization system will remain connected to fuel vent disconnect (4) until launching of vehicle.

E. *Fill gas generant (GG) tank*

1. Attach GG tank vent line to GG tank vent valve (37).
2. Attach GG tank fill line to GG tank fill valve (36).
3. Fill GG tank to required capacity.
4. Remove GG tank fill line from GG tank fill valve (36) and install cap on new crush gasket.
5. Remove GG tank vent line from GG tank vent valve (37) and install cap on new crush gasket.

F. *Charging helium supply systems*

1. Check position of tank pressurization valves (9) and (10), and dome loader valve (17) and solenoid valve (35). If all are closed, proceed.
2. Connect helium fill line to helium disconnect (15).
3. Connect helium fil line to GG helium fill and vent disconnect (38).

G. *Final preparation of main propellant valve actuation system and GG ignition system*

1. Make visual observation of main propellant valve linkage position to insure that valves (23) and (24) are in the closed position and main propellant valve lock device is in position.

[1]Numbers in parentheses refer to component numbers on Fig. 11.

2. Remove nitrogen fill disconnect cap and attach nitrogen fill line to nitrogen tank disconnect (19). Fill nitrogen system to 3000 psi.
3. Detach nitrogen fill line from nitrogen tank disconnect (19) and replace nitrogen disconnect cap.
4. Remove fill cap (28) and attach N_2 fill line to oxidizer cartridge. Fill N_2 to 600 psia.
5. Detach N_2 fill line and replace oxidizer cartridge cap (28).
6. Remove main propellant valve lock pin (27).
7. Note: This is the final operation by personnel on the 6,000-lb-thrust stage propulsion system. All subsequent preflight operations will be remotely controlled.

F. Charging main helium supply system (Continued)

4. When the area around the missile is clear of personnel, fill both helium systems to 3000 psi. Monitor helium tank pressures in the blockhouse by direct gauge and telemetry.
5. Allow sufficient time for helium-system to come to thermal equilibrium and recheck pressure.

H. Pressurization of propellant tanks

1. Approximately 5 minutes prior to launch, pressurize the ullage in the oxidizer and fuel tanks by means of the ground pressurization system.

I. At launch

1. Oxidizer vent disconnect, fuel vent disconnect, and helium fill disconnects all pull away.

J. Flight operation

1. At the launch signal (a) solenoid valve (17) opens admitting helium to the dome loader regulator (18) which slowly pressurizes the dome of the helium regulator (13) through restrictor (12), pressurizing the helium line to 250 psi. (b) solenoid valve (35) opens admitting helium to regulator (34) pressurizing the ullage of the GG tank.

2. At the appropriate point in stage separation, and while the vehicle is under positive acceleration, (a) the propellant valve actuator opening valve (20) opens admitting high pressure nitrogen to both

   (a) main valve actuator (22) which opens main propellant valves (23) and (24).

   (b) pressurization valve actuators (11.a and 11.b) which open pressurization valves (9) and (10).

   (c) valves (33) and (39) are actuated initiating ignition of the gas generator and hence delivering decomposition gases to the fuel tank.

3. One second after valve (20) opens, valve (21) closes to shut off nitrogen flow to the opening side of main propellant valve actuator (22).

   Note: 6K stage is now operating.

K. Propulsion system shutoff

1. At the appropriate signal, main propellant valve actuation control valve for closing (25) opens, admitting nitrogen (a) to the closing side of main propellant valve actuator (22) closing main propellant valves (23) and (24) and (b) to the closing side of the tank pressurization valve actuators (11.a and 11.b) closing tank pressurization valves (9) and (10).

2. Simultaneously with K-1 above, the shutoff signal closes the dome loader supply valve (17). Helium regulator (13) then locks up. The shutoff signal also actuates GG shutoff valve (32) and closes GG pressurization valve (35).

3. Closing motion of main propellant valve actuator (22) opens port in actuator admitting high pressure nitrogen from nitrogen accumulation into the injector purge line for post operation purge of fuel side of injector.

II. MALFUNCTION ANALYSIS. POST PREFLIGHT CHECK.

A. *Fill oxidizer tank*

1. Dissipate leakage by purging affected area with nitrogen, helium, or dry air.
2. Leakage at any point in the system requires remedial action before proceeding with filling operation.
   (a) Stop leaks and replace defective components.
   (b) Inspect equipment for corrosion. Replace affected components where necessary.
   (c) Pressure check entire system. See preflight check procedure.

   Note: No leakage can be tolerated.

B. *Fill fuel tank*

1. Dissipate leakage by water flush.
2. Leakage at any point in the system requires remedial action before proceeding with filling operation.
   (a) Stop leaks and replace defective components.
   (b) Inspect equipment for corrosion. Replace affected components where necessary.
   (c) Pressure check entire system. See preflight check procedure.
3. Evidence of heat generation or gas evolution in tank requires immediate evacuation of personnel. Reverse filling procedure so as to drain tank.

   Note: Unsafe or inconvenient remedial operation should be undertaken only after tanks have been drained and purged.

C. *Final preparation of main propellant valve actuation system*

1. If propellant valve lockpin shows indication of main bipropellant valve motion, check to see if oxidizer is leaking out of motor nozzle.
   (a) If no leakage can be detected, proceed with preparation.
   (b) If leakage is detected, drain propellant and replace valve.
2. If main propellant valve linkage moves or causes the lockpin to bind upon or subsequently to charging nitrogen accumulator, vent N_2, and replace explosive valves. Leakage through normally closed valve will be indicated by flow from bleed in main valve actuator.
3. If N_2 system leaks to atmosphere, vent and take proper remedial action.
4. If, upon disconnecting nitrogen fill line, the nitrogen disconnect leaks, vent and replace the disconnect.

D. *Charging main helium supply system*

1. If tank pressurization valves and dome loader valves are not in proper position, ascertain reason and remedy.
2. If external leakage is noted, vent and take appropriate remedial action.
3. If regulator leaks, manifest by buildup in regulated pressure, vent helium system. Replace regulator.

E. *Flight operation*

1. Dome loader supply valve fails to open – S F (Stage Failure).
2. Regulator
   (a) Fails to open – S F
   (b) Bleed plugs – may over-pressurize tanks – S F
   (c) Regulates low-burning time increases, p_c low – may become unstable, error in trajectory in pitch angle. May not be able to cool thrust chamber.
   (d) Regulating high, short burning time, p_c high, error in pitch angle, burst tanks if too high.
   (e) Break diaphragm over pressurize tank.
3. If either propellant tank is over-pressurized, the appropriate burst diaphragm will rupture venting the pressure.
4. Firing sequence
   (a) If valve (20) fails to open – S F
   (b) If valve (21) fails to close, lose N_2 pressure, run to exhaustion which can cause explosive failure of main engine.

F. Propulsion system shutoff

1. If main valve actuator shutoff valve (25) fails to close, run to propellant exhaustion which can cause explosive failure or burnout of the main engine.
2. If main valves fail to close, same as F-1.
3. If pressurization valves fail to close, possible mixing of propellants and explosion.
4. If supply valve for dome loader fails to close, no problem except if helium regulator leaks more than relief valve capacity.
5. If injector purge fails to operate, possible explosion in injector.

G. Non-scheduled operation of components

1. With the exception of non-scheduled normal operation of the entire pressurization system, which would give a reasonable probability for successful operation, non-scheduled operation will result in an abort.

   (c) Main valve actuator fails to open – S F

   (d) Main valve actuator sticks, operate anywhere from monopropellant oxidizer to normal mixture ratio.

   (e) Main valve linkage failure or main valve failure – S F

   (f) Pressurization valve sticks or fails to open, operate at reduced thrust with T/C failure – S F or at low thrust at long burning time.

H. Post operation tank pressure increase

1. Post operation pressure increase in the propellant tank due to helium warmup will be relieved by the burst diaphragms, designed to relieve at some pressure less than the failure pressure of the tanks.

REFERENCES

1. Rupe, Jack H., A Correlation Between the Dynamic Properties of a Pair of Impinging Streams and the Uniformity of Mixture-Ratio Distribution in the Resulting Spray, Progress Report No. 20-209. Pasadena: Jet Propulsion Laboratory, March 28, 1956.

2. Lee, D. H., A Survey of the Compatibility of Various Materials with Hydrazine and Mixtures of Hydrazine, Hydrazine Nitrate, and Water, Memorandum No. 20-152, Pasadena: Jet Propulsion Laboratory, December 22, 1957 (Confidential).

3. Bartz, D. R., Noel, M. B., Grant, A. F. Jr., Evaluation of Hydrazine As a Regenerative Coolant (presented at 3rd Bipropellant Conference, Navy Bureau of Aeronautics, Sacramento), Publication No. 111. Pasadena: Jet Propulsion Laboratory, October 16, 1957 (Confidential).

4. Bartz, D. R., "The Role of Transport Properties in the Problems of Jet Engines and Rockets," in Transport Properties in Gases. Evanston: Northwestern University Press, 1958.

5. Landsbaum, E., Thrust of a Conical Nozzle, (presented at American Rocket Society Meeting, New York City, November 17-20, 1958). Pasadena: Jet Propulsion Laboratory, External Publication No. 560.

6. Jet Propulsion, American Rocket Society, Inc., Easton, Pennsylvania, January, 1957.

7. Grant, A. F., Jr., Basic Factors Involved in the Design and Operation of Catalytic Monopropellant-Hydrazine Reaction Chambers, Report No. 20-77. Pasadena: Jet Propulsion Laboratory (Confidential).